eman ta zabal zazu

Universidad del País Vasco

Euskal Herriko Unibertsitatea

Synthesis of Molecularly Imprinted Polymers for the Speciation of Chiral Compounds

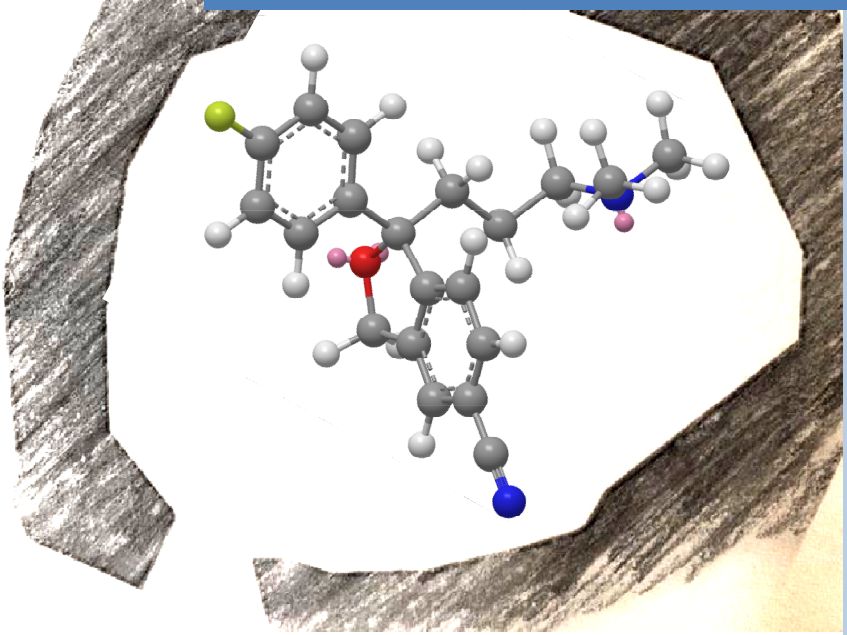

TESIS DOCTORAL

Raquel Gutiérrez Climente

2015

eman ta zabal zazu

Universidad del País Vasco Euskal Herriko Unibertsitatea

SYNTHESIS OF MOLECULARLY IMPRINTED POLYMERS FOR THE SPECIATION OF CHIRAL COMPOUNDS

SÍNTESIS DE POLÍMEROS DE HUELLA MOLECULAR PARA LA ESPECIACIÓN DE COMPUESTOS QUIRALES

This Doctoral Thesis has been carried out in the Forensic Analysis Doctorate Programme at the University of the Basque Country, UPV/EHU

Faculty of Pharmacy, Vitoria-Gasteiz

RAQUEL GUTIÉRREZ CLIMENTE

Diciembre 2015

Esta tesis ha sido realizada, y consecuentemente será defendida, con el propósito de obtener el título de Doctorado Internacional por la Universidad del País Vasco/Euskal Herriko Unibertsitatea (UPV-EHU).

Previamente a la defensa de esta Tesis Doctoral, este trabajo ha sido evaluado por dos expertos pertenecientes a Instituciones de Educación Superior directamente relacionados con el área de Investigación:

- **Dr. Antonio Guerreiro,** Department of Chemistry of the University of Leicester, Leicester (UK).

- **Dr. Josino Costa Moreira,** Departamento de Química da Pontifícia Universidade Católica do Rio de Janeiro, Río de Janeiro (Brasil).

A mi Familia, en especial a mis padres

En primer lugar me gustaría agradecer a mis directores, la Dra. Arantxa Goicolea y el Dr. Alberto Gómez, todo el esfuerzo realizado en esta tesis, las horas dedicadas y el conocimiento que me han aportado a lo largo de estos años. Sin su gran esfuerzo y dedicación, todo este trabajo no hubiera sido posible.

Del mismo modo, quiero agradecer al Dr. Ramón Barrio mi admisión en el programa de doctorado y en el grupo de investigación en el que se ha llevado a cabo esta investigación.

También me gustaría agradecer, por un lado, al Gobierno Vasco el apoyo económico que me ha ofrecido mediante la concesión de una beca predoctoral (BFI-2011-122) y por otro, a la Unidad de Formación e Investigación en Neuroquímica, Neuropsicofarmacología y Psiquiatría de la UPV/EHU (UFI 11/35) la financiación de las dos estancias de investigación que he tenido el placer de realizar a lo largo de estos años. Así mismo, agradecer a la Universidad del País Vasco (EHU/UPV), al servicio central de análisis SGIker y al departamento de Química Analítica las instalaciones, equipamiento y medios ofrecidos sin los cuales este trabajo no hubiera sido posible.

I gratefully acknowledge Dr. Börje Sellergren and Dr. Sergey Piletsky who accepted me in their research groups in Dortmund and Leicester respectively, giving me the opportunity to form part of those wonderful groups. Of course, I would like to thank all the people I met there, for their knowledge, guidance and support.

Finalmente, y no por ello menos importante, agradecer a mis compañeros de laboratorio, familia y amigos el apoyo ofrecido en todos estos años. Su fuerza, ayuda y el ánimo ofrecido en los malos momentos, me han permitido seguir adelante. En especial, agradecer a aquellos que me vieron comenzar, pero que no están aquí para compartir conmigo esta alegría que conlleva acabar un proyecto de tantos años. Para acabar, e incumpliendo mi palabra de no citar a nadie individualmente, Eriz, Dei y Dani, gracias por vuestra paciencia y apoyo en este tramo final.

‘Life is not easy for any of us. But what of that? We must have perseverance and above all confidence in ourselves. We must believe that we are gifted for something and that this thing must be attained’.

Marie Curie

CONTENTS

LIST OF ACRONYMS

ACN	Acetonitrile
AIBN	2,2'-Azobisisobutyronitrile
APTES	3-Aminopropyltriethoxysilane
ATR	Attenuated total reflectance
ATRP	Atom transfer radical polymerisation
BEHS	Bis(2-ethylhexyl)sebacate
CD	Cyclodextrin
CF	Chloroform
CIT	Citalopram
CSP	Chiral stationary phase
CTA	Chain transfer agent
DBP	Dibutyl phthalate
DCM	Dichloromethane
DDCPTS	N, N'-Diethylaminodithiocarbamoylpropyl (trimethoxy)silane
DMSO	Dimethyl sulfoxide
DOP	Dioctyl phthalate
DLS	Dynamic light scattering
EA	Elemental analysis
EDC	1-Ethyl-3-(3-dimethylaminopropyl)-carbodiimide
EDMA	Ethylene glycol dimethacrylate
EMF	Electromotive force
EtOH	Ethanol
FIM	Fixed interference method
FLD	Fluorescence detector
FRP	Free radical polymerisation
FT-IR	Fourier transform infrared spectroscopy
HPLC	High performance liquid chromatography
IA	Itaconic acid
IF	Imprinting factor
Iniferter	Initiator-transfer agent-terminator
ISE	Ion-selective electrode
PETMP	Pentaerythritol tetrakis(3-mercaptopropionate)

LOD	Limit of detection
LOQ	Limit of quantitation
LU	Luminescence
MAA	Methacrylic acid
MeOH	Methanol
MIN	Molecularly imprinted nanoparticles
MIP	Molecularly imprinted polymer
MSM	Mixed solution method
NHS	N-Hydroxysuccinimide
NIN	Non-imprinted nanoparticles
NIP	Non-imprinted polymer
NMP	Nitroxide mediated polymerisation
NPOE	2-nitrophenyl octyl ether
PBS	Phosphate buffered saline
PSI	Pounds per square inch
PVC	Poly(vinyl chloride)
RAFT	Reversible addition fragmentation chain transfer polymerisation
RCIT	R-citalopram
RDRP	Reversible deactivation radical polymerization
RT	Room temperature
RU	Response units
SCIT	S-citalopram
SEM	Scanning electron microscopy
Si-P-MIN	Silica modified with molecularly imprinted nanoparticles synthesised by precipitation polymerisation
Si-SP-MIN	Silica modified with molecularly imprinted nanoparticles synthesised by solid-phase approach
Si-MIP	Molecularly imprinted polymer modified silica
Si-NIP	Non-molecularly imprinted polymer modified silica
SPR	Surface plasmon resonance
TGA	Thermogravimetric analysis
THF	Tetrahydrofuran
TRIM	Trimethylolpropane trimethacrylate

Resumen

La quiralidad es una característica inherente a la mayor parte de los sistemas macromoleculares de reconocimiento biológico. Este hecho, provoca que la unión de uno de los enantiómeros de un fármaco a un receptor biológico desencadene una actividad biológica significativamente distinta a la que provocaría el otro enantiómero. Esto se traduce en diferencias en el mecanismo de acción, toxicidad, farmacocinética e incluso en el metabolismo entre las dos enantioformas de un mismo fármaco.

Por este motivo, es necesario disponer de técnicas analíticas específicas que permitan separar y determinar de una forma eficaz y rápida cada uno de los enantiómeros de una mezcla racémica. La disponibilidad de estas técnicas, permitirá llevar a cabo estudios basados en el comportamiento farmacológico de cada enantiómero, lo que se traduce en un ajuste de las dosis y una mejora en el efecto terapéutico.

En este sentido, la presente tesis se centra en el desarrollo de técnicas analíticas basadas en la implementación de polímeros de huella molecular (MIP) que permitan separar y/o determinar la enantioforma activa de fármacos. Los polímeros de huella molecular, son polímeros altamente entrecruzados que se han generado en presencia de un compuesto empleado como plantilla (*template*) para el que se desea obtener un reconomiento selectivo. Una vez sintetizado el polímero, el *template* es extraído de la matriz, dejando en su lugar cavidades complementarias, en tamaño, forma y funcionalidad, al compuesto objetivo.

Para este trabajo, se ha seleccionado como *template* el enantiómero S del antidepresivo citalopram, perteneciente al grupo de antidepresivos inhibidores selectivos de la recaptación de serotonina. Este fármaco es comúnmente utilizado tanto para el tratamiento de la depresión como para el tratamiento de transtornos de pánico y ansiedad. La enantioforma R (RCIT) de este compuesto reduce la eficiencia del fármaco y, por ello, resulta de gran interés el desarrollo de técnicas que permitan separar y/o monitorizar de forma sencilla la enantioforma S (SCIT), la cual presenta actividad terapeútica.

El objetivo principal de esta tesis, consiste en avanzar en el conocimiento y las posibilidades de los polímeros de huella molecular como materiales de reconocimiento de compuestos quirales. Para ello, el trabajo experimental ha sido dividido en dos secciones principales, en función de la técnica analítica en la que ha sido implementado el material impreso desarrollado. Inicialmente, se presenta una metodología para el desarrollo y aplicación de un receptor sintético MIP como selector quiral en sensores potenciométricos ion selectivos. Como segunda sección del trabajo, se describen distintas técnicas de impresión molecular, controlada mediante polimerización radical por desactivación reversible, para la obtención de películas y nanopartículas MIP sobre microesferas de sílice como sustrato soporte. Los materiales desarrollados, han sido evaluados como fases estacionarias quirales para la separación de mezclas racémicas por cromatografía líquida de afinidad.

Se estableció como principal objetivo de la primera etapa experimental, el diseño de un sensor potenciométrico basado en nanopartículas molecularmente impresas que permitiera la determinación del enantiómero S del antidepresivo citalopram en muestras de orina. La razón de la elección de nanopartículas como formato para el desarrollo del MIP subyace en las ventajas que presentan los nanomateriales MIP. Sobre todo en lo que se refiere a su mayor accesibilidad de sitios de unión y sus cinéticas de asociación-disociación más rápidas, lo que mejora notablemente su selectividad. Estas nanopartículas han sido sintetizadas por polimerización por precipitación, siendo posteriormente caracterizadas química y morfológicamente por

Espectroscopía Infrarroja con Transformada de Fourier y Microscopia Electrónica de Barrido. Asimismo, las propiedades de unión del MIP, como receptor macromolecular sintético, fueron evaluadas por ensayos de unión ligando-receptor realizados en estático.

Las nanopartículas desarrolladas fueron incorporadas en una membrana plástica de policloruro de vinilo, la cual fue implementada en un cuerpo electródico para la construcción de un sensor potenciométrico ion selectivo. Se evaluó el efecto de la composición de dicha membrana en el comportamiento electroquímico del sensor desarrollado. Finalmente, se midió la señal potenciométrica proporcionada por el dispositivo en orina, con el fin de determinar la aplicabilidad del mismo a esta matriz. Asimismo, fue necesario llevar a cabo ensayos de especificidad del sensor tanto para el enantiómero objetivo como para otros iones que habitualmente están presentes a niveles mucho más elevados en orina. Del trabajo realizado se pudo concluir que el sensor potenciométrico desarrollado era capaz de determinar selectivamente el enantiómero S del antidepresivo citalopram en muestras de orina. El dispositivo ha resultado ser una herramienta rápida, fiable y de bajo coste para la monitorización de este antidepresivo en muestras clínicas.

Como segunda parte del trabajo se han evaluado materiales impresos sintetizados en base a distintas estrategias de desarrollo controlado para su uso como selectores quirales en cromatografía líquida. A fin de tener un mayor control sobre el peso molecular, polidispersidad y arquitectura del polímero de huella molecular, en este apartado, la síntesis polimérica se ha llevado a cabo por polimerización radical por desactivación reversible (RDRP), en sustitución a la polimerización radical convencional. Ambas polimerizaciones se basan en el mismo mecanismo radical y pueden ser utilizados para un mismo grupo de monómeros. Sin embargo, en los sistemas de RDRP existe un equilibrio entre radicales propagantes y durmientes, que hacen que el número de cadenas muertas se vea reducido de prácticamente la totalidad en polimerizaciones radicales convencionales, a menos del 10% en RDRP. Además existen otras diferencias significativas como, por ejemplo, el mayor tiempo de

vida de las cadenas en crecimiento en RDRP, la velocidad de iniciación, que pasa de ser lenta en la polimerización radical convencional a rápida en RDRP, o la posibilidad de reiniciar la polimerización en sistemas de RDRP.

Inicialmente, como primera estrategia de síntesis, se llevó a cabo la impresión en superficie del polímero MIP mediante la técnica de injerto conocida como *grafting from* utilizando un *iniferter* (*initiator, transfer agent, terminator*), el cual además de actuar como iniciador, actúa como agente de transferencia de cadena y permite la terminación de la reacción. Por medio de esta técnica es posible sintetizar una capa fina y controlada sobre la superficie de partículas de sílice porosa, manteniendo la estructura, homogeneidad y porosidad del material original. El material sintetizado ha sido caracterizado a través de técnicas como la Espectroscopía Infrarroja con Transformada de Fourier, Microscopia Electrónica de Barrido, Análisis Elemental y Análisis Termogravimétrico. El material desarrollado, fue empleado como fase estacionaria en cromatografía de afinidad. No obstante, a pesar de que la separación era enantioespecífica, la resolución cromatográfica no resultó adecuada, debido fundamentalmente a la anchura de los picos cromatográficos. Tales anchuras de banda, podrían derivar del elevado grado de entrecruzamiento del material MIP sobre el soporte de sílice, lo que originaría una baja accesibilidad a los sitios de unión en el material. En este sentido, se planteó la hipótesis de que las ventajas que presentan los nanomateriales MIP, podrían ser extrapolables al ámbito cromatográfico, pudiendo obtener materiales con sitios de unión más accesibles y con equilibrios de asociación-disociación más rápidos, lo que en teoría podría contribuir a obtener menores anchuras de banda y, en consecuencia, mayor resolución cromatográfica. Para tal fin, se han desarrollado nanopartículas molecularmente impresas, sintetizadas siguiendo dos estrategias diferentes: por síntesis en fase sólida y por polimerización por precipitación. El anclaje de tales nanopartículas en la superficie del soporte de sílice es una estrategia novedosa que ha sido diseñada para aprovechar las ventajas que supone el uso de nanomateriales MIP, sin sufrir desventajas como la sobrepresión, resultante de la reducción del tamaño de partícula en las fases estacionarias.

En la síntesis de nanopartículas en fase sólida, el *template* se inmoviliza sobre la superficie de esferas de vidrio, empleadas como soporte sólido. Éstas son dispuestas en una mezcla para polimerización, la cual contiene los monómeros funcionales y el iniciador oportuno. Los monómeros funcionales interaccionan con el *template* inmovilizado, dando lugar a un complejo monómero-*template* en la superficie de las esferas de vidrio. Este complejo se inmoviliza espacialmente gracias a la acción de varios monómeros entrecruzadores, dando lugar a nanopartículas MIP de elevada afinidad con sitios impresos localizados en su superficie. Dado que las partículas, una vez sintetizadas, se encuentran unidas al *template* sobre la superficie de vidrio, es necesario llevar a cabo etapas de lavado que permitan obtener las partículas en suspensión, libres del soporte sólido. Para ello, se procedió al lavado de las esferas de vidrio empleando, en primer lugar, acetonitrilo a temperatura ambiente y, a continuación, acetonitrilo a 60ºC. El primero, para eliminar de la superficie del soporte los restos de monómeros y las nanopartículas de polímero de menor afinidad, y el segundo para obtener las de mayor afinidad. La afinidad de las nanopartículas obtenidas en el segundo lavado, tanto para el SCIT como para el RCIT, fue determinada por Resonancia de Plasmones Superficiales (SPR). Asimismo, el tamaño del material desarrollado, así como su podispersidad fue caracterizado por Dispersión Dinámica de Luz.

Los resultados obtenidos por SPR, donde se observaba una constante de afinidad aproximadamente 50 veces superior para el enantiómero S que para el R, invitaban a pensar que el nanomaterial MIP podría presentar capacidad para resolver cromatográficamente ambos enantiómeros. No obstante, los ensayos cromatográficos llevados a cabo *a posteriori*, rechazaron tal hipótesis. La falta de capacidad para separar la mezcla racémica podría deberse, probablemente, al hecho de que al unir covalentemente el *template* sobre el soporte sólido para la síntesis, uno de los grupos funcionales, en este caso el grupo nitrilo, del SCIT quedaba inutilizado para su participación en la impresión molecular. Además, este grupo funcional es el que, según la predicción computacional, establece uniones más fuertes entre el SCIT y el

monómero funcional, siendo notablemente más débiles con el enantiómero R. En consecuencia, los sitios impresos generados en su ausencia, presentarían menor enantioespecificidad, hecho que fue corroborado experimentalmente.

Por el contrario, la utilización de nanopartículas sintetizadas por polimerización por precipitación, en la que el SCIT fue utilizado sin inmovilización previa sobre soporte sólido alguno, dio lugar a una columna cromatográfica con buena resolución quiral. En polimerización por precipitación el *template* se encuentra libre en disolución y en consecuencia, todos sus grupos funcionales polares pueden interaccionar con el monómero funcional para establecer el complejo monómero-*template*. Complejo en el cual se basan los posteriores sitios impresos. Como resultado, se obtuvieron materiales que presentaron mayor enantioespecificidad que los sintetizados por síntesis en fase sólida. En base a los resultados obtenidos, se concluyó que la técnica de polimerización en fase sólida, a pesar de ser conocida por dar lugar a nanomateriales MIP de mayor afinidad que los sintetizados por otras técnicas, no resultó ser eficaz para obtener fases estacionarias con capacidad para separar cromatográficamente los enantiómeros del citalopram. No obstante, la síntesis de nanopartículas por precipitación dio lugar a fases estacionarias que permitían la separación quiral del fármaco con una resolución comparable a la proporcionada por fases estacionarias comerciales. Con todo ello, quedó corroborado que las ventajas de los nanomateriales MIP pueden ser explotadas en separación cromatográfica, obteniendo bandas más estrechas y mejor resueltas que con MIP desarrollados por polimerización convencional en bloque.

Se puede afirmar que se han sintetizado y aplicado de forma satisfactoria, polímeros de huella molecular a dos técnicas analíticas diferentes. Permitiendo así, determinar y separar las dos enantioformas del antidepresivo citalopram.

Finalmente, mencionar que las metodologías aquí presentadas pueden ser extrapoladas a otros compuestos quirales, sean fármacos o no, permitiendo desarrollar técnicas analíticas capaces de separar una mezcla racémica. Lo que supone un gran avance en el desarrollo de técnicas rápidas y fiables para la especiación de compuestos quirales.

Chapter 1

Introduction

This Page Intentionally Left Blank

1. Introduction

Most of natural ligands in living organisms present chirality as a hallmark; even if they present the same chemical structure, they exhibit remarkable differences concerning biological activities. This is particularly determinant in the pharmaceutical field in what concerns drug development, in its mechanism of action, toxic effects, pharmacokinetics or even its metabolism. As a consequence, the Food and Drug Administration has recommended that chiral drugs must be tested and regulated separately [1].

The enantiomers of the antidepressant citalopram (S-citalopram and R-citalopram) are among the ones exhibiting differences in terms of bioactivity, pharmacological and toxicological properties (figure 1.1). Citalopram, (RS)-1-[3-(dimethylamino) propyl]-1-(4-fluorophenyl)-1,3-dyhydroisobenzofuran-5-carbonitrile, is a racemic mixture of R-citalopram and S-citalopram widely used as serotonin reuptake inhibiting antidepressant [2]. It is widely used to treat anxiety and panic disorders and it is prescribed off-label for a number of anxiety conditions [3]. In 2004 the group of Sánchez *et al.* [4, 5] confirmed the preclinical evidences about the efficiency reduction of citalopram when the drug was supplied as a racemate. In fact, in 2013, more accurate studies [6, 7] indentified some brain activity changes depending on the drug type. Despite these findings, in some instances this drug is still being

prescribed as a racemic mixture rather than as a pure form of the pharmacologically active enantiomer. Therefore, it still exists the need of developing specific chiral separation techniques capable of determining target enantiomers of these drugs in pharmaceutical and clinical samples.

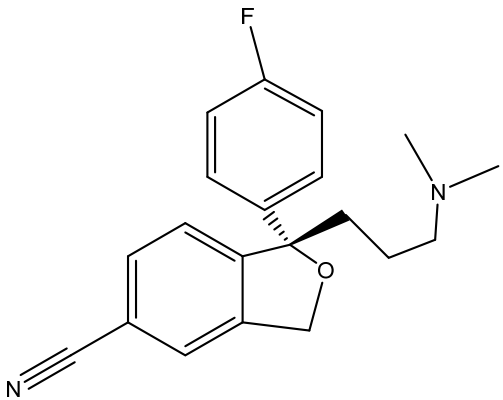

(*S*)-1-(3-(dimethylamino)propyl)-1-(4-fluorophenyl)-1,3-dihydroisobenzofuran-5-carbonitrile

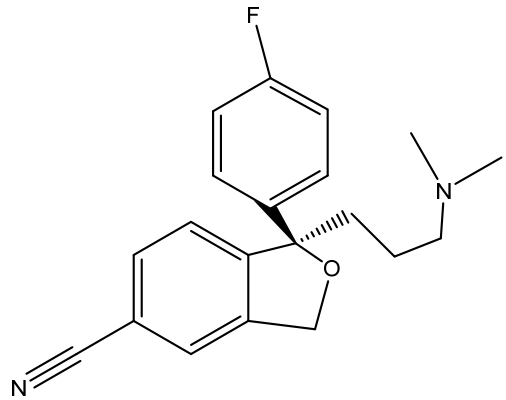

(*R*)-1-(3-(dimethylamino)propyl)-1-(4-fluorophenyl)-1,3-dihydroisobenzofuran-5-carbonitrile

Figure 1.1. Structures of S-citalopram (SCIT) and R-citalopram (RCIT).

Generally speaking, there are two different approaches to achieve pure enantiomers, the chiral and the racemic approach. The chiral approach is based on developing an asymmetric synthesis of only a single enantiomers, whereas the racemic approach is based on separating racemic mixtures of both enantiomers [8]. In the latter, almost the entire spectrum of separation techniques, both on analytical or on preparative scale, can be employed as potential tools for enantiomer resolution (figure 1.2).

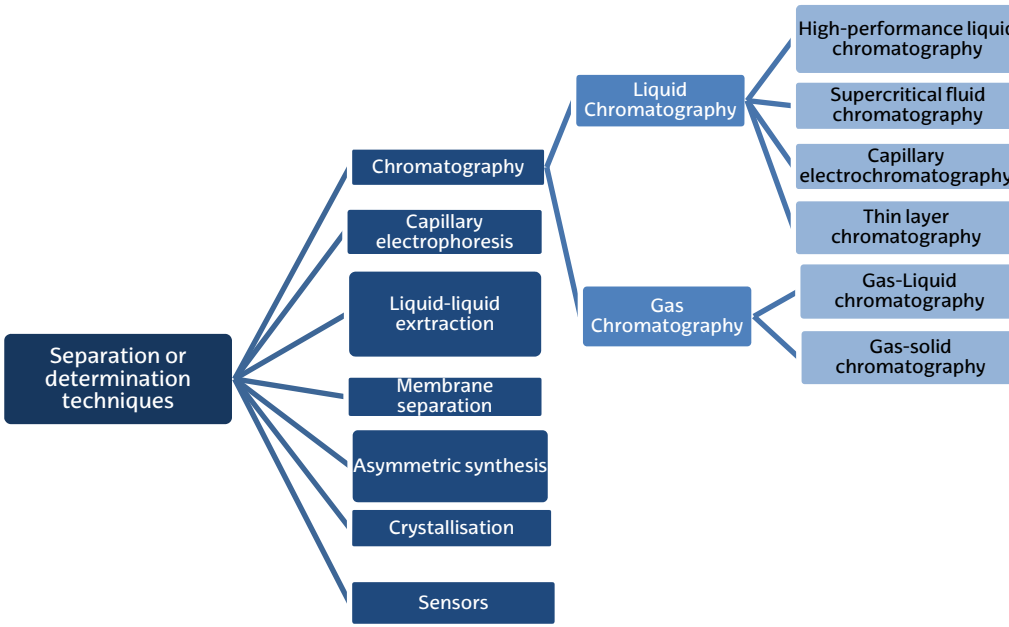

Figure 1.2. Techniques used for the separation and/or determination of enantiomers.

In this work, high-performance liquid chromatography has been selected as separation technique for the chiral resolution of citalopram. Novel chiral stationary phases have been developed using plastic enantiospecific receptors as chiral selectors immobilised on silica beads, as solid support. These chiral selectors have been synthesised by the Molecular Imprinting Technology in different formats. Thin receptor layers and also nanoparticles of these artificial receptors have been developed on silica particles to be employed as stationary phases in chiral chromatography.

Molecular Imprinting of Polymers consists in a technique for developing synthetic polymers in the presence of a target molecule, which is responsible for originating nanocavities in the polymer matrix during the synthesis process. After the synthesis, this molecule is extracted from the polymer matrix obtaining Molecularly Imprinted Polymers (MIP), which behave as synthetic receptors with binding sites

complementary, chemically and sterically, in shape, size and functionality to the target molecule (known as template) used in the synthesis of the material. Advantages such as high physical and chemical stability, combined with their low costs and predetermined selectivity, make these materials a really attractive tool to be used in chromatography.

In MIP development, an adduct is formed betweeen the target molecule and one or even more functional monomers in a prepolymerisation solution. This adduct is later immobilised thanks to the addition of a high amount of a cross-linking monomer which immobilises spatially the prepolymerisation adduct. As a final step, the template is removed from the polymer matrix, whereas, the nanocavities generated by it remain in the polymer, providing it with specific recognition capability. Based on the type of interaction between the template and the functional monomers in the prepolymerisation adduct, Molecular Imprinting of Polymers can be carried out by different approaches including the covalent and non-covalent ones. The first report of MIP was published by Wulff *et al*. in 1972 [9] based on the covalent approach. However, the non-covalent one, which is based on interactions such as hydrogen bonds, dipole-dipole interactions, ionic interactions and hydrophobic interactions, is, currently, the most commonly applied technique due to its flexibility and faster rebinding kinetics [10, 11].

The potential benefits of imprinted materials can undoubtedly be exploited not only for chromatographic separation but also for their use as recognition elements in sensor development. Based on the high specificity of MIP, in some instances comparable to that presented by natural receptors, they can be implemented in different types of electrodes for selective sensing of target analytes. This simplifies or almost eliminates the need of performing tedious sample treatment steps, reducing considerably the global analysis time.

Regarding to these premises, as the first stage of the developed research, molecularly imprinted nanoparticles were developed by precipitation polymerisation in order to integrate them in a liquid membrane of an Ion Selective Electrode. The sensor

fabricated this way, would allow for the direct quantification of S-citalopram in urine by potentiometric transduction. It was also hypothesised that using MIP in nanoparticle format, instead of using irregular MIP coming from traditional bulky syntheses, could lead to faster binding-release kinetics, what may favour sensor performance.

In a second step of the experimental, the research work was focussed on the development of chiral stationary phases based on MIP synthesised by Reversible Deactivation Radical Polymerisation (RDRP) capable of resolving chromatographically the citalopram racemate. To this end, different polymerisation strategies were assessed in order to obtain a chiral stationary phase which could be comparable, in terms of chromatographic peak resolution, with the commercial ones based on other chiral selectors like cyclodextrins. Undoubtedly, this will open a new research area where the specificity of MIP could give rise to new chiral stationary phases, more specifically designed and with predictable elution order.

References

1. Rauws AG, Groen K: **Current regulatory (draft) guidance on chiral medicinal products: Canada, EEC, Japan, United States**. *Chirality* 1994, **6**(2):72-75.
2. Li M, Bao Z, Su B, Xing H, Yang Y, Ren Q: **Enantiomeric separation of citalopram base by supercritical fluid chromatography**. *Journal of Separation Science* 2013, **36**(18):3093-3100.
3. Peikova L, Pencheva I, Petrova G, Zlatkov A: **Stereo chemical determination of stability of citalopram enanthiomers: HPLC chirality test**. *International Journal of Pharmaceutical Sciences Review and Research* 2013, **19**(2):7-11.
4. Sanchez C, Kreilgaard M: **R-citalopram inhibits functional and 5-HTP-evoked behavioural responses to the SSRI, escitalopram**. *Pharmacolology Biochemistry and Behavior* 2004, **77**(2):391-398.
5. Sanchez C, Bogeso KP, Ebert B, Reines EH, Braestrup C: **Escitalopram versus citalopram: the surprising role of the R-enantiomer**. *Psychopharmacology* 2004, **174**(2):163-176.
6. Henry ME, Lauriat TL, Lowen SB, Churchill JH, Hodgkinson CA, Goldman D, Renshaw PF: **Effects of citalopram and escitalopram on fMRI response to affective stimuli in healthy volunteers selected by serotonin transporter genotype**. *Psychiatry Research: Neuroimaging* 2013, **213**(3):217-224.
7. **FDA Drug Safety Communication: Revised recommendations for Celexa (citalopram hydrobromide) related to a potential risk of abnormal heart rhythms with high doses**
   [http://www.fda.gov/Drugs/DrugSafety/ucm297391.htm]. **Access Data**: 2015.11.12
8. Lorenz H, Seidel-Morgenstern A: **Processes to separate enantiomers**. *Angewandte Chemie International Edition* 2014, **53**(5):1218-1250.
9. Wulff G, Sarhan A: **Use of polymers with enzymeanalogous structures for resolution of racemates** *Angewandte Chemie International Edition* 1972, **11**(4):341.
10. Sellergren B: **The non-covalent approach to molecular imprinting**. In: *Molecularly Imprinted Polymers Man-made mimics of antibodies and their applications in analytical chemistry*. Edited by Sellergren B, vol. 23, 1 edn. Amsterdam: Elsevier; 2001: 113-184.
11. Zhang H, Ye L, Mosbach K: **Non-covalent molecular imprinting with emphasis on its application in separation and drug development**. *Journal of Molecular Recognition* 2006, **19**(4):248-259.

Chapter 2

Objectives

This Page Intentionally Left Blank

1. Objectives

The development of new chiral methodologies for the direct determination and quantification of chiral drugs is vital in order to fulfill the requirements of the regulatory authorities about the stereoisomeric composition of chiral substances. This aspect, together with the increasing interesting in the specific recognition carried out by synthetic receptors, made us to suggest the following main objective of this work:

Development of synthetic polymeric receptors for their direct application in chromatography and potentiometric sensing for the separation and/or determination of the chiral antidepressant citalopram.

In order to achieve this general objective this work has been structured in two chapters, one of them for the synthesis nanoparticles and their application on the development of a potentiometric sensor, and another one for the synthesis of a chiral stationary phase for its use in high performance liquid chromatography.

In the first section, chapter 3, the main objective that has been described in order to contribute to the accomplishment of the general objective consists in:

- ***The design of a potentiometric sensor based on molecularly imprinted nanoparticles for the determination of the S enantiomer of the antidepressant citalopram in urine samples.***

On the other hand, the objective of the second section, chapter 4, has been focused on:

- ***The development of chiral molecularly imprinted polymers in a controlled manner on solid supports, in order to develop chiral stationary phases for the enantiomeric resolution of the antidepressant drug citalopram.***

In each of these sections several operational objectives have been more extensively detailed in the corresponding chapters.

Capítulo 3

Síntesis de un sensor potenciométrico para la determinación directa de S-citalopram en muestras de orina

This Page Intentionally Left Blank

Índice

This Page Intentionally Left Blank

1. Introducción

1.1. Sensores potenciométricos

Los sensores potenciométricos constituyen un grupo de dispositivos electroanalíticos que permiten determinar la diferencia de potencial eléctrico respecto a un determinado electrodo de referencia. A través de esta diferencia de potencial, puede determinarse la actividad de una especie iónica en disolución. Han sido empleados en análisis clínicos de rutina para la determinación de hemoglobina y hematocrito, pH, O_2 y CO_2 en sangre, electrolitos y otros parámetros de interés como la urea o la glucosa [1]. También se han utilizado en el campo medioambiental, por ejemplo, para la determinación de contaminantes en aguas, como pesticidas [2] y metales pesados [3-5], medida de pH o fluoruros también en aguas [6], o medida de gases como el CO_2 o el O_2 presentes en la atmósfera [7].

En potenciometría directa, se emplea una celda electroquímica que consta de un electrodo indicador y uno de referencia, conectados por un puente salino. Esta técnica está limitada a la medida de potenciales de equilibrio de sistemas rápidos, a los que puede aplicarse la ecuación de Nernst (3.1):

$$E = E^0 + \frac{0.059}{n} log \frac{a_{Ox}}{a_{Red}} \qquad 3.1$$

El electrodo indicador, el cual se sumerge en la disolución del analito, adquiere un potencial (E) que depende de la actividad del propio analito.

Como electrodos indicadores, habitualmente se emplean electrodos metálicos o electrodos selectivos de iones (ISE), también conocidos como electrodos de membrana [8].

1.1.1. Electrodos metálicos

Los electrodos metálicos generan un potencial eléctrico en respuesta a una reacción redox que tiene lugar en la interfase electrodo-disolución. Estos electrodos se dividen en electrodos de primera, segunda y tercera especie [8].

Los **electrodos de primera especie** consisten en electrodos metálicos que están en equilibrio directo con su propio catión en disolución, implicando únicamente una reacción. Debido a su reducida selectividad y a su respuesta frente a otros cationes, estos electrodos no son muy utilizados. Además, muchos de ellos, únicamente pueden emplearse en disoluciones neutras o básicas debido a su solubilidad en medios ácidos.

Los **electrodos de segunda especie** están compuestos por metales que no sirven únicamente como electrodos indicadores de sus propios cationes, sino que también responden ante aniones con los que forman precipitados o complejos estables. Por ejemplo, la plata puede servir como un electrodo de segunda especie para haluros y pseudohaluros. Dos electrodos de segunda especie habituales son los electrodos de referencia de calomelanos y de Ag/AgCl.

Finalmente, los **electrodos de tercera especie** están compuestos por un metal inerte el cual responde al potencial de los sistemas de oxidación-reducción con los que se pone en contacto.

1.1.2. Electrodos selectivos de iones

Un electrodo selectivo de iones (ISE) consiste en un electrodo provisto de una membrana que responde selectivamente a un determinado ion. La parte externa de la membrana se pone en contacto con una disolución del ion a determinar mientras que

la disolución interna, contiene una disolución de actividad fija del ion en contacto con un electrodo de referencia interno, habitualmente de Ag/AgCl.

El potencial de celda (E_{cel}) consta de tres componentes: el potencial de membrana (E_m), el potencial del electrodo de referencia (E_{ref}) y el potencial de unión líquida (E_j) tal y como se expresa en la ecuación 3.2. El potencial de membrana se relaciona con la actividad de los iones en las disoluciones (interna a_1 y externa a_2) a ambos lados de la membrana mediante una ecuación similar a la de Nernst (ecuación 3.3). En una situación ideal, este potencial debe ser igual a 0. Sin embargo, debido a que la cara interna y externa de la membrana no son idénticas, es necesario establecer un potencial de asimetría (E_{asim}) que puede verse ligeramente alterado con el tiempo. Para eliminar los errores que resultan del potencial de asimetría, todos los ISE deben calibrarse frecuentemente frente a una o más disoluciones patrón de analito.

$$E_{cel} = E_m + E_{ref} + E_j \qquad 3.2$$

$$E_m = E_{asim} - \frac{RT}{zF} ln \frac{a_1}{a_2} \qquad 3.3$$

Los ISE presentan la ventaja de permitir ensayos no destructivos que dan lugar a una respuesta rápida. No obstante, la respuesta electroquímica puede verse afectada por iones interferentes. Además, algunos compuestos pueden quedar adsorbidos en la membrana, evitando la adecuada difusión de las especies a su través [7].

Los ISE pueden clasificarse en función del tipo de membrana, en electrodos de membranas cristalinas y no cristalinas, pudiendo dentro de estas últimas incluir las membranas de vidrio y las membranas líquidas.

Electrodos de membrana cristalina

Estos electrodos poseen una membrana compuesta por un cristal inorgánico de una sal de muy baja solubilidad. En este grupo, uno de los más conocidos es el electrodo de fluoruros, que está constituido por una sal de fluoruro de lantano [9]. También pertenecen a este grupo los electrodos fabricados para iones como Cl^-, Br^-, I^-, Cu^{2+}, Pb^{2+},

CN^-, Ag^+ y S^{2-} [10]. En estos dos últimos, la sal utilizada Ag_2S permite la medida tanto del ion sulfuro como del ion plata siempre y cuando ésta no tenga lugar de forma simultánea [7].

Electrodos de membrana de vidrio

Son los electrodos más comunes dentro de los ISE, siendo el más conocido el electrodo de pH [9]. Este tipo de electrodos únicamente pueden ser utilizados para un número reducido de iones como el H^+ o Na^+, ya que su selectividad para otros iones se ve significativamente reducida [7].

Electrodos de membrana líquida

Este grupo de electrodos, a diferencia de los dos tipos de electrodos descritos anteriormente, permite la medida de un amplio grupo de compuestos. Las primeras membranas líquidas se prepararon a partir de líquidos inmiscibles intercambiadores de iones, que estaban retenidos en un soporte sólido inerte y poroso en forma de disco. El disco poroso, de dimensiones habituales de 3 x 0.15 mm, estaba constituido por un plástico hidrófobo que permitía mantener la capa orgánica intercambiadora entre los medios interno y externo acuosos. Como alternativa al uso del disco poroso, se han conseguido inmovilizar líquidos intercambiadores en membranas poliméricas como las de policloruro de vinilo (PVC). La membrana de estos electrodos consiste en un polímero orgánico hidrófobo impregnado con un plastificante, habitualmente un ftalato, y un intercambiador iónico capaz de permitir el paso del ion analito [11]. En el interior hay un electrodo Ag/AgCl, cuyo potencial varía en función de la concentración del analito que entra [9]. Comercialmente, los más conocidos son aquellos que permiten la determinación de Ca^{2+}, Mg^{2+}, $K^{+,}$ o NO_3^- [10].

1.2. Electrodos Ion Selectivos enantioespecíficos

El primer trabajo publicado sobre sensores electroquímicos enantioselectivos data de 1975 [12]. En éste y en trabajos sucesivos [13-16], se estudió el efecto de los éteres corona como ionóforos macrocíclicos quirales en sensores basados en membranas de policloruro de vinilo (PVC) selectivos para el ion α-fenil etil amonio. Desde entonces, la mayoría de los sensores electroquímicos enantioselectivos desarrollados, se basan en la incorporación de ionóforos quirales a membranas líquidas de PVC.

1.2.1. Electrodos Ion Selectivos basados en ionóforos quirales

Los selectores quirales utilizados en potenciometría, son ionóforos ópticamente activos capaces de formar diastereoisómeros mediante uniones por puentes de hidrógeno, interacciones electrostáticas, acoplamientos π-π y/o fuerzas de Van der Waals. Habitualmente se emplean selectores como los éteres corona, las ciclodextrinas o bien antibióticos macrocíclicos. La selección del selector quiral es la que determinará la enantioselectividad en la medida electroquímica.

Los **éteres corona** son poliéteres macrocíclicos que presentan cierta polaridad en su cavidad y que forman complejos anfitrión-huésped con iones metálicos y especies catiónicas. Se han utilizado como ionóforos quirales selectivos de fármacos con grupos amino en su estructura, como la efedrina [17], así como para aminoácidos y sus derivados [16, 18].

La discriminación de enantiómeros también puede tener lugar empleando **ciclodextrinas (CD) o sus derivados** como ionóforos. Las CDs son oligosacáridos compuestos por 6, 7 y 8 unidades de D-glucopiranosa, denominándose CDs α, β y δ respectivamente. Estas macromoléculas de estructura cilíndrica presentan grupos hidroxilo en el exterior de los anillos macrocíclicos, lo que les dota de carácter hidrofílico necesario para permitir su solubilidad en medios acuosos y en disolventes apróticos moderadamente polares. Así mismo, presentan una cavidad hidrófoba que permite la inclusión selectiva de una gran variedad de compuestos formando complejos diasteroisómeros reversibles [19]. Estudios como los llevados a cabo por los

grupos de Bates *et al.* [20] y Kataky *et al.* [21] demuestran la efectividad de estos selectores para la determinación de fármacos como la efedrina, propranolol y norefedrina. Por otro lado Kaniewska *et al.* [22] estudiaron el efecto de diferentes plastificantes en la elaboración de membranas con derivados de CDs para el 1,4-nitrofenil etil amina y la efedrina. Aboul-Enein *et al.* [23, 24] y Stefan R.I *et al.* [25, 26] también emplearon este selector quiral para el análisis de varios inhibidores de la enzima convertidora de la angiotensina (IECA).

En ocasiones, aunque con menor frecuencia, también se utilizan **antibióticos macrocíclicos** como la teicoplanina [22, 27, 28] y derivados de la monensina [29] como ionóforos quirales. La teicoplanina es un glipopéptido compuesto por anillos macrocíclicos enlazados que dan lugar a estructuras hidrófobas en forma de canasta. En el reconocimiento enantioselectivo, estos antibióticos son capaces de establecer uniones hidrofóbicas, enlaces iónicos, uniones dipolo-dipolo, interacciones π-π y/o enlaces por puentes de hidrógeno [30].

Otro ejemplo de selector quiral lo constituye el alcaloide **quinina.** La enantioespecificidad de este selector ha sido evaluada para los aminoácidos triptófano, ácido aspártico y ácido glutámico, incorporándolo en un sensor potenciométrico de membrana de PVC [31]. Este compuesto ha sido asimismo implementado recientemente como selector quiral en electrodos de pasta de carbono para la determinación de los enantiómeros R y S de la 3,5-dinitrobenzoil leucina, derivado del aminoácido esencial leucina [32].

En menor medida, también se han empleado **sales de manganeso** como selectores quirales en la determinación de los isómeros del ácido mandélico. Para ello, se ha empleado un complejo quiral de salicilaldehido y etilendiamida (ligando SALEN) con Mn(II) recubierto de una monocapa de polianilina [33]. De forma similar, se han empleado selectores basados en un complejo de **sales de cobalto** sobre electrodos de óxido de indio dopado con estaño (ITO) modificados previamente con una monocapa de (3-aminopropil) trietoxisilano [34].

En la tabla 3.1 se resumen los sensores potenciométricos enantioselectivos más relevantes que se han desarrollado empleando ionóforos quirales.

Tabla 3.1. Resumen de los trabajos publicados relacionados con sensores potenciométricos enantioselectivos basados en ionóforos quirales.

Selector quiral	Analito	Coeficiente de enantioselectividad log K^{pot}	Referencia	Año
Éter corona	Ion α-fenil etil amonio	0.41	Bussmann W *et al.* [16]	1981
	Efedrina	0.71	Horvath V. *et al.* [17]	1997
	Iones de fenil etil amonio	0.03; -0.11	Pilbath Z *et al.* [18]	2010
Derivados de CDs	Efedrina	0.41	Bates P.S *et al* [20]	1994
	Efedrina	-2.6	Kataky R. *et al.* [21]	1995
	Propranolol	-2.7	Kataky R. *et al.* [21]	1995
	Norefedrina	-1.5	Kataky R. *et al.* [21]	1995
	1,4-Nitrofenil etil amina y efedrina	0.53; - 0.31	Kaniewska *et al.* [22]	2008
	IECA	< -3	Aboul-Enein H.Y. *et al.* [23] [24] y Stefan R.I *et al.* [25, 26]	1999
Teicoplanina	L-carnitina	0.42	Kaniewska *et al.* [22]	2008
	Baclofeno	-2.38	Rat'ko A. A. *et al.* [27]	2004
	Ácido D-2-hidroxiglutárico	-2,42	Stefan R.I *et al.* [28]	2005
Monensina	Leucina metil éster	0.88	Maruyama K. *et al.* [29]	1992
Quinina y sus derivados	Aminoácidos	-	Chibvongodze, H. *et al.* [31]	2001
	3,5-Dinitrobenzoil leucina	-2,66	Stefan-van Staden R.I *et al.* [32]	2013
Sales de Mn	Ácido mandélico	-4.0	Xu L *et al.* [33]	2009
Sales de Co	Ácido mandélico	-2.71	Yang Y *et al.* [34]	2010

IECA: Inhibidores de la enzima convertidora de la angiotensina

1.2.2. Electrodos Ion Selectivos basados en Polímeros de Huella Molecular

Los Polímeros de Huella Molecular (MIP) han sido utilizados como elemento de reconocimiento en una amplia variedad de sensores químicos, incluyendo sensores conductimétricos [35], amperométricos [36-38], voltamperométricos [39, 40], potenciométricos [2, 41-43] sensores basados en microbalanzas de cristal de cuarzo (QCM) [44, 45] y sensores basados en la resonancia de plasmones superficiales (SPR)

[46]. Entre ellos, los sensores potenciométricos basados en MIP, dada su estabilidad, simplicidad y versatilidad, resultan verdaderamente atractivos como herramienta en el análisis electroquímico [47].

La investigación focalizada a la elaboración de ISEs basados en MIP sufre un importante desarrollo a comienzos de siglo, para monitorizar la concentración de enantiómeros en tiempo real, de forma fiable y a bajo coste [48]. La amplia aceptación que han ido ganando estos materiales durante los últimos años es atribuible a su habilidad de reconocimiento específico del compuesto objetivo, su estabilidad térmica y resistencia mecánica, así como su relativa facilidad de síntesis a bajo coste.

1.2.2.1. Electrodos Ion Selectivo basados en Nanopartículas Impresas

En los últimos años, el desarrollo de nuevas metodologías para la elaboración de nanopartículas molecularmente impresas (MIN) ha ido cobrando especial relevancia debido a las mejoras significativas que poseen los MIP a nanoescala frente a los MIP convencionales [49, 50]. La relación superficie-volumen es mayor para las MIN que en los MIP tradicionales, lo que favorece la accesibilidad del compuesto objetivo a las cavidades impresas, dando lugar a cinéticas de unión más rápidas [51]. Existen diferentes estrategias que permiten sintetizar este tipo de nanomateriales, entre ellas, la polimerización por precipitación y polimerización por emulsión, ya sea por polimerización convencional [52-57] o mediante polimerización radical por desactivación reversible [58, 59], han sido las más empleadas hasta la fecha. La síntesis de MIP en fase sólida, descrita recientemente para el desarrollo de estos materiales, supone un paso adelante en la fabricación de nanomateriales MIP [60-62].

Polimerización por precipitación

Este tipo de polimerización tiene lugar de forma análoga a la polimerización en bloque, pero utilizando un volumen de porógeno entre 50 y 100 veces superior. El proceso de polimerización puede dividirse en dos etapas: la etapa de nucleación y la de crecimiento [63]. Al comienzo de la polimerización, se forman radicales primarios como consecuencia de la descomposición térmica o fotoquímica del iniciador de

polimerización. Estos radicales interaccionan con los grupos vinílicos de los monómeros en disolución, facilitando su unión en cadena y dando lugar a estructuras poliméricas. Este proceso continúa hasta alcanzar un determinado peso molecular formándose núcleos de cadenas poliméricas (figura 3.1a). Cuando estos núcleos alcanzan una masa determinada, si el disolvente en el cual se encuentran no es apropiado para su gelificación, precipitan, deteniéndose así su crecimiento.

El proceso de crecimiento puede ocurrir de dos formas: por captación de radicales oligoméricos y monómeros en la superficie de la partícula (figura 3.1b), o por agregación de núcleos a través de un proceso conocido como homocoagulación (figura 3.1c) [63, 64]. La adecuada elección del disolvente resulta determinante en la morfología de las partículas, puesto que, por ejemplo, para evitar la gelificación de los núcleos iniciales (figura 3.1d), conocidos como partículas en estado sol, el porógeno en el que transcurre la síntesis debe ser un disolvente en el que el polímero presente baja solubilidad [63].

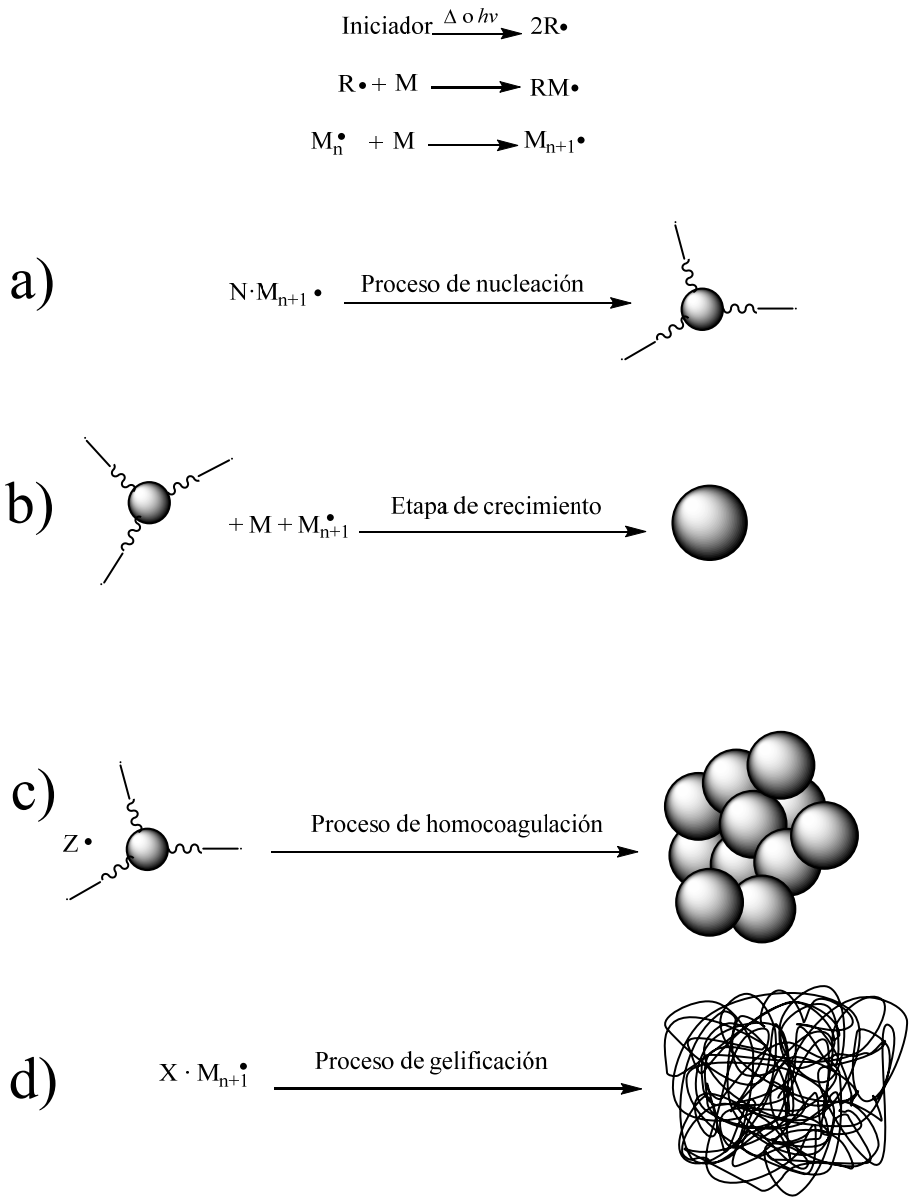

Figura 3.1. Etapas de síntesis polimérica por precipitación

M: monómero, **M_{n+1}:** cadenas poliméricas propagantes, **n:** número de monómeros promedio que forman la cadena polimérica y **N:** número de cadenas propagantes. [63]

En muchas ocasiones, para seleccionar el disolvente óptimo en el que se va a realizar la polimerización, se utiliza el parámetro de Hildebrand (δ) [52, 65-67]. Este parámetro refleja la energía cohesiva de un material y viene dado por la ecuación 3.4:

$$\delta = \left(\frac{\Delta E}{V}\right)^{1/2} = \left(\frac{\Delta H - RT}{M/\rho}\right)^{1/2} \qquad 3.4$$

Donde ΔE es la energía de vaporización, V el volumen molar, ΔH el calor latente de vaporización, R la constante de los gases, T la temperatura, M la masa molecular y ρ la densidad.

Cuanto más próximos sean los parámetros de solubilidad de dos sustancias, más miscibles serán éstas entre sí. Sin embargo, en la práctica, materiales con valores de δ similares pueden presentar afinidades diferentes [68]. Esto es debido a que el parámetro de solubilidad, al igual que el proceso de solvatación, involucra interacciones moleculares por puentes de hidrógeno (δ_h), uniones dipolo-dipolo (δ_p) y fuerzas de dispersión de London (δ_d). Por lo que para definir de forma correcta la solubilidad en cada disolvente, resulta conveniente utilizar los parámetros de solubilidad de Hansen (ecuación 3.5) [69].

$$\delta = \left(\delta_d^2 + \delta_p^2 + \delta_h^2\right)^{1/2} \qquad 3.5$$

La importancia de utilizar los parámetros de solubilidad de Hansen en lugar de los de Hildebrand queda, por ejemplo, reflejada en el trabajo llevado a cabo por Yan *et al.* [70] en el que estudió el efecto del disolvente, en la morfología de partículas de polidivinilbenceno sintetizadas por polimerización por precipitación. Observaron que en la mayoría de los trabajos publicados para divinilbenceno, únicamente se obtenían partículas esféricas cuando la polimerización se llevaba a cabo en disolventes con un parámetro δ comprendido entre 16 y 24 $MPa^{1/2}$. Este amplio abanico de resultados, les llevó a estudiar este comportamiento teniendo en cuenta los parámetros de

solubilidad tridimensionales de Hansen (δ_h, δ_p y δ_d). Observaron como el valor de solubilidad dependiente de las fuerzas de dispersión de London, δ_d, resultaba ser el que verdaderamente afectaba a la morfología de las partículas, ya que únicamente se obtenían partículas esféricas cuando el valor de δ_d era aproximadamente 15.4 $MPa^{1/2}$. Valores próximos a él, tanto por encima como por debajo (15-20.2 $MPa^{1/2}$), daban lugar a microgeles o macrogeles debido a la alta solubilidad en el disolvente, mientras que valores muy bajos (‹15 $MPa^{1/2}$) o muy elevados (›24.3 $MPa^{1/2}$) daban lugar a aglomerados debido a una solubilidad demasiado baja. Estas conclusiones, aunque con menor profundidad, también habían sido descritas anteriormente por Shim *et al.* [71].

Experimentalmente, a la hora de seleccionar el disolvente adecuado, se evalúa la miscibilidad del monómero entrecruzador en el medio, por ser el reactivo mayoritario en la mezcla de polimerización, y por tanto, el que contribuye, en mayor medida, a la estructura final del polímero.

La polimerización por precipitación favorece la generación de partículas esféricas con mayor capacidad de unión y con una distribución de sitios de unión más homogénea que por polimerización en bloque [52]. Además del disolvente, para controlar el proceso de polimerización y, con ello, controlar el tamaño final de las partículas, se deben optimizar tanto la cantidad de iniciador y monómeros en disolución, como el tipo de entrecruzador a emplear [72]. Se ha observado que la relación molar entre dos entrecruzadores distintos, así como la relación entre el monómero funcional y el entrecruzador influyen de forma determinante en la morfología de las nanopartículas resultantes [52]. Del mismo modo, el tipo de *template*, así como la cantidad de éste, juegan un papel crucial en la homogeneidad en cuanto al tamaño de las nanopartículas. Cabe destacar el trabajo realizado por Chen *et al.* [53] en el que evaluaron las modificaciones en cuanto a la morfología y homogeneidad en el tamaño de las nanopartículas sintetizadas para el pesticida atrazina, al adicionar pequeñas cantidades de otro *template*, como el propranolol, en la etapa de síntesis. Otro ejemplo, lo constituye el descrito por Pardeshi *et al.* [73] en el que observaron como el hecho de añadir diferentes cantidades de tolueno al ACN, utilizado como porógeno en la síntesis, provocaba la modificación del tamaño de las nanopartículas

resultantes, aumentando el tamaño de partícula a medida que se añadía más tolueno a la mezcla para la polimerización. Este disolvente puede afectar a la superficie de las nanopartículas puesto que provoca un aumento del tamaño de poro y en consecuencia, el área superficial interna se ve incrementada [73, 74].

Habitualmente se obtienen partículas con un tamaño del orden de una micra. No obstante, en estudios en los que se utiliza el divinilbenceno como agente entrecruzador han llegado a obtenerse tamaños medios de 5 µm [66, 75-77].

La rapidez en la preparación junto con el mayor rendimiento (›85%) que ofrece la polimerización por precipitación frente a otras técnicas, hacen que ésta sea una alternativa muy atractiva para la preparación de MIN [78].

Polimerización por emulsión

Este tipo de polimerización tiene lugar cuando una mezcla de monómero entrecruzador, monómero funcional y *template* emulsiona en una fase acuosa gracias a la presencia de un compuesto surfactante. Este tipo de polimerización implica el uso de monómeros líquidos o disoluciones de éstos como fase dispersa. Con la aplicación de un estabilizante a la fase dispersa, como por ejemplo el tensioactivo aniónico dodecilsulfato sódico (SDS), se forman micelas donde queda contenido el monómero. Algunas micelas son activas, es decir, la reacción de polimerización tiene lugar en su interior, mientras que otras son inactivas constituyendo una fuente de monómero. A medida que cursa la reacción, las micelas inactivas suministran monómero a las activas, que crecen hasta formar el polímero sólido (figura 3.2) [79]. Este proceso se llama polimerización por mini-emulsión y da lugar a emulsiones estables que resultan en la formación de nanopartículas homogéneas con forma de gota y un tamaño comprendido entre los 50 nm y 1 µm de diámetro [56]. El tamaño de las gotas está determinado por la velocidad de agitación y la naturaleza y concentración del tensioactivo, mientras que la morfología de las partículas queda determinada principalmente por la solubilidad del monómero y del polímero dentro de las micelas.

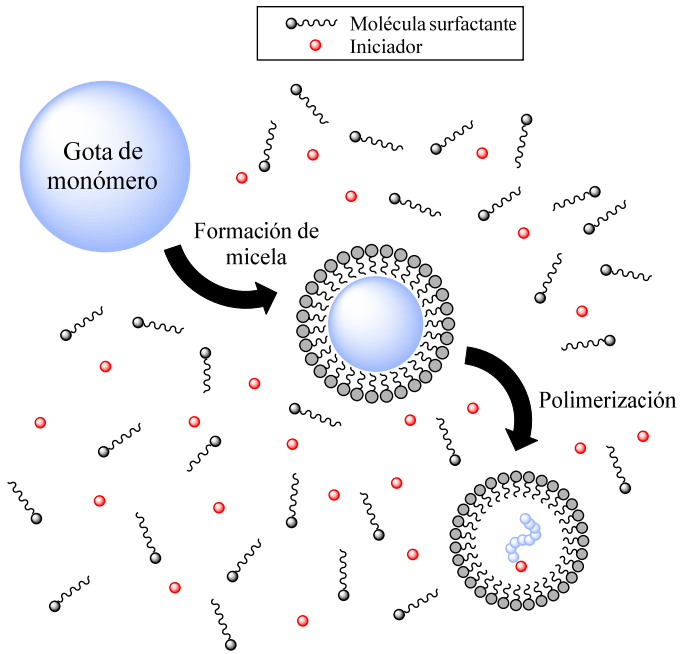

Figura 3.2. Representación esquemática del mecanismo de polimerización por emulsión.

Esta metodología presenta la desventaja de que el agua empleada como fase continua afecta de forma negativa a las interacciones monómero funcional-*template*. Además, estas interacciones pueden verse alteradas por la presencia del surfactante, lo que perjudica de forma significativa el proceso de impresión molecular [80]. Para solventar estos inconvenientes, se han sintetizado MIN monodispersas por polimerización por mini-emulsión en medio no acuoso en presencia de un emulsificante no iónico [80]. Esta metodología de síntesis de nanopartículas da lugar a mayores rendimientos en comparación con la síntesis convencional.

Una modificación de este tipo de polimerización consiste en la utilización de la técnica de impresión en superficie, que combina las ventajas del método semi-covalente junto con el método de síntesis por mini-emulsión, permitiendo obtener nanopartículas con elevada capacidad de unión. En este sentido, Curcio *et al*. proponen la unión covalente del *template* glucopiranosido al surfactante mediante un enlace

éster que actúa como separador, favoreciendo la estabilidad del complejo de prepolimerización (figura 3.3). La naturaleza del surfactante fuerza al *template* a posicionarse entre la fase acuosa y la orgánica, permitiendo que la impresión se produzca en la superficie de las partículas poliméricas, mejorando de forma notable las capacidades de unión de éstas [81].

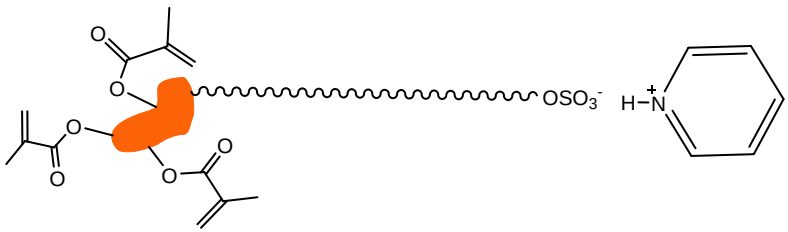

Template con el surfactante polimerizable

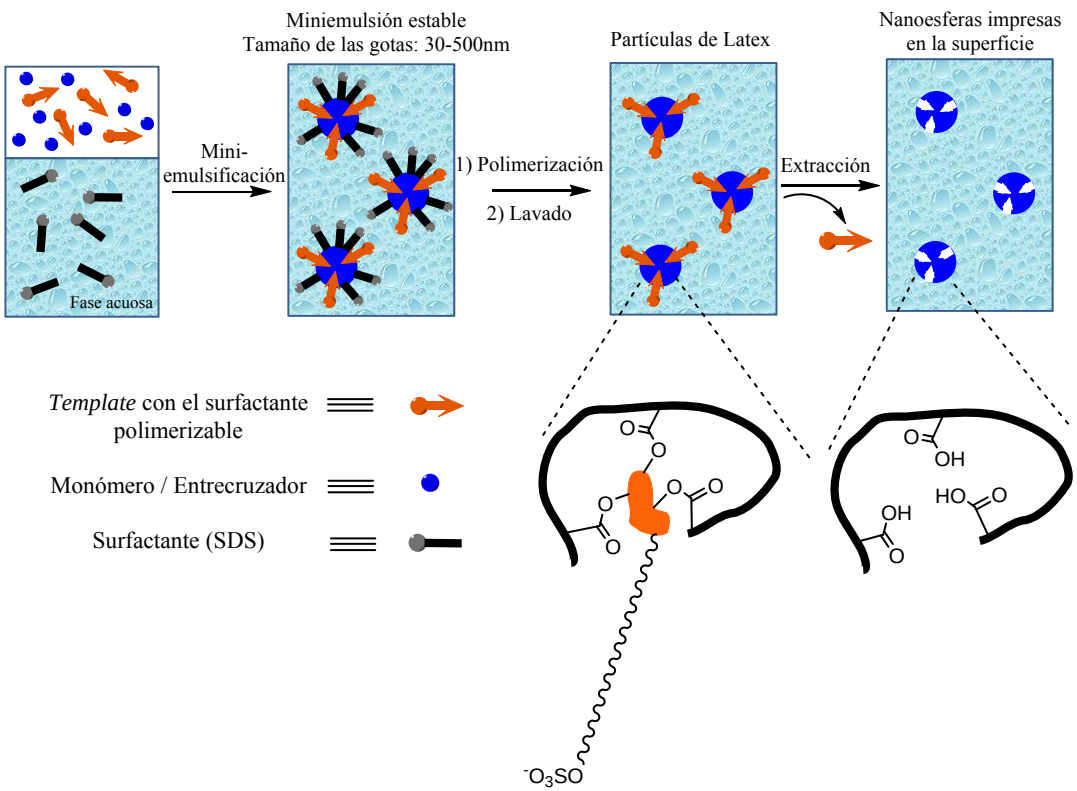

Figura 3.3. Representación esquemática de la técnica de impresión en superficie que combina el método semi-covalente junto con el método de síntesis por mini-emulsión. [81]

Ambas polimerizaciones, por precipitación y por mini-emulsión, pueden llevarse a cabo por **polimerización radical por desactivación reversible** (RDRP). Las RDRP, conocidas hasta la fecha como polimerizaciones radicales controladas o vivas, permiten controlar el peso molecular y la distribución y longitud de las cadenas poliméricas en crecimiento, dando lugar a polímeros más homogéneos que los obtenidos por la polimerización radical tradicional [82]. Entre estas polimerizaciones, aquellas mediadas por el uso de un *iniferter* (del inglés *ini*tiator-*transfer* agent-*ter*minator) permiten un mejor control sobre las cinéticas de reacción, ofreciendo la posibilidad de reiniciar la polimerización por exposición a radiación UV, polimerización en la que las propias nanopartículas actuarían como macroiniciadores [59].

Los *iniferters* [83] son iniciadores que al fragmentarse se descomponen en dos radicales, un radical activo capaz de iniciar la polimerización y otro, denominado durmiente, que favorece la recombinación entre radicales dando lugar a la finalización de la polimerización [84]. Uno de los *iniferter*s más utilizados para la elaboración de nanopartículas es el éster bencílico del ácido dietilditiocarbámico [59]. En este tipo de reacción, se utilizan tiempos de polimerización muy cortos para evitar la gelificación de la mezcla de polimerización, lo que da lugar a rendimientos muy bajos. El grupo de Piletsky *et al.* [59] mejoró el rendimiento, hasta valores del 14%, sin que se produjera el proceso de gelificación, mediante la adición de un agente de transferencia de cadena a la mezcla de polimerización y la disminución de la cantidad de *iniferter* [58].

La principal ventaja de este tipo de polimerización es que permite la elaboración de MIN para *templates* sensibles a la temperatura, puesto que estas polimerizaciones se inician por radiación UV. Además, se trabaja a temperaturas más bajas que en polimerizaciones térmicas, lo que resulta beneficioso para la formación del aducto de prepolimerización entre el monómero funcional y el *template*.

Síntesis en fase sólida

Aunque en 2006, Zourob *et al.* [85] desarrollaran un reactor automatizado para la obtención de partículas MIP para el fármaco propranolol, no fue hasta el 2013 cuando Poma *et al.* [62] desarrollaron el primer reactor automático utilizado para la síntesis de

nanopartículas mediante la técnica de síntesis en fase sólida. Esta técnica consiste en inmovilizar el template en una fase sólida (microesferas de vidrio de 75 µm de diámetro), que es empaquetada en una columna translúcida conectada a un sistema de bombeo que permite el paso de la mezcla para la polimerización. La etapa de síntesis polimérica tiene lugar fotoquímicamente irradiando la columna con luz UV en presencia de un iniferter. Esta técnica ha sido utilizada para sintetizar MIN para *templates* como la melamina [86], el antibiótico vancomicina [87], los fármacos diclofenaco [88] y propofol [89], histamina [90], enzimas como la tripsina [61], o algunos microorganismos [91].

Una vez obtenidas las nanopartículas, varias son las técnicas que se han llevado a cabo para la fabricación de electrodos potenciométricos basados en MIP [92]. Entre ellas, la más sencilla consiste en la elaboración de membranas de PVC con partículas MIP dispersas. En este procedimiento, se ha comprobado que la uniformidad de las partículas MIP es un aspecto crítico a tener en cuenta, puesto que aquellas membranas elaboradas con partículas homogéneas presentan mejores tiempos de respuesta que las preparadas con materiales irregulares [90, 93]. Este hecho puede ser atribuido a la mejora que conlleva el uso de materiales homogéneos en la dispersión del material en las membranas de PVC, lo que se traduce en una mayor accesibilidad a los sitios de unión [93].

2. Objetivos

La quiralidad es una propiedad inherente a los fármacos, que hace que ambas enantioformas presentes en un fármaco racémico, puedan presentar diferente comportamiento farmacocinético y farmacodinámico. El ahondar en el conocimiento del comportamiento farmacológico de cada una de las dos enantioformas, resulta beneficioso en cuanto a que puede lograrse la exposición al paciente a una menor dosis con el mismo efecto terapéutico y se pueden reducir las interacciones entre ambos enantiómeros y con otros fármacos. Este hecho, hace necesaria la monitorización del tratamiento farmacológico siendo indispensables técnicas analíticas específicas que permitan determinar de forma rápida y efectiva, la enantioforma activa del fármaco en muestras biológicas.

En este sentido el objetivo principal de este trabajo engloba el diseño de un sensor potenciométrico basado en nanopartículas molecularmente impresas que permita la determinación del enantiómero S del antidepresivo citalopram en muestras de orina.

Para alcanzar este objetivo principal, es necesario el cumplimiento de los siguientes objetivos metodológicos:

- Síntesis de nanopartículas impresas con el antidepresivo SCIT. Caracterización química y morfológica.
- Caracterización de la capacidad del polímero a partir de ensayos de unión ligando-receptor.
- Inmovilización de las nanopartículas en una membrana plástica de un cuerpo electródico y evaluación del dispositivo como transductor potenciométrico para la medida directa de S-citalopram en muestras de orina.
- Evaluación de la selectividad del sensor a partir del estudio de la especificidad en el reconocimiento del enantiómero de interés.

- Comprobación de la selectividad del sensor para el enantiómero objetivo, respecto de otros iones que pueden coexistir con éste en la matriz orina.

3. Material y equipamiento

En este apartado se detallará el material utilizado en la síntesis de las nanopartículas y la fabricación de la membrana potenciométrica, así como el equipamiento necesario para la caracterización del material polimérico y del sensor.

3.1. Reactivos y disoluciones

Los enantiómeros R y S del citalopram (RCIT y SCIT), fueron suministrados como oxalatos por Shanghai Peiyang Chemical Co., Ltd (Shanghai, China). A partir de oxalato de S citalopram, por extracción líquido-líquido, se obtuvo la forma neutra del fármaco, ya que para la síntesis del MIP se requería que el SCIT estuviera en su forma no ionizada. A tal efecto, se disolvió 1 g de oxalato de SCIT en 50 mL de agua milli-Q trasvasándose posteriormente a un embudo de decantación. Seguidamente, se adicionaron 100 mL de carbonato sódico 0.5 M, 10 mL de cloruro sódico saturado y 100 mL de diclorometano como fase extractante. Tras agitación y decantación, la fase orgánica fue separada y evaporada en un rotavapor obteniéndose un producto oleoso que fue almacenado en refrigeración y bajo atmósfera inerte.

El monómero funcional ácido itacónico de pureza $\geq$ 99% (IA), el entrecruzador etilen glicol dimetacrilato al 98% (EDMA), así como la benzofenona (99%) utilizada como iniciador fotoquímico, se obtuvieron de Sigma-Aldrich (Madrid, España). De la misma casa comercial, se adquirieron los distintos componentes de la membrana como el policloruro de vinilo (PVC), dioctil ftalato (DOP), dibutil ftalato (DBP), bis (2-etilhexil) sebacato (BEHS) y 2-nitrofenil octil éter (NPOE). Los disolventes acetonitrilo (ACN) y tetrahidrofurano (THF) fueron suministrados por Scharlab (Barcelona, España), ambos de calidad para HPLC.

Para la elaboración de los medios tamponados, el acetato de sodio trihidratado, el ácido acético, el hidrogenofosfato de disodio anhidro y el dihidrogenofosfato de sodio monohidratado fueron adquiridos a través de Merck (Madrid, España). Para las disoluciones se empleó agua ultrapura desmineralizada mediante ósmosis inversa en

un sistema Elix20 de Millipore (Bedford, EE.UU.) y purificada con un sistema de filtración Milli-Q de la misma casa comercial.

3.2. Equipamiento

Previamente a la síntesis de las nanopartículas y para la selección del monómero funcional, se realizó una simulación computacional de las interacciones monómero-template. Para ello se utilizó un sistema operativo CentOS 5 de GNU/Linux el cual controlaba la ejecución del software orientado a la química computacional SYBYL 7.0 TM (Tripos Inc., St. Louis, Missouri, USA). Con el fin de evaluar la energía de enlace entre cada uno de los monómeros estudiados y la molécula *template,* se partió de una librería virtual, con 22 monómeros de distinta funcionalidad, comúnmente utilizados en impresión molecular. Se incluyeron monómeros ácidos, básicos y neutros capaces de formar enlaces por fuerzas electrostáticas, uniones por formación de puentes de hidrógeno, fuerzas de Van der Waals y/o dipolo/dipolo con el enantiómero objetivo. Para la selección de los monómeros funcionales capaces de formar los complejos más estables con la molécula objetivo se utilizó el algoritmo Leapfrog®, que permite evaluar las posibles estructuras de ligandos en base a sus energías de enlace con un determinado compuesto. Éstas son calculadas empleando repetidamente distintos ligandos en distintas posiciones del *template* a modo de barrido estérico o electrostático. Los ligandos, subestructuras y energías de enlace, se almacenan en una base de datos que sirve como plataforma para lanzar nuevas evaluaciones. Los monómeros que presentaron una menor energía de enlace y una mayor enantioselectividad fueron utilizados en el proceso posterior de síntesis del polímero.

3.2.1. Síntesis y caracterización de las nanopartículas molecularmente impresas

La síntesis polimérica se llevó a cabo por radiación UV con una lámpara modelo UVACube 100 de la casa comercial Dr. Hönle (Gräfelfing, Alemania). Después de la polimerización, las nanopartículas fueron centrifugadas a una temperatura de 20ºC en una centrifuga modelo Allegra X-15R de la casa Beckman Coulter (Brea, U.S.A).

La caracterización morfológica y química de las nanopartículas se llevó a cabo por Microscopía Electrónica de Barrido (SEM) y Espectroscopia Infrarroja con Transformada de Fourier (FTIR). Las imágenes SEM se realizaron utilizando un microscopio electrónico de barrido modelo JSM-7000F de JEOL (Tokio, Japón) con una resolución de 1.2 nm y a 30 kV. Por otro lado, los análisis IR se llevaron a cabo en un equipo FTIR modelo 6300 de Jasco (Tokio, Japón) provisto de un módulo de reflectancia total atenuada (ATR) de la casa comercial Pike (Madison, EE.UU.) y equipado con un cristal de diamante.

En los ensayos de unión las medidas para la determinación de S citalopram libre, se realizaron por cromatografía líquida. Para ello, se utilizó un cromatógrafo de líquidos de la serie 1100 de Agilent Technologies (Palo Alto, EE.UU.) provisto de una bomba cuaternaria, un desgasificador de vacío en línea, un inyector automático y un detector de fluorescencia. El control del sistema y el análisis de datos se llevaron a cabo a través del software Agilent LC ChemStation (Agilent Technologies, EE.UU.). Para la separación cromatográfica, se utilizó una columna ZORBAX Eclipse XDB-C18 (4.6 x 150 mm, 5µm) también de la casa Agilent. Se trabajó en modo isocrático a un flujo de 1 mL/min empleando como fase móvil una mezcla 70:30 de tampón fosfato 40 mM, ajustada a pH 4, y acetonitrilo como modificador orgánico. Para las medidas de fluorescencia se seleccionó 240 nm como longitud de onda de excitación y 308 nm como la de emisión.

3.2.2. Medidas potenciométricas

Las nanopartículas impresas fueron inmovilizadas en una membrana plástica, que fue colocada en un cuerpo electródico adquirido en Sigma-Aldrich (Madrid, España). Para las medidas de potencial se utilizó un milivoltímetro de MeterLab (Radiometer, Dinamarca) modelo PHM220. Las medidas se realizaron bajo agitación constante y a temperatura ambiente, utilizando un electrodo de referencia Ag/AgCl modelo 5241 suministrado por la casa comercial Crison (Barcelona, España).

La celda potenciométrica empleada puede esquematizarse tal y como se detalla a continuación:

Ag/AgCl(s), KCl (3M) // disolución de medida/membrana MIP/AgCl(s), SCIT (10^{-5}M) /Ag.

3.3. Muestras de orina

Las muestras de orina se obtuvieron de un voluntario en tratamiento diario con el medicamento Esertia®, que contiene una dosis de 10 mg de SCIT por comprimido. Estas muestras fueron recogidas en contenedores estériles suministrados por Deltalab (Barcelona, España) a diferentes horas tras la ingesta del fármaco. Todas ellas fueron almacenadas en congelación a -42 ºC hasta su medida analítica. Las muestras de orina control fueron recogidas del mismo individuo antes de que comenzara el tratamiento. Con anterioridad a la medida, todas las muestras fueron filtradas a través de un filtro de polifluoruro de vinilideno (PVDF) de 0.22 µm de diámetro de poro, Millipore (Bedford, EE.UU.).

4. Desarrollo de nanopartículas impresas para el enantiómero S del antidepresivo citalopram

Entre las diferentes estrategias que se pueden llevar a cabo para la elaboración de nanopartículas MIP homogéneas, se seleccionó la polimerización por precipitación por ser la metodología que da lugar, de una forma rápida, sencilla y económica, a partículas esféricas monodispersas con elevado rendimiento y pureza [60] y con tamaños que varían desde los nanómetros hasta diámetros comprendidos entre 1 y 3 micrómetros. [94, 95].

4.1. Diseño, síntesis y optimización

4.1.1. Selección del monómero funcional

En base a los resultados obtenidos en la simulación computacional para las interacciones entre distintos monómeros y el *template* se seleccionó el ácido itacónico como monómero funcional, ya que tal y como se muestra en la tabla 3.2, resultaba ser el monómero que formaba complejos más estables con el enantiómero S del citalopram y no formaba conjugados tan estables con el enantiómero R.

Tabla 3.2. Energías de unión de los monómeros funcionales que dan lugar a los conjugados más estables con los enantiómeros S y R citalopram como iones monovalentes y el grupo funcional del fármaco al que se une preferentemente el monómero funcional.

Energías de Unión (Kcal/mol)	
SCIT	RCIT
Ácido Itacónico (-28.26)	Bisacrilamida (-27.88)
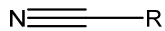	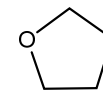
Acrilamida (-24.48)	Acrilamida (-26.62)
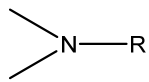	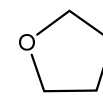
Bisacrilamida (-23.75)	Alilamina (-23.68)
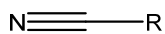	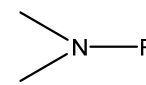
Alilamina (-22.57)	EGMP (-22.45)
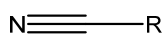	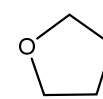
EGMP (-18.71)	TFMAA (-20.29)
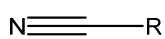	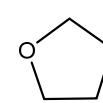

EGMP: Etilenglicol metacrilato fosfato, **TFMAA:** Ácido 2-(trifluorometil) acrílico

4.1.2. Selección del medio de polimerización

La selección del medio de polimerización es uno de los parámetros clave a optimizar en la polimerización por precipitación. Para que se produzca la precipitación, el medio seleccionado debe ser un mal disolvente para las cadenas poliméricas resultantes. La mejor forma de establecer la solubilidad del polímero en el medio es mediante el estudio de los parámetros de solubilidad.

Para sustancias de bajos pesos moleculares como es el caso de los disolventes, los parámetros de solubilidad pueden calcularse de forma sencilla a través de la entalpía de vaporización, la cual se obtiene mediante los datos resultantes de la medida de la presión de vapor a diferentes temperaturas o a partir de las medidas de la capacidad calorífica en función de la temperatura [96]. No obstante, existen muchas referencias bibliográficas que recogen estos parámetros para un amplio grupo de disolventes [68, 69, 97]. Los parámetros de solubilidad para los disolventes comúnmente utilizados en la elaboración de polímeros vienen recogidos en la tabla 3.3. Por el contrario, obtener los parámetros de solubilidad de materiales como los polímeros con elevados pesos moleculares es extremadamente complejo debido a que la entalpía de vaporización o el punto de ebullición no son parámetros que se puedan medir en estos materiales, ya que se degradan antes de llegar a vaporizarse [96]. Por ello, se han desarrollado metodologías indirectas como la medida del grado de hinchamiento de un polímero en diferentes disolventes o la medida de la viscosidad intrínseca para poder calcular los distintos parámetros de solubilidad. No obstante, ante la complejidad de estos procesos, se suelen seleccionar los disolventes en base al parámetro de solubilidad total, o parámetro de solubilidad de Hildebrand.

Tabla 3.3. Parámetros de solubilidad para algunos de los disolventes más utilizados.

Disolventes	δ (MPa)$^{1/2}$	δ_d (MPa)$^{1/2}$	δ_p (MPa)$^{1/2}$	δ_h (MPa)$^{1/2}$
Acetona	19.9	15.5	10.4	7.0
Acetonitrilo	24.4	15.3	18.0	6.1
Benceno	18.5	18.4	0.0	2.0
Cloroformo	18.9	17.8	3.1	5.7
Ciclohexano	16.8	16.8	0.0	0.2
Diclorometano	20.2	18.2	6.3	6.0
Dimetilsulfóxido	26.7	18.4	16.4	10.2
Etanol	26.5	15.8	8.8	19.4
Heptano	15.3	15.3	0.0	0.0
Hexano	14.9	14.9	0.0	0.0
Metanol	29.4	14.7	12.3	22.3
N,N-Dimetilformamida	24.9	17.4	13.7	11.3
2-Propanol	23.6	15.8	6.1	16.4
Tetrahidrofurano	19.5	16.8	5.7	8.0
Tolueno	18.2	18.0	1.4	2.0

δ: parámetro de solubilidad de Hildebrand, **δ_d**: parámetro de solubilidad basado en las fuerzas de dispersión, **δ_p**: parámetro de solubilidad basado en las fuerzas producidas por las interacciones dipolo-dipolo y **δ_h**: parámetro de solubilidad basado en las interacciones por formación de puentes de hidrógeno.

Partiendo de esta premisa, habitualmente se selecciona como medio de polimerización, aquel disolvente cuyo parámetro de solubilidad (δ) no diste en más de 3-5 MPa$^{1/2}$ [52] respecto al del monómero que se encuentra en mayor proporción en la mezcla de polimerización, en este caso el entrecruzador EDMA (δ=18.6 MPa$^{1/2}$). Entre los disolventes que presentan un valor de δ próximo al del EDMA, el tolueno,

diclorometano (DCM) y cloroformo (CF) son los disolventes que se consideran más adecuados para la impresión molecular debido a sus bajas permitividades relativas (constante dieléctrica) que permiten que las interacciones no covalentes entre monómero y *template* sean más fuertes que las que se producen en disolventes polares [98-100]. Otro disolvente que es comúnmente utilizado en la síntesis de MIP es el acetonitrilo, su interés radica en que, al igual que el tolueno o el cloroformo, es un disolvente aprótico y por ello no inhibe los enlaces por puentes de hidrógeno entre monómeros y *template* [101]. Este disolvente no presenta un parámetro de solubilidad en el intervalo recomendable, sin embargo, tal y como se aprecia en la tabla 3.4, es un disolvente comúnmente utilizado en polimerizaciones por precipitación para la síntesis de MIP en las que el EDMA resulta ser el monómero entrecruzador.

Tabla 3.4. Resumen de las condiciones de polimerización de MIP sintetizados por polimerización por precipitación utilizando como monómero entrecruzador EDMA.

Medio de polimerización	*Template*	Monómero funcional	Iniciador	Referencia	Año
ACN	2,6-diclorofenol	MAA	AIBN	Wei X. *et al.* [102]	2015
ACN : DMSO (1 :1.5 v/v)	Ácido t,t-mucónico y 1, 2, 4-tri-hidroxibenceno	MAA	AIBN	Chauhan A. *et al.* [103]	2015
ACN, Tolueno , CF	Tramadol	MAA	AIBN	Seifi M. *et al.* [54]	2014
ACN	Vanilina	MAA	AIBN	Su L. *et al.* [104]	2014
CF	Haloperidol	MAA	AIBN	Ebrahimzadeh H. *et al.* [105]	2013
MeOH	Cloruro de rodio (III)	ANA	AIBN	Yang B. *et al.* [106]	2013
ACN: DMSO (2:1 v/v)	Nitrato de cesio	MAA	AIBN	Shamsipur M. *et al.* [107]	2013
DCM	Rodamina B	AA	AIBN	Ma Y *et al.* [108]	2013
MeOH: Agua (4:1 v/v)	Ácido 2,4-di-clorofenoxiacético	4-VP	AIBN	Cao H. *et al.* [109]	2013
Tolueno: ACN (1:1 v/v)	Mezcla de fármacos ácidos	2-VP	AIBN	Dai C.M. *et al.* [110]	2012
ACN	Carbofurano	AA	AIBN	Ge S. *et al.* [111]	2012
ACN	Verde de malaquita	AA	AIBN	Liu H. *et al.* [112]	2012
ACN	Sulfametazina	MAA	AIBN	Chen C. *et al.* [113]	2012

Continuación tabla 3.4. Resumen de las condiciones de polimerización de MIP sintetizados por polimerización por precipitación utilizando como monómero entrecruzador EDMA.

Medio de polimerización	*Template*	Monómero funcional	Iniciador	Referencia	Año
Tolueno	2-(3,4-dimetoxifenil) etilamina	MAA	1,1´-azobis (ciclohexanocarbonitrilo)	Lulinski P. *et al.* [114]	2012
ACN: MeOH (1:1 v/v)	Quercetina	MAA	AIBN	Curcio M. *et al.* [115]	2012
Acetona	Quercetina	AA	AIBN	Qiu H. *et al.* [116]	2012
ACN : Tolueno (1:3 v/v)	(D)-naproxeno	MAA	AIBN	Jiang X. *et al.* [117]	2012
ACN	Gatifloxacina	MAA	AIBN	Shi Y. *et al.* [67]	2012
Tolueno	Diclofenaco	2-VP	AIBN	Dai C.M. *et al.* [118]	2011
CF : MeOH (3:1 v/v)	Ácido oleanólico	AA	AIBN	Zhang W. *et al.* [119]	2011
ACN	Ácido salvianolico	AA	AIBN	Zhu L. *et al.* [120]	2011
ACN	Atrazina	MAA	AIBN	Xu S. *et al.* [121]	2011
ACN	Fluoroquinolonas	MAA+ HEMA	AIBN	Rodriguez E. *et al.* [122]	2011
MeOH	Ciprofloxacino	MAA	AIBN	Prierto A. *et al.* [123]	2011
ACN	Nitrato de cobre (II)	AQ	AIBN	Shamsipur M. *et al.* [124]	2010
ACN : Tolueno (3:1 v/v)	Triazofos	AA	AIBN	Xie C. *et al.* [125]	2010
ACN	dexametasona-21 fosfato disódico	HEMA+DEAEMA	DMDPL	Wang C. *et al.* [126]	2010
ACN	Colorante	4-VP	AIBN	Long C. *et al.* [127]	2009
Aceite mineral : Tolueno (2:3 v/v)	Bisfenol A	4-VP	AIBN	Jiang M. *et al.* [128]	2009
ACN	17β-estradiol	MAA	AIBN	Nemulenzi O. *et al.* [129]	2009
MeOH	Complejo entre z-histidina y acetato de cobalto	4-VP	AIBN	Chaitidou S. *et al.* [130]	2009
ACN: Tolueno (3:1 v/v)	Tiabendazol	MAA	AIBN	Cacho C. *et al.* [131]	2009
ACN	Verde de Malaquita	MAA	AIBN	Long C. *et al.* [132]	2009

Continuación tabla 3.4. Resumen de las condiciones de polimerización de MIP sintetizados por polimerización por precipitación utilizando como monómero entrecruzador EDMA.

Medio de polimerización	*Template*	Monómero funcional	Iniciador	Referencia	Año
Agua: ACN (1:19 v/v)	Cetirizina dihidrocloruro	MAA	AIBN	Javanbakht M. *et al.* [133]	2008
ACN	Carbaril	MAA	AIBN	Yao W. *et al.* [134]	2008
CF	Hidroxicina dihidrocloruro	MAA	AIBN	Javanbakht M. *et al.* [135]	2008
DCM o MeOH	Ciprofloxacino	MAA	AIBN	Turiel E. *et al.* [136]	2007
Tolueno	Propazina monometacrilato	-	AIBN	Cacho C. *et al.* [137]	2006
Tolueno	Propazina	MAA	AIBN	Carabias-Martinez R. *et al.* [138]	2005
2 metoxietanol	Complejo del ion paladio (II) con aminoquinolina	4-VP + HEMA	AIBN	Daniel S. *et al.* [139]	2005
ACN: Tolueno (3.5:1 v/v)	Sulfasalazina	MAA	AIBN	Puoci F. *et al.* [140]	2004

MAA: ácido metacrílico, **ANA**: ácido 2-(aliltio) nicotínico, **4-VP:** 4-vinilpiridina, **2-VP:** 2-vinilpiridina, **AA:** acrilamida, **AQ:** 1-hidroxi-4-(prop-2'-eniloxi)-9,10 antraquinona, **HEMA:** poli-hidroxietilmetacrilato, **DEAEMA**: 2-(dietilamino) etil metacrilato, **AIBN:** azobisisobutironitrilo y **DMDPL:** 2,2-Dimetoxi-1,2-difeniletan-1-ona.

Los disolventes cloroformo, tolueno y diclorometano no fueron considerados debido a la baja solubilidad que presentaba en ellos el monómero funcional ácido itacónico. Se seleccionó ACN, ya que además de ser habitualmente utilizado en este tipo de polimerizaciones (tabla 3.4), existe evidencia de su efectividad a la hora de obtener partículas esféricas y homogéneas [52, 67, 72]. Las mezclas entre ACN y otros disolventes como tolueno, cloroformo o tetrahidrofurano fueron descartadas ya que la adición de estos disolventes favorecía la solubilidad del polímero en el medio, lo que, en algunos casos, se traducía en un aumento del tamaño de poro, y por consiguiente, en un indeseado aumento del tamaño de partícula [65, 66, 76].

4.1.3. Síntesis de nanopartículas impresas

La síntesis por polimerización por precipitación fue realizada en un vial de vidrio borosilicatado de 40 mL. Para ello, fueron disueltos 0.033 g de SCIT, 0.049 g de IA, 0.450 g de EDMA y 0.010 g de benzofenona en 30 mL de acetonitrilo previamente desgasificado. La relación *template*: monómero funcional: entrecruzador fue 1:4:24. Una vez disueltos todos los componentes, la mezcla para la polimerización fue desoxigenada con una corriente de gas nitrógeno de elevada pureza durante 3 minutos, con la finalidad de evitar la inhibición de los radicales provenientes de la fotólisis del iniciador. A continuación, la mezcla fue sometida a radiación UV durante 3 horas. Para eliminar los posibles restos de monómeros que no hubieran reaccionado en la etapa de polimerización, las nanopartículas resultantes se sometieron a un proceso de lavado por centrifugación. Se realizaron 3 ciclos de centrifugado con 30 mL de acetonitrilo a 8000 rpm durante 10 min a 20ºC.

Las nanopartículas no impresas (NIN) fueron sintetizadas en las mismas condiciones que las molecularmente impresas pero en ausencia del *template* (SCIT) en la mezcla de polimerización.

Es importante destacar que para la medida del potencial de membrana no es necesario realizar una etapa de extracción o lavado del *template*. Esto supone un beneficio debido a que la etapa de eliminación del analito plantilla para liberar los sitios de unión, suele conllevar cierta pérdida de sensibilidad del material [141].

4.1.4. Optimización de las condiciones de polimerización

El efecto del porcentaje de monómeros, el porcentaje de iniciador, el tiempo de polimerización, así como su curso bajo agitación, fueron evaluados con la finalidad de determinar aquellas condiciones de polimerización que dieran lugar a nanopartículas con el tamaño y la uniformidad deseada. Para ello, se llevó a cabo la síntesis de distintas series de MIN variando en cada serie el valor de un único parámetro. Las nanopartículas obtenidas en cada caso fueron examinadas por microscopía

electrónica de barrido, obteniendo de este modo información visual sobre su tamaño y homogeneidad.

En primer lugar, se sintetizaron una serie de MIN empleando tres porcentajes de monómeros: 2%, 4% y 6% (w/w) respecto al disolvente. Por otro lado, se evaluó el efecto del porcentaje de iniciador empleando porcentajes del mismo comprendidos entre 0.5 y 6% (0.5%; 1%, 2%, 4% y 6%) (w/w) respecto al peso de monómeros. En lo referente al tiempo de polimerización, se sintetizaron MIN manteniendo la mezcla de polimerización bajo radiación UV durante 3 h, 6 h y 9 h con el fin de determinar el tiempo adecuado de síntesis. Finalmente, se evaluó el efecto de la agitación de la mezcla en el transcurso de la polimerización, para ello, se sintetizaron las nanopartículas tanto en ausencia de agitación como a dos velocidades (100 y 500 rpm).

Tal y como se aprecia en la figura 3.4, para el estudio del **efecto del porcentaje de monómeros**, se observó que un aumento en la cantidad de monómeros en la disolución, favorecía la agrupación de las nanopartículas dando lugar a la formación de aglomerados y por ello, a una mayor irregularidad en las partículas. Por este motivo se seleccionó como óptimo el valor de un 2% (w/w) de monómeros respecto al disolvente.

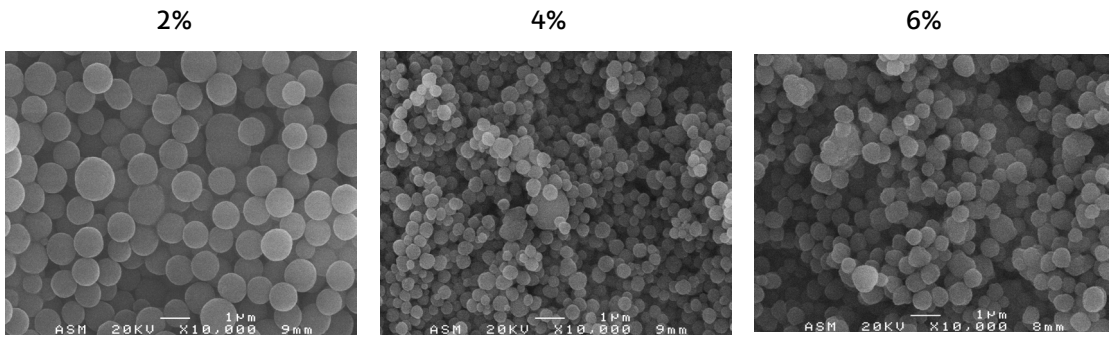

Figura 3.4. Imágenes SEM obtenidas en la serie de MIN sintetizadas para tres porcentajes distintos de monómeros: 2%, 4% y 6% (w/w) respecto al disolvente.

En una segunda serie realizada para evaluar el **efecto del porcentaje de iniciador,** no se apreciaron diferencias significativas en cuanto al tamaño de partícula obtenido. Sin embargo, se puede apreciar (figura 3.5) un ligero aumento en el tamaño de partícula a medida que el porcentaje de iniciador se incrementaba y cómo para

porcentajes menores (0.5% o 1%) se observaba una mayor irregularidad en los tamaños de las partículas. Por este motivo, y a fin de obtener los tamaños más pequeños y con mayor regularidad, se seleccionó un 2% de iniciador (w/w) respecto al porcentaje de monómeros como el valor óptimo para la etapa de polimerización.

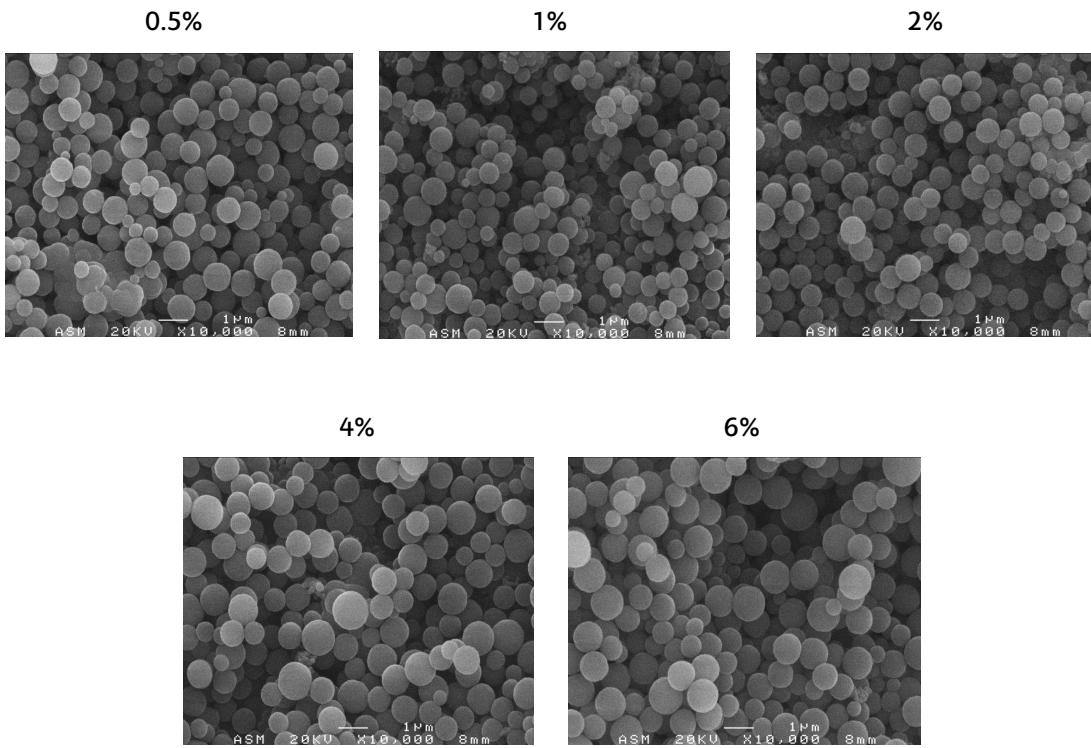

Figura 3.5. Imágenes SEM obtenidas en la serie de MIN sintetizadas para diferentes porcentajes de iniciador (0.5%, 1%, 2%, 4% y 6% (w/w)) respecto al peso de monómeros.

A continuación fue estudiado el **efecto del tiempo de polimerización** (figura 3.6). Se pudo apreciar como 3 horas era un tiempo suficiente para la polimerización, y que el hecho de aumentar dicho tiempo no suponía un cambio significativo en el tamaño de las nanopartículas. A fin de reducir el tiempo requerido en la etapa de síntesis y evitar la formación de acúmulos que pueden generarse en algunas ocasiones por tiempos elevados de polimerización [65], se seleccionó el tiempo de 3 horas.

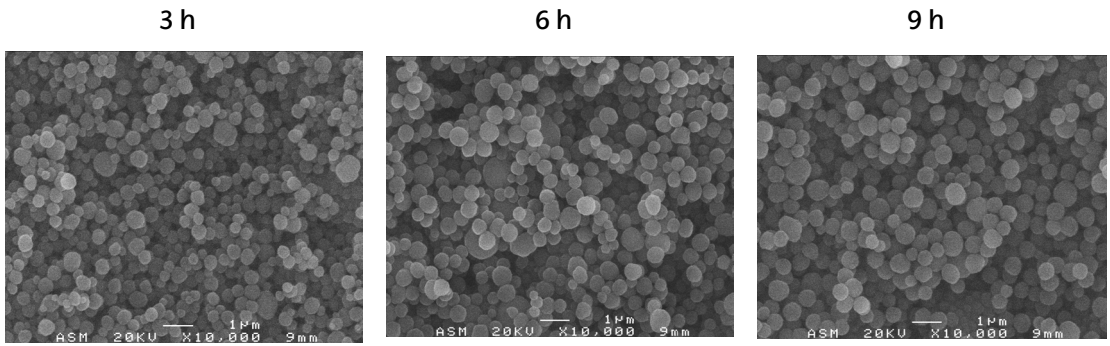

Figura 3.6. Imágenes SEM obtenidas en la serie de MIN sintetizadas a diferentes tiempos de polimerización, 3 h, 6 h y 9 h.

Finalmente, se realizó una última serie de MIN para evaluar el **efecto de la agitación** en el tamaño y forma de las nanopartículas ya que se ha demostrado en otros estudios la relación entre la agitación y la monodispersidad de las partículas [52, 142]. En esta ocasión no se apreciaron diferencias significativas entre ambas síntesis (figura 3.7), por lo que se decidió llevar a cabo la polimerización en ausencia de agitación debido a la mayor simplicidad del proceso.

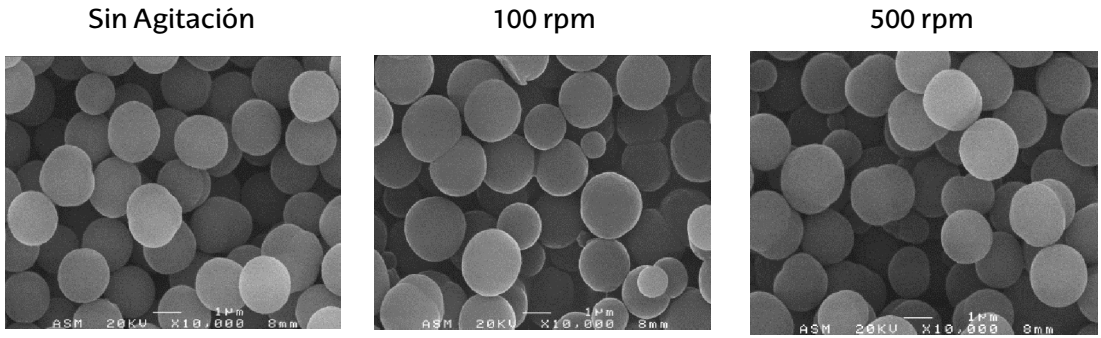

Figura 3.7. Imágenes SEM obtenidas en la serie de MIN sintetizadas en ausencia de agitación, a 100 rpm y a 500 rpm.

Cabe destacar que, en todas las series realizadas, el tamaño de partícula varió desde unos cientos de nanómetros hasta la obtención de tamaños de partícula comprendidos entre una y dos micras. A modo resumen, la tabla 3.5 recoge los valores

seleccionados como óptimos, para los parámetros que influyen en la síntesis de las nanopartículas impresas (MIN) por polimerización por precipitación.

Tabla 3.5. Condiciones para la síntesis de MIN por polimerización por precipitación.

Condiciones finales
2 % (en peso) de monómeros en la mezcla de polimerización
2 % de iniciador respecto al peso de monómeros.
3 horas de polimerización
Sin agitación

4.2. Caracterización de las nanopartículas impresas

4.2.1. Caracterización química por Espectroscopía Infrarroja con Transformada de Fourier (FTIR)

Mediante Espectroscopía Infrarroja con Transformada de Fourier (FTIR) se puede obtener el espectro vibracional de una molécula, el cual es considerado como una propiedad física única y característica de ésta. Es por ello que un espectro infrarrojo puede ser considerado como una huella dactilar para la identificación de una molécula desconocida mediante comparativa con un espectro de referencia previamente registrado [143].

Esta técnica es comúnmente utilizada en la caracterización de polímeros [144-146] puesto que, además de su utilidad en la determinación de la composición mediante la identificación de grupos funcionales, permite determinar los cambios estructurales de la muestra debidos a esfuerzos extremos, microdefectos, impurezas, recubrimientos, etc., permitiendo de ese modo monitorizar los procesos de polimerización y los de degradación [144]. En el caso de los MIP, los espectros FTIR permiten obtener información cuantitativa sobre la composición del polímero, esto es posible en los casos en los que las variaciones químicas del material, por ejemplo

debidas a distintas proporciones entre el monómero funcional y el entrecruzador, proporcionen bandas que no estén solapadas entre sí. Asimismo, a través de esta técnica puede comprobarse la existencia de interacciones no covalentes monómero-*template*, tales como los enlaces por puentes de hidrógeno [147].

El espectro IR se obtiene como consecuencia de la absorción de radiación infrarroja por parte de cada tipo de enlace. Esta absorción se produce a una frecuencia distinta según la vibración específica de los enlaces químicos, permitiendo de ese modo determinar qué tipo de grupos funcionales posee la molécula objeto de estudio. La zona del espectro de infrarrojo de mayor interés analítico es la que se corresponde con el infrarrojo medio en el espectro electromagnético (intervalo entre 4000 y 400 cm^{-1}).

En función de la estructura espacial de la molécula y el número de átomos, la vibración que se produzca será diferente. En general, se puede considerar que hay dos tipos de vibraciones [148]:

- **Vibración de tensión** (*stretching*). Ocurre en átomos unidos por enlaces simples, dobles o triples cuando se acercan y alejan siguiendo la dirección del enlace. A su vez, esta vibración puede ser simétrica o asimétrica.
- **Vibración de flexión** (*bending*). En este tipo de vibración, los átomos vibran de modo que varían los ángulos, pero no las longitudes de enlace.

El espectrómetro FTIR ha ido evolucionando con el acoplamiento de accesorios para la medida de la reflexión total atenuada (ATR) [149]. El ATR en el espectrofotómetro de IR permite poner en contacto la muestra con un cristal ópticamente denso (prisma de diamante o ZnSe) de elevado índice de refracción, posibilitando la medida de los cambios que se producen en un ambiente de reflexión interna total. La reflexión es producida cuando un haz de radiación pasa de un medio más denso a uno menos denso. Esta radiación es dirigida al borde biselado del prisma mediante un conjunto de espejos en los que se va reflejando sucesivamente con cierto ángulo hasta alcanzar el detector (figura 3.8). A pesar de que la reflexión interna se produce en el interfaz prisma-aire, la radiación penetra en la superficie de la muestra

que está colocada en la parte superior del prisma, absorbiendo cierta energía y dando lugar a un espectro de absorbancia [150].

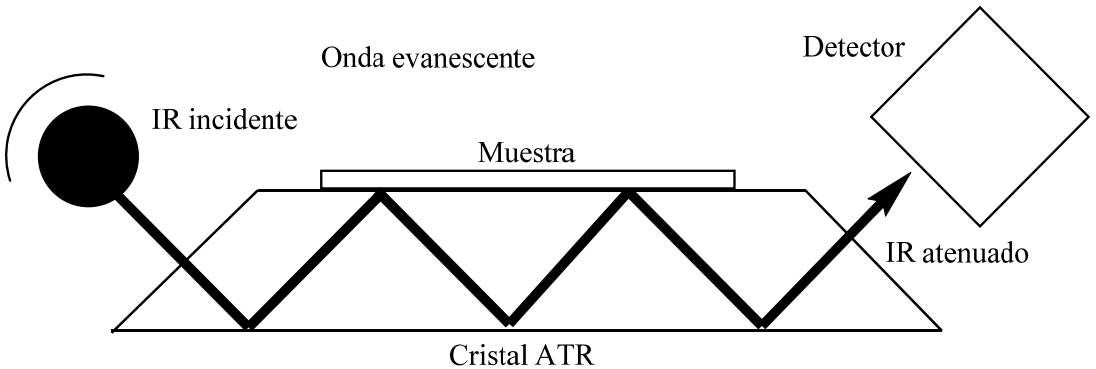

Figura 3.8. Esquema del proceso de reflectancia total atenuada.

En este estudio, la espectroscopia FTIR/ATR fue utilizada para la elucidación de grupos funcionales específicos presentes en el compuesto y característicos de los monómeros funcional y entrecruzador utilizados en la etapa de polimerización, permitiendo de este modo caracterizar y confirmar la correcta síntesis de los materiales objeto de estudio.

Con el objetivo de obtener los espectros IR característicos de las nanopartículas MIP y NIP, se analizó el material de forma directa colocándolo sobre el cristal ATR del equipo de medida. Para ello, previamente, el material fue secado al vacío durante 48 horas en un desecador a temperatura ambiente.

En la figura 3.9 se muestra el espectro IR para el compuesto SCIT. La banda a 2934 cm^{-1} podría atribuirse a la vibración de tensión del enlace C-H, mientras que las bandas entre 2851 y 2760 cm^{-1} podrían ser correspondientes a la vibración de este mismo enlace cuando el carbono está unido, además, a un átomo de nitrógeno, lo que podría atribuirse a los grupos metilo de la amina terciaria del compuesto. La presencia de anillos aromáticos en la molécula puede deducirse, por un lado, por la presencia de la banda a 3055 cm^{-1} propia de la vibración de tensión del enlace =C-H. Por otro lado, las bandas debidas a los armónicos y combinados, que aparecen en el intervalo 2018 -

1771 cm^{-1}, así como las vibraciones de tensión del enlace C-C del anillo aromático, a 1597 y 1505 cm^{-1}, confirmarían la aromaticidad de la molécula. A 2228 cm^{-1}, puede apreciarse una banda intensa aislada correspondiente a la vibración de tensión del grupo -CΞN- del SCIT, al estar unido a un anillo aromático, este grupo nitrilo aparece desplazado de sus frecuencias habituales (2260-2240 cm^{-1}). A 1223 cm^{-1} puede apreciarse una banda intensa atribuible a la vibración de tensión del enlace -C-N-. Por último, las bandas a 1032 cm^{-1} y 733 cm^{-1}, podrían atribuirse al enlace C-F de la molécula.

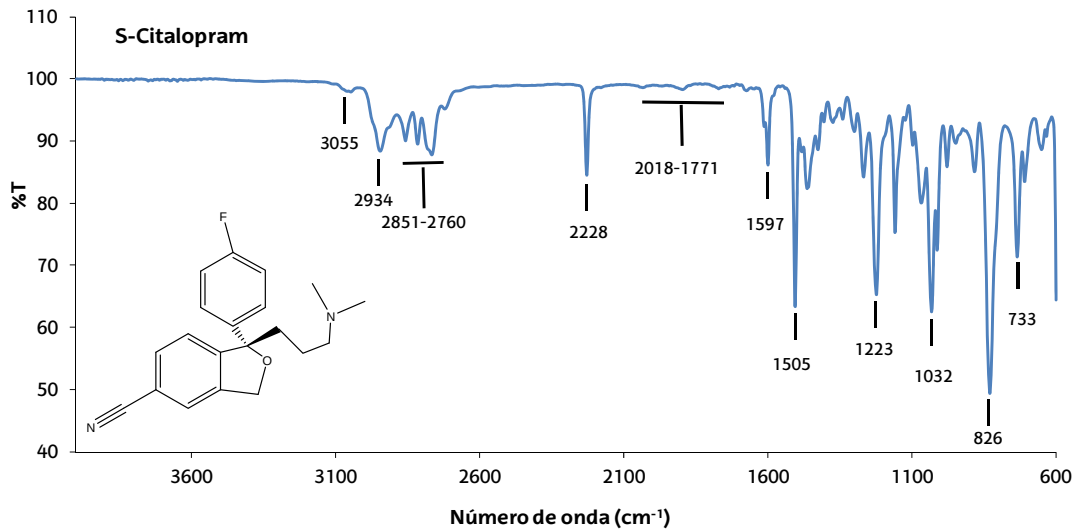

Figura 3.9. Espectro IR correspondiente a la molécula SCIT

Los espectros obtenidos analizando las nanopartículas molecularmente impresas (MIN) y las no impresas (NIN) (figura 3.10) fueron prácticamente idénticos, a excepción de una pequeña banda a 2228 cm^{-1} que puede asignarse a vibraciones de tensión correspondientes al grupo nitrilo del SCIT, confirmando la existencia de éste en las cavidades impresas de las MIN. Esta banda se puede apreciar de forma muy intensa en el espectro del SCIT. Como cabía esperar, dado que las NIN se sintetizaron en ausencia de *template*, esta banda no aparece en su espectro. Además, en los espectros

de las MIN y NIN, pueden apreciarse otras bandas relativas a grupos funcionales propios del entramado polimérico. A 1722 cm^{-1}, aparece una banda intensa que podría asignarse a la vibración de tensión del grupo C=O presente tanto en el monómero funcional como en el entrecruzador. Así mismo, las dos bandas intensas que pueden distinguirse a 1252 y 1121 cm^{-1} podrían deberse a la vibración de tensión del enlace C-O de los grupos éster del polímero. Las bandas pertenecientes a la vibración de tensión del enlace C-H de los grupos alcanos del polímero pueden apreciarse a 2986 y 2938 cm^{-1}.

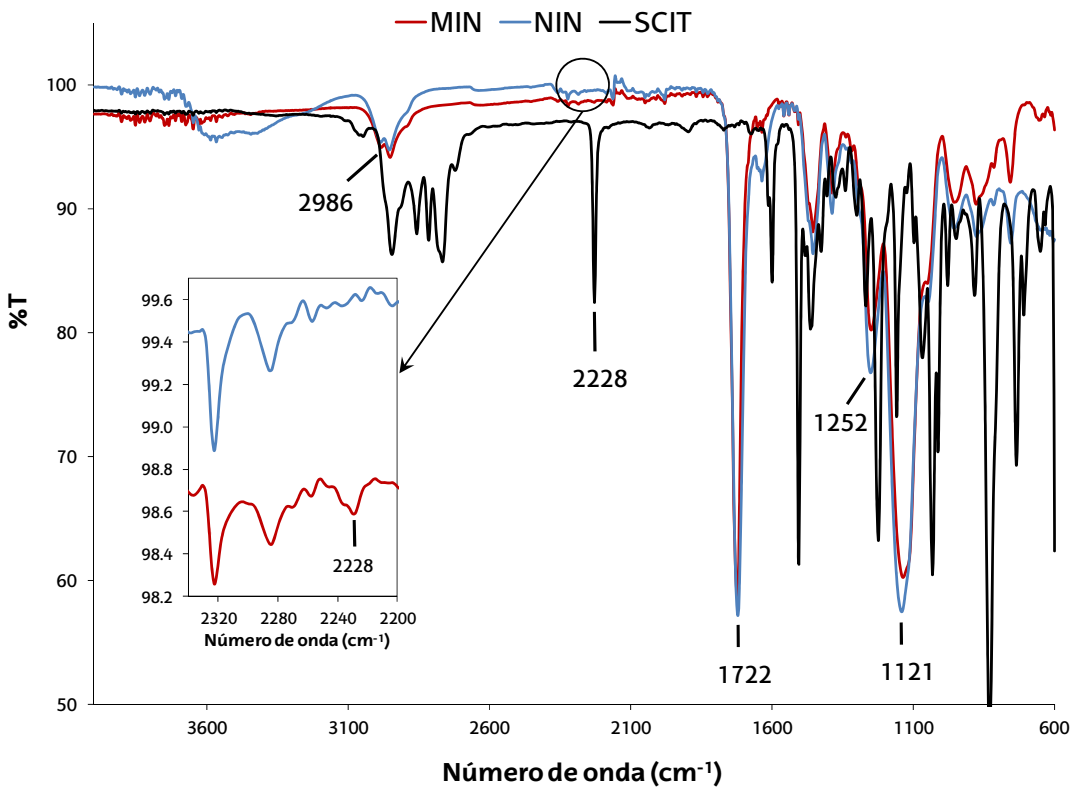

Figura 3.10. Espectros IR del SCIT y de las nanopartículas impresas (MIN) y no impresas (NIN).

4.2.2. Caracterización morfológica por Microscopía Electrónica de Barrido (SEM)

La Microscopía Electrónica de Barrido (SEM) es una técnica ampliamente utilizada en la investigación de materiales poliméricos debido a su alta resolución y capacidad para analizar características morfológicas y estructurales. Esta técnica se basa en el mismo principio de la microscopía óptica en la que la radiación se sustituye por un haz de electrones acelerados. El microscopio electrónico de barrido forma la imagen con los electrones secundarios que se generan en la interacción de la radiación electrónica con una capa superficial y fina de la muestra mediante un proceso de rastreo. El hecho de que la observación de la muestra se haga punto a punto, permite la utilización de muestras de cualquier tamaño y forma y con una gran profundidad de campo, lo que da a las imágenes una apariencia tridimensional. En una muestra observada por SEM, las áreas oscuras corresponden a las zonas de baja reflectividad y las rugosas a los relieves superficiales, pudiendo tener un contraste composicional o topográfico. La resolución espacial de una observación SEM viene dada por el área de la muestra reflectante y dependerá del grado de interacción de la radiación con la muestra. Esta interacción genera electrones reflejados que son atraídos por un detector para dar imágenes topográficas.

Para las medidas por Microscopía Electrónica de Barrido, se depositó una pequeña cantidad de nanopartículas, previamente secadas al vacío durante 48 horas, sobre un soporte metálico recubriéndolas, a continuación por pulverización catódica, con una capa de cromo de 5 nm, con el fin de dotar a la muestra de conductividad eléctrica suficiente para el análisis microscópico.

Tal y como puede observarse en la figura 3.11, la síntesis por polimerización por precipitación dio lugar a partículas esféricas y uniformes con tamaños menores o iguales a un micrómetro y sin observarse acúmulos. Las nanopartículas no impresas presentaron un tamaño ligeramente mayor que las impresas debido a la influencia del SCIT en la solubilidad de las partículas en estado sol (etapa de nucleación) y por

consiguiente en el proceso de crecimiento de las nanopartículas durante la etapa de polimerización [52].

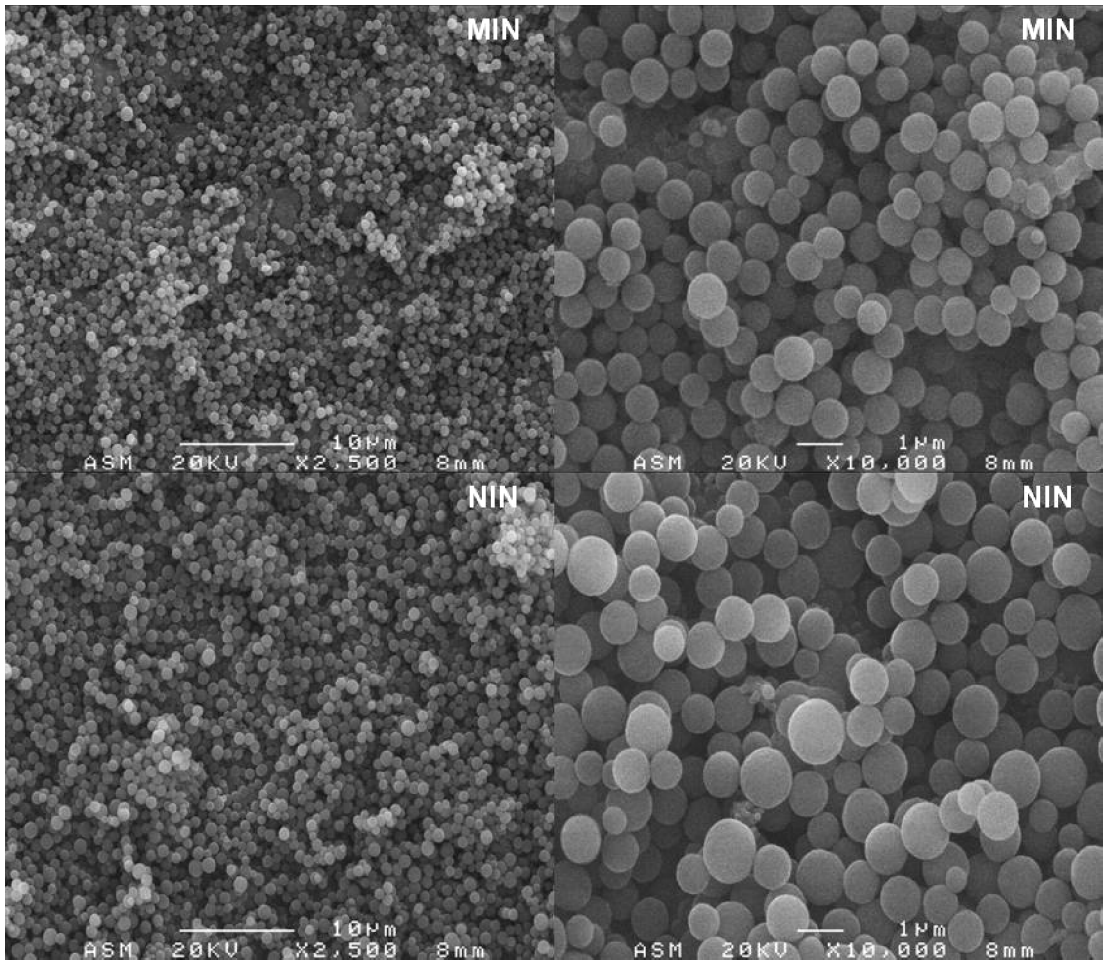

Figura 3.11. Imágenes SEM para las nanopartículas impresas (MIM) y no impresas (NIN) a diferentes aumentos.

4.2.3. Caracterización de la capacidad de los polímeros mediante ensayos de unión

Los ensayos de unión permiten conocer las propiedades de interacción para un ligando, por un determinado receptor, bien sea de origen natural o sintético. En este tipo de ensayos, se ponen en contacto cantidades determinadas de un receptor con su correspondiente ligando a distintos niveles de concentración.

Como resultado, se obtienen las correspondientes isotermas de unión experimentales, en las cuales se representa, para cada nivel de concentración de ligando, la concentración unida al receptor (B) frente a la concentración que ha quedado libre en disolución (F) tras el ensayo.

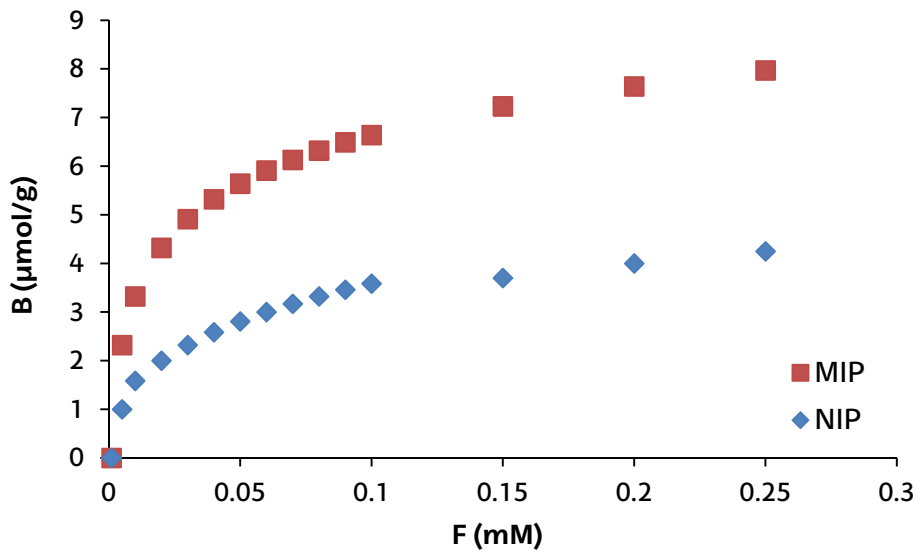

Figura 3.12. Representación de las isotermas de unión para el polímero impreso (MIP) y no impreso (NIP).

Los ensayos de unión, fundamentalmente pueden llevarse a cabo por cromatografía frontal [151-155] o por ensayos en estático [156-160]. En los **ensayos en**

estático, se mantiene una cantidad determinada de polímero en contacto con una disolución de concentración fija de analito hasta alcanzar el equilibrio termodinámico, habitualmente 24 horas [159, 160]. Si no se alcanzara el equilibrio, la accesibilidad a los sitios de unión podría influir en el resultado subestimándose la capacidad real del polímero [151]. Alcanzado este tiempo, el MIP es eliminado por filtración y la concentración del ligando remanente en disolución (F), es determinada, con o sin separación cromatográfica previa, por espectroscopia UV o fluorescencia.

En **cromatografía frontal**, se emplea, como fase estacionaria, el MIP empaquetado en una columna cromatográfica. El ligando, disuelto en la fase móvil, transcurre a flujo constante a través de dicha columna quedando retenido en ésta hasta su saturación. Como resultado se obtienen cromatogramas en forma sigmoidea de cuyo punto de inflexión se determina el volumen de ruptura. La concentración constante que se hace pasar por la fase estacionaria MIP es considerada como la concentración libre (F), mientras que la concentración de analito unido (B) es calculada a partir de la ecuación (3.6) en la que V (L) es el volumen de retención, el cual se obtiene a partir del máximo de la 1ª derivada de la curva de ruptura obtenida como cromatograma (figura 3.13), V_0 (L) es el volumen muerto de la columna, calculado a partir del tiempo muerto, y m (g) es la masa del polímero utilizada en el empaquetado de la columna cromatográfica.

$$B(\mu mol/g) = \frac{F(V - V_0)}{m} \qquad 3.6$$

Las isotermas calculadas por cromatografía frontal también se ven afectadas por factores relativos a la cinética de absorción-liberación del analito. Debido a ello, las interacciones entre analito y MIP suelen ser más débiles, lo que suele dar lugar a capacidades y afinidades más bajas. Por este motivo, se observan menores diferencias entre isotermas, lo que, en ocasiones, dificulta apreciar diferencias significativas al comparar adsorbentes de distinta naturaleza [161].

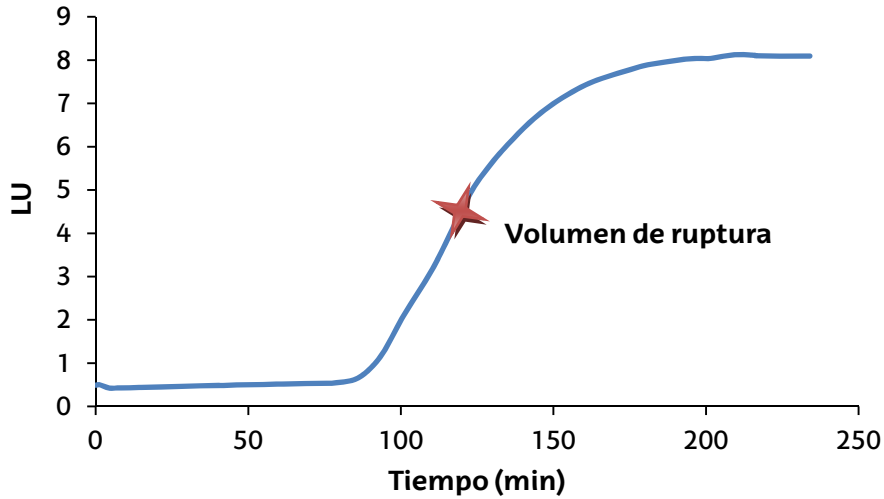

Figura 3.13. Ejemplo de un cromatograma frontal.

Los datos experimentales que componen las isotermas de unión (figura 3.12) son ajustados a distintos modelos matemáticos de regresión no lineal con el fin de estimar el valor de los distintos parámetros que describen el comportamiento del sistema en la unión ligando-receptor. La relación matemática de los valores experimentales con cada modelo está basada en presunciones acerca de las propiedades del polímero, especialmente en lo que concierne al número de sitios de unión, así como sus poblaciones relativas [162]. Los modelos más utilizados en la caracterización de MIP son el modelo Langmuir [160, 163, 164], Bi-Langmuir [165, 166], Freundlich-Langmuir [154, 167, 168] y Freundlich [169, 170]. El primero de ellos presume la existencia de una población homogénea de sitios de unión (N_t) y permite conocer la cantidad de analito unido (B) en función de la concentración libre (F), a partir de una única constante de afinidad (K). El resto de modelos son modelos heterogéneos que asumen la existencia de dos o más clases de sitios de unión, cada uno de ellos con su constante de afinidad particular (K_i).

Modelo Langmuir

El modelo Langmuir es un modelo de unión que asume que todos los sitios de unión (N_t) son idénticos y que presentan la misma afinidad por el ligando. Estos comportamientos de unión suelen darse en sistemas estructuralmente homogéneos como enzimas, anticuerpos monoclonales o receptores moleculares sintéticos, entre los que se pueden encontrar algunos tipos de MIP [162]. El comportamiento de los MIP sintetizados por el método covalente o bien en aquellos sintetizados por el método no covalente donde la constante de formación del aducto de prepolimerización funcional-*template* es elevada ($K_a \geq 10^3\ M^{-1}$), lo que se le conoce como método estequiométrico no covalente, quedan perfectamente descritos por este método a través de la ecuación (3.7):

$$B = \frac{N_t K F}{1 + K F} \qquad 3.7$$

El cálculo de los parámetros del ajuste del modelo puede realizarse a partir de la representación de la ecuación de Scatchard (ecuación 3.11), la cual es una reorganización de la ecuación de Langmuir que permite transformar la isoterma hiperbólica inicial en una recta, que permite calcular de forma sencilla el número de sitios de unión (N_t) y la constante de afinidad (K) a partir de la pendiente (-K) y la ordenada en el origen (N_tK), ya que para y=0 se cumple que $B=N_t$.

A partir de la ecuación (3.7) de Langmuir se obtiene que,

$$B = \frac{N_t K F}{1 + K F} = \frac{N_t K}{\frac{1}{F} + K} \qquad 3.8$$

Lo que llevaría a,

$$B\left(\frac{1}{F} + K\right) = N_t K \qquad 3.9$$

O lo que es lo mismo,

$$\frac{B}{F} + KB = N_t K \qquad 3.10$$

Dando lugar a la ecuación de Scatchard:

$$\frac{B}{F} = N_t K - KB \qquad 3.11$$

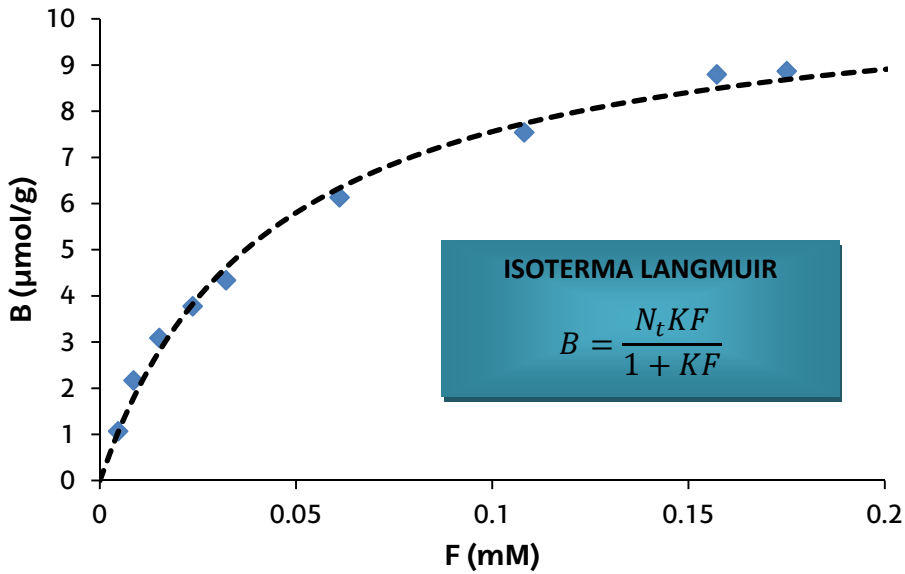

Figura 3.14. Representación de la isoterma de Langmuir

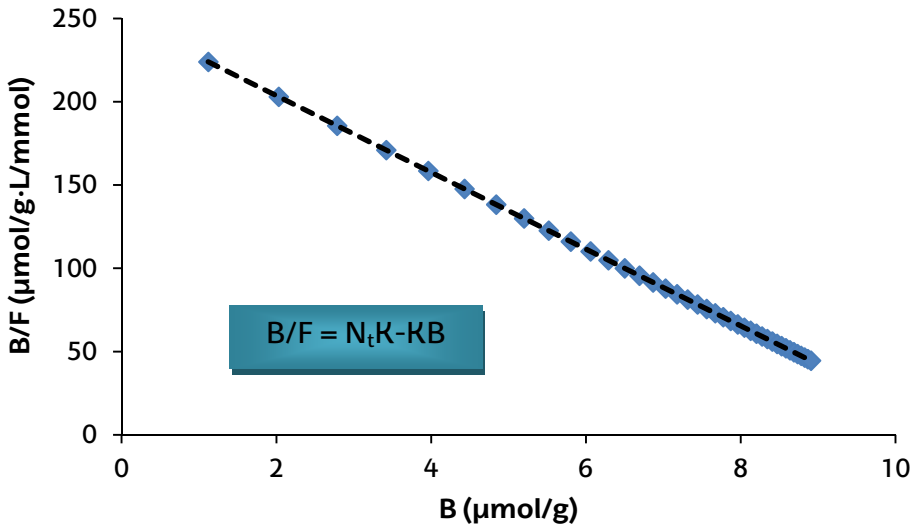

Figura 3.15. Representación de Scatchard correspondiente a una isoterma de Langmuir.

Modelo Bi-Langmuir

En la mayoría de los MIP sintetizados por el método no covalente y debido a la heterogeneidad de sitios de unión, al representar la ecuación de Scatchard, en lugar de apreciarse una tendencia lineal, se obtiene una curva. Ajustando esta curva a dos rectas independientes (figura 3.16) pueden calcularse los distintos parámetros de unión, cada uno de ellos con su constante de afinidad particular (K_1, N_{t1} y K_2, N_{t2}). Estas dos rectas, representan dos tipos distintos de sitios de unión. Este modelo queda descrito por la ecuación 3.12.

$$B = \frac{N_{t1}K_1F}{1+K_1F} = \frac{N_{t2}K_2F}{1+K_2F} \qquad 3.12$$

Donde debe cumplirse que $N_{t2}K_2 \gg N_{t1}K_1$ [171].

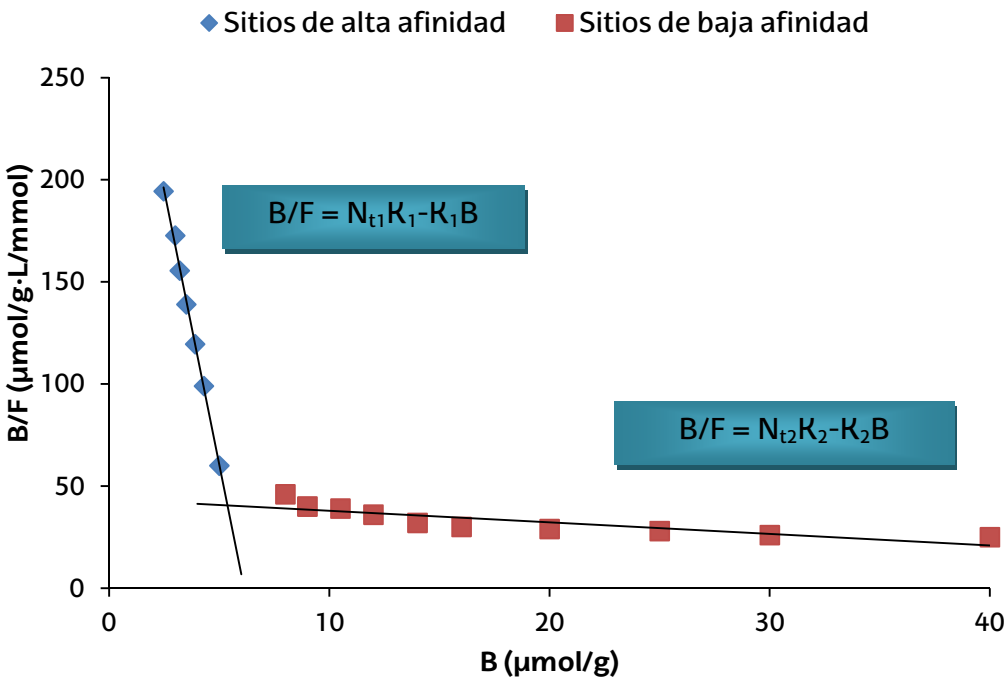

Figura 3.16. Representación de Scatchard para una isoterma ajustada con el modelo Bi-Langmuir.

De la misma forma que el modelo bi-Langmuir asume la existencia de dos poblaciones de sitios de unión, existen otros modelos que consideran tres, cuatro o incluso más poblaciones. Estos modelos se describen de acuerdo a las ecuaciones 3.13 y 3.14.

$$B = \frac{N_{t1}K_1F}{1+K_1F} = \frac{N_{t2}K_2F}{1+K_2F} = \frac{N_{t3}K_3F}{1+K_3F} \qquad 3.13$$

$$B = \frac{N_{t1}K_1F}{1+K_1F} = \frac{N_{t2}K_2F}{1+K_2F} = \frac{N_{t3}K_3F}{1+K_3F} = \frac{N_{t4}K_4F}{1+K_4F} \qquad 3.14$$

Habitualmente, estos modelos basados en un número limitado de sitios de unión son demasiado sencillos para describir la heterogeneidad propia de la mayoría de los MIP. Lo normal es que los MIP posean una distribución continua de sitios de unión que englobe tanto sitios de alta como de baja afinidad. Los modelos que describen este comportamiento son los modelos Freundlich y Freundlich-Langmuir.

Modelo Freundlich

El modelo Freundlich está basado en la relación de la concentración libre y unida mediante una función potencial (ecuación 3.15). Los parámetros de unión a y m hacen referencia a la afinidad de unión media y al factor de heterogeneidad respectivamente. El factor preexponencial, a, es una medida del número de sitios de unión (N_t) y de la constante de afinidad media (K_0). El factor de heterogeneidad, aporta información acerca del grado de heterogeneidad de los sitios de unión en el receptor. Adquiere un valor comprendido entre 0 y 1, de manera que cuanto más se aproxime el valor a la unidad más homogénea será la distribución de los sitios de unión, mientras que la proximidad de este valor a 0, indica una distribución más heterogénea [158, 161].

$$B = aF^m \qquad 3.15$$

La representación en forma logarítmica de las concentraciones libres y unidas obtenidas experimentalmente permite la obtención de los parámetros a y m, siendo m la pendiente de la recta y log a la ordenada en el origen, tal y como se deduce de la ecuación 3.16 (figura 3.17).

$$logB = m\,logF + loga \qquad 3.16$$

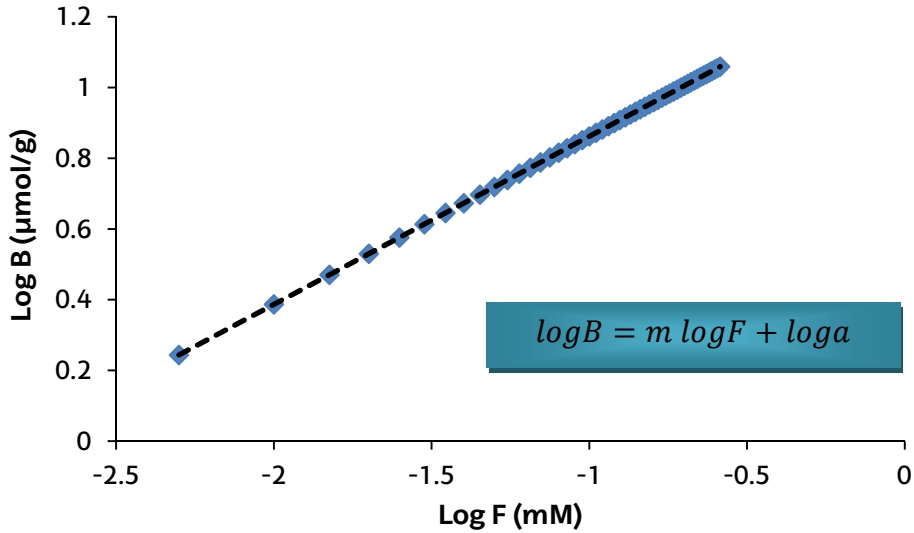

Figura 3.17. Representación logarítmica de la isoterma de Freundlich.

La ecuación 3.17 es una expresión que permite calcular el número de sitios de unión (N_i) que presentan una misma afinidad K_i. En ella se incluyen los parámetros de ajuste a y m, necesarios para el cálculo de la distribución de afinidades. Conocidos los valores de a y m, podría representarse N_i en función de K_i obteniéndose una curva semejante a la que se recoge en la figura 3.18.

$$N_i = 2.3am(1 - m^2)K_i^{-m} \qquad 3.17$$

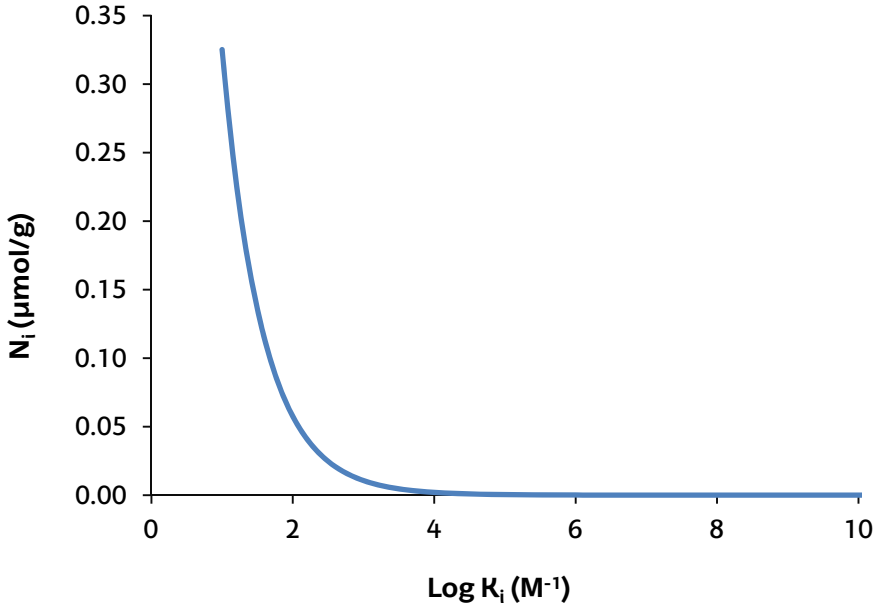

Figura 3.18. Diagrama de distribución de afinidades basada en el modelo Freundlich.

Aunque la mayoría de las isotermas para MIP se ajusten adecuadamente al modelo Freundlich, en algunos casos, se han observado variaciones en los índices de heterogeneidad en función de las concentraciones de ligando empleadas en los ensayos de unión [158]. Para los casos en los que se estudia el comportamiento del MIP tanto a altas concentraciones de ligando, próximas a la saturación del polímero, como a bajas concentraciones, se requiere un modelo con capacidad de describir el comportamiento del polímero en todo el intervalo de concentraciones del ligando. Dado que el modelo Freundlich no describe adecuadamente el comportamiento a bajas concentraciones de ligando, se emplea en su lugar el modelo Freundlich-Langmuir.

Modelo Freundlich-Langmuir

Umpleby *et al*. [172] demostraron que el mejor modelo de ajuste para describir los MIP era el modelo Freundlich-Langmuir, debido a que es capaz de modelizar tanto los sistemas homogéneos como los heterogéneos, a altas y bajas concentraciones de ligando. La ecuación matemática que explica este modelo (ecuación 3.18) presenta tres coeficientes de ajuste: N_t, a y m, siendo N_t el número total de sitios de unión, a el valor de afinidad de unión media, relacionada con la constante de afinidad media (K_0) mediante la ecuación $K_0=a^{1/2}$, y m el factor de heterogeneidad.

$$B = \frac{N_t a F^m}{1 + a F^m} \qquad 3.18$$

A partir de los valores de los parámetros de ajuste, puede calcularse el número determinado (N_i) de sitios de unión con una constante de afinidad (K_i) particular (ecuación 3.19).

$$N_i = N_t a m \left(\frac{1}{K_i}\right)^m \frac{\left(1 + 2a\left(\frac{1}{K_i}\right)^m + a^2\left(\frac{1}{K_i}\right)^{2m} + 4a\left(\frac{1}{K_i}\right)^m m^2 - a^2\left(\frac{1}{K_i}\right)^{2m} m^2 - m^2\right)}{\left(1 + a\left(\frac{1}{K_i}\right)^m\right)^4} \qquad 3.19$$

4.2.3.1. Isoterma de unión experimental para el ligando S citalopram

Las isotermas de adsorción para el ligando SCIT fueron obtenidas mediante ensayos en estático. Para ello, se pesaron 20 mg de MIN o NIN en viales de vidrio de 5 mL y se les añadieron 2 mL de diferentes disoluciones estándar de SCIT en acetonitrilo con concentraciones comprendidas entre 2.5 y 80 mg/L (7.71 x 10^{-3} - 0.25 mM). A continuación, dichos viales fueron agitados a 15 rpm y a temperatura ambiente en un agitador de tubos MovilROB (P.Selecta, Barcelona, España). Tras 24 h, las

nanopartículas se dejaron decantar y el sobrenadante fue filtrado y analizado por cromatografía líquida con detección de fluorescencia. La representación de la concentración de SCIT libre frente a la unida se muestra en la figura 3.19.

Puede apreciarse como la concentración unida del SCIT aumenta a medida que la concentración libre es mayor. Este incremento es más pronunciado en el caso del MIP que en el NIP. Cuando todos los sitios de unión en el polímero están ocupados, se alcanza la saturación y la concentración unida de ligando permanece constante. En la figura 3.19 se aprecia como esta saturación se alcanza mucho antes en el caso de las NIN.

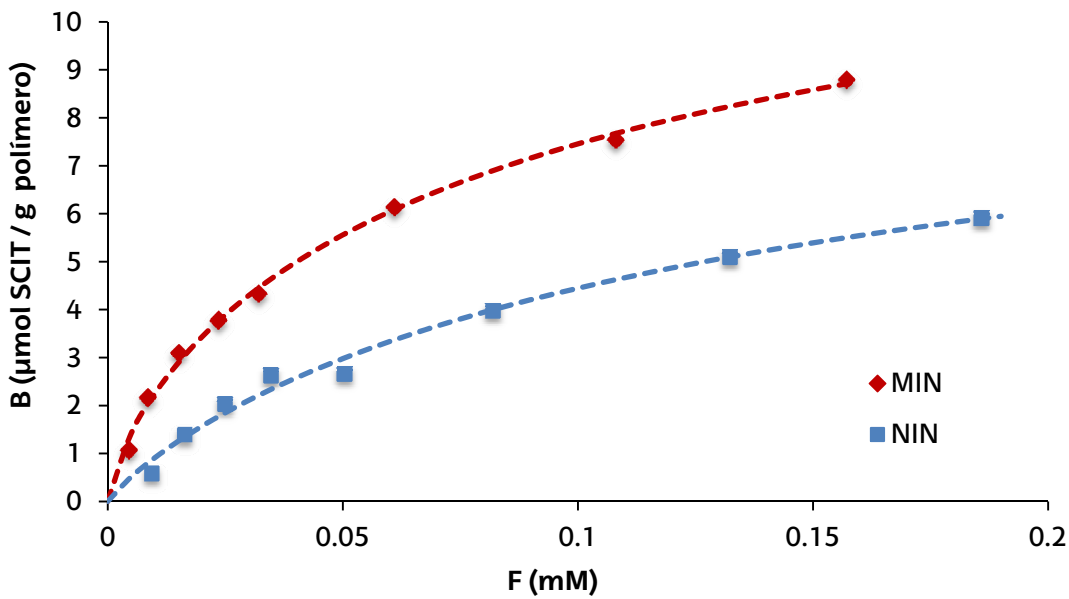

Figura 3.19. Isotermas de unión para las nanopartículas impresas (MIN) y no impresas (NIN) ajustadas al modelo Freundlich-Langmuir

La isoterma de unión experimental fue ajustada por regresión no lineal empleando los modelos de unión descritos anteriormente. Los parámetros de unión obtenidos para cada modelo se resumen en la tabla 3.6.

Tabla 3.6. Parámetros de ajuste para los modelos Langmuir, Bi-Langmuir, Freundlich y Freundlich-Langmuir

Modelo Langmuir			**MIN**	**NIN**
Constante de afinidad	K_a	(mM^{-1})	$2.30\ 10^{-2} \pm 0.26\ 10^{-2}$	$1.03\ 10^{-2} \pm 0.17\ 10^{-2}$
Número de sitios de unión	N_t	(µmol/g)	10.84 ± 0.49	8.88 ± 0.72
Coeficiente de determinación		R^2	0.991	0.984
Suma absoluta de los cuadrados			0.281	0.337
Modelo Bi-Langmuir			**MIN**	**NIN**
Constante de afinidad	K_{a1}	(mM^{-1})	$5.70\ 10^{-2} \pm 3.38\ 10^{-2}$	$6.59\ 10^{-2} \pm 29.04\ 10^{-3}$
	K_{a2}	(mM^{-1})	$2.77\ 10^{-3} \pm 6.41\ 10^{-3}$	$3.58\ 10^{-3} \pm 10.72\ 10^{-3}$
Número de sitios de unión	N_{t1}	(µmol/g)	5.18 ± 3.04	1.70 ± 5.81
	N_{t2}	(µmol/g)	13.41 ± 14.29	10.90 ± 8.90
Coeficiente de determinación		R^2	0.997	0.988
Suma absoluta de los cuadrados			0.116	0.118
Modelo Freundlich			**MIN**	**NIN**
Afinidad de unión media	a	(mM^{-1})	0.82 ± 0.09	0.29 ± 0.06
Factor de heterogeneidad		m	0.48 ± 0.03	0.58 ± 0.04
Coeficiente de determinación		R^2	0.988	0.979
Suma absoluta de los cuadrados			0.624	0.501
Modelo Freundlich-Langmuir			**MIN**	**NIN**
Número de sitios de unión	N_t	(µmol/g)	14.90 ± 2.58	10.62 ± 4.11
Afinidad de unión media	a	(mM^{-1})	$3.14\ 10^{-2} \pm 0.31\ 10^{-2}$	$1.22\ 10^{-2} \pm 0.34\ 10^{-2}$
Factor de heterogeneidad		m	0.75 ± 0.08	0.89 ± 0.19
Coeficiente de determinación		R^2	0.997	0.986
Suma absoluta de los cuadrados			0.171	0.314

La simple comparación de estos parámetros, obtenidos del ajuste por regresión no lineal, no permite establecer el modelo que mejor describe el comportamiento experimental. A fin de establecer una comparación más precisa, se realizó un test estadístico mediante el software Graphpad®. Este programa realiza una adaptación del análisis de la varianza (ANOVA), conocido como test de Fischer o test F, el cual está

basado en un cociente modificado de la suma de los cuadrados residuales de los dos modelos a comparar. De este modo, calcula el valor de Fischer (F) y su correspondiente valor p para cada estudio comparativo. El valor F se calcula tal y como se muestra en la ecuación 3.20, a partir de la suma de los cuadrados (SS) y los grados de libertad (DF), que son indicativos de la complejidad del modelo. Si el modelo más simple (descrito como hipótesis nula, h_0), es el que mejor se ajusta a los datos experimentales, cabe esperar que el aumento relativo en la suma de los cuadrados sea aproximadamente igual al incremento relativo de los grados de libertad, dando lugar a valores de F cercanos a 1. Por el contrario, si el modelo más complejo (hipótesis alternativa, h_1) es el que mejor se ajusta, entonces es de esperar que el incremento relativo en la suma de los cuadrados, sea mucho mayor que el incremento relativo en los grados de libertad, dando valores de F significativamente superiores a 1.

$$F = \frac{(SS_{nula} - SS_{alt})/SS_{alt}}{(DF_{nula} - DF_{alt})/DF_{alt}} \qquad 3.20$$

A continuación, el programa calcula el valor p a partir de este valor F. Si este valor es inferior a 0.05 debería aceptarse la hipótesis alternativa. De lo contrario, se aceptaría el modelo más simple, que se corresponde con la hipótesis nula.

Tal y como se aprecia en la en la tabla 3.7 el modelo que mejor describe el comportamiento experimental fue el modelo de Freundlich-Langmuir (ecuación 3.18). Observando los parámetros de ajuste a partir de este modelo, se aprecia como la afinidad de unión media en el material MIP ($3.14\ 10^{-2} \pm 0.31\ 10^{-2}\ mM^{-1}$) es notablemente mayor que la observada en las partículas NIP ($1.22\ 10^{-2} \pm 0.34\ 10^{-2}\ mM^{-1}$). Respecto a los sitios de unión, el valor observado en las MIN es mayor que el observado en las NIN 14.90 ± 2.58 µmol/g frente a 10.62 ± 4.11. De cualquier modo, el elevado número de sitios de unión observado en las nanopartículas NIP puede ser debido a las uniones electrostáticas inespecíficas del SCIT con los grupos carboxílicos de los monómeros funcionales distribuidos de forma aleatoria en el entramado polimérico.

Tabla 3.7. Resultados obtenidos en la comparación entre los modelos de ajuste de las isotermas de unión.

Test Comparativo entre modelos			
Comparación	**Modelo preferido**	**Valor de F**	**Valor de p**
Langmuir (h_0) frente a Freundlich-Langmuir (h_1)	Freundlich-Langmuir	8.887	0.031
Freundlich (h_0) frente a Freundlich-Langmuir (h_1)	Freundlich-Langmuir	13.260	0.015
Freundlich-Langmuir (h_0) frente a Bi-Langmuir (h_1)	Freundlich-Langmuir	1.919	0.238

A partir de la isoterma de Freundlich-Langmuir, cuyos parámetros se observan en la tabla 3.6, se trazó el diagrama de distribución de afinidades de los sitios de unión en base a la ecuación descrita anteriormente (ecuación 3.19). Este diagrama es típico de modelos heterogéneos que asumen la existencia de un elevado número de tipos de sitios de unión, cada uno con su constante de afinidad particular (figura 3.20).

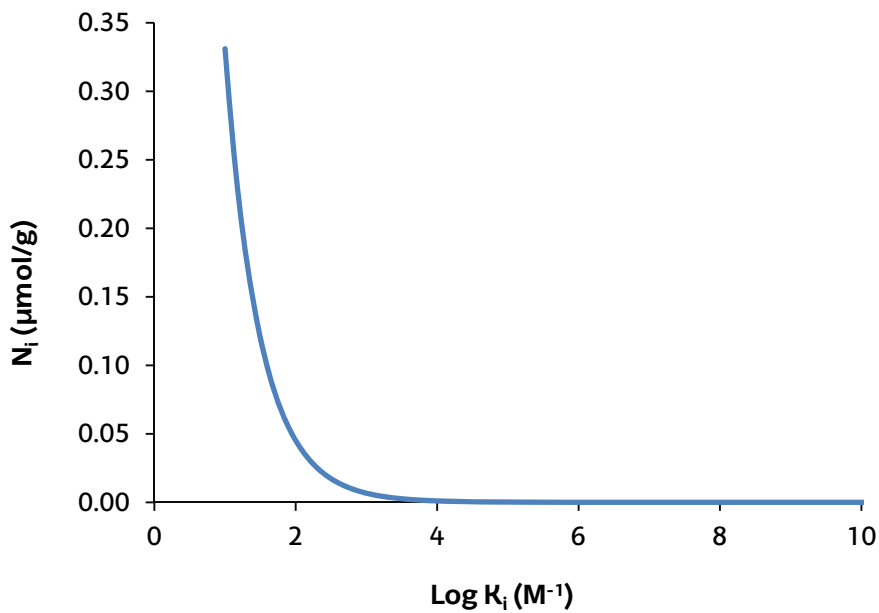

Figura 3.20. Diagrama de distribución de afinidades para la isoterma de Freundlich-Langmuir.

5. Fabricación de un sensor potenciométrico empleando nanopartículas MIP quirales como elemento de reconocimiento

Un electrodo selectivo de iones (ISE) basado en membranas líquidas, consiste en un sensor con una membrana selectiva para un ion determinado. La membrana es un polímero orgánico hidrofóbico impregnado con una disolución orgánica que contiene un intercambiador iónico que se une selectivamente al ión analito. En general, como consecuencia de la diferencia de potenciales electroquímicos a uno y otro lado de la membrana, se produce un fenómeno de transporte de iones de una cara a la otra hasta que los potenciales se igualan, estableciéndose en ese momento una diferencia de potencial denominada potencial de membrana, cuyo valor está relacionado con la diferente actividad del ión a ambos lados de la misma.

En la figura 3.21 se puede observar un esquema de la celda electroquímica empleada, la cual está compuesta por un electrodo selectivo de iones y un electrodo de referencia, a través de los cuales se determina la fuerza electromotriz o diferencia de potencial eléctrico bajo condiciones de corriente cero.

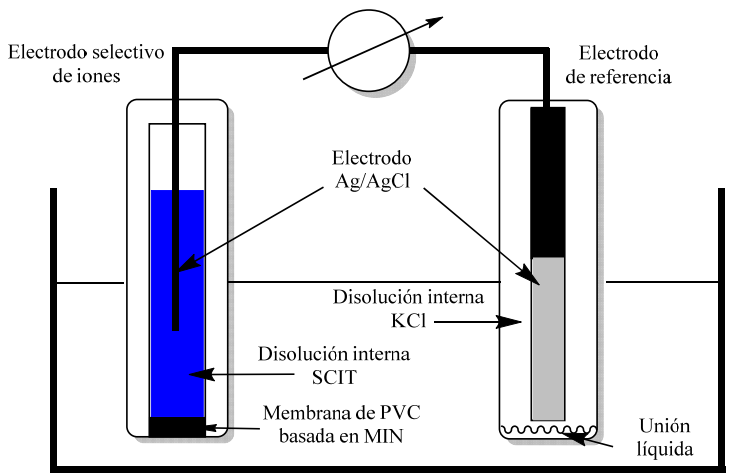

Figura 3.21. Esquema de una celda electroquímica típica para ISE.

En condiciones ideales, el potencial varía de forma proporcional al logaritmo de la actividad del ion. Esta relación ideal viene determinada por la Ley de Nernst (ecuación 3.21) adaptada a electrodos selectivos de iones, la cual se representa de forma simplificada como:

$$E_{cel} = K + \frac{0.059}{n} loga \qquad 3.21$$

Donde K es una constante, determinada experimentalmente, que representa los potenciales de los electrodos de referencia, cualquier potencial de unión líquida, el potencial de asimetría y la concentración del analito en la disolución interna; n es la carga del ion implicado y a la actividad de dicho ion en disolución. Los potenciales de membrana se deben a una interacción química entre el analito y los lugares activos de la superficie de la membrana. Como la señal depende del proceso químico, en su mayoría ninguna membrana es completamente específica de un único ion, siendo el potencial de membrana proporcional a la concentración de todos los iones existentes en la disolución que sean capaces de establecer interacciones con los lugares activos de la membrana. Esta modificación de la ecuación de Nernst, que tiene en cuenta iones interferentes, es conocida como la ecuación de Nicolsky (ecuación 3.22), si los iones interferentes tienen la misma carga, o la ecuación de Nicolsky-Eisenman cuando el ion primario y el interferente tienen cargas distintas (ecuación 3.23):

$$E_i = K_i + \frac{s}{z_i} log\left(a_i + \sum_{j \neq i} K_{i,j}^{pot} a_j\right) \qquad 3.22$$

$$E_i = K_i + \frac{s}{z_i} log\left(a_i + \sum_{j \neq i} K_{i,j}^{pot} {a_j}^{z_i/z_j}\right) \qquad 3.23$$

Siendo $K_{i,j}^{pot}$ el coeficiente de selectividad, el cual refleja la capacidad del electrodo para discriminar entre el ion primario y el ion interferente, y a_j la actividad del ion interferente [7]. El coeficiente de selectividad puede definirse como:

$$K_{i,j}^{pot} = \frac{a_i}{a_j^{z_i/z_j}} \qquad 3.24$$

Donde a_i y a_j son las actividades del analito y el interferente y z_i y z_j representan sus respectivas cargas. Cuando el coeficiente de selectividad es 1, la respuesta de la membrana es idéntica para el analito y el interferente. Por el contrario, si una membrana presenta elevada especificidad para el analito, el coeficiente de selectividad es significativamente inferior a la unidad.

5.1. Fabricación de la membrana

La membrana selectiva para el SCIT fue preparada disolviendo 100 mg de PVC en 3 mL de THF. Posteriormente, se añadieron 5 mg de nanopartículas impresas (o, en su caso, las no impresas) así como 200 mg de plastificante DBP. La mezcla fue sometida durante 5 minutos a sonicación para facilitar la dispersión de las nanopartículas. Posteriormente se transvasó a un vaso de precipitados de 10 mL y después de 48 horas de secado a temperatura ambiente, se obtuvo un material plástico flexible. Por último, este material fue recortado para obtener una membrana de 7 mm de diámetro y 0.2 mm de grosor. Ésta, fue dispuesta en el extremo de un cuerpo electródico comercial proporcionado por Sigma-Aldrich (Madrid, España) el cual se rellenó internamente con una disolución acuosa de SCIT de concentración 10^{-5} M. Previo a su uso, los electrodos fueron sumergidos en una disolución de esta misma concentración durante 24 horas para su acondicionamiento.

La fabricación de la membrana potenciométrica se resume, de forma esquematizada, en la figura 3.22.

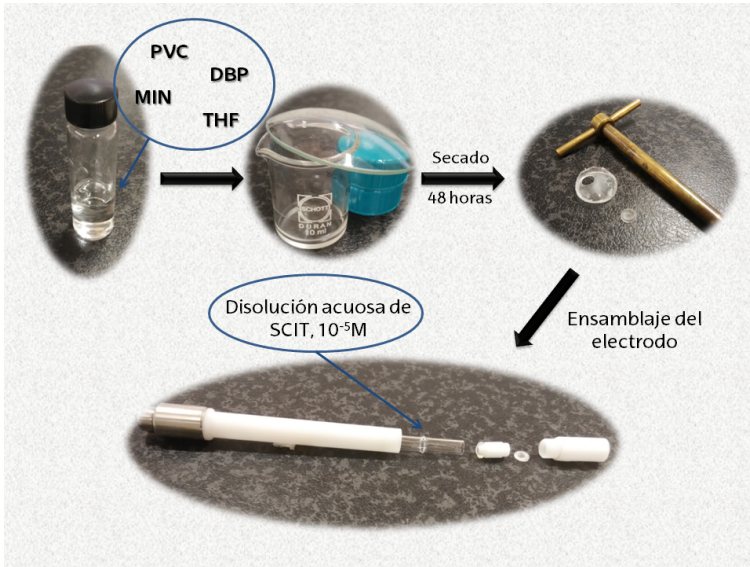

Figura 3.22. Proceso de fabricación de la membrana y su montaje en el cuerpo electródico.

5.2. Optimización de la composición de la membrana

El comportamiento electroquímico de los sensores potenciométricos depende, en amplia medida, de la composición de la membrana electródica. La naturaleza del plastificante, la proporción de PVC, la cantidad de ionóforo y la concentración de la disolución interna, son algunos de los parámetros clave para obtener un comportamiento electródico adecuado, con un valor de pendiente lo más próximo al valor ideal establecido por la ley de Nernst.

Con el fin de determinar la composición de la membrana que permitiera obtener una respuesta electroquímica ajustada a la ley de Nernst, se prepararon diferentes membranas a partir de distintas cantidades de cada componente. A continuación, se midió la fuerza electromotriz de la celda electroquímica utilizando disoluciones de SCIT de concentración comprendida entre 10^{-7} y 10^{-3} M en tampón acético/acetato 10 mM (pH 6). Los resultados obtenidos quedan resumidos en la tabla 3.8.

Tabla 3.8. Resultados obtenidos para la pendiente en membranas electródicas fabricadas con diferentes composiciones.

Membrana nº	MIN (mg)	NIN (mg)	PVC (mg)	NPOE (mg)	DBP (mg)	DOP (mg)	BEHS (mg)	Pendiente (mV/década)
1	-	-	100	200	-	-	-	20,9
2	-	-	100	-	200	-	-	24,8
3	-	-	100	-	-	200	-	33,0
4	-	-	100	-	-	-	200	26,7
5	10	-	100	200	-	-	-	48,3
6	10	-	100	-	200	-	-	49,9
7	10	-	100	-	-	200	-	42,6
8	10	-	100	-	-	-	200	21,4
9	10	-	100	-	250	-	-	19,4
10	10	-	100	-	150	-	-	40,2
11	10	-	100	-	100	-	-	16,4
12	5	-	100	-	200	-	-	50,1
13	15	-	100	-	200	-	-	34,5
14	20	-	100	-	200	-	-	25,0
15	25	-	100	-	200	-	-	8,4
16	-	5	100	-	200	-	-	30,2

PVC: policloruro de vinilo, **NPOE:** 2-nitrofenil octil éter, **DBP**: dibutil ftalato, **DOP**: dioctil ftalato y **BEHS:** bis(2-etilhexil)sebacato.

Las propiedades físicas de una membrana están determinadas por la naturaleza del plastificante, el cual facilita la movilidad de los iones a través de la misma. Los plastificantes más utilizados son el NPOE, DBO, BEHS y DOP (figura 3.23). Inicialmente Shamsipur *et al*. [173] y luego Prathish *et al*. [174] observaron que la sensibilidad de un

electrodo puede estar directamente relacionada con la constante dieléctrica del plastificante. Este razonamiento se basa en que cuanto mayor es el valor de la constante dieléctrica (ε) mayor es la conductividad eléctrica, y por ende mayor resulta la movilidad de los iones a través de la membrana. En este estudio se observó un comportamiento similar, ya que aquellas membranas 5 y 6 elaboradas con NPOE (ε = 24) y DBP (ε = 8.5) proporcionaron valores de pendientes más próximos al valor ideal, 48.3 y 49.9 mV/década respectivamente. Mientras que las membranas 7 y 8 elaboradas con DOP (ε = 5) y BEHS (ε = 4) aportaron valores inferiores, 42.60 y 21.40 mV/década respectivamente.

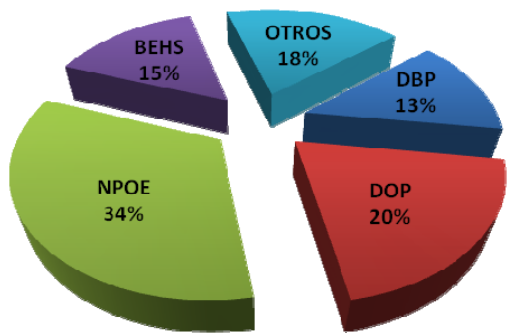

Figura 3.23. Plastificantes habitualmente utilizados para la fabricación de membranas potenciométricas líquidas (2007-2015).

Otro factor determinante para que el funcionamiento de las membranas ISE se aproxime a lo establecido por la ley de Nernst, lo constituye la proporción de PVC. Por ello, una vez seleccionado el plastificante adecuado, con el objetivo de conocer la proporción DBP: PVC óptima se fabricaron una serie de membranas empleando relaciones 2.5:1, 2:1, 1.5:1 y 1:1, obteniéndose los mejores resultados con la relación 2:1, es decir, 200 mg de DBP y 100 mg de PVC (membrana 6, tabla 3.8). Proporción que otros

estudios también avalan como óptima para el desarrollo de membranas potenciométricas líquidas basadas en PVC [175].

Fijado el tipo de plastificante, así como su relación frente al PVC, se procedió a optimizar la cantidad de nanopartículas MIP a emplear puesto que el número de sitios de unión disponibles para el reconocimiento del analito depende directamente de la cantidad de MIN [174]. Como se observa en la tabla 3.8 los valores de pendiente más próximos al valor ideal se obtuvieron al emplear bajas cantidades de nanopartículas. Esto puede atribuirse al hecho de que elevadas cantidades de material pudieran dar lugar a una dispersión poco homogénea de las nanopartículas, restringiendo la interacción del SCIT con los sitios de unión y dando lugar a una pobre respuesta electródica. En ausencia de MIN, como puede observarse en la tabla 3.8, sea cual sea el plastificante utilizado, los valores de pendiente obtenidos son significativamente inferiores a los obtenidos cuando se le añaden las nanopartículas impresas, lo que demuestra que el potencial de membrana se establece a través de los sitios de unión presentes en el material impreso. Con todo ello, la membrana número 12, preparada con 5 mg de MIN, 100 mg de PVC y 200 mg de DBP fue seleccionada como óptima dada la proximidad del valor de la pendiente obtenida con el valor ideal. A fin de evaluar el comportamiento de la membrana cuando se utilizaban nanopartículas no impresas, se preparó una nueva membrana (membrana número 16) con las condiciones óptimas seleccionadas para las membranas impresas. El bajo valor de pendiente que se obtuvo en esta membrana (30.2 mV/década) permite afirmar que, efectivamente, los sitios de unión presentes en el material impreso son los encargados de establecer el potencial de membrana y no la estructura del entramado polimérico.

5.3. Optimización del pH del medio de medida

Puesto que el sensor fabricado reconoce la forma catiónica del SCIT (pKa 9.57), cabe esperar que los mejores resultados se obtengan cuando el monómero funcional, ácido itacónico, esté en su forma ionizada (pKa 3.85 y 5.45). Por este motivo, se evaluó la respuesta del sensor en un intervalo de pH entre 5 y 8, empleando para ello tampón acético/acetato 10 mM ajustado a pH 5 y 6 y tampón fosfato 10 mM a pH 7 y 8. En la

figura 3.24 se representan los valores de potencial (mV) registrados empleando distintas disoluciones patrón de SCIT a niveles de concentración comprendidos entre 10^{-7} M y 10^{-3} M. Tras evaluar la respuesta electroquímica del sensor en los distintos medios tamponados se seleccionó el valor de pH 6, ya que fue para el que se observó un mayor intervalo de linealidad manteniéndose una pendiente próxima al valor establecido por la ley de Nernst.

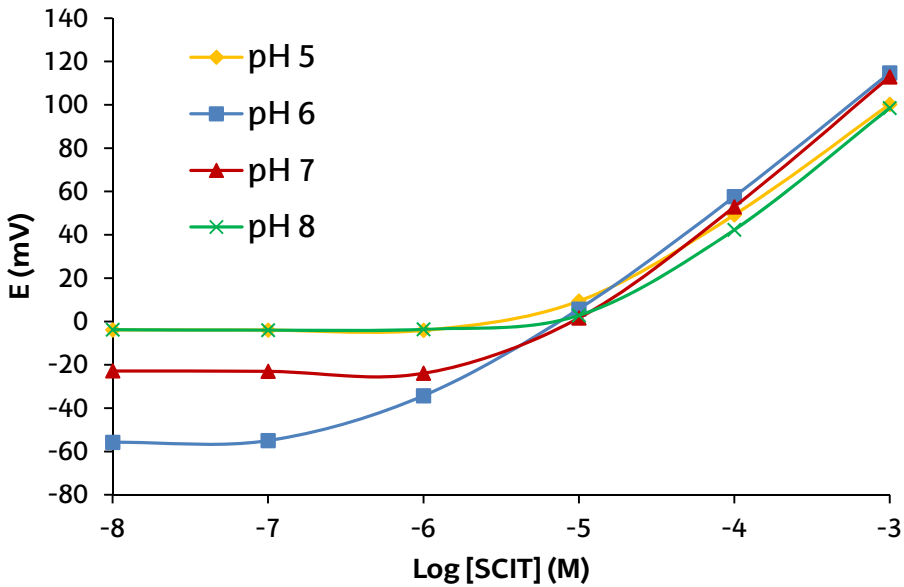

Figura 3.24. Respuesta del sensor registrada a diferentes concentraciones de SCIT y diferentes valores de pH.

5.4. Optimización de la concentración de la disolución interna

La transferencia de analito desde la disolución interna a la externa a través de la membrana sensora, limita la sensibilidad de los ISE basados en membranas líquidas. Estas pérdidas dan lugar a una concentración de analito en la parte externa de la membrana, del mismo orden que la existente en la disolución interna, disminuyendo

así la sensibilidad [9, 176]. Reduciendo la concentración del ion primario en el interior del electrodo, la concentración en la cara exterior de la membrana decrece en varios órdenes de magnitud y consecuentemente disminuye el límite de detección tal y como describieron Sokalski *et al.* [177] para el Pb^{2+}.

La importancia de la disolución interna en la respuesta electródica es tal, que resulta indispensable su optimización con el fin de mejorar la señal analítica. Para ello, se fabricaron diferentes sensores potenciométricos empleando como disolución interna disoluciones acuosas de SCIT a concentraciones comprendidas entre 10^{-3} y 10^{-9} M. Cada sensor fue sometido a calibración empleando distintas concentraciones de SCIT en tampón acético/acetato 10 mM a pH 6. Tal y como cabía esperar, la sensibilidad del sensor mejoraba significativamente a medida que la concentración interna disminuía, sin embargo, un descenso de la concentración interna por debajo de 10^{-5} M no mejoraba la sensibilidad. El sensor que poseía una disolución interna 10^{-5} M de SCIT fue el que proporcionó una mejor respuesta, obteniéndose una pendiente de calibración muy próxima al valor Nernstiano tal y como se muestra en la figura 3.25.

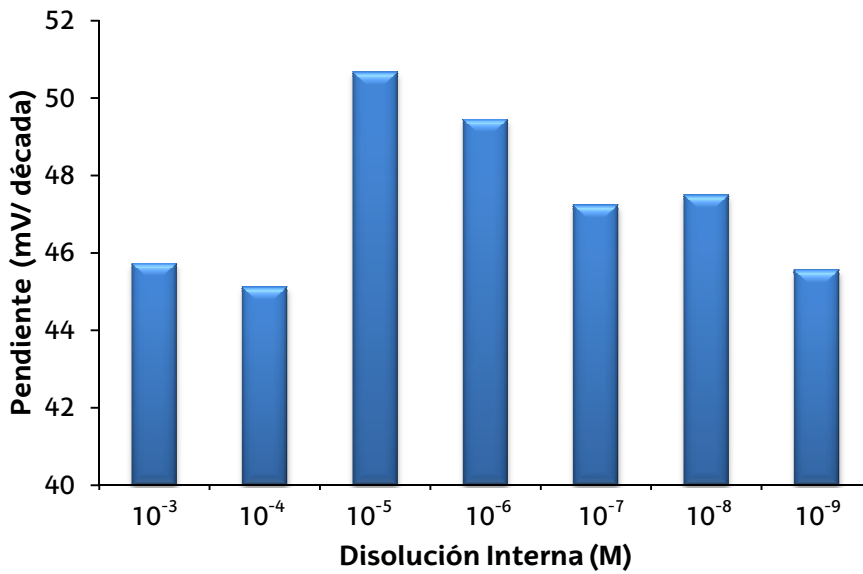

Figura 3.25. Sensibilidad de la calibración en función de la concentración de la disolución interna de SCIT.

6. Evaluación analítica del sensor

6.1. Calibración

Un electrodo ion selectivo puede ser calibrado mediante disoluciones con actividades o concentraciones conocidas de un determinado analito. La calibración a partir de disoluciones con actividades conocidas requiere el conocimiento del coeficiente de actividad de dicho ion, lo que requiere recurrir a supuestos y asunciones que denotan cierta arbitrariedad a la calibración. Sin estos parámetros la preparación de una disolución estándar con una actividad conocida de un ion es estrictamente imposible [178]. Debido a la complejidad de este procedimiento, la mayoría de las veces se lleva a cabo la calibración mediante disoluciones estándar de concentraciones conocidas de un ion determinado. Estas disoluciones fueron preparadas a partir del oxalato de SCIT, para un intervalo de concentraciones comprendidas entre 10^{-9} y 10^{-3} M, en medio tampón acético/acetato 10 mM a pH 6.

Se representó el potencial o fuerza electromotriz (EMF) de la celda frente al logaritmo de la concentración de SCIT. La representación obtenida fue ajustada por regresión lineal, empleando el método de mínimos cuadrados [9]. Se observó una dependencia lineal de la señal analítica (E, mV) y el logaritmo de la concentración de SCIT en un intervalo comprendido entre 2.5 x 10^{-7} y 10^{-3} M con un coeficiente de determinación (R^2) de 0.998.

$$E(mV) = (50.77 \pm 1.32)\log[SCIT] + (401.09 \pm 8.07) \qquad 3.25$$

6.1.1. Límite de detección

La IUPAC define el límite de detección en sensores ISE como la concentración del analito en el punto de intersección entre el tramo lineal de la curva de calibrado y la parte inicial de respuesta constante [179]. Estas dos rectas se corresponden con los tramos relativos a niveles de concentración medios-altos, donde existe un

comportamiento lineal Nernstiano, y los tramos de concentraciones bajas donde el sensor prácticamente no responde a los cambios de concentración (figura 3.26).

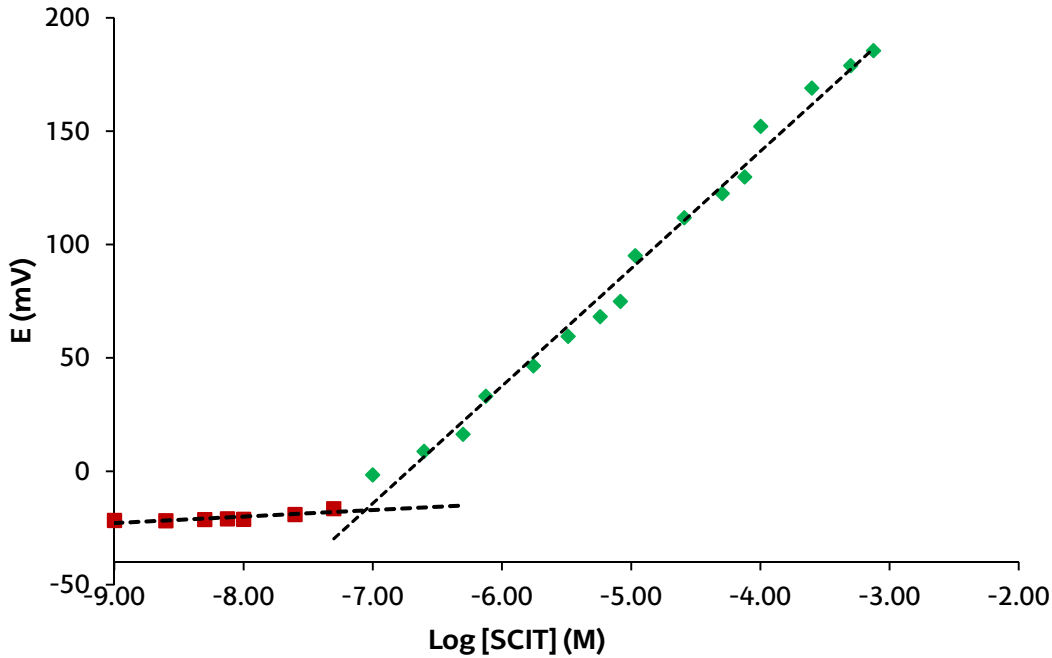

Figura 3.26. Ejemplo gráfico del punto de intersección entre rectas, para el cálculo del límite de detección.

El límite de detección instrumental empleando el sensor desarrollado fue de 1.25 x 10^{-7} mol/L. Este parámetro fue posteriormente analizado (ver apartado 7.1) para evaluar la influencia del efecto matriz en la medida.

6.2. Precisión

De acuerdo con el Vocabulario Internacional de Metrología (VIM) [180] la precisión de los resultados consiste en "la concordancia entre los resultados de mediciones sucesivas del mismo mesurando bajo las mismas condiciones de medición". Para ello,

se llevaron a cabo sucesivas calibraciones (n=5) de un mismo sensor en un intervalo de concentraciones en el tramo de linealidad (entre 2.5 $x10^{-7}$ y 10^{-3} M).

Paralelamente, fue evaluada la variabilidad del proceso global de fabricación electródica, sometiendo distintos sensores a calibración, en un intervalo de concentración de SCIT comprendido entre 2.5 $x10^{-7}$ y 10^{-3} M (n=5).

A partir de los valores de la pendiente obtenidos en cada caso, se calculó el valor medio de la pendiente y su correspondiente desviación estándar relativa. Tal y como se observa en la tabla 3.9, los valores de RSD son inferiores al 2% lo que indica que en ambos casos, la medida se da con una elevada precisión.

Tabla 3.9. Resumen de los valores medios obtenidos en las calibraciones para la evaluación de la precisión del método analítico.

	Rango de concentración estudiado (M)	Pendiente media (mV/década)	Desviación estándar (mV/década)	RSD (%)
Repetitividad	$2.5 x10^{-7}$-10^{-3}	50.07	0.88	1.75
Precisión intermedia	$2.5 x10^{-7}$-10^{-3}	51.00	0.78	1.53

6.3. Selectividad

Los sensores potenciométricos ISE no son completamente específicos para un único ion. Su selectividad depende, fundamentalmente, de las características del intercambiador de iones y del disolvente. En ocasiones, las interferencias están relacionadas con la estabilidad relativa de los quelatos formados por el ion interferente y la especie de interés. En otras ocasiones, la polaridad del disolvente puede facilitar la selectividad de la membrana respecto a ciertos iones [181].

La influencia de los iones interferentes y el comportamiento de respuesta del ISE se describen habitualmente en términos de coeficientes de selectividad.

Los coeficientes de selectividad para los diferentes iones que podrían interferir en este estudio ($RCIT^+$, Na^+, K^+, NH_4^+, Ca^{2+}, Mg^{2+}) fueron obtenidos mediante el método

de disoluciones conjuntas (MSM) conocido como método de interferencia fija (*Fixed Interference Method*, FIM) tal y como estable la IUPAC [179, 182, 183]. Los coeficientes de selectividad se obtuvieron tras realizar la medida de concentraciones crecientes del analito objetivo, en una disolución que contenía una concentración fija del ion interferente. Este método está basado en la ecuación de Nicolskii − Eisenman, que asume que la respuesta Nernstiana del ISE no se debe únicamente al ion primario, sino que es debida también a los iones interferentes [182], cuyos coeficientes de selectividad son considerados una constante y están relacionados con los potenciales medidos mediante la ecuación 3.26:

$$logK_{i,j}^{pot} = -\left(\frac{z_i}{z_j}\right) loga_j + loga_i \qquad 3.26$$

Con el objetivo de determinar la capacidad del sensor para discriminar entre enantiómeros, se evaluó como ion interferente el $RCIT^+$. El resto de iones interferentes, Na^+, K^+, NH_4^+, Ca^{2+}, Mg^{2+}, fueron evaluados por ser los cationes mayoritarios presentes en orina [184] (tabla 3.10).

Tabla 3.10. Concentraciones de los cationes mayoritarios en orina [184].

Ion	(g/24 h)
Na^+	1.70-4.60
K^+	1.40-3.90
NH_4^+	0.54-1.26
Ca^{2+}	0.10-0.25
Mg^{2+}	0.07-0.21

Todos fueron evaluados como iones interferentes para una concentración 10^{-4} M. Cuanto menor sea el valor de los coeficientes de selectividad, mayor es la preferencia del sensor por el ion primario. Tal y como se muestra en la tabla 3.11, ninguno de los iones estudiados interfiere significativamente en la respuesta del sensor. El valor negativo obtenido para el RCIT corrobora la preferencia del sensor por la forma S del citalopram.

Tabla 3.11. Valores de los coeficientes de selectividad para los iones interferentes.

	Log K^{pot}
	10^{-4} mol/L
$RCIT^{+}$	-0.310
Na^{+}	-2.045
K^{+}	-1.920
Ca^{2+}	-4.044
Mg^{2+}	-3.742
NH_4^{+}	-1.893

7. Aplicación del sensor a la medida de SCIT en muestras de orina

Hasta el momento, todo el trabajo experimental y el método desarrollado se han aplicado a estándares acuosos. Sin embargo, el objetivo de este estudio era la aplicación de esta metodología a la determinación de SCIT en orina. La medida potenciométrica fue realizada directamente sobre la muestra de orina previamente filtrada y sin necesidad de ajustar el pH, ya que las muestras de orina recogidas presentaban un pH comprendido entre 6.0 y 6.5, que coincidía con el pH para el cual el sensor presentaba mayor sensibilidad.

7.1. Calibración en la matriz orina

Con objeto de evaluar el efecto matriz, se llevó a cabo un estudio de la influencia de los componentes de la orina en la determinación potenciométrica de SCIT. Con este fin se realizó un calibrado en matriz, para ello muestras de orina blanco se doparon con volúmenes adecuados de disoluciones estándar de SCIT en distintas concentraciones, para que el volumen a añadir a la matriz fuese siempre equiparable y, en todos los casos, despreciable frente al volumen total, de modo que no se alterase la naturaleza propia de la muestra biológica.

Los parámetros de calibración obtenidos, fueron comparados con los obtenidos a partir de medidas de SCIT en disolución tampón con el fin de evaluar el efecto matriz. El límite de detección se vio ligeramente incrementado desde 1.25×10^{-7} mol/L obtenido al realizar las medidas en medio tamponado hasta 1.46×10^{-6} mol/L, obtenido en la matriz orina.

7.2. Exactitud del método

La exactitud (precisión y veracidad) del método se evaluó mediante la determinación directa de SCIT en muestras blanco de orina dopadas previamente con SCIT a distintos niveles de concentración (1, 2 y 5 µg/mL). Los resultados obtenidos se resumen en la tabla 3.12. Tal y como se observa, las recuperaciones fueron superiores al 91% y las desviaciones estándar relativas (RSD%) fueron inferiores al 7 % en todos los casos, lo que indica la idoneidad del método para la cuantificación directa del SCIT en muestras de orina.

Tabla 3.12. Resumen de la validación de los parámetros en muestras de orina (n=5).

Muestra	Añadido (µg/mL)	Cuantificado (µg/mL)	RSD (%)	Recuperación (%)
QC 1	1	0.97 ± 0.04	4.12	97.34 ± 3.52
QC 2	2	1.83 ± 0.12	6.56	91.61 ± 5.75
QC 3	5	4.82 ± 0.10	2.07	96.40 ± 1.91

7.3. Determinación potenciométrica de S-citalopram en orina

La metodología analítica desarrollada se aplicó a la cuantificación de SCIT en muestras de orina de un voluntario tratado crónicamente con dicho antidepresivo. Las muestras fueron recogidas cada día durante una semana y a diferentes tiempos después de la toma del fármaco. En la tabla 3.13 se recogen los valores de los niveles de SCIT cuantificados en orina. Estos valores son los esperados en pacientes sometidos a tratamiento crónico [185]

Tabla 3.13. Niveles de SCIT en orina a distintos tiempos desde la toma del fármaco (n=5).

Tiempo (h)	Cuantificado (µg/mL)	RSD (%)
0-6	1.34 ± 0.11	8.21
6-12	2.03 ± 0.14	6.89
12-15	1.70 ± 0.03	1.76

8. Conclusiones

En base al objetivo principal establecido y conforme a los resultados presentados a lo largo de este capítulo, puede concluirse que se ha fabricado un sensor potenciométrico basado en nanopartículas molecularmente impresas que es capaz de determinar el enantiómero S del antidepresivo citalopram en muestras de orina. El dispositivo resulta una herramienta rápida, fiable y de bajo coste para la monitorización de este antidepresivo en muestras clínicas.

Así mismo, se han alcanzado los objetivos operativos previamente descritos, permitiendo concluir que:

- Se ha comprobado mediante la caracterización química y morfológica, que se han sintetizado de forma satisfactoria nanopartículas impresas para el enantiómero S del antidepresivo citalopram.

- Se ha evaluado el comportamiento del polímero impreso mediante ensayos de unión ligando-receptor. Habiéndose caracterizado los sitios de unión por isotermas de adsorción ajustadas al modelo de Freundlich-Langmuir.

- Se ha fabricado un electrodo de membrana de PVC basado en nanopartículas MIP que permiten la determinación de SCIT por potenciometría directa en orina.

- Se ha confirmado la enantioespecificidad del sensor para el SCIT frente a su enantiómero RCIT.

- Se ha comprobado que los iones presentes de forma habitual en orina no afectan a la cuantificación del enantiómero SCIT en la matriz biológica.

Bibliografía

1. Wang J: **Ion-selective electrode in clinical medicine**. En: *Electroanalytical techniques in clinical chemistry and laboratory medicine*. Editado por Wang J, 1 edn. Weinheim: Wiley-VCH; 1988: 49-79.
2. Javanbakht M, Akbari-Adergani B: **Molecularly imprinted polymer-based potentiometric sensors for the determination of drugs in pharmaceutical, biological, and environmental samples**. En: *Molecularly imprinted sensors: overview and applications*. Editado por Li S, Ge Y, Piletsky SA, Lunec J, 1 edn. Oxford: Elsevier Ltd.; 2012: 247-273.
3. Di Natale C, Davide F, Brunink JAJ, D'Amico A, Vlasov YG, Legin AV, Rudnitskaya AM: **Multicomponent analysis of heavy metal cations and inorganic anions in liquids by a non-selective chalcogenide glass sensor array**. *Sensors and Actuators B: Chemical* 1996, **34**(1–3):539-542.
4. Zamani HA, Rajabzadeh G, Masrornia M, Dejbord A, Ganjali MR, Seifi N: **Determination of Cr^{3+} ions in biological and environmental samples by a chromium(III) membrane sensor based on 5-amino-1-phenyl-1H-pyrazole-4-carboxamide**. *Desalination* 2009, **249**(2):560-565.
5. Heidari P, Jalali S, Mofidi Z, Zamani A, Yaftian MR: **Preparation of a lead ion-selective electrode based upon crown ether nitrobenzo18-crown-6**. *Analytical & Bioanalytical Electrochemistry* 2013, **5**(3):305-315.
6. Ismail ABM, Furuichi K, Yoshinobu T, Iwasaki H: **Light-addressable potentiometric fluoride (F^-) sensor**. *Sensors and Actuators B: Chemical* 2002, **86**(1):94-97.
7. Bakker E: **Potentiometric sensors**. En: *Environmental analysis by electrochemical sensors and biosensors*. Editado por Moretto L, Kalcher K, 1 edn. New York: Springer-Verlag; 2014: 193-238.
8. Skoog DA, West DM, Holler JF, Crough SR: **Potenciometría**. En: *Fundamentos de química analítica*. Editado por Skoog DAW, Donald M., Holler JF, Crough SR, 8 edn. Mexico: Thomson; 2005: 597-642.
9. Harris DC: **Electrodos y potenciometría**. En: *Análisis químico cuantitativo*. Editado por Harris DC, 3 edn. Barcelona: Editorial Reverté; 2007: 314-346.
10. Monk PMS: **Equilibrium measurements: 'frustated' equilibrium with no net electron transfer**. En: *Fundamentals of electroanalytical chemistry*. Editado por Monk PMS, 1 edn. Chichester: John Wiley & Sons LTD; 2001: 25-85.
11. Pingarrón Carrazón JM, Sánchez Batanero P: **Las técnicas electroanalíticas potenciométricas no redox. Los electrodos selectivos de iones**. En: *Química electroanalítica. Fundamentos y aplicaciones*. Editado por Pingarrón Carrazón JM, Sánchez Batanero P, 1 edn. Madrid: Editorial Síntesis, S.A.; 1999: 139-155.
12. Thoma AP, Cimerman Z, Fiedler U, Bedekovic D, Gueggi M, Jordan P, May K, Pretsch E, Prelog V, Simon W: **Enantiomer-selective behavior in membranes of a chiral, electrically neutral ionophore**. *Chimia* 1975, **29**(8):344-346.

13. Thoma AP, Pretsch E, Horvai G, Simon W: **Chiral recognition of biogenic amines by synthetic neutral ionophores in membranes**. En: *Biochemistry of Membrane Transport FEBS Symposium: 1977; Zlirich*. Springer-Verlag 116-122.
14. Thoma AP, Viviani-Nauer A, Schellenberg KH, Bedekovic D, Pretsch E, Prelog V, Simon W: **Electrochemical studies on the enantiomer selective behavior of chiral ionophores in liquid membranes**. *Helvetica Chimica Acta* 1979, **62**(7):2303-2316.
15. Bussmann W, Simon W: **Determination of the enantiomeric excess of chiral ammonium ions using liquid membrane electrodes**. *Helvetica Chimica Acta* 1981, **64**(7):2101-2108.
16. Bussmann W, Lehn JM, Oesch U, Plumere P, Simon W: **Enantiomer-selectivity for phenylethylammonium ion of membranes based on a chiral macrocyclic polyether**. *Helvetica Chimica Acta* 1981, **64**(3):657-661.
17. Horvath V, Takacs T, Horvai G, Huszthy P, Bradshaw JS, Izatt RM: **Enantiomer selectivity of ion-selective electrodes based on a chiral crown-ether ionophore**. *Analytical Letters* 1997, **30**(9):1591-1609.
18. Pilbath Z, Horvath V, Horvai G, Huszthy P: **Enantiomeric discrimination of chiral crown ether ionophores containing phenazine subcyclic unit by ion-selective potentiometry**. *Periodica Polytechnica Chemical Engineering* 2010, **54**(1):3-8.
19. Rouessac F, Rouessac A: **High-performance liquid chromatography**. En: *Chemical analysis modern instrumentation methods and techniques*. Editado por Rouessac F, Rouessac A, 2 edn. Chichester: John Wiley & Sons Ltd; 2007: 63-89.
20. Bates PS, Kataky R, Parker D: **Chiral sensors based on lipophilic cyclodextrins: interrogation of enantioselectivity by combined NMR, structural correlation and electrode response studies**. *Journal of the Chemical Society, Perkin Transactions 2* 1994(4):669-675.
21. Kataky R, Parker D, Kelly PM: **Potentiometric, enantioselective sensors for alkyl and aryl ammonium ions of pharmaceutical significance, based on lipophilic cyclodextrins**. *Scandinavian Journal of Clinical and Laboratory Investigation* 1995, **55**(5):409-419.
22. Kaniewska M, Sikora T, Kataky R, Trojanowicz M: **Enantioselectivity of potentiometric sensors with application of different mechanisms of chiral discrimination**. *Journal of Biochemical and Biophysical Methods* 2008, **70**(6):1261-1267.
23. Aboul-Enein HY, Stefan RI, Van Staden JF: **Potentiometric enantioselective membrane electrode for S-enalapril assay**. *Analusis* 1999, **27**(1):53-56.
24. Aboul-Enein HY, Stefan RI, Van Staden JF: **Analysis of several angiotensin-converting enzyme inhibitors using potentiometric, enantioselective membrane electrodes**. *Analytical Letters* 1999, **32**(4):623-632.
25. Stefan RI, Van Staden JF, Aboul-Enein HY: **A new construction for a potentiometric, enantioselective membrane electrode-its utilization to the S-captopril assay**. *Talanta* 1999, **48**(5):1139-1143.

26. Stefan RI, Van Staden JF, Aboul-Enein HY: **S-perindopril assay using a potentiometric, enantioselective membrane electrode**. *Chirality* 1999, **11**(8):631-634.
27. Rat'ko AA, Stefan RI: **Teicoplanin-based enantioselective, potentiometric membrane electrodes for the determination of R-baclofen in pharmaceutical formulations**. *Analytical Letters* 2004, **37**(15):3161-3173.
28. Stefan RI, Nejem RaM, van Staden JF, Aboul-Enein HY: **Determination of D-2-hydroxyglutaric acid in urine samples using enantioselective, potentiometric membrane electrodes based on antibiotics**. *Sensors and Actuators B* 2005, **106**(2):791-795.
29. Maruyama K, Sohmiya H, Tsukube H: **Enantiomer recognition of organic ammonium salts by podand- and crown-type monensin amides: new synthetic strategy for chiral receptors**. *Tetrahedron* 1992, **48**(5):805-818.
30. Ward TJ, Farris AB: **Chiral separations using the macrocyclic antibiotics: a review**. *Journal of Chromatography A* 2001, **906**(1-2):73-89.
31. Chibvongodze H, Hayashi K, Toko K: **Discrimination of D-amino acids from L-amino acids using electric potential changes of a membrane**. *Sensors and Materials* 2001, **13**(2):99-106.
32. Stefan-van Staden RI, van Staden JF: **Quinine, quinidine and their tert-butyl carbomylated derivatives as chiral selectors in the enantioselective, potentiometric membrane electrodes design: their application for the assay of (S) and (R) enantiomers of 3,5-dinitrobenzoyl leucine**. *Journal of the Electrochemical Society* 2013, **160**(10):B196-B200.
33. Xu L, Yang Y, Wang Y, Gao J: **Chiral salen Mn(III) complex-based enantioselective potentiometric sensor for L-mandelic acid**. *Analytica Chimica Acta* 2009, **653**(2):217-221.
34. Yang Y, Hou J, Li B, Xu L: **Enantioselective ITO electrode modified with chiral salen Co(II) complex**. *Chemical Letters* 2010, **39**(7):690-691.
35. Chai C, Liu G, Li F, Liu X, Yao B, Wang L: **Towards the development of a portable sensor based on a molecularly imprinted membrane for the rapid determination of salbutamol in pig urine**. *Analytica Chimica Acta* 2010, **675**(2):185-190.
36. Kriz D, Mosbach K: **Competitive amperometric morphine sensor based on an agarose-immobilized molecularly imprinted polymer**. *Analytica Chimica Acta* 1995, **300**(1-3):71-75.
37. Zhao YG, Chen XH, Pan SD, Zhu H, Shen HY, Jin MC: **Self-assembly of a surface bisphenol A-imprinted core-shell nanoring amino-functionalized superparamagnetic polymer**. *Journal of Materials Chemistry A* 2013, **1**(38):11648-11658.
38. Chen PY, Vittal R, Nien PC, Liou GS, Ho KC: **A novel molecularly imprinted polymer thin film as biosensor for uric acid**. *Talanta* 2010, **80**(3):1145-1151.
39. Sadeghi S, Motaharian A, Moghaddam AZ: **Electroanalytical determination of sulfasalazine in pharmaceutical and biological samples using molecularly**

imprinted polymer modified carbon paste electrode. *Sensors and Actuators B* 2012, **168**:336-344.

40. Tarley CRT, Kubota LT: **Molecularly-imprinted solid phase extraction of catechol from aqueous effluents for its selective determination by differential pulse voltammetry**. *Analytica Chimica Acta* 2005, **548**(1-2):11-19.
41. Bektasoglu E, Ozkutuk EB, Ersoz A, Say R: **Double-imprinted potentiometric sensors based on ligand exchange for the determination of dimethoate**. *Korean Journal of Chemical Engineering* 2015, **32**(8):1613-1617.
42. Anirudhan TS, Alexander S: **Design and fabrication of molecularly imprinted polymer-based potentiometric sensor from the surface modified multiwalled carbon nanotube for the determination of lindane (-hexachlorocyclohexane), an organochlorine pesticide**. *Biosensors and Bioelectronics* 2015, **64**:586-593.
43. El-Naby EH, Kamel AH: **Potential transducers based man-tailored biomimetic sensors for selective recognition of dextromethorphan as an antitussive drug**. *Materials Science and Engineering C* 2015, **54**:217-224.
44. Cao L, Zhou XC, Li SFY: **Enantioselective sensor based on microgravimetric quartz crystal microbalance with molecularly imprinted polymer film**. *Analyst* 2001, **126**(2):184-188.
45. Zhou W-H, Tang S-F, Yao Q-H, Chen F-R, Yang H-H, Wang X-R: **A quartz crystal microbalance sensor based on mussel-inspired molecularly imprinted polymer**. *Biosensors and Bioelectronics* 2010, **26**(2):585-589.
46. Hao HX, Zhou H, Chang J, Zhu J, Wei TX: **Molecularly imprinted polymers for highly sensitive detection of morphine using surface plasmon resonance spectroscopy**. *Chinese Chemical Letters* 2011, **22**(4):477-480.
47. Blanco-Lopez MC, Lobo-Castañón MJ, Miranda-Ordieres AJ, Tuñón-Blanco P: **Electrochemical sensors based on molecularly imprinted polymers**. *Trends in Analytical Chemistry* 2004, **23**(1):36-48.
48. Bakker E, Chumbimuni-Torres K: **Modern directions for potentiometric sensors**. *Journal of the Brazilian Chemical Society* 2008, **19**(4):621-629.
49. Flavin K, Resmini M: **Imprinted nanomaterials: a new class of synthetic receptors**. *Analytical and Bioanalytical Chemistry* 2009, **393**(2):437-444.
50. Bompart M, Haupt K, Ayela C: **Micro and nanofabrication of molecularly imprinted polymers**. En: *Molecular imprinting*. Editado por Haupt K, vol. 325, 1 edn. Heidelberg: Springer; 2012: 83-110.
51. Tokonami S, Shiigi H, Nagaoka T: **Review: micro- and nanosized molecularly imprinted polymers for high-throughput analytical applications**. *Analytica Chimica Acta* 2009, **641**(1-2):7-13.
52. Yoshimatsu K, Reimhult K, Krozer A, Mosbach K, Sode K, Ye L: **Uniform molecularly imprinted microspheres and nanoparticles prepared by precipitation polymerization: The control of particle size suitable for different analytical applications**. *Analytica Chimica Acta* 2007, **584**(1):112-121.

53. Chen Z, Ye L: **Controlling size and uniformity of molecularly imprinted nanoparticles using auxiliary template**. *Journal of Molecular Recognition* 2012, **25**(6):370-376.
54. Seifi M, Hassanpour Moghadam M, Hadizadeh F, Ali-Asgari S, Aboli J, Mohajeri SA: **Preparation and study of tramadol imprinted micro-and nanoparticles by precipitation polymerization: Microwave irradiation and conventional heating method**. *International Journal of Pharmaceutics* 2014, **471**(1-2):37-44.
55. Piacham T, Nantasenamat C, Isarankura-Na-Ayudhya C, Prachayasittikul V: **Synthesis and computational investigation of molecularly imprinted nanospheres for selective recognition of alpha-tocopherol succinate**. *Experimental and Clinical Sciences* 2013, **12**:701-718.
56. Vaihinger D, Landfester K, Krauter I, Brunner H, Tovar GEM: **Molecularly imprinted polymer nanospheres as synthetic affinity receptors obtained by miniemulsion polymerisation**. *Macromolecular Chemistry and Physics* 2002, **203**(13):1965-1973.
57. Sener G, Ozgur E, Yilmaz E, Uzun L, Say R, Denizli A: **Quartz crystal microbalance based nanosensor for lysozyme detection with lysozyme imprinted nanoparticles**. *Biosensors and Bioelectronics* 2010, **26**(2):815-821.
58. Subrahmanyam S, Guerreiro A, Poma A, Moczko E, Piletska E, Piletsky S: **Optimisation of experimental conditions for synthesis of high affinity MIP nanoparticles**. *European Polymer Journal* 2013, **49**(1):100-105.
59. Guerreiro AR, Chianella I, Piletska E, Whitcombe MJ, Piletsky SA: **Selection of imprinted nanoparticles by affinity chromatography**. *Biosensors and Bioelectronics* 2009, **24**(8):2740-2743.
60. Wackerlig J, Lieberzeit PA: **Molecularly imprinted polymer nanoparticles in chemical sensing - Synthesis, characterisation and application**. *Sensors and Actuators B* 2015, **207**(Part A):144-157.
61. Poma A, Guerreiro A, Caygill S, Moczko E, Piletsky S: **Automatic reactor for solid-phase synthesis of molecularly imprinted polymeric nanoparticles (MIP NPs) in water**. *RSC Advances* 2014, **4**(8):4203-4206.
62. Poma A, Guerreiro A, Whitcombe MJ, Piletska EV, Turner APF, Piletsky SA: **Solid-phase synthesis of molecularly imprinted polymer nanoparticles with a reusable template-"plastic antibodies"**. *Advanced Functional Materials* 2013, **23**(22):2821-2827.
63. Medina-Castillo AL, Fernandez-Sanchez JF, Segura-Carretero A, Fernandez-Gutierrez A: **Micrometer and submicrometer particles prepared by precipitation polymerization: thermodynamic model and experimental evidence of the relation between Flory's parameter and particle size**. *Macromolecules* 2010, **43**(13):5804-5813.
64. Downey JS, Frank RS, Li W-H, Stoever HDH: **Growth mechanism of poly(divinylbenzene) microspheres in precipitation polymerization**. *Macromolecules* 1999, **32**(9):2838-2844.

65. Lime F, Irgum K: **Preparation of divinylbenzene and divinylbenzene-co-glycidyl methacrylate particles by photoinitiated precipitation polymerization in different solvent mixtures**. *Macromolecules* 2009, **42**(13):4436-4442.
66. Wang J, Cormack PAG, Sherrington DC, Khoshdel E: **Monodisperse, molecularly imprinted polymer microspheres prepared by precipitation polymerization for affinity separation applications**. *Angewandte Chemie International Edition* 2003, **42**(43):5336-5338.
67. Shi Y, Lv H, Lu X, Huang Y, Zhang Y, Xue W: **Uniform molecularly imprinted poly(methacrylic acid) nanospheres prepared by precipitation polymerization: the control of particle features suitable for sustained release of gatifloxacin**. *Journal of Materials Chemistry* 2012, **22**(9):3889-3898.
68. Hansen CM: **Solubility parameters - an introduction**. En: *Hansen Solubility Parameters: A User's Handbook*. Editado por Hansen CM, 2 edn. Boca Raton: CRC Press; 2007: 1-27.
69. Hansen CM: **Three-dimensional solubility parameter-key to paint-component affinities: I. solvents, plasticizers, polymers, and resins**. *Journal of Paint Technology* 1967, **39**(505):104-117.
70. Yan Q, Zhao T, Bai Y, Zhang F, Yang W: **Precipitation polymerization in acetic acid: study of the solvent effect on the morphology of poly(divinylbenzene)**. *The Journal of Physical Chemistry B* 2009, **113**(10):3008-3014.
71. Shim SE, Yang S, Jin MJ, Chang YH, Choe S: **Effect of the polymerization parameters on the morphology and spherical particle size of poly(styrene-co-divinylbenzene) prepared by precipitation polymerization**. *Colloid and Polymer Science* 2004, **283**(1):41-48.
72. Li GL, Moehwald H, Shchukin DG: **Precipitation polymerization for fabrication of complex core-shell hybrid particles and hollow structures**. *Chemical Society Reviews* 2013, **42**(8):3628-3646.
73. Pardeshi S, Dhodapkar R, Kumar A: **Molecularly imprinted microspheres and nanoparticles prepared using precipitation polymerisation method for selective extraction of gallic acid from *Emblica officinalis***. *Food Chemistry* 2014, **146**:385-393.
74. Li WH, Stover HDH: **Porous monodisperse poly(divinylbenzene) microspheres by precipitation polymerization**. *Journal of Polymer Science Part A: Polymer Chemistry* 1998, **36**(10):1543-1551.
75. Turiel E, Tadeo JL, Cormack PAG, Martin-Esteban A: **HPLC imprinted-stationary phase prepared by precipitation polymerization for the determination of thiabendazole in fruit**. *Analyst* 2005, **130**(12):1601-1607.
76. Valero-Navarro A, Gomez-Romero M, Fernandez-Sanchez JF, Cormack PAG, Segura-Carretero A, Fernandez-Gutierrez A: **Synthesis of caffeic acid molecularly imprinted polymer microspheres and high-performance liquid chromatography evaluation of their sorption properties**. *Journal of Chromatography A* 2011, **1218**(41):7289-7296.

77. Lai JP, Xie L, Sun H, Chen F: **Synthesis and evaluation of molecularly imprinted polymeric microspheres for highly selective extraction of an anti-AIDS drug emtricitabine**. *Analytical and Bioanalytical Chemistry* 2013, **405**(12):4269-4275.
78. Tamayo FG, Casillas JL, Martin-Esteban A: **Highly selective fenuron-imprinted polymer with a homogeneous binding site distribution prepared by precipitation polymerization and its application to the clean-up of fenuron in plant samples**. *Analytica Chimica Acta* 2003, **482**(2):165-173.
79. Yamak HB: **Emulsion polymerization: effects of polymerization variables on the properties of vinyl acetate based emulsion polymers**. En: *Polymer Science*. Editado por Yilmaz F, 1 edn. http://www.intechopen.com/books/polymer-science/emulsion-polymerization-effects-of-polymerization-variables-on-the-properties-of-vinyl-acetate-based **Consulta:** 23-11-2015: InTech; 2013: 35-72.
80. Dvorakova G, Haschick R, Klapper M, Muellen K, Biffis A: **Nonaqueous emulsion polymerization: A practical synthetic route for the production of molecularly imprinted nanospheres**. *Journal of Polymer Science Part A: Polymer Chemistry* 2013, **51**(2):267-274.
81. Curcio P, Zandanel C, Wagner A, Mioskowski C, Baati R: **Semi-covalent surface molecular imprinting of polymers by one-stage mini-emulsion polymerization: glucopyranoside as a model analyte**. *Macromolecular Bioscience* 2009, **9**(6):596-604.
82. Bompart M, Haupt K: **Molecularly imprinted polymers and controlled/living radical polymerization**. *Australian Journal of Chemistry* 2009, **62**(8):751-761.
83. Otsu T, Yoshida M: **Role of initiator-transfer agent-terminator (iniferter) in radical polymerizations: polymer design by organic disulfides as iniferters**. *Macromolecular Rapid Communications* 1982, **3**(2):127-132.
84. Otsu T: **Iniferter concept and living radical polymerization**. *Journal of Polymer Science Part A: Polymer Chemistry* 2000, **38**(12):2121-2136.
85. Zourob M, Mohr S, Mayes AG, Macaskill A, Perez-Moral N, Fielden PR, Goddard NJ: **A micro-reactor for preparing uniform molecularly imprinted polymer beads**. *Lab on a Chip* 2006, **6**(2):296-301.
86. Moczko E, Guerreiro A, Piletska E, Piletsky S: **PEG-stabilized core-shell surface-imprinted nanoparticles**. *Langmuir* 2013, **29**(31):9891-9896.
87. Chianella I, Guerreiro A, Moczko E, Caygill JS, Piletska EV, De Vargas Sansalvador IMP, Whitcombe MJ, Piletsky SA: **Direct replacement of antibodies with molecularly imprinted polymer nanoparticles in ELISA-development of a novel assay for vancomycin**. *Analytical Chemistry* 2013, **85**(17):8462-8468.
88. Altintas Z, Guerreiro A, Piletsky SA, Tothill IE: **NanoMIP based optical sensor for pharmaceuticals monitoring**. *Sensors and Actuators B* 2015, **213**:305-313.
89. Karim K, Giannoudi L, Piletska E, Chianella I, Henry OYF, Laitenberger P, Piletsky SA, Cowen T: **Development of MIP sensor for monitoring propofol in clinical procedures**. *Journal of the Chinese Advanced Materials Society* 2015, **3**(3):149-160.

90. Basozabal I, Guerreiro A, Gomez-Caballero A, Goicolea MA, Barrio RJ: **Direct potentiometric quantification of histamine using solid-phase imprinted nanoparticles as recognition elements**. *Biosensors and Bioelectronics* 2014, **58**:138-144.
91. Altintas Z, Gittens M, Guerreiro A, Thompson KA, Walker J, Piletsky S, Tothill IE: **Detection of waterborne viruses using high affinity molecularly imprinted polymers**. *Analytical Chemistry* 2015, **87**(13):6801-6807.
92. Gurtova O, Ye L, Chmilenko F: **Potentiometric propranolol-selective sensor based on molecularly imprinted polymer**. *Analytical and Bioanalytical Chemistry* 2013, **405**(1):287-295.
93. Liang RN, Song DA, Zhang RM, Qin W: **Potentiometric sensing of neutral species based on a uniform-sized molecularly imprinted polymer as a receptor**. *Angewandte Chemie International Edition* 2010, **49**(14):2556-2559.
94. Ye L, Cormack PAG, Mosbach K: **Molecularly imprinted monodisperse microspheres for competitive radioassay**. *Analytical Communications* 1999, **36**(2):35-38.
95. Ye L, Weiss R, Mosbach K: **Synthesis and characterization of molecularly imprinted microspheres**. *Macromolecules* 2000, **33**(22):8239-8245.
96. Miller-Chou BA, Koenig JL: **A review of polymer dissolution**. *Progress in Polymer Science* 2003, **28**(8):1223-1270.
97. **The official Hansen solubility parameter site.** http://hansen-solubility.com/ **Consulta**: 23.11.2015
98. Lanza F, Hall AJ, Sellergren B, Bereczki A, Horvai G, Bayoudh S, Cormack PAG, Sherrington DC: **Development of a semiautomated procedure for the synthesis and evaluation of molecularly imprinted polymers applied to the search for functional monomers for phenytoin and nifedipine**. *Analytica Chimica Acta* 2001, **435**(1):91-106.
99. Martin-Esteban A: **Molecularly imprinted polymers: new molecular recognition materials for selective solid-phase extraction of organic compounds**. *Fresenius Journal of Analytical Chemistry* 2001, **370**(7):795-802.
100. Komiyama M, Takeuchi T, Mukawa T, Asanuma H: **Experimental methods (1) - procedures of molecular imprinting**. En: *Molecular imprinting from fundamentals to applications*. Editado por Komiyama M, Takeuchi T, Mukawa T, Asanuma H, 1 edn. Weinheim: WILEY-VCH Verlag GmbH & Co. KGaA; 2003: 21-47.
101. Chen L, Xu S, Li J: **Recent advances in molecular imprinting technology: current status, challenges and highlighted applications**. *Chemical Society Reviews* 2011, **40**(5):2922-2942.
102. Wei X, Zhou Z, Hao T, Li H, Yan Y: **Molecularly imprinted polymer nanospheres based on Mn-doped ZnS QDs via precipitation polymerization for room-temperature phosphorescence probing of 2,6-dichlorophenol**. *RSC Advances* 2015, **5**(26):19799-19806.

103. Chauhan A, Bhatia T, Gupta MK, Pandey P, Pandey V, Saxena PN, Mudiam MKR: **Imprinted nanospheres based on precipitation polymerization for the simultaneous extraction of six urinary benzene metabolites from urine followed by injector port silylation and gas chromatography-tandem mass spectrometric analysis**. *Journal of Chromatography B* 2015, **1001**:66-74.
104. Su L, Guo X, Han S: **Preparation and evaluation of vanillin molecularly imprinted polymer microspheres by reversible addition-fragmentation chain transfer precipitation polymerization**. *Analytical Methods* 2014, **6**(8):2512-2517.
105. Ebrahimzadeh H, Dehghani Z, Asgharinezhad AA, Shekari N, Molaei K: **Determination of haloperidol in biological samples using molecular imprinted polymer nanoparticles followed by HPLC-DAD detection**. *International Journal of Pharmaceutics* 2013, **453**(2):601-609.
106. Yang B, Zhang T, Tan W, Liu P, Ding Z, Cao Q: **Determination of rhodium by resonance light-scattering technique coupled with solid phase extraction using Rh(III) ion-imprinted polymers as sorbent**. *Talanta* 2013, **105**:124-130.
107. Shamsipur M, Rajabi HR: **Flame photometric determination of cesium ion after its preconcentration with nanoparticles imprinted with the cesium-dibenzo-24-crown-8 complex**. *Microchimica Acta* 2013, **180**(3-4):243-252.
108. Ma Y, Pan G, Zhang Y, Guo X, Zhang H: **Narrowly dispersed hydrophilic molecularly imprinted polymer nanoparticles for efficient molecular recognition in real aqueous samples including river water, milk, and bovine serum**. *Angewandte Chemie International Edition* 2013, **52**(5):1511-1514.
109. Cao H, Xu F, Li DX, Zhang XG, Yu J-S: **Preparation and performance valuation of high selective molecularly imprinted polymers for malachite green**. *Research on Chemical Intermediates* 2013, **39**(6):2321-2337.
110. Dai CM, Zhang J, Zhang YL, Zhou XF, Duan YP, Liu SG: **Selective removal of acidic pharmaceuticals from contaminated lake water using multi-templates molecularly imprinted polymer**. *Chemical Engineering Journal* 2012, **211-212**:302-309.
111. Ge S, Zhao P, Yan M, Zang D, Yu J: **Multi-branch chemiluminescence-molecular imprinting sensor for sequential determination of carbofuran and omethoate in foodstuff**. *Analytical Methods* 2012, **4**(10):3150-3156.
112. Liu H, Lei X, Zhai Y, Li L: **Electrospun nanofiber membranes containing molecularly imprinted polymer (MIP) for rhodamine B (RhB)**. *Advances in Chemical Engineering and Science* 2012, **2**(2):266-274.
113. Chen C, Zhang X, Long Z, Zhang J, Zheng C: **Molecularly imprinted dispersive solid-phase microextraction for determination of sulfamethazine by capillary electrophoresis**. *Microchimica Acta* 2012, **178**(3-4):293-299.
114. Lulinski P, Maciejewska D: **Effective separation of dopamine from bananas on 2-(3,4-dimethoxyphenyl)ethylamine imprinted polymer**. *Journal of Separation Science* 2012, **35**(8):1050-1057.

115. Curcio M, Cirillo G, Parisi OI, Iemma F, Picci N, Puoci F: **Quercetin-imprinted nanospheres as novel drug delivery devices**. *Journal of Functional Biomaterials* 2012, **3**:269-282.
116. Qiu H, Luo C, Sun M, Lu F, Fan L, Li X: **A novel chemiluminescence sensor for determination of quercetin based on molecularly imprinted polymeric microspheres**. *Food Chemistry* 2012, **134**(1):469-473.
117. Jiang X, Liu Z: **Uniformly-sized, molecularly imprinted polymers for naproxen by precipitation polymerization**. *Advanced Materials Research* 2012, **399-401**:713-717.
118. Dai CM, Zhou XF, Zhang YL, Liu SG, Zhang J: **Synthesis by precipitation polymerization of molecularly imprinted polymer for the selective extraction of diclofenac from water samples**. *Journal of Hazardous Materials* 2011, **198**:175-181.
119. Zhang W, Zhang H, Zhang Q, Cui Y, Wu Z, Zheng R, Liu L: **Molecularly imprinted polymers prepared by precipitation polymerization and used for inducing crystallization of oleanolic acid in supercritical CO2**. *Separation and Purification Technology* 2011, **81**(3):411-417.
120. Zhu L, Fu S, Li L, Zhu J: **Characterization and evaluation of binding properties of salvianolic acid A imprinted polymers prepared by precipitation polymerization**. *Advanced Materials Research* 2011, **239-242**:2423-2426.
121. Xu S, Li J, Chen L: **Molecularly imprinted polymers by reversible addition-fragmentation chain transfer precipitation polymerization for preconcentration of atrazine in food matrices**. *Talanta* 2011, **85**(1):282-289.
122. Rodriguez E, Navarro-Villoslada F, Benito-Pena E, Marazuela MD, Moreno-Bondi MC: **Multiresidue determination of ultratrace levels of fluoroquinolone antimicrobials in drinking and aquaculture water samples by automated online molecularly imprinted solid phase extraction and liquid chromatography**. *Analytical Chemistry* 2011, **83**(6):2046-2055.
123. Prieto A, Schrader S, Bauer C, Moeder M: **Synthesis of a molecularly imprinted polymer and its application for microextraction by packed sorbent for the determination of fluoroquinolone related compounds in water**. *Analytica Chimica Acta* 2011, **685**(2):146-152.
124. Shamsipur M, Besharati-Seidani A, Fasihi J, Sharghi H: **Synthesis and characterization of novel ion-imprinted polymeric nanoparticles for very fast and highly selective recognition of copper(II) ions**. *Talanta* 2010, **83**(2):674-681.
125. Xie C, Zhou H, Gao S, Li H: **Molecular imprinting method for on-line enrichment and chemiluminescent detection of the organophosphate pesticide triazophos**. *Microchimica Acta* 2010, **171**(3-4):355-362.
126. Wang C, Javadi A, Ghaffari M, Gong S: **A pH-sensitive molecularly imprinted nanospheres/hydrogel composite as a coating for implantable biosensors**. *Biomaterials* 2010, **31**(18):4944-4951.

127. Long C, Mai Z, Yang Y, Zhu B, Xu X, Lu L, Zou X: **Synthesis and characterization of a novel molecularly imprinted polymer for simultaneous extraction and determination of water-soluble and fat-soluble synthetic colorants in chilli products by solid phase extraction and high performance liquid chromatography**. *Journal of Chromatography A* 2009, **1216**(47):8379-8385.
128. Jiang M, Shi Y, Zhang RL, Shi CH, Peng Y, Huang Z, Lu B: **Selective molecularly imprinted stationary phases for bisphenol A analysis prepared by modified precipitation polymerization**. *Journal of Separation Science* 2009, **32**(19):3265-3273.
129. Nemulenzi O, Mhaka B, Cukrowska E, Ramstrom O, Tutu H, Chimuka L: **Potential of combining of liquid membranes and molecularly imprinted polymers in extraction of 17-estradiol from aqueous samples**. *Journal of Separation Science* 2009, **32**(11):1941-1948.
130. Chaitidou S, Kotrotsiou O, Kiparissides C: **On the synthesis and rebinding properties of [Co(C2H3O2)2(z-Histidine)] imprinted polymers prepared by precipitation polymerization**. *Materials Science and Engineering C* 2009, **29**(4):1415-1421.
131. Cacho C, Turiel E, Perez-Conde C: **Molecularly imprinted polymers: An analytical tool for the determination of benzimidazole compounds in water samples**. *Talanta* 2009, **78**(3):1029-1035.
132. Long C, Mai Z, Yang Y, Zhu B, Xu X, Lu L, Zou X: **Determination of multi-residue for malachite green, gentian violet and their metabolites in aquatic products by high-performance liquid chromatography coupled with molecularly imprinted solid-phase extraction**. *Journal of Chromatography A* 2009, **1216**(12):2275-2281.
133. Javanbakht M, Fard SE, Abdouss M, Mohammadi A, Ganjali MR, Norouzi P, Safaraliee L: **A biomimetic potentiometric sensor using molecularly imprinted polymer for the cetirizine assay in tablets and biological fluids**. *Electroanalysis* 2008, **20**(18):2023-2030.
134. Yao W, Fang Y, Li G, Gao Z, Cheng Y: **Adsorption of carbaryl using molecularly imprinted microspheres prepared by precipitation polymerization**. *Polymers for Advanced Technologies* 2008, **19**(7):812-816.
135. Javanbakht M, Fard SE, Mohammadi A, Abdouss M, Ganjali MR, Norouzi P, Safaraliee L: **Molecularly imprinted polymer based potentiometric sensor for the determination of hydroxyzine in tablets and biological fluids**. *Analytica Chimica Acta* 2008, **612**(1):65-74.
136. Turiel E, Martin-Esteban A, Tadeo JL: **Molecular imprinting-based separation methods for selective analysis of fluoroquinolones in soils**. *Journal of Chromatography A* 2007, **1172**(2):97-104.
137. Cacho C, Turiel E, Martin-Esteban A, Ayala D, Perez-Conde C: **Semi-covalent imprinted polymer using propazine methacrylate as template molecule for the clean-up of triazines in soil and vegetable samples**. *Journal of Chromatography A* 2006, **1114**(2):255-262.

138. Carabias-Martinez R, Rodriguez-Gonzalo E, Herrero-Hernandez E: **Determination of triazines and dealkylated and hydroxylated metabolites in river water using a propazine-imprinted polymer**. *Journal of Chromatography A* 2005, **1085**(2):199-206.
139. Daniel S, Rao PP, Rao TP: **Investigation of different polymerization methods on the analytical performance of palladium(II) ion imprinted polymer materials**. *Analytica Chimica Acta* 2005, **536**(1-2):197-206.
140. Puoci F, Iemma F, Muzzalupo R, Spizzirri UG, Trombino S, Cassano R, Picci N: **Spherical molecularly imprinted polymers (SMIPs) via a novel precipitation polymerization in the controlled delivery of sulfasalazine**. *Macromolecular Bioscience* 2004, **4**(1):22-26.
141. Blanco-Lopez MC, Lobo-Castañón MJ, Miranda-Ordieres AJ, Tuñón-Blanco P: **Electrochemical sensors based on molecularly imprinted polymers**. *Trends in Analytical Chemistry* 2004, **23**(1):36-48.
142. Li K, Stover HDH: **Synthesis of monodisperse poly(divinylbenzene) microspheres**. *Journal of Polymer Science Part A: Polymer Chemistry* 1993, **31**(13):3257-3263.
143. Coates J: **Interpretation of infrared spectra, a practical approach.** En: *Encyclopedia of analytical chemistry*. Editado por Meyers RA, 1 edn. Chichester: John Wiley & Sons Ltd; 2000: 10815-10837.
144. Stuart BH: **Polymers**. En: *Infrared spectroscopy-fundamentals and applications*. Editado por Stuart BH, 1 edn. Chichester: John Wiley & Sons; 2004: 113-135.
145. Koenig JL: **Infrared and raman spectroscopy of polymers**. En: *Infrared and raman spectroscopy of polymers*. Editado por Koenig JL, 1 edn. Shawbury: Smithers Rapra Press; 2001: 16-39.
146. Koenig JL: **Fourier transform infrared spectroscopy of polymers**. En: *Spectroscopy: NMR, fluorescence, FT-IR*. Editado por Koenig JL, vol. 54, 1 edn. Heidelberg: Springer; 1984: 87-154.
147. Kumar R, Agrawal YK: **Analytical strategies for characterization of molecular imprinted polymers: a current review**. *International Journal of ChemTech Research* 2014, **6**(2):1162-1167.
148. Skoog DA, Holler FJ, Crouch SR: **Principios de análisis instrumental**. En: *Principios de análisis instrumental*. Editado por Skoog DAH, F. James, Crouch SR, 6 edn. Madrid: Ediciones Paraninfo S.A.; 2009: 430-455.
149. Smith BC: **Introduction to infrared spectroscopy**. En: *Fundamentals of Fourier transform infrared spectroscopy*. Editado por Smith BC, 2 edn. New York: CRC Press; 2011: 1-19.
150. Dole MN, Patel PA, Sawant SD, Shedpure PS: **Advance applications of Fourier transform infrared spectroscopy**. *International Journal of Pharmaceutics* 2011, **7**(2):159-166.
151. Baggiani C, Giraudi G, Giovannoli C, Tozzi C, Anfossi L: **Adsorption isotherms of a molecular imprinted polymer prepared in the presence of a polymerizable template. Indirect evidence of the formation of template clusters in the binding site**. *Analytica Chimica Acta* 2004, **504**(1):43-52.

152. Shea KJ, Spivak DA, Sellergren B: **Polymer complements to nucleotide bases. Selective binding of adenine derivatives to imprinted polymers**. *Journal of the American Chemical Society* 1993, **115**(8):3368-3369.
153. Manesiotis P, Osmani O, McLoughlin P: **An enantio-selective chromatographic stationary phase for S-ibuprofen prepared by stoichiometric molecular imprinting**. *Journal of Materials Chemistry* 2012, **22**(22):11201-11207.
154. Basozabal I, Gomez-Caballero A, Diaz-Diaz G, Guerreiro A, Gilby S, Goicolea MA, Barrio RJ: **Rational design and chromatographic evaluation of histamine imprinted polymers optimised for solid-phase extraction of wine samples**. *Journal of Chromatography A* 2013, **1308**:45-51.
155. Sajonz P, Kele M, Zhong G, Sellergren B, Guiochon G: **Study of the thermodynamics and mass transfer kinetics of two enantiomers on a polymeric imprinted stationary phase**. *Journal of Chromatography A* 1998, **810**(1-2):1-17.
156. Sellergren B: **Molecular imprinting by noncovalent interactions. Enantioselectivity and binding capacity of polymers prepared under conditions favoring the formation of template complexes**. *Die Makromolekulare Chemie* 1989, **190**(11):2703-2711.
157. Rampey AM, Umpleby RJ, II, Rushton GT, Iseman JC, Shah RN, Shimizu KD: **Characterization of the imprint effect and the influence of imprinting conditions on affinity, capacity, and heterogeneity in molecularly imprinted polymers using the Freundlich isotherm-affinity distribution analysis**. *Analytical Chemistry* 2004, **76**(4):1123-1133.
158. Rushton GT, Karns CL, Shimizu KD: **A critical examination of the use of the Freundlich isotherm in characterizing molecularly imprinted polymers (MIPs)**. *Analytica Chimica Acta* 2005, **528**(1):107-113.
159. Diñeiro Y, Menendez MI, Blanco-Lopez MC, Lobo-Castañón MJ, Miranda-Ordieres AJ, Tuñón-Blanco P: **Computational predictions and experimental affinity distributions for a homovanillic acid molecularly imprinted polymer**. *Biosensors and Bioelectronics* 2006, **22**(3):364-371.
160. Ng SM, Narayanaswamy R: **Molecularly imprinted polymers as optical sensing receptors: Correlation between analytical signals and binding isotherms**. *Analytica Chimica Acta* 2011, **703**(2):226-233.
161. Umpleby RJ, Baxter SC, Rampey AM, Rushton GT, Chen Y, Shimizu KD: **Characterization of the heterogeneous binding site affinity distributions in molecularly imprinted polymers**. *Journal of Chromatography B* 2004, **804**(1):141-149.
162. Shimizu KD: **Binding isotherms**. En: *Molecularly imprinted materials science and technology*. Editado por Yan M, Ramström O, 1 edn. New York: Marcel Dekker; 2005: 419-434.

163. Kim H, Guiochon G: **Adsorption on molecularly imprinted polymers of structural analogues of a template. Single-component adsorption isotherm data**. *Analytical Chemistry* 2005, **77**(19):6415-6425.
164. Ma W, Dai J, Dai X, Da Z, Yan Y: **Core-shell molecularly imprinted polymers based on magnetic chitosan microspheres for chloramphenicol selective adsorption**. *Chemical Monthly* 2015, **146**(3):465-474.
165. Djozan D, Mahkam M, Ebrahimi B: **Preparation and binding study of solid-phase microextraction fiber on the basis of ametryn-imprinted polymer. Application to the selective extraction of persistent triazine herbicides in tap water, rice, maize, and onion**. *Journal of Chromatography A* 2009, **1216**(12):2211-2219.
166. Djozan D, Baheri T: **Preparation and evaluation of solid-phase microextraction fibers based on monolithic molecularly imprinted polymers for selective extraction of diacetylmorphine and analogous compounds**. *Journal of Chromatography A* 2007, **1166**(1-2):16-23.
167. Tamayo FG, Casillas JL, Martin-Esteban A: **Evaluation of new selective molecularly imprinted polymers prepared by precipitation polymerization for the extraction of phenylurea herbicides**. *Journal of Chromatography A* 2005, **1069**(2):173-181.
168. Cacho C, Turiel E, Martin-Esteban A, Perez-Conde C, Camara C: **Characterization and quality assessment of binding sites on a propazine-imprinted polymer prepared by precipitation polymerization**. *Journal of Chromatography B* 2004, **802**(2):347-353.
169. Zhu X, Yang J, Su Q, Cai J, Gao Y: **Molecularly imprinted polymer for monocrotophos and its binding characteristics for organophosphorus pesticides**. *Analytical Chemistry* 2005, **95**(11-12):877-884.
170. Zhao Z, Fu D, Zhang B: **Novel molecularly imprinted polymer prepared by palygorskite as support for selective adsorption of bisphenol A in aqueous solution**. *Desalination and water treatment* 2015:DOI: 10.1080/19443994.19442015.11052989.
171. Spivak DA, Campbell J: **Systematic study of steric and spatial contributions to molecular recognition by non-covalent imprinted polymers**. *Analyst* 2001, **126**(6):793-797.
172. Umpleby RJ, II, Baxter SC, Chen Y, Shah RN, Shimizu KD: **Characterization of molecularly imprinted polymers with the Langmuir-Freundlich isotherm**. *Analytical Chemistry* 2001, **73**(19):4584-4591.
173. Shamsipur M, Yousefi M, Hosseini M, Ganjali MR: **Lanthanum(III) PVC membrane electrodes based on 1,3,5-trithiacyclohexane**. *Analytical Chemistry* 2002, **74**(21):5538-5543.
174. Prathish KP, Prasad K, Rao TP, Suryanarayana MVS: **Molecularly imprinted polymer-based potentiometric sensor for degradation product of chemical warfare agents**. *Talanta* 2007, **71**(5):1976-1980.

175. Sadeghi HB, Ebrahimi SA, Tamaddon A, Bozorgvar F, Afifinia H, Almasian N, Mollaei S: **Potentiometric sensing of lamotrigine based on molecularly imprinted polymers**. *Electroanalysis* 2011, **23**(11):2716-2723.
176. Gyurcsanyi RE, Pergel E, Nagy R, Kapui I, Lan BTT, Toth K, Bitter I, Lindner E: **Direct evidence of ionic fluxes across ion-selective membranes: a scanning electrochemical microscopic and potentiometric study**. *Analytical Chemistry* 2001, **73**(9):2104-2111.
177. Sokalski T, Ceresa A, Zwickl T, Pretsch E: **Large improvement of the lower detection limit of ion-selective polymer membrane electrodes**. *Journal of the American Chemical Society* 1997, **119**(46):11347-11348.
178. Buck RP, Cosofret V: **Recommended procedures for calibration of ion-selective electrodes**. *Pure and Applied Chemistry* 1993, **65**(8):1849-1858.
179. Buck RP, Lindner E: **Recommendations for nomenclature of ion-selective electrodes**. *Pure and Applied Chemistry* 1994, **66**(12):2527-2536.
180. Joint committee for guides in metrology (JCGM): **VIM-vocabulario internacional de metrología conceptos fundamentales y generales, y términos asociados**. En: *JCGM 200:2012*. http://www.cem.es/ **Consulta:** 23.11.2015: Centro Español de metrología (CEM); 2012.
181. Hernández-Hernández L, Gónzalez-Pérez C: **Métodos potenciométricos**. En: *Introducción al análisis instrumental*. Editado por Hernández-Hernández L, Gónzalez-Pérez C, 1 edn. Barcelona: Ariel Ciencia; 2002: 233-265.
182. Umezawa Y, Buhlmann P, Umezawa K, Tohda K, Amemiya S: **Potentiometric selectivity coefficients of ion-selective electrodes Part I. Inorganic cations**. *Pure and Applied Chemistry* 2000, **72**(10):1851-2082.
183. Guilbault GG: **Recommendations for publishing manuscripts on ion-selective electrodes**. *Pure and Applied Chemistry* 1981, **53**(10):1907-1912.
184. Consejo General de Colegios Oficiales de Farmacéuticos: **Análisis clínicos**. En: *Catálogo de especialidades farmaceúticas*. Editado por Consejo General de Colegios Oficiales de Farmacéuticos, 1 edn. Madrid: Einsa; 1997: 2071-2082.
185. Unceta N, Gomez-Caballero A, Garcia D, Diaz G, Guerreiro A, Piletsky S, Goicolea MA, Barrio RJ: **Enantioselective extraction of (+)-(S)-citalopram and its main metabolites using a tailor-made stir bar chiral imprinted polymer for their LC-ESI-MS/MS quantitation in urine samples**. *Talanta* 2013, **116**:448-453.

Chapter 4

Development of chiral imprinted stationary phases for the chromatographic resolution of citalopram enantiomers

This Page Intentionally Left Blank

Contents

This Page Intentionally Left Blank

1. Introduction

Chiral separation by liquid chromatography represents the most common technique used for the resolution of enantiomers. The different existing approaches for the separation of enantiomers, can be classified into non-chiral stationary phase based (non-CSP) or chiral stationary phase (CSP) based ones. The formers involve the derivatisation of the analyte with a chiral reagent, obtaining two different diastereomers which can be easily separated in a non-CSP, or the use of chiral mobile phase additives. As regards CSP, they can be employed to directly separate enantiomers or even to separate such compounds after derivatisation with a non-chiral reagent [1].

One direct and straightforward approach for the development of new CSP is the use of small organic compounds as chiral selectors, immobilised on solid support such as silica beads. In this regard, cyclodextrins [2, 3], proteins [4], chiral crown ethers [5, 6], macrocyclic glycopeptides [7] or polysaccharides [8] have been successfully used as chiral selectors. In the pharmaceutical field, the most popular CSP are the ones based on polysaccharides due to their high site density and broad applicability [8-11]. The main disadvantages of these CSP are their limited predictability of the elution order and separability [12]. Alternatively, Molecularly Imprinted Polymers (MIP) may be employed, which consist in synthetic polymers with predetermined selectivity. Since chiral MIP are made specific for a target enantiomer, using it as template in the

polymer synthesis, stronger retention of this enantiomer may be later expected [13]. The first application of MIP for enantiomer resolution by liquid chromatography was carried out by Sellergren and Nilsson in 1989 [14]. Since then, the use of molecular imprinting in chiral chromatography has been widely extended [15], mainly due to their mechanical and chemical stability, reproducibility, high selectivity, predictable elution order and relatively low cost [12].

Chiral MIP have been synthesised by both covalent [16] and non-covalent approaches [17]. In the covalent approach, the exact stoichiometric template to monomer ratio is employed, what means that functional groups for binding the analyte are exclusively located inside the imprinted cavities of the resulting polymer [16]. In contrast, polymers developed by the non-covalent approach are synthesised employing large amounts of monomers in the polymerisation mixture, in order to favour the establishment of the template-functional monomer adduct. Due to this excess, there may be functional monomers, randomly distributed in the polymer matrix, outside the binding sites. These monomers are responsible for non-specific binding interactions between the target ligand and the functional monomer. Nevertheless, as the association/dissociation kinetics of non-covalent MIP is faster than those polymers synthesised by the covalent approach, non-covalent MIP are preferably better for stationary phases in chromatographic applications [1].

Amino acids [14, 18-21], peptides [19, 22] as well as drugs such as timolol [23], naproxen [24], ibuprofen [25], ephedrine [26, 27] and benzyl benzodiazepine [28] have been imprinted by the non-covalent approach to develop chiral stationary phases based on MIP. More recently, chiral MIP research has focused on the separation of racemates using chiral monomers as cross-linkers [21] or even as a functional monomers [29-31]. This approach aims to finish with the need of using a single target enantiomer as template in the polymer synthesis, allowing for the use of the racemic mixture and thereby reducing the costs.

Depending on the MIP application, different methodologies can be employed to synthesise these materials (table 4.1), giving rise to different physical forms of MIP. So far, most of reports concerning MIP describe the synthesis of these materials by conventional free radical polymerisation (FRP), due to its higher flexibility in terms of reagent purity, experimental conditions or monomer availability. Alternatively, Reversible-Deactivation Radical Polymerisation (RDRP) provides a new polymerisation strategy that aims overcoming common disadvantages of FRP such as the lack of control over the size, architecture or molecular weight of the polymers [32].

Table 4.1. Benefits and limitations of the different methodologies used in the synthesis of MIP.

Methodology	Benefits	Limitations
Bulk polymerisation	- Simplicity and universality. - Does not require particular skills or sophisticated instrumentation.	- Tedious procedures of grinding, sieving and column packing. - Irregular particle size and shape, low performance.
Suspension polymerisation	- Spherical particles. - Highly reproducible results.	- Phase partitioning of complicated systems. - Water is incompatible with most imprinted procedures. - Surfactant required.
Multi-step swelling polymerisation	- Monodisperse beads of controlled diameter. - Excellent particle for HPLC	- Complicated procedures and reaction conditions. - Need for aqueous emulsions.
Precipitation polymerisation	- Imprinted microspheres. - Uniform size and high yields.	- Large amount of template. - High dilution factor.
Surface polymerisation	- Monodisperse product. - Thin imprinted layers.	- Complicated system. - Time consuming.
***In-situ* polymerisation**	- One-step, in-situ preparation. - Cost-efficient, good porosity.	- Extensive optimisation required for each new template system.

1.1. Free radical polymerisation

MIP have been mainly synthesised by FRP so far. This is the most simple and straightforward technique for large-scale preparation of polymers involving vinylic or acrylic monomers [33]. Principally, this chain polymerisation consists of three steps, namely initiation, propagation and termination (figure 4.1). During the initiation, a small amount of an initiator is required, which is a compound that fragments under temperature or UV irradiation, leading to free radicals. The most commonly employed initiators are benzoyl peroxide and azobis(isobutyronitrile) (AIBN) [34]. Free radicals react with double bonds of vinyl monomers resulting in intermediate free radical species. Thereafter, the propagation starts, where the intermediate free radical species at the end of the growing chains react with single monomers allowing the chain lengthen. There are two main mechanisms for termination: by recombination of two radical species or by disproportionation obtaining a double bond and C-H bond at the chain terminus. Besides this, termination can also take place due to: interaction of two active chain ends, the reaction of an active chain end with an initiator radical, termination by transfer of the active centre to another molecule (solvent, initiator, monomer or template), or interaction with impurities such as oxygen or polymerisation inhibitors.

Despite its advantages arising from its flexibility in terms of reagent purity and experimental conditions, FRP has some major drawbacks, such as the lack of control over initiation, propagation, termination and chain transfer reaction steps during polymerisation [33, 35]. These reactions determine the structure of the polymer chain and therefore the molecular weight distribution, sequence distribution and stereoregularity. The lack of control of the polymer structure favours the synthesis of MIP which suffer from slow mass transfer, non uniform binding sites, template leaching, low saturation capacity, poor site accessibility, low yield and/or high amounts of template consumption [36].

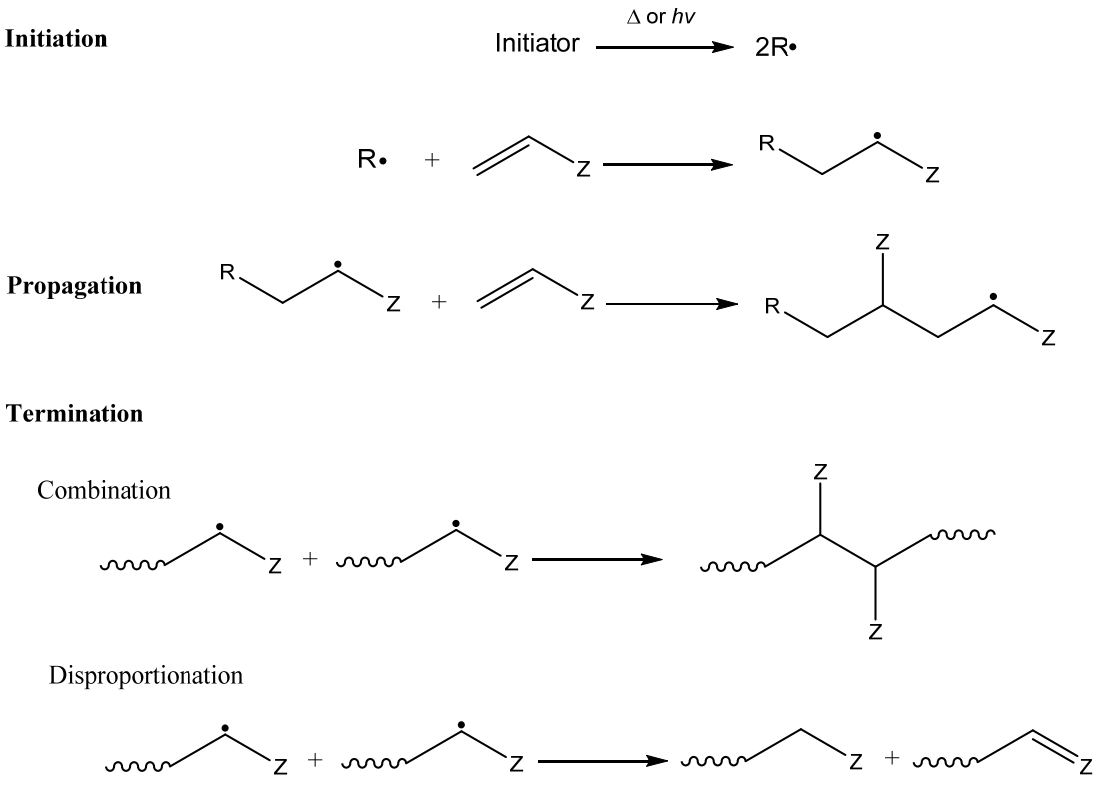

Figure 4.1. Free radical polymerisation mechanism.

FRP has been almost exclusively used in bulk polymerisation to synthesise MIP based stationary phases. This technique leads to irregular polymer particles due to grinding and sieving processes after radical synthesis of bulk monoliths. However, despite its advantages, such as its simplicity and low cost, this procedure is far from ideal since the process is time-consuming and often leads to highly irregular MIP particles with variable dimensions and poor yield. In addition, it causes a substantial loss of useful polymer that can be estimated between 50-75% of the initial powder [37].

In order to have a better control of MIP particle morphology and to provide materials having improved chromatographic characteristics, different strategies such as suspension polymerisation [38], multi-swelling polymerisation [39], precipitation polymerisation [40] and imprinting core-shell particles [41] have been employed. However, the conditions required to generate high affinity binding sites are, in most cases, incompatible with the conditions required to obtain the desired particle characteristics (size, porosity, pore volume and surface area) [42].

1.2. Reversible-deactivation radical polymerisation

To overcome limitations of FRP, Reversible Deactivation Radical Polymerisation emerged (RDRP) [43]. RDRP is a type of chain polymerisation which is propagated by radicals that are deactivated reversibly, bringing them into active and dormant equilibria [44]. This polymerisation was previously known as "living" or "controlled" radical polymerisation. These terms were used to describe a set of polymerisations techniques where the chain growth of the polymer is controlled by an extremely fast, reversible activation and deactivation of reacting species. Here, the termination processes are almost non-existent and the polymerisation proceeds until all monomers are consumed, although it may further continue if more monomer is added to the mixture [35, 45]. Although the term "living" was recommended by the IUPAC in 1996 [46], for a radical polymerisation, termination by radical-radical reactions will always occur, which means that this step can never be eliminated, even when such processes are undetectable. In consequence, IUPAC does not accept the use of the word "living" for radical polymerisations, no matter how minimal the termination might be within such systems. As regards the term "controlled", its use is frequent and is most commonly applied to the synthesis conditions or under which a measurement is carried out. Because of this, it is unacceptable to use the term "controlled" by itself to describe a specific form of control without specifying what is being controlled, and the term "controlled polymerisation" cannot be used as a polymerisation type name where

the outcome is controlled by reversible-deactivation [44]. Based on these premises the IUPAC recommends the term Reversible Deactivation Radical Polymerisation (RDRP) for this type of polymerisations.

RDRP mechanisms provide polymers of controlled composition, architecture and molecular weight distribution [34, 35] since the polymer chains grow at a more constant rate than in traditional polymerisation, achieving similar chain lengths with very low polydispersity index. There are a number of properties that make RDRP advantageous over FRP:

- In traditional FRP, initiation is rather slow and some initiator is usually not consumed in the process. In RDRP reactions, due to the fast dissociation rate of iniferters, initiation is quick and all chains start growing at almost the same time, what makes it possible to control final polymer architecture.

- The lifetime of growing chain increases from about 1s in FRP to more than 1h in RDRP, thanks to the intermittent activation-deactivation processes of dormant and active radicals.

- In FRP, almost all chains are dead, whereas in RDRP, dead chain proportion is below 10%.

- Polymerisation by RDRP is usually slower than FRP, but rates may be similar if the desired molecular weight of the polymer is small enough.

- The polymerisation can be restarted at any time. One important aspect of this condition is that a block copolymer can be synthesised if a different monomer is added to the system before restarting the polymerisation.

- In FRP, termination occurs between the growing chains and the new chains that are constantly being generated due to the slow initiation kinetics and the remaining small amounts of unconsumed initiator. In early stages of RDRP, when all chains are

short, termination is more likely to happen. However, as they become longer, termination significantly decreases, mainly due to the fact that reversible deactivation becomes the controlling factor of polymerisation [47].

In FRP, the steady state concentration of propagating radicals is approximately 10^{-7} M. Taking into account the abovementioned short lifetime of growing chains, long chains are formed early in the process and as polymerisation is going by, molecular weights of new chains decrease due to monomer depletion. In contrast, in RDRP all chains are initiated at the beginning of the reaction and grow until all monomer is consumed. As a result, molecular weight increases linearly with conversion and, therefore, the molecular weight distribution is narrow. Even though in RDRP the concentration of propagating radicals is usually similar or lower than in FRP (i.e. $\leq 10^{-7}$ M), to have a high amount of living chains, in RDRP the lifetime of chains in their active state must be significantly lower ($\ll$1-10 s) than in FRP in order for all propagating species to have an equal opportunity for chain growth. Therefore, a fast equilibration between active and dormant radical must be ensured [35]. Several sub-classes of RDRP processes can be differentiated according to their mechanism, namely, nitroxide-mediated polymerisation (NMP), atom transfer radical polymerisation (ATRP), reversible addition-fragmentation chain transfer (RAFT) polymerisation and iniferter polymerisation.

1.2.1. Nitroxide-mediated polymerisation

Nitroxide-mediated polymerisation was first described in a patent application reported by Solomon *et al.* in 1985 [48], where it was reported the use of an alkoxyamine that acted as a unimolecular agent, as polymerisation initiator for producing block and end-functional polymers by NMP. The alkoxyamine provides both the reactive initiating radical and the stable mediating nitroxide radical which acts as a deactivator which allows deactivation by reversible coupling. Traditionally, nitroxides were well known as inhibitors of polymerisation and they were widely used in polymer stabilisation. These

applications are based on the capability of nitroxides to efficiently scavenge carbon-centred radicals, by combining with them at near diffusion-controlled rates, to form alkoxyamines. A simplified mechanism of NMP is shown in figure 4.2.

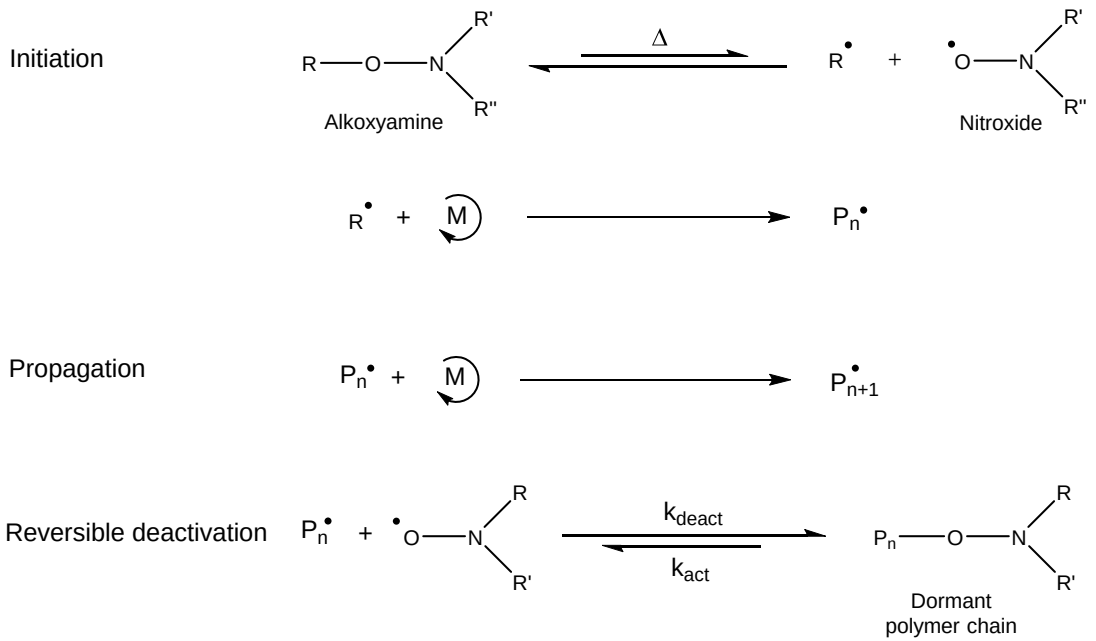

Figure 4.2. Nitroxide mediated polymerisation.

Where $P_n\bullet$ is a propagating radical (an active chain) and the nitroxide is a stable radical which acts as the deactivator, giving a dormant chain. The constant values of activation and deactivation (k_{act} and k_{deact}) depend on the structure of both the reactive radical and the nitroxide fragment. The stability of the nitroxide fragment is influenced by several factors such as the degree of the steric compression around de C-O bond in the alkoxyamine and the electronegativity or capability of forming hydrogen bonds of its substituent groups [49-51].

Although this type of polymerisation is widely used for several polymer syntheses [52, 53], concerning MIP, there is only a reported work carried out by Boonpangrak *et al.* [54]. They synthesised a cholesterol-imprinted bulk polymer via the covalent approach. They concluded that the imprinted hydrolysed MIP prepared by NMP displayed higher selective for cholesterol than that prepared by traditional radical polymerisation.

1.2.2. Atom transfer radical polymerisation

Atom transfer radical polymerisation (ATRP) differs from other RDRP techniques in the use of transition metal-catalysed reversible atom transfer to generate the propagating radicals [55]. The first reports concerning this technique were published simultaneously in 1995 by the groups of Matyjaszewski [56-58], Sawamoto [59] and Percec [60]. It was developed from the Kharasch reaction named as atom transfer radical addition (ATRA) [61], which consisted of the addition of halocarbons (RX) across alkene double bonds in a radical chain process. In contrast to ATRA reactions, ATRP requires reactivation of the first formed alkyl halide adduct with the unsaturated compound (monomer) and further reaction of the intermittently formed radical with additional monomers [62]. The general mechanism for ATRP is shown in figure 4.3.

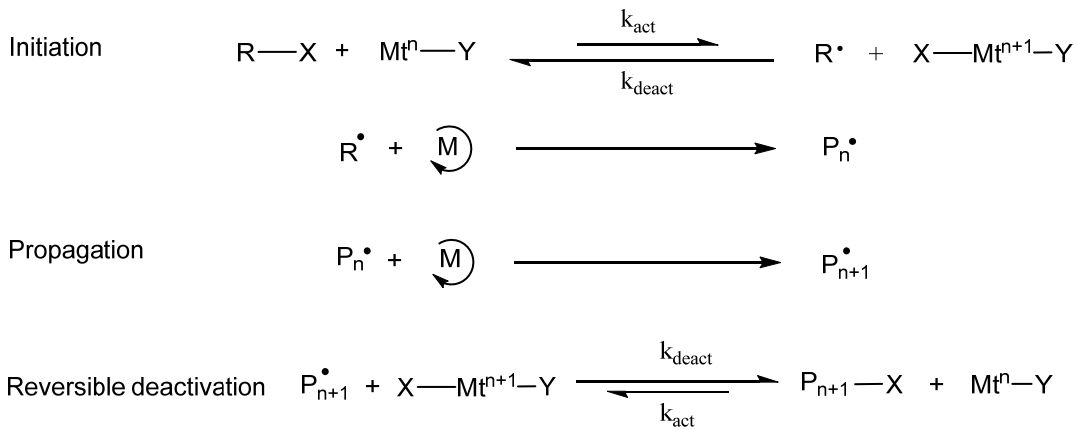

Figure 4.3. Mechanism of ATRP. The transition state metal, Mt^n, can be Ti, Mo, Re, Fe, Ru, Os, Rh, Co, Ni, Pd and Cu [47].

The active radicals are generated through a reversible redox process catalysed by a transition metal complex (Mt^n-Y where Mt^n is the metal in its lowest oxidation state and Y a ligand or a counterion) which undergoes a one electron oxidation with concomitant abstraction of a (pseudo)halogen atom, X, from a dormant species, R-X. Figure 4.4 shows most commonly employed ligands.

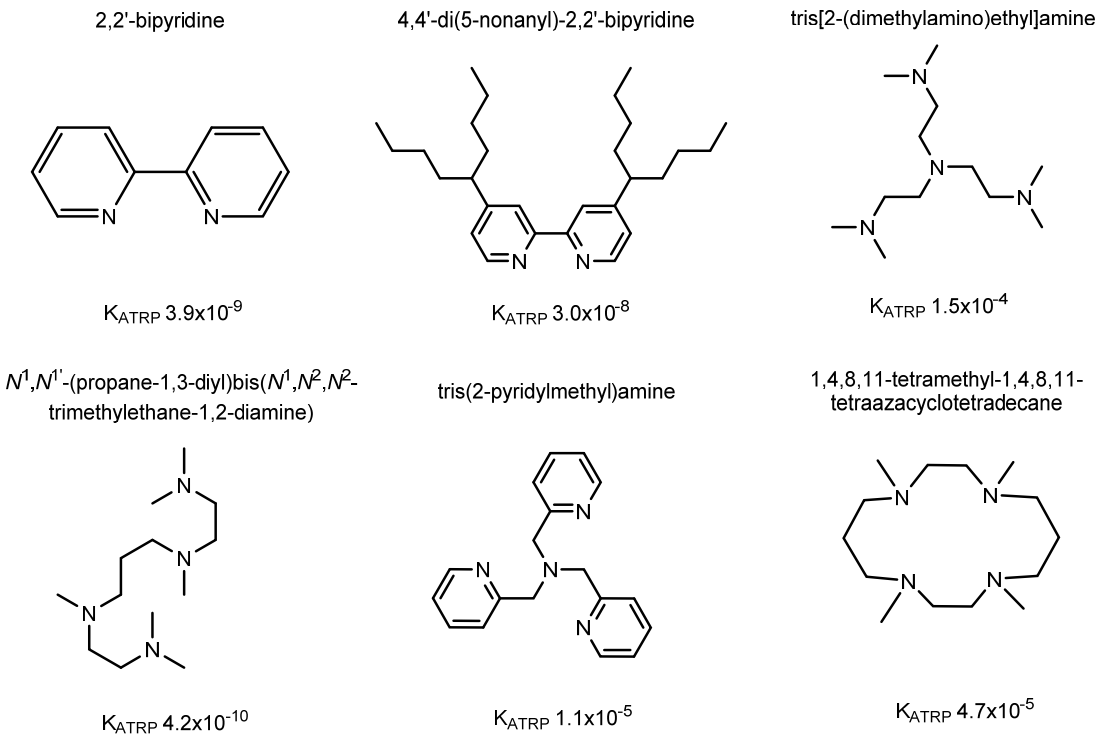

Figure 4.4. ATRP ligands and their equilibrium constants [47].

The ATRP process occurs with constant activation, k_{act}, and deactivation, k_{deact}, rates. In a similar way to conventional radical polymerisation, polymer chains grow by the addition of the intermediate radicals to monomers with a constant propagation

rate k_p. Termination reactions (k_t) also happen in ATRP, mainly through radical coupling and disproportionation; however, in a well-controlled ATRP, no more than a few percent of the polymer chains undergo termination [62].

There are different methods, based on the way to initiate ATRP polymerisation: reverse ATRP, activator generated by electron transfer (AGET) ATRP, activator regenerated by electron transfer (ARGET) ATRP, initiators for continuous activator regeneration (ICAR) ATRP, etc [55]. Among them, reverse ATRP is the most widely employed.

Reverse ATRP (figure 4.5) differs from conventional ATRP in the initiation process. In conventional ATRP initiating radicals are generated from an alkyl halide in the presence of a transition metal in its lowest oxidation state. However, in reverse ATRP, the initiator is a traditional radical initiator, e.g. AIBN which decomposes forming two radicals which, in turn, extract a halogen atom from transition-metal compound in its higher oxidation state and forms a dormant halide species and the reduced transition metal species activator. In the propagation step, equilibrium is established between propagating chains and dormant chains.

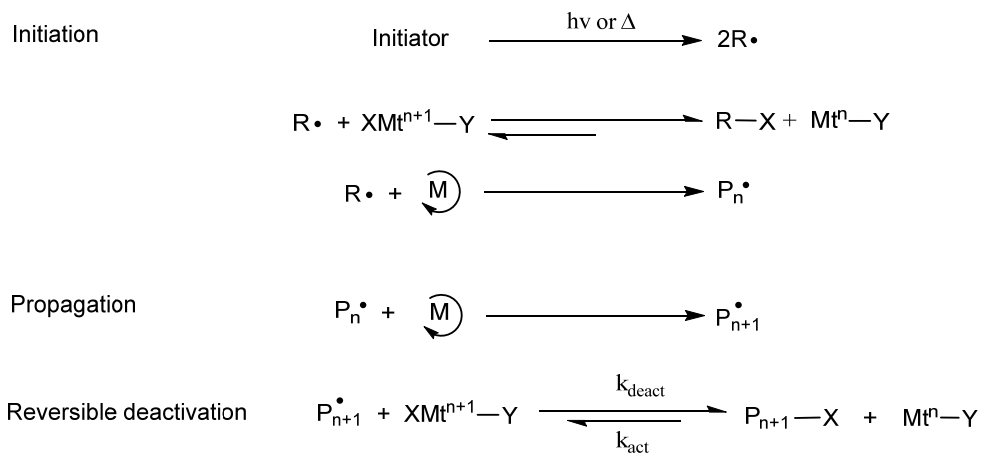

Figure 4.5. Reverse ATRP using a free radical initiator.

ATRP can be successfully applied to a great number of monomers: styrenes, (meth)acrylates, (meth)acrylamides, dienes, acrylonitrile, and other monomers that contain substituents that can stabilise the propagating radicals. However, even using the same catalysts under the same conditions, each monomer has its own equilibrium constant for its active and dormant species, which determines the polymerisation rate [62]. This constitutes the major limitation of this procedure for MIP development. In molecular imprinting, the most widely employed monomer is methacrylic acid, which inhibits the metal-ligand complex, and therefore it is incompatible with ATRP. Moreover, other less reactive monomers such as methacrylamide or vinylpiridine have not yet been successful in ATRP [63]. The limited number of monomers with suitable functional groups for ATRP, and considering that template molecules often contain functional groups that may inhibit the catalysis, this technique has not been widely used for the synthesis of MIP so far. However, over the last four years, there has been a slight increase in the development of MIP via ATRP (figure 4.6), especially when this technique is used for surface initiated polymerisation [64-67].

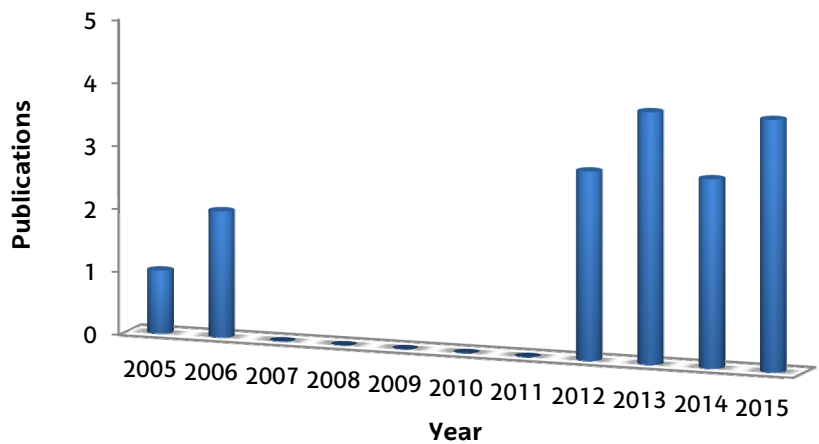

Figure 4.6. Number of publications in the last 10 years concerning MIP developed by ATRP [68].

1.2.3. Reversible addition-fragmentation chain transfer polymerisation.

Reversible addition-fragmentation chain transfer polymerisation (RAFT polymerisation) was first developed in 1998 by Moad *et al.* [69] as a new RDRP of superlative effectiveness and versatility. Due to the tolerance of RAFT polymerisation for a wide range of reaction conditions and of functional monomers, such as acids, esters, amines and alcohols, it rapidly aroused much research interest [35, 70].

Although the term RAFT is sometimes used in a more general sense, it is most closely associated with reactions that involve thiocarbonylthio compounds [35], including dithioesters, dithiocarbamates, or trithiocarbonates (figure 4.7). When it involves the thiocarbonylthio compound xanthate, it is sometimes also called Macromolecular Design via the Interchange of Xanthates (MADIX) [71].

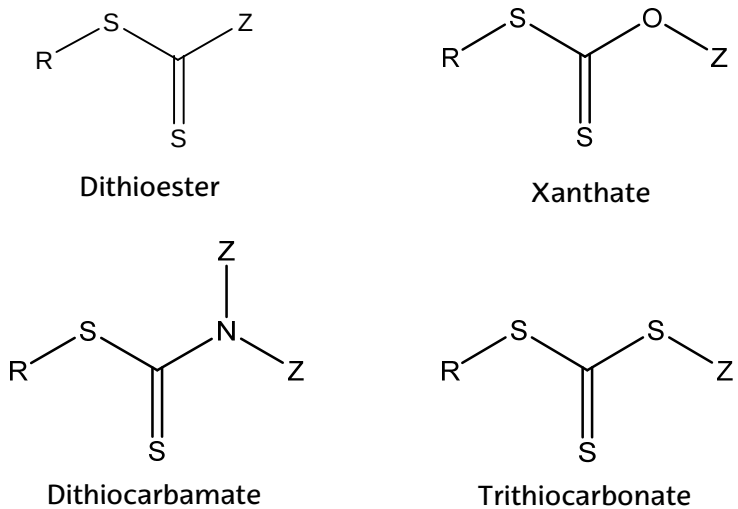

Figure 4.7. Thiocarbonylthio compounds.

Figure 4.8 shows the mechanism of RAFT polymerisation. In the early stages of polymerisation (figure 4.8, chain transfer step), the presence of propagating radicals (P_n•) in a medium containing thiocarbonylthio compounds, known as chain transfer agents (CTA), give rise to a polymeric CTA (new dormant polymeric CTA) and a new radical (R•). The radical (R•) reacts with new monomers (M) to form new propagating radicals (P_m•). A rapid equilibrium between the active propagating radicals (P_n• and P_m•) and the dormant polymeric CTA provides equal probability for all chains to grow and allows for the production of narrow dispersity polymers [69]. With particular attention to the reaction conditions, the vast majority of chains will retain the thiocarbonylthio end group when the polymerisation is complete (or stopped). Radicals are neither formed nor destroyed in the chain equilibration process. Thus, once the equilibria are established, the rates of polymerisation should be similar to those in FRP [35].

A key feature of the mechanism of RAFT polymerisation is the sequence of addition-fragmentation equilibria, where the transfer constants and therefore the polymerisation activity of RAFT agents are greatly affected by the R and Z substituents [69]. The R groups normally refer to the living radical groups that can reinitiate polymerisation, while Z groups refer to groups bonded to the carbon sulphur double bond, which is used to modify the activity of RAFT agent.

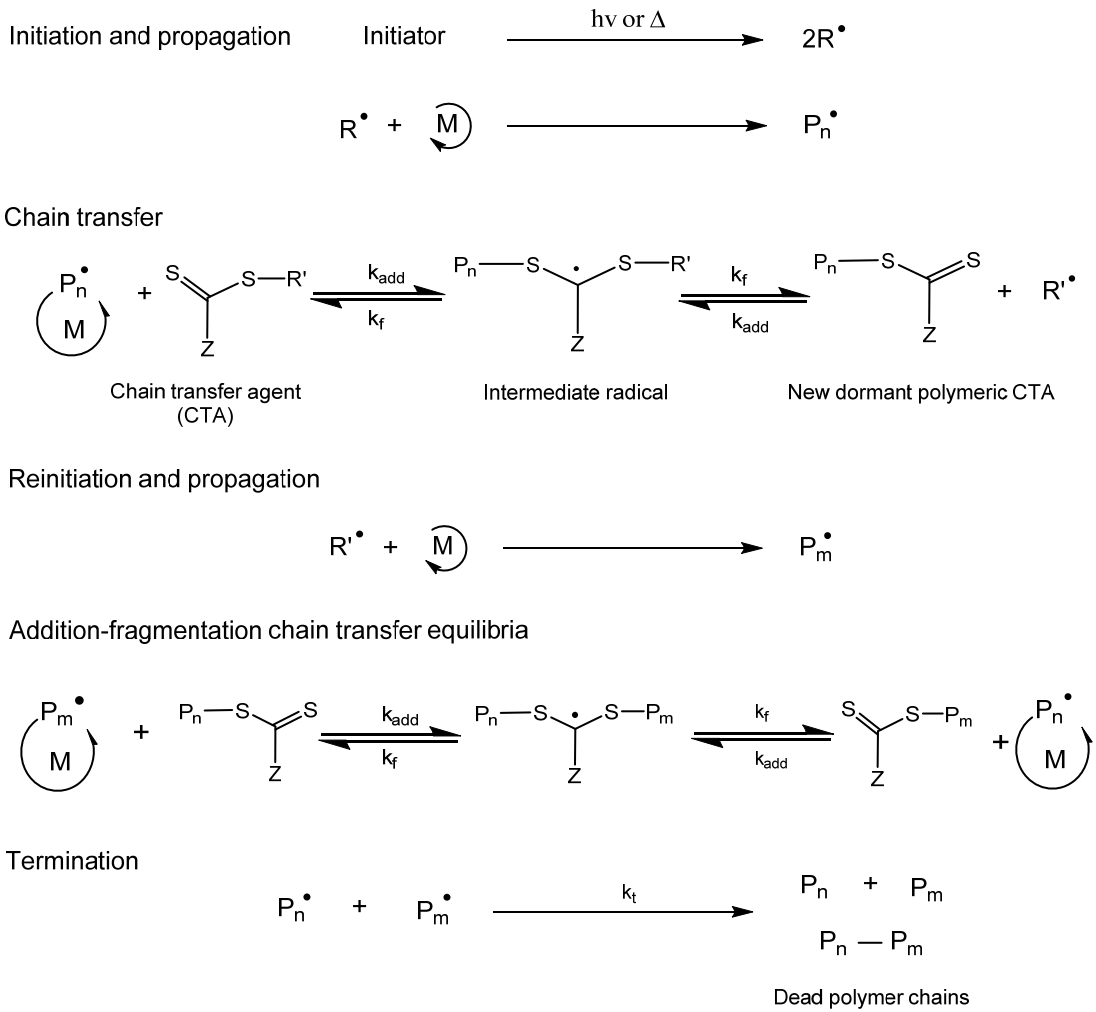

Figure 4.8. Mechanism of RAFT polymerisation.

To ensure a high transfer constant, Z should activate (or at least not deactivate) the C-S double bond towards radical addition. Suitable Z groups are aryl and alkyl (figure 4.9). In addition, for an efficient RAFT polymerisation: 1) both the initial (CTA)

and polymeric RAFT agents should have a reactive C=S double bond (high k_{add}), 2) the intermediate radicals should fragment rapidly (high k_f, weak S-R bond) and give no side reactions and 3) finally, the expelled radicals (R•) should efficiently re-initiate polymerisation [35].

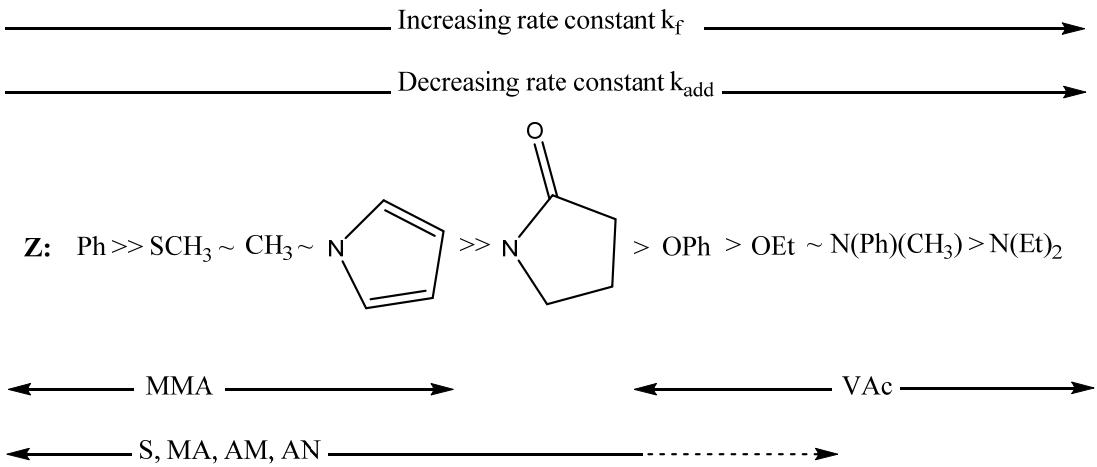

Figure 4.9. Effect of Z substituent on effectiveness of RAFT agents. Dashed line implies limited effectiveness with a particular monomer.

MMA: methyl methacrylate, **VAc**: vinyl acetate, **S**: styrene, **MA:** methyl acrylate, **AM:** acrylamide, **AN:** acrylonitrile **[72].**

In the imprinting field, RAFT polymerisation has been widely used as a technique to modify the material surface obtaining uniform and controlled polymer films. As a result, spherical shape monodisperse particles, with improved imprinting efficiency and mass transfer kinetics, are obtained in comparison with MIP fabricated by FRP [73].

RAFT polymerisation has been employed for many analytical applications including solid phase extraction (SPE) sorbents [74, 75], chromatographic chiral separation of phenylalanine [76-78] and aminoglutethimide [79], electrochemical sensing [80, 81] or the development of optical sensors, for example, for the direct

quantification of drugs in complex biological samples [82] or for the determination of low molecular compounds such as the nicotine [83].

1.2.4. Iniferter polymerisation.

In 1955, Ferington and Tobolsky [84] observed in their first attempt of control over radical polymerisations of vinyl monomers, that dithiuram disulfides in radical polymerisations led to higher transfer constants, which resulted in retardation of the polymerisation. However, it was not until 1982 when Otsu and Yoshida [85] provided, for the first time, a model for RDRP to describe styrene and methyl methacrylate polymerisation in the presence of phenylazotriphenylmethane and benzyl-N,N-diethyldithiocarbamate. It was also then, when it was first proposed the term iniferter (*ini*tiator-trans*fer* agent-*ter*minator).

Iniferters are initiators that induce radical polymerisation involving initiation, propagation, and termination steps. As bimolecular termination and other transfer reactions are negligible, these polymerisations are performed by the insertion of the monomer into the iniferter bond, leading to polymers with two iniferter fragments at the chain ends [86]. Some of the most commonly employed iniferters are depicted in figures 4.10 and 4.11.

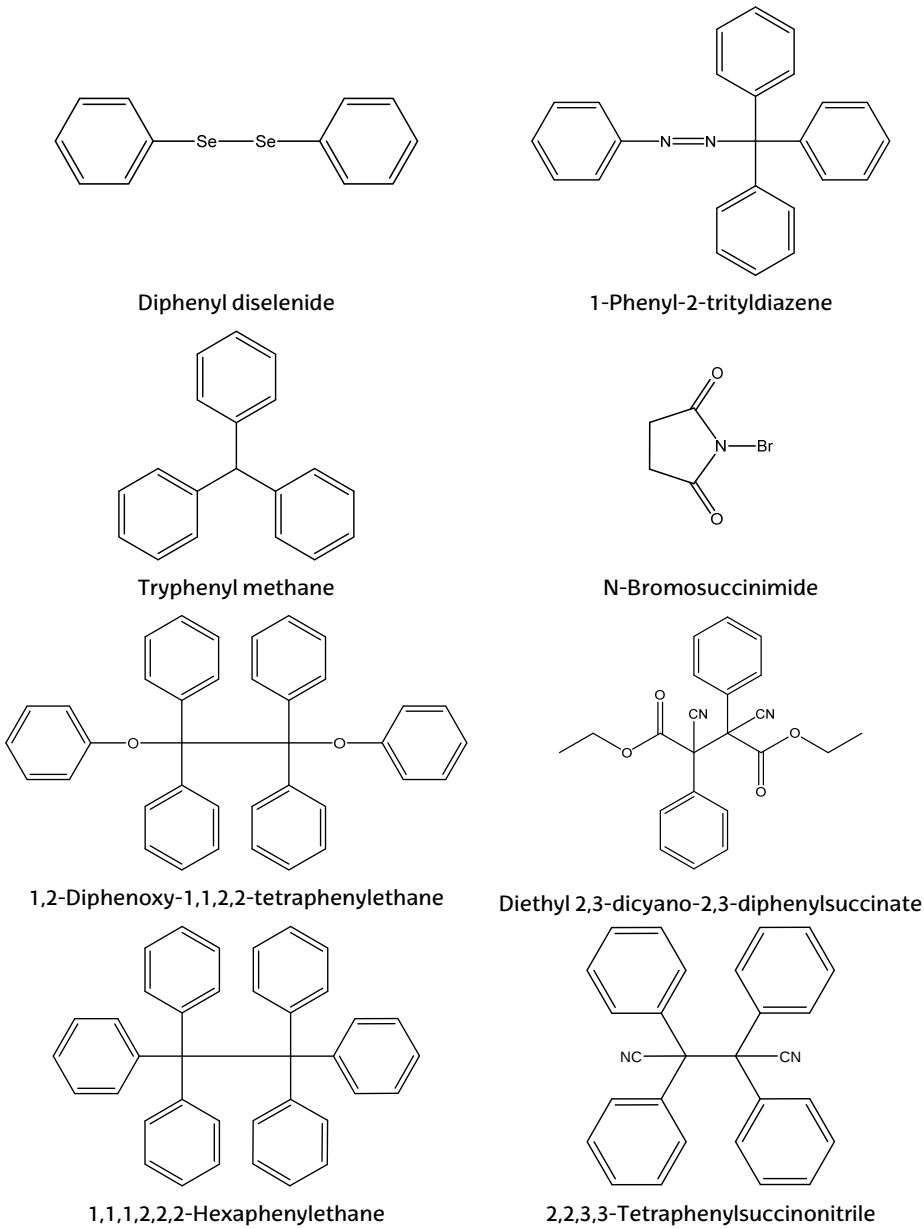

Diphenyl diselenide

1-Phenyl-2-trityldiazene

Tryphenyl methane

N-Bromosuccinimide

1,2-Diphenoxy-1,1,2,2-tetraphenylethane

Diethyl 2,3-dicyano-2,3-diphenylsuccinate

1,1,1,2,2,2-Hexaphenylethane

2,2,3,3-Tetraphenylsuccinonitrile

Figure 4.10. Chemical structures of common thermal iniferters.

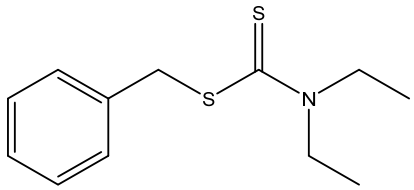

Benzyl diethyldithiocarbamate

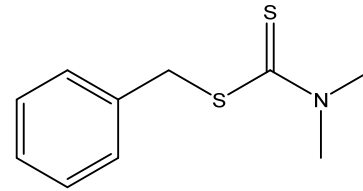

Benzyl dimethyldithiocarbamate

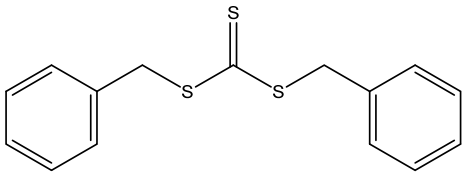

bis(benzylsulfanyl)methanethione

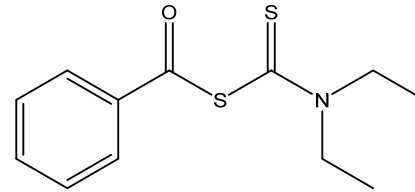

Benzoyl diethyldithiocarbamate

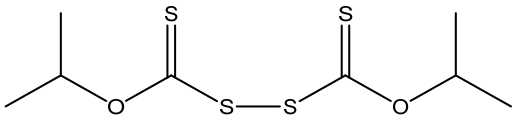

Isopropylxanthic disulfide

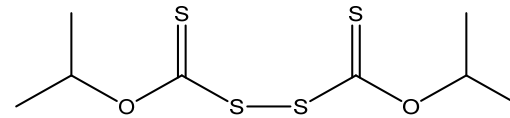

2,3-Dihydroxypropyl diethylcarbamodithioate

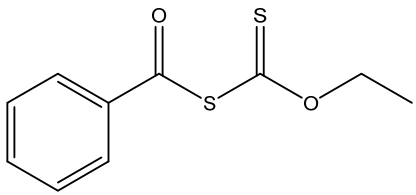

S-Benzoyl O-ethyl xanthate

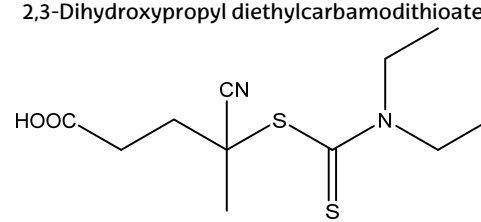

4-Cyano-4-(diethyldithiocarbamyl)pentanoic acid

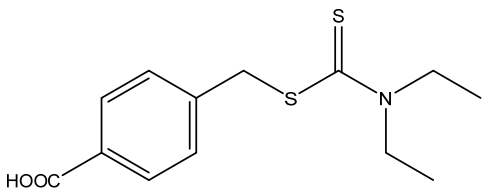

4-Diethyl thiocarbonyl sulfanylmethyl-benzoic acid

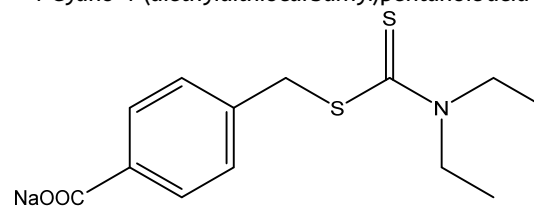

Sodium 4-diethyl thiocarbonyl sulfanylmethyl-benzoate

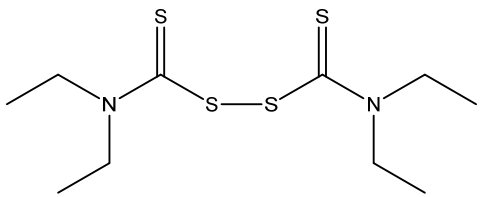

Tetraethylthiuram disulfide

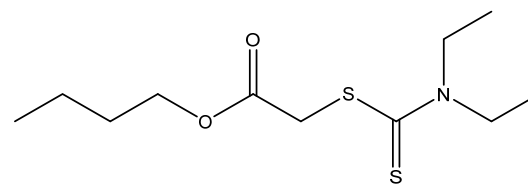

n-Butyl N,N′-diethyldithiocarbamylacetate

Figure 4.11. Chemical structures of common photoiniferters.

As it is shown in figure 4.12, the initiation step relies on the photochemical or thermal dissociation of the iniferter molecule into a reactive carbon-centered radical (R•) and a relatively stable diethylcarbamylthiyl radical (dormant radical).

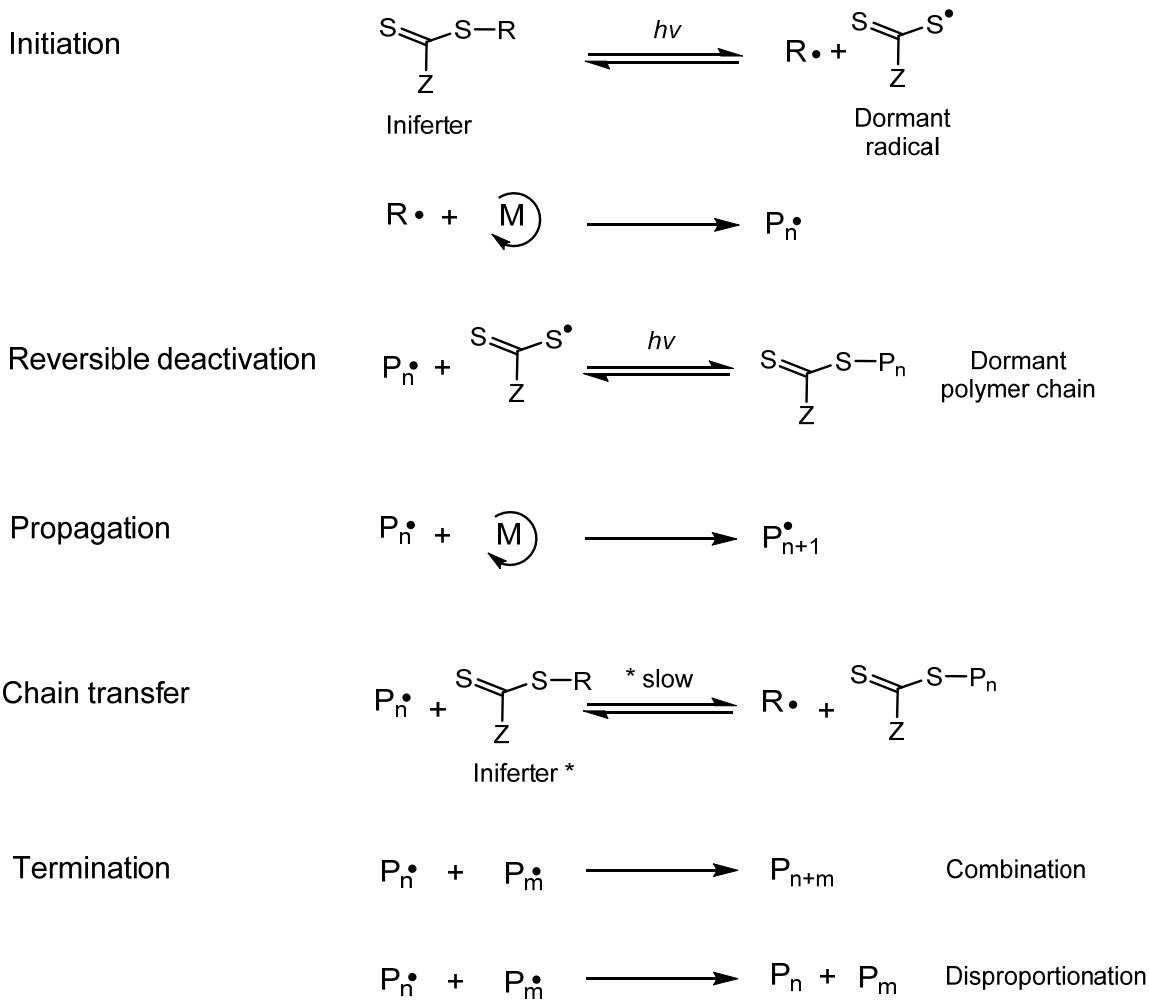

Figure 4.12 General mechanism of iniferter polymerisation.

The carbon radicals (R•) produced in these reactions are extremely reactive and they initiate the polymerisation by reacting with a double bond of a monomer to generate a macroradical (P_n•). In contrast, the dormant radical is less or nonreactive and cannot promote initiation. After the addition of a certain number of monomer species (chain transfer and reinitiation steps), the macroradical recombines reversibly with the dormant radical and it is converted into a polymeric macroiniferter molecule, also named as dormant polymeric chain. This macroiniferter can reactivate again to continue propagation. Growing polymer chains can combine through irreversible carbon-carbon radical reactions known as recombination or disproportionation, what leads to dead unreactive polymers. The unique feature of this iniferter polymerisation is that it proceeds in a controlled manner, in which "active" and "dormant" propagating chain ends are reversibly equilibrated throughout the course of polymerisation [87]. These reactions prevent from irreversible termination processes or even other side reactions, thereby proceeding in a controlled way.

Iniferters can be classified in two groups according to the structures of the formed radicals: symmetrical B-B and unsymmetrical A-B type iniferters.

Symmetrical type iniferters dissociate into two identical radicals where B• is the dormant radical which can enter into both initiation and primary radical termination. This type of iniferters has a major drawback compared with the unsymmetrical ones: the low reactivity of the dormant radicals results in a broadening of the molecular weight distribution and a loss of molecular weight control. Commonly, symmetrical iniferters are thermal iniferters which have been mainly used for the polymerisation of acrylic monomers such as methyl methacrylate [87].

Unsymmetrical type iniferters decompose into two different radicals where A• is the reactive radical that takes part only in initiation, and B• is the dormant radical, which acts as a primary radical terminator. These iniferters are more versatile and, in most cases, they are activated by UV energy. Photopolymerisations offer many

advantages such as temporal and spatial control of initiation, cost efficiency, and solvent-free systems. In fact, since the dithiocarbamyl end groups (dormant radicals) are thermally stable but photochemically labile, at usual polymerisation temperatures, only photoinitiated polymerisations have the potential to show typical characteristics of RDRP [35].

1.3. Surface imprinting by reversible-deactivation radical polymerisation

Surface imprinting lies in grafting imprinted polymer thin films on the surface of solid substrates. End-functionalised monomers or polymeric chains can be inserted on the surface of solid supports by grafting to or grafting from approaches (figure 4.13). These grafting methods allow for the growth of MIP on preformed supporting materials of predetermined morphology [88, 89].

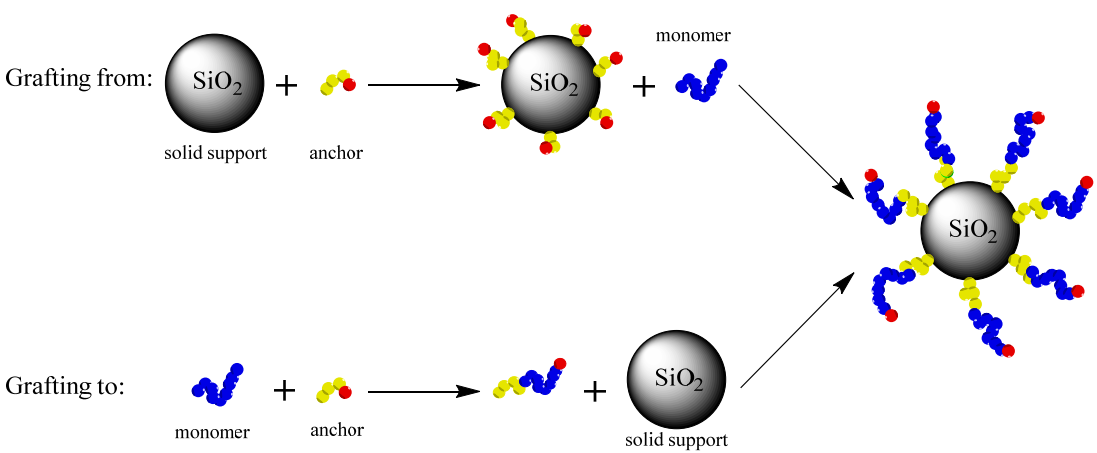

Figure 4.13. Schematic representation of the grafting from and grafting to approaches.

1.3.1. The grafting to approach

In the grafting to approach, the polymer can be chemically attached to a solid surface, provided the performed polymer possesses a functional group capable of being attached to the surface [90], e.g. a polymer containing a primary amine could form an amide bond with a carboxylic acid-terminated self-assembled monolayer (SAM).

The first report concerning surface imprinting was published in 1984, when Norrloew *et al.* [91] introduced this technique to synthesise a non-covalent MIP film for different dyes (safranin O and rhodamine blue) on porous silica surface. It dealt with functionalising the surface of silica microparticles with acrylate groups and then, it was coated with a thin shell of acrylic polymers under similar conditions to conventional bulk polymerisation [92-94]. So far, the preparation of conventional bonded stationary phases based on silica has been carried out almost exclusively by the grafting to approach, attaching alkyl chains (typically octadecyl chains) to porous silica particles through silane coupling reactions [95].

Despite its potential benefits, such as kinetic improvement and procedure simplicity, the synthesis of imprinted thin layers by the grafting to approach is not a simple goal due to the difficulties in controlling film thickness [96] due to the presence of the initiator in the polymerisation mixture. Moreover, grafting densities are limited due to kinetic and steric factors [97, 98], limiting the thickness of the polymer to a few tens of nanometres [99]. To overcome these effects and to increase the density of grafted layers, monomers are polymerised from surface-bound initiators using the grafting from approach [96, 99].

1.3.2. The grafting from approach

This approach refers to an *in situ* method of polymer synthesis covalently attached to the solid substrate. Due to its simplicity and versatility, this technique is more frequently used in solid support modification [100]. In the grafting from approach, the

initiator is immobilised on the silica surface in a preliminary step. Then, the polymer chains grows directly on the surface, which leads to well-defined grafts [35].

Although the first report of MIP surface imprinting using immobilised initiators on porous silica was carried out via conventional FRP, this technique can be accomplished by almost all known mechanisms for polymer synthesis [42, 100]. The use of RDRP, together with the grafting from approach, allows homogeneously grafting thin MIP layers with reduced mass-transfer resistance. In addition, desirable formats such as particles, tubes or microchips with desirable properties of size, porosity and surface area, can be obtained.

Grafting via photoiniferter technique is much faster than others, usually providing thicknesses of hundreds of nanometres in a few minutes. Additionally, it can be performed at room temperature with or without solvent (pure monomer), requires no catalyst/ligand system, and is compatible with a wide range of vinyl monomers. In the case of photoiniferter based surface initiated polymerisation, the iniferter molecules can be easily immobilised on surfaces by self-assembly or by chemically modifying the precursor surfaces through the introduction of dithiocarbamate moieties [101]. To avoid irreversible termination reactions, and to increase the thickness of the polymers, a strategy of adding a symmetric iniferter such as tetraethylthiuram disulfide was introduced [102-104]. This strategy leads to an increase of the amount of deactivating species to the polymerisation mixture, which is mandatory to provide controlled radical polymerisation behaviour.

Over the last years, thin films of MIP grafted from preformed silica particles using an immobilized iniferter-type initiator have been synthesised [111-113]for their use as stationary phases, for templates such as pesticides [105], organotin compounds [106] and drugs [107, 108]; or as packing material for solid phase extraction cartridges for the analysis of pesticides [109, 110]. In all cases, surface imprinting via iniferter polymerisation has allowed for the synthesis of polymer beads with shape and size compatible with chromatographic techniques. With respect to the development of

CSPs, the only reported work is the one carried out by Halhalli *et al* [78] where a MIP based CSP is synthesised by both RAFT and iniferter polymerisation, but only the first strategy provides polymers capable of chiral resolution.

2. Objectives

The potential benefits that provides RDRP on polymer architecture control, have been exploited here to develop chiral MIP in a controlled manner on solid supports. In this regard, the development of different strategies based on iniferter mediated polymerisation of MIP was established as the principal aim of the work described along this chapter. These strategies were focused on the development of chiral stationary phases for the enantiomeric resolution of the antidepressant drug citalopram. To achieve this general objective, the following operational objectives are to be fulfilled:

- Development of chiral MIP grafting the polymer from the surface of silica beads functionalised with a silane iniferter.
- Alternative development of chiral MIP in nanoparticle format: Solid-phase imprinting and precipitation polymerisation. Attachment of the nanoparticles to silica beads as solid support.
- Characterisation of the surface imprinted material by Elemental Analysis (EA), Fourier Transform Infrared Spectroscopy (FTIR), Thermogravimetric Analysis (TGA) and Scanning Electron Microscopy (SEM).
- Development of chiral chromatographic columns packed with silica beads coated with different MIP formats. Application of the stationary phases to the chiral resolution of the citalopram racemate.
- Determination of the binding capacity of the materials by adsorption isotherms recorded by batch rebinding. Fitting of the isotherm to different binding models and selection of the best fitting one.
- Analytical evaluation of the chiral stationary phase.

3. Materials and equipment

3.1. Materials

(S)-citalopram (SCIT), (R)-citalopram (RCIT) and carboxylated SCIT oxalate were purchased from Trademax (Shanghai, China). For MIP synthesis, SCIT was required to be used in its neutral form, to this end, the procedure described in chapter 3 (section 3.1) was followed.

The monomers itaconic acid (IA) ≥99%, acrylamide 99%, methacrylic acid 99% (MAA) trimethylolpropane trimethacrylate (TRIM) 90% and ethylene glycol dimethacrylate (EDMA) 98%, as well as the initiator 1, 1'-Azobis (cyclohexanecarbonitrile) 98%, were supplied from Sigma-Aldrich (Madrid, Spain). The chain transfer agent pentaerythritol tetrakis (3-mercaptopropionate) was also purchased from Sigma-Aldrich and the iniferter diethyldithiocarbamic acid benzyl ester was obtained from TCI Europe (Zwijndrecht, Belgium).

Porous silica particles (SiliCycle®) were acquired from Teknokroma (Barcelona, Spain) whose average diameter, pore size and surface area were 10 µm, 9 nm and 432 m^2/g respectively. For the amino funtionalisation of the silica, 3-aminopropyl (trimethyloxysilane) (APTMS) was employed from Sigma-Aldrich. Hexamethyldisilazane (HMDS), employed for the end-capping, was acquired from the same company.

Solid glass beads (Spheriglass® 2429) whose diameter was between 65 µm and 106 µm (average 90 µm) were purchased from Blagden Chemicals (Westerham, UK).

Sodium diethyl dithiocarbamate trihydrate and 3-chloropropyl (trimethoxysilane), required for the synthesis of the iniferter N, N'-diethylaminodithiocarbamoylpropyl (trimethoxy)silane (DDCPTS), were obtained from Sigma-Aldrich.

Solvents such as acetone, acetonitrile (ACN), ethanol (EtOH), methanol (MeOH) and dimethylformamide (DMF) were acquired from Scharlab (Barcelona, Spain) and dry

toluene and dimethyl sulfoxide (DMSO) from Panreac (Barcelona, Spain). All of them were analytical or high-performance liquid chromatography (HPLC) grade and used as received. Mass spectrometry grade ammonium formate ›99% and formic acid ≥98% used for buffer preparation, were acquired from Sigma-Aldrich (Madrid, Spain). Every buffer solution was prepared with ultra-pure water obtained from Elix20 reverse osmosis and Milli-Q water purification systems.

3.2. Equipment

For MIP synthesis by bulk or precipitation polymerisation, a UVAcube 100 UV lamp (100 W) purchased from Dr. Hönle UV-technology (Gräfelfing, Germany) was employed. For the coating of the silica support by grafting, a Philips UV device model HP/3151/A (Amsterdam, the Netherlands) fitted with 4 × 75 W lamps was used.

Characterisation of the silica coating by Elemental Analysis (EA) was performed with a Eurovector 3000 (Milan, Italy) elemental analyser. Fourier Transform Infrared Spectroscopy analysis of polymers was performed using a FTIR spectrometer, model 6300 type A, from Jasco (Madrid, Spain). Thermogravimetric Analysis (TGA) was carried out in a Mettler Toledo SDTA 851 analyser (Mettler Toledo International Inc., Greifensee, Switzerland) at a heating rate of 10 °C/min up to 900 °C under nitrogen atmosphere. Morphological studies were carried out by Scanning Electron Microscopy (SEM) in a JSM- 6400 scanning microscope (JEOL Ltd., Tokyo, Japan), with an accelerating voltage set to 20 kV. Samples were mounted on conductor tape and were chromium coated (5 nm thickness). EA, FTIR, TGA, and SEM analysis were performed by the Advanced Research Facilities (SGIker) of the University of Basque Country.

For the characterisation of the molecularly imprinted nanoparticles (MIN), Dynamic Light Scattering (DLS) measurements were carried out using a Zetasizer Nano equipment (Nano-S) from Malvern Instruments Ltd (UK). Surface Plasmon Resonance (SPR) experiments were performed using a Biacore 3000 SPR system (GE Healthcare

Life Sciences) and SPR Au-coated chips (SIA Kit Au, Biacore). Both of them, were purchased from GE Healthcare Life Science (UK).

Chromatographic experiments were carried out using stainless-steel columns (4.6 × 100mm, 4.6 × 150mm and 4.6 × 250mm) (Phenomenex-Micron Analítica, Madrid, Spain) packed with surface-modified silica. The packing was performed using the Pack in a Box column packing system from Restek (Bellefonte, USA) comprised of a dual piston pump and a 20 mL reservoir. Chromatographic evaluation of MIP and non-imprinted polymer (NIP) columns was performed in an Agilent 1100-series binary pump system (Agilent Technologies Inc., Palo Alto, CA, USA) at a flow rate of 1ml/min and a temperature of 40 °C. The mobile phase consisted of a mixture of formate buffer and ACN. Fluorescence detection was carried out at 240nn (excitation) and 308 nm (emission). For batch rebinding experiments, a ZORBAX Eclipse XDB-C18 (4.6×150mm, 5 µm) column from Agilent Technologies (Palo Alto, CA, USA) was used, and a mixture of tetramethylammonium chloride (0.4%, pH4) and ACN (70:30 v/v) was employed as mobile phase at a flow rate of 1ml/min at room temperature.

4. Pre-screening of molecularly imprinted polymers for the enantioselective recognition of S-citalopram

Based on computational predictions of binding energies described in the previous chapter, functional monomers that led to strongest adducts with SCIT were selected for MIP development. Both IA and acrylamide were preselected as possible candidates for imprinting the target enantiomer. IA is the monomer that strongest binds to SCIT, whereas computational binding energy of the RCIT-IA complex was too weak to consider this monomer appropriate to bind the R enantiomer. Therefore, it was hypothesised that if a MIP was developed using IA as functional monomer, it could probably have moderate to high specificity to the S form over the R.

On the other hand, acrylamide was the second monomer among the top five giving strongest complexes with the target. Moreover, the predicted SCIT-acrylamide complex is established by hydrogen bonding between the amide group of the monomer and the tertiary amine of the template, in contrast, in the RCIT-acrylamide adduct, hydrogen bonding happens preferably between the amide and the heterocyclic oxygen of the template (figure 4.14). These binding differences could be *a priori* considered good enough to be exploited in the development of a MIP selective for SCIT.

Not only functional monomers play a crucial role in binding efficiency of MIP, but also the cross-linker. Proper selection of the cross-linking monomer is to be done to minimise non specific binding, thereby increasing enantiospecificity. In this sense, both trimethylolpropane trimethacrylate (TRIM) and ethylene glycol dimethacrylate (EDMA) were preselected as possible candidates for imprinting. The former was chosen due to the fact that it leads to polymers with higher cross-linking degree and, in consequence, higher rigidity. Usually, polymers with lowest plasticity, lead to lowest cross reactivities, as imprinted sites suffer from lower swelling/shrinking capacity. Studies reported elsewhere have demonstrated that polymer rigidity directly influences MIP selectivity for a target enantiomer [114, 115]. TRIM is one of the less

polar cross-linkers commonly used for imprinting (log Kow: 3.93), therefore, non specific hydrophobic binding with the polymer backbone is more likely to happen. Thus, EDMA (log Kow: 1.93) was also selected for MIP development due to its higher polar character, since lower hydrophobic binding may be presumed using this cross-linker.

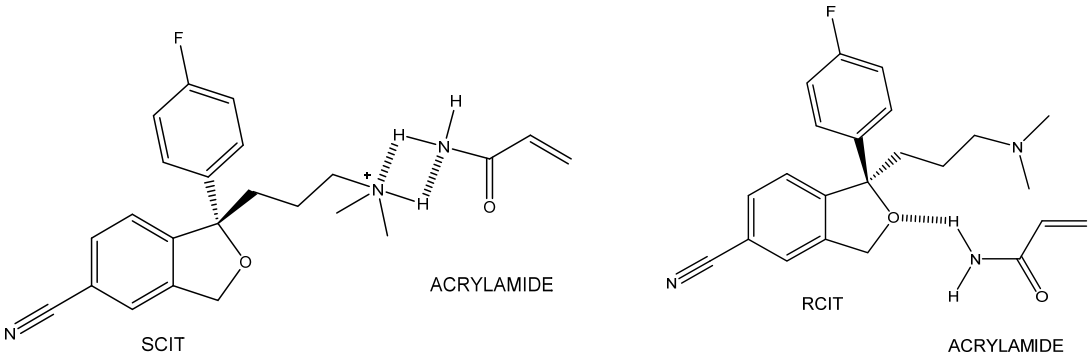

Figure 4.14. Hydrogen bonding interactions between each enantiomer and acrylamide.

In the efficiency of MIP, not only polymer rigidity plays a key role, but also binding site accessibility [1]. As the polymer porosity directly depends on the solvent used in the polymerisation mixture, its proper selection may be critical in many cases. The solvent should preferably not interfere with functional monomer-template interactions during the self-assembly. Aprotic organic solvents of low polarity and low hydrogen bonding capacity are therefore preferred, since prepolymerisation template-monomer adducts in non covalent imprinting are mainly established through polar interactions. As this regards, toluene, acetonitrile and chloroform are the most commonly employed solvents [116]. Moreover, it has also been reported that, the rebinding performance of MIP is best when it is carried out in the same solvent used for imprinting, thereby requiring the same or very similar solvation conditions to those used in the polymerisation step [117]. Two aprotic solvents of different polarities were

tested in this work, ACN and DMSO. Nevertheless, ACN was preferred due to its much weaker hydrogen bonding capacity in comparison with DMSO. However, the solubility of IA in ACN is too low for bulk polymer synthesis. Therefore, when IA was used as functional monomer, DMSO was employed as solvent due to the act that it was the solvent with lowest polarity among the ones that dissolved all the polymerisation components of the mixture.

Using the preselected functional monomers and cross-linkers, a preliminary experiment was carried out first, in order to determine the monomers that provided MIP with best chiral recognition capability. To this end, SCIT imprinted polymers where synthesised, in bulk format, by free radical polymerisation using a 1:4:24 template:functional monomer:cross-linker molar ratio. The compositions of the polymerisation mixtures are summarised in table 4.2. Once prepared, each polymerisation mixture was degassed with pure nitrogen and then irradiated with UV energy for 40 min. The resulting polymer monoliths were ground and wet-sieved in MeOH through 25 and 50 μm pore size sieves.

Polymer suspensions were packed in chromatographic columns of 100 mm in length and 4.6 mm in diameter. The slurry was packed at a constant pressure of 2000 psi.

Template removal was performed by continuously flowing, at 1 mL/min, a 200 mM solution of formic acid in MeOH through the columns until a stable baseline, indicative of template absence, was registered by HPLC-FD (approximately after 5 h). Non-imprinted polymers were synthesised using the same protocol but in the absence of SCIT in the MIP synthesis.

Table 4.2. Polymerisation mixtures used for MIP syntheses by bulk polymerisation.

	MIP1	MIP2	MIP3
TRIM	2 g	-	-
EDMA	-	2 g	2 g
IA	-	-	0.219 g
Acrylamide	0.331 g	0.120 g	-
SCIT	0.094 g	0.136 g	0.136
1,1'-Azobis (cyclohexanecarbonitrile)	0.025 g	0.025 g	0.025 g
DMSO	-	-	2.5 g
ACN	2.5 g	2.5 g	-

Once the template was removed, it was proceed to chromatographic evaluation of the MIP and the NIP polymers. To this end, the retention times of SCIT and RCIT in MIP and NIP columns were compared. The retention time differences between the MIP and the NIP columns indicate the existence of specific interactions of the target compound and the binding sites. Usually, the degree of such interaction is quantified based on the imprinting factor (IF), which is calculated based on retention factors of the target compound on the MIP and NIP column through the expression 4.1:

$$IF = \frac{k_{MIP}}{k_{NIP}} \qquad 4.1$$

The retention factor (k) is a measure of the time the sample component resides in the stationary phase relative to the time it resides in the mobile phase; it expresses how much longer a compound is retarded by the stationary phase than it would take to pass through the column with the mobile phase [118]. It is calculated through the equation 4.2 where t_r is the retention time of the analyte and t_0 is the void time.

$$k = \frac{t_r - t_0}{t_0} \qquad 4.2$$

In the first instance, it was assessed the effect of the cross-linker on MIP enantioselectivity. With this purpose, MIP 1 and MIP 2 (table 4.2) were evaluated injecting 20 μL of a solution of 25 μg/mL of SCIT or RCIT in ACN in the chromatographic system. As mobile phase, acetonitrile: water (90:10 v/v) was used in all cases. Registered retention times and the corresponding imprinting factors are depicted in figure 4.15. As it can be observed, non-imprinted columns packed with TRIM are capable of retaining both enantiomers longer than imprinted columns, providing IF values lower than 1. That could be indicative of high non specific binding of the enantiomers with the polymer backbone, what minimises the imprinting effect observed in MIP columns. In contrast, retention times observed with MIP synthesised with EDMA were always higher than the ones observed with the NIP, thereby demonstrating the imprinting effect. Based on the presented results, EDMA was selected as cross-linker for further experimental.

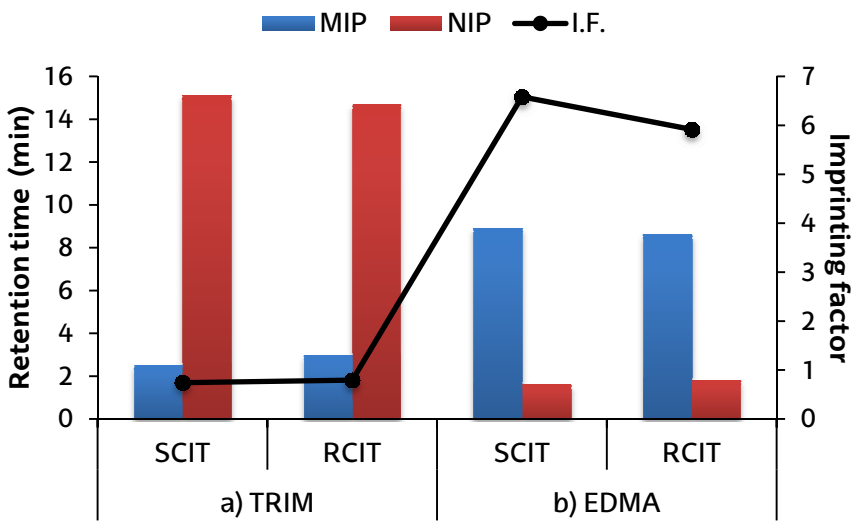

Figure 4.15. Retention times and imprinting factors of SCIT and RCIT using acetonitrile: water (90:10 v/v) as mobile phase. In all polymers acrylamide was used as functional monomer.

The effect of the functional monomer on MIP enantioselectivity was evaluated next. For this purpose, the stationary phases MIP 2 and MIP 3 (table 4.2), made with acrylamide and IA respectively, were evaluated. First of all, different solvents such as MeOH, EtOH and ACN were evaluated as mobile phase. When MIP 2 was used, no retention was observed when MeOH or EtOH were employed as mobile phase. However, using ACN as the mobile phase favoured analyte retention, but both RCIT and SCIT behaved similarly, not observing any enantiospecificity (figure 4.16).

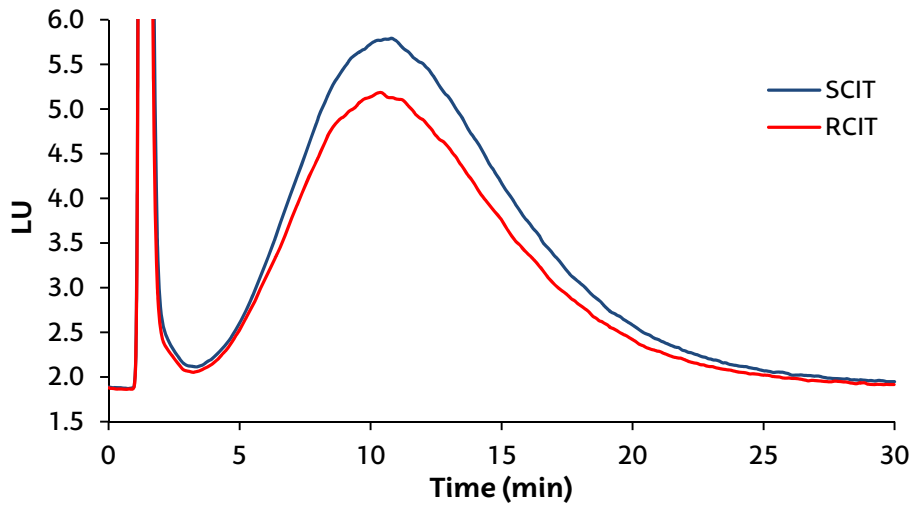

Figure 4.16. Chromatograms obtained for SCIT and RCIT when MIP2 was used. Mobile phase: 90:10 v/v ACN: water.

In order to test whether the presence of water in the mobile phase could contribute to enantioseparation or not, different ACN: water mixtures were tested. Figure 4.17 represents the retention factor of SCIT and RCIT in MIP 2 and NIP 2 columns in relation to the percent of water in the mobile phase. As depicted, the presence of water in the mobile phase made the retention factors of both enantiomers decrease. However, even if at certain water percentages a small difference between enantiomers

is observed, the registered peak width was too high for a good resolution of the racemic mixture. It was therefore concluded, that the use of acrylamide as the functional monomer provided MIP materials with moderate to high IF, but with poor chiral resolution capability, being the retention time differences between enantiomers not enough for chromatographic resolution.

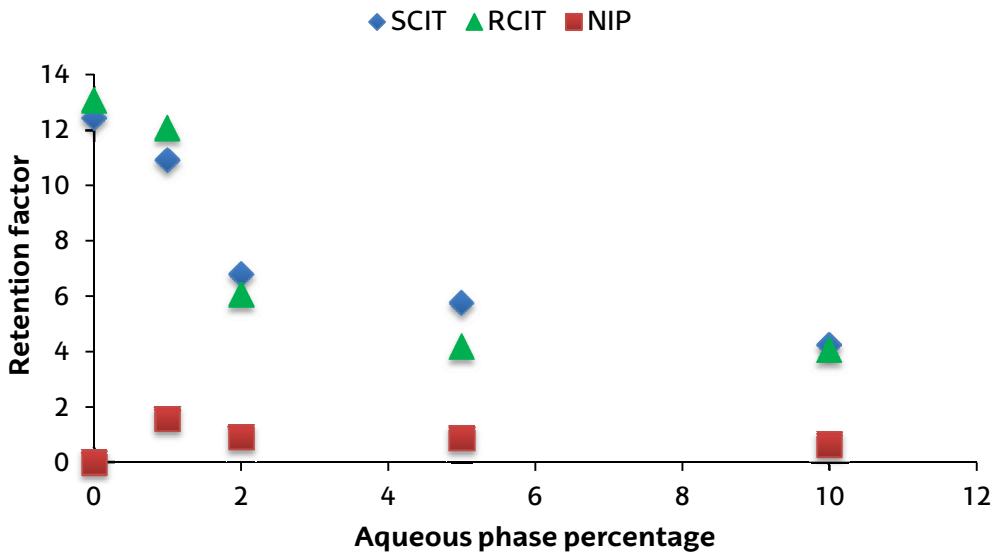

Figure 4.17. Retention factor of RCIT and SCIT in MIP 2 and NIP 2 materials, synthesised with acrylamide as functional monomer, with relation to aqueous percentage in the mobile phase.

In addition, the separation factor (α), which describes the separation of two species (A and B, being A the analyte which elutes first) in a column, was calculated as detailed in equation 4.3. α was lower or equal to 1 in all tested ACN:water mixtures, indicating that there was no separation between both species (table 4.3). Based on these premises, acrylamide was discarded for further experiments.

$$\alpha = \frac{k_B}{k_A} \qquad 4.3$$

Table 4.3. Separation parameters calculated using different aqueous phase percentages. Mobile phase composition: ACN : water.

%	Enantiomer	k (NIP)	k (MIP)	α (MIP)	IF
1	RCIT	0.75	12.08	0.90	16.03
	SCIT	1.58	10.92		6.91
2	RCIT	0.85	6.08	1.12	7.15
	SCIT	0.91	6.80		7.47
5	RCIT	0.65	4.19	1.37	6.45
	SCIT	0.88	5.75		6.53
10	RCIT	0.65	4.08	1.04	6.29
	SCIT	0.64	4.25		6.64

When IA was used as functional monomer (MIP 3), retention times were different for the S and the R enantiomers. When 100 % MeOH, EtOH or ACN were used as mobile phase, RCIT and SCIT were retained for long times. Particularly with ACN, full retention of both enantiomers was observed. In order to facilitate analyte elution, different amounts of formic acid were added to the organic phase. As it can be deduced from figure 4.18, when MeOH was employed as mobile phase, the addition of small amounts of formic acid to this solvent (1 mM, 2.5 mM and 5 mM) made the retention time of both enantiomers drastically decrease, leading to poor enantiomer resolution. In addition, this retention time drop made the MIP to NIP differences fall, obtaining worse imprinting factors.

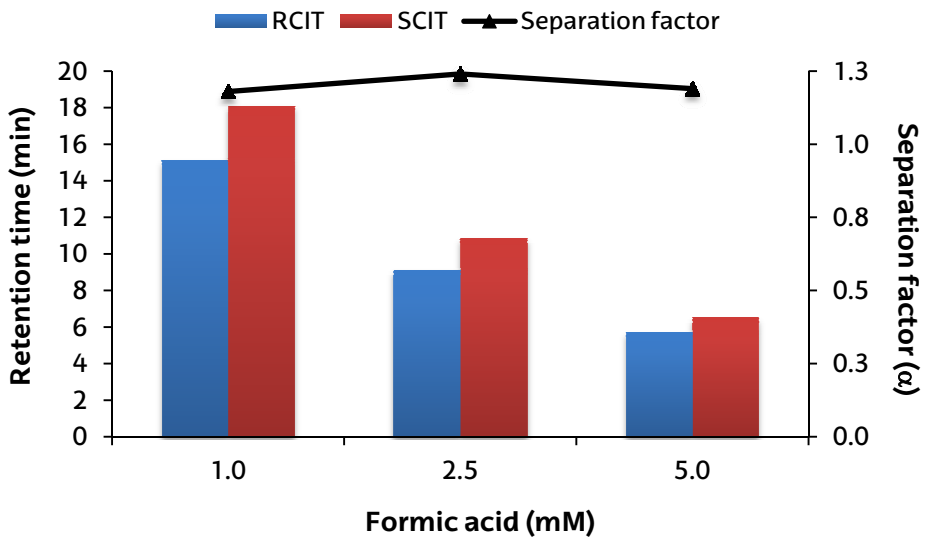

Figure 4.18. Retention times of RCIT and SCIT in column MIP 3 registered using different concentrations of formic acid in MeOH as mobile phase.

When ACN was used as mobile phase, higher amounts of formic acid than with MeOH were required to favour analyte elution. This higher retention, favoured the existence of retention time differences between enantiomers, however, an excessive peak widening was appreciated what hindered proper chiral resolution.

Best results were obtained with MIP 3 when EtOH was used as mobile phase. To this solvent, increasing concentrations of formic acid (from 5 mM to 160 mM) were added as detailed in figure 4.19. It was found that the differences between the retention times of RCIT and SCIT were significantly higher than with MeOH or ACN. However the width of the peaks was still too broad.

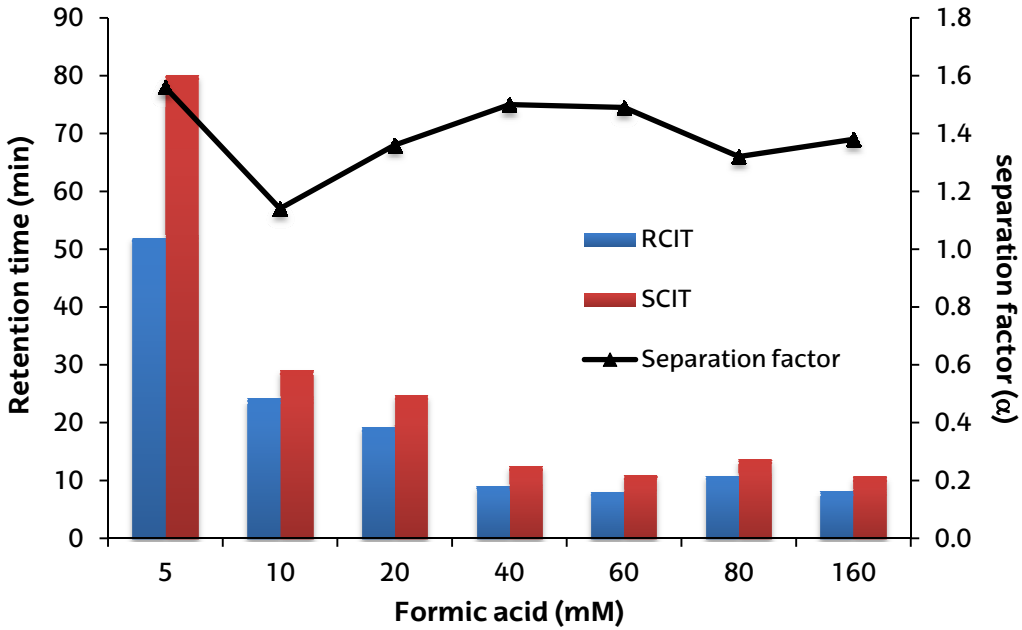

Figure 4.19. Retention time of RCIT and SCIT in MIP 3, Data recorded employing different concentrations of formic acid in EtOH as mobile phase.

As depicted in figure 4.19, the retention time of both enantiomers decreases when higher concentration of formic acid was used in the mobile phase. However, reducing the retention time has, oppositely, a negative effect on the enantioseparation.

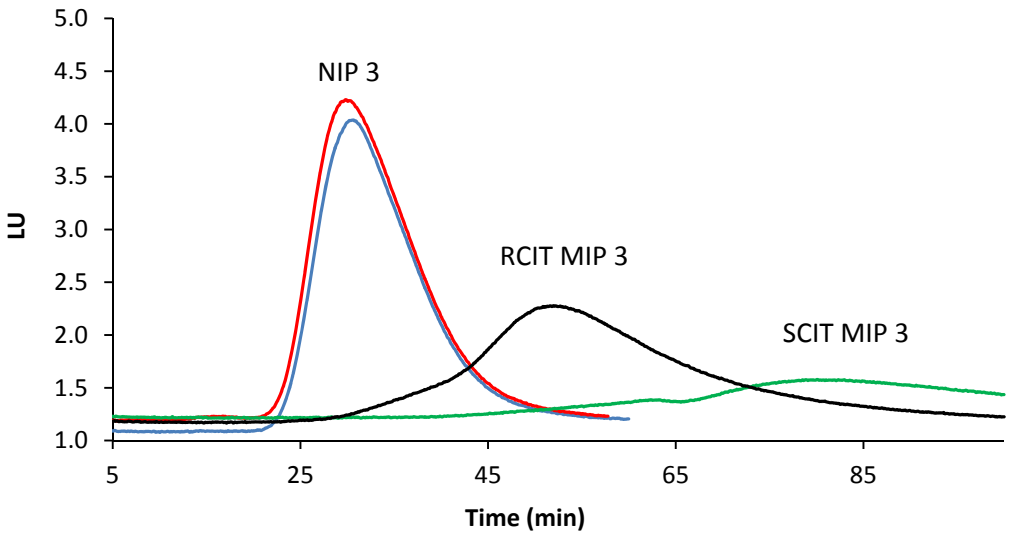

Figure 4.20. Chromatograms corresponding to 10 µg/mL of RCIT and SCIT using MIP3 and NIP3 as stationary phases. The mobile phase consisted of 5 mM formic acid in EtOH.

Based on the obtained preliminary results, it was corroborated that IA was the functional monomer that led to better chiral separation, being EDMA the cross-linker that provided less non specific binding. Bulk polymers synthesised under these conditions behaved differently for SCIT and RCIT and showed good imprinting factor, however, an excessive peak widening was observed with MIP what hindered proper chiral resolution (figure 4.20). Nevertheless, the results obtained with these bulk materials served as a platform to develop new MIP using other polymerisation techniques that would provide MIP with better chromatographic behaviour. To this end, the best monomers preliminary selected in these tests could be potentially employed for efficient racemic resolution of the selected chiral drug.

5. Development a chiral stationary phase based on molecularly imprinted polymer thin films coated on porous silica support

Chiral stationary phases (CSP) can be classified into three groups depending on the chiral selector employed in the separation of the racemic mixture [119]. Phases based on chiral organic polymers are classified as type I CSP. These polymers can be used as they are, or even coated on the surface of inorganic supports. Oligo- and polysaccharides and their derivatives, polyacrylamides, polyacrylesters and protein-based phases are included in this group [4, 120]. In type II CSP, a chiral selector such as amino acid derivatives, crown ethers, cinchona alkaloids, carbohydrates, amines, tartaric acid derivatives, cyclodextrins or binaphthol are linked by ionic or covalent bonds to an achiral support which, commonly silica [3, 5, 6]. Finally, type III, includes those obtained by the imprinting technique and they have been intensively investigated by Mosbach [22, 121, 122], Sellergen [36, 79, 123], and Haginaka [39, 124, 125].

In this work, a type III CSP was developed for the chromatographic separation of the enantiomers of citalopram. To this end, the grafting from approach has been employed to develop a surface-imprinted chiral stationary phase consisting in a silica based achiral matrix modified with imprinted thin films.

5.1. Silica surface activation

In many cases, the silica manufacturer applies calcination processes to the material, and it is well known, that any excessive heat treatment can influence silica surface chemistry, leading to a lower concentration of silanols. Because of that, rehydroxylation of the silica surface is often required before the synthesis of chemically

bonded phases. Rehydroxylation provides a concentration of 8.0±1.0 µmol of SiOH per m^2 of silica surface [126, 127]. Köhler and Kirkland [128, 129], and later Unger *et al*. [130], studied rehydroxylation by different acidic/hydrothermal treatments of a series of commercially available silicas. According to them, acid treatment did not change the specific surface area and improved the column performance in terms of plate numbers and peak symmetry.

In this study, the rehydroxylation process was accomplished using an acid treatment with HCl. 4 g of silica were suspended in 150 mL of a 17% HCl solution, and the mixture was kept under reflux during 24 h (figure 4.21). Once the mixture had cooled down, silica particles were filtered and rinsed several times with water and then twice with 250 mL of MeOH to avoid clotting during drying [95]. Finally, silica particles were dried at 120 °C at least for 12 h.

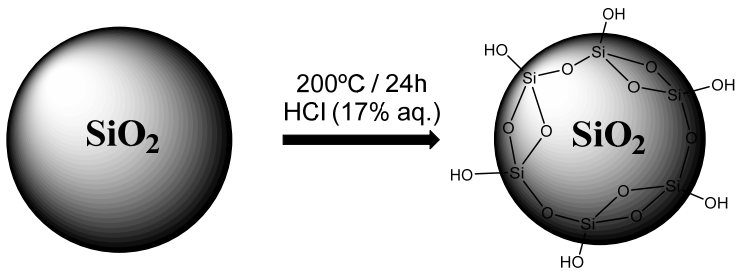

Figure 4.21. Silica surface activation.

5.2. Silica surface functionalisation

Prior to polymer synthesis on silica surface, it was functionalised so that the polymer coating could be properly grafted on it. This would allow for obtaining mechanically stable stationary phases. The silica was functionalised linking the iniferter N, N-diethylaminodithiocarbamoylpropyl(trimethoxy)silane (DDCPTS) to its surface.

5.2.1. Synthesis and characterisation of the silane iniferter

The iniferter DDCPTS was synthesised as reported by Bossi *et al*. [103]. Initially, sodium diethyl dithiocarbamate trihydrate (3.42 g) was ground obtaining a fine powder that was lyophilised at -80 ºC and 0.2 bars during 24 hours in order to remove crystallisation water. Dehydrated sodium diethyl dithiocarbamate (2.65 g) was suspended in 40 mL of dry acetone in a round bottom flask, fitted with a stirrer and condenser, and then 2.48 g of 3-chloropropyl(trimethoxysilane) was added dropwise to get a 1.2:1 mol:mol ratio of dithiocarbamate:trimethoxysilane. The mixture was heated at 50 °C during 15 hours (figure 4.22). Thereafter, insoluble salts were removed by filtration, and the solvent evaporated by a nitrogen stream, obtaining a yellowish oily product.

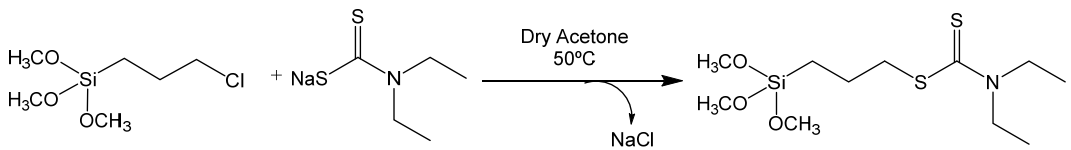

Figure 4.22. Synthesis of the iniferter.

The synthesised iniferter was characterised by FTIR and Nuclear Magnetic Resonance Spectroscopy (RMN). Figure 4.23 depicts IR spectra of the iniferter and the reagents employed to synthesise it. Figure 4.23a, is relative to the IR spectrum of the iniferter compound, the bands that can be appreciated here between 2968 and 2831 cm^{-1} could be related with characteristic absorption frequencies of the -C-H stretching vibrations. The bands at 1482, 1414 and 1355 cm^{-1} were attributed to bending vibrations of $-CH_2-$ and $-CH_3$ functional groups bound to the tertiary amine. These three bands are also present in the spectrum relative to sodium diethyl dithiocarbamate (figure 4.23c) at very close wavenumbers: 1470, 1407 and 1353 cm^{-1}, whereas in the 3-chloropropyl (trimethoxysilane) spectrum (figure 4.23b), no significant band is observed in this interval, what reinforces the performed attribution.

At 1268 and 1204 cm^{-1} two bands of moderate intensity can be appreciated in figure 4.23a. These bands were assigned to stretching vibration frequencies of the C=S and the C-N functional groups respectively. These bands are also noteworthy at 1260 and 1204 cm^{-1} in the spectrum relative to the dithiocarbamate (figure 4.23c).

The broad intense band observable at 1067 cm^{-1} was attributed to the Si-OR stretching vibration of the silane group which usually presents two well defined bands at 1110-1000 cm^{-1} and 800-850 cm^{-1} [131, 132]. This band can also be appreciated at 1073 cm^{-1} in the 3-chloropropyl(trimethoxysilane) spectrum (figure 4.23b), what corroborates this assignation. It should be noticed that this band is not observable in the dithiocarbamate spectrum (figure 4.23c). The band at 807 cm^{-1}, which is also present in the 3-chloropropyl(trimethoxysilane) spectrum (figure 4.23b) at 799 cm^{-1}, was also attributed to the stretching vibration of the SI-OR group.

In addition to the described ones, other intense bands can also be appreciated in these spectra. Particularly in spectrum 4.23c, the bands observed between 3270 and 3211 cm^{-1} were assigned O-H stretching vibrations due to the presence of water of crystallisation in the reagent.

In conclusion, the IR spectrum of the iniferter compound includes bands that match with the ones present in both spectra of the reagents employed in the iniferter synthesis. In this regard, it could be stated that the iniferter synthesis had been correctly performed.

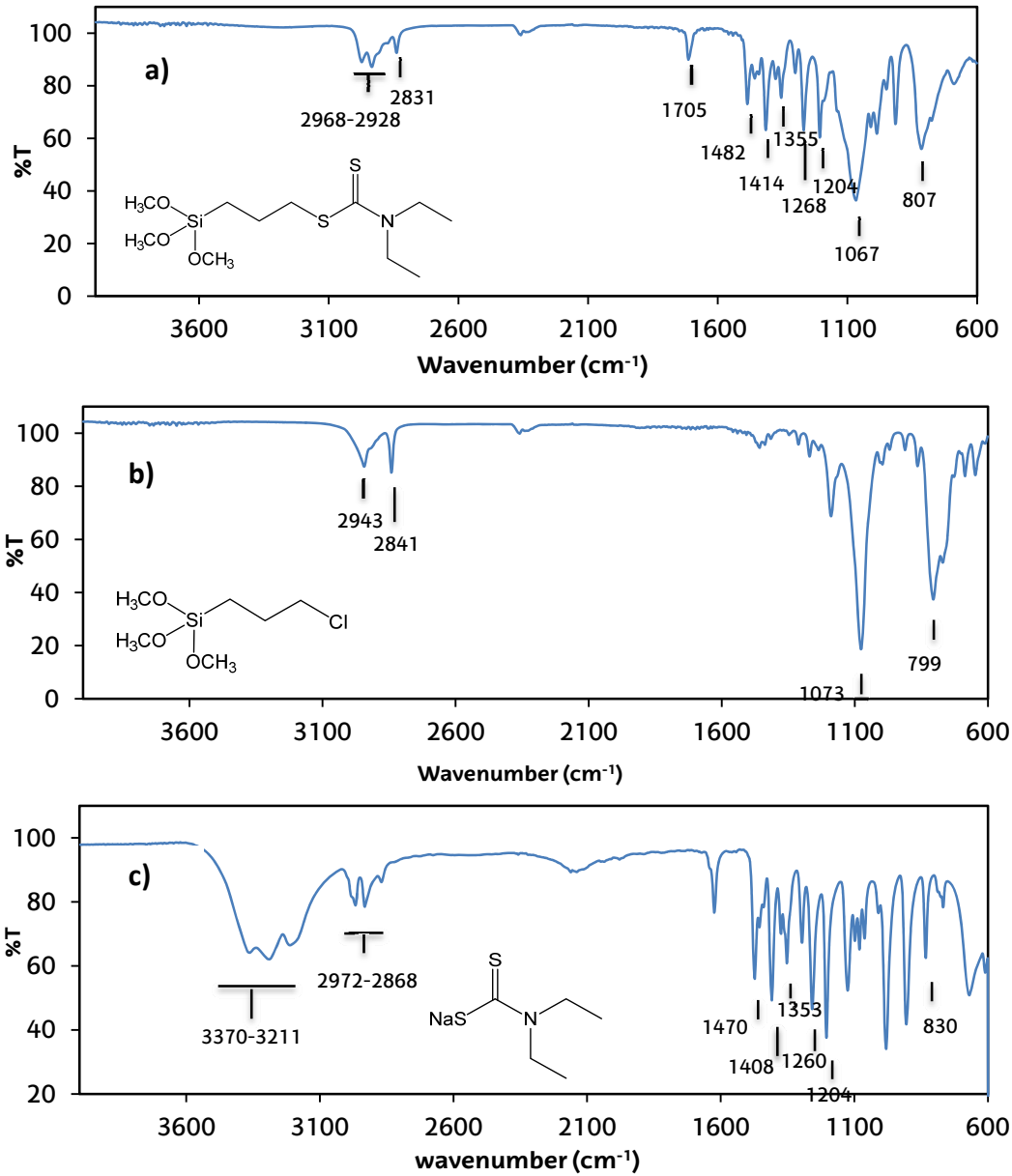

Figure 4.23. FTIR spectra of a) the iniferter, b) 3-chloropropyl(trimethoxysilane) and c) sodium diethyl dithiocarbamate trihydrate.

Nevertheless, additionally, this synthesis was corroborated by ^{1}H RMN. The DDCPTS iniferter as well as sodium diethyl dithiocarbamate, were characterised using ^{1}H NMR spectroscopy (figure 4.24) shows two defined peaks around 4 and 1.2 ppm which were assigned to the two methylene and the two methyl groups respectively of sodium diethyl dithiocarbamate (5 and 6 in figure 4.24). These peaks are also present in the iniferter ^{1}HRMN spectrum which could be indicative of the presence of unreacted reagent. However the presence of new peaks, such as the peak at 3.9 ppm 1.7 and 0.7 ppm, is clearly an indicative of the formation of the iniferter molecule.

These results can be summarised as: ^{1}H NMR ($CDCl_3$) δ (ppm): 0.6-0.72 (2H, J 0.52, Si-$\underline{CH_2}$-CH_2), 1.1-1.23 (6H, J 2.38, CH_2-$\underline{CH_3}$), 1.62-1.8 (2H, J 0.55, CH_2-$\underline{CH_2}$-CH_2), 3.1-3.22 (2H, J 0.42, CH_2-$\underline{CH_2}$-S), 3.4-3.55 (9H, J 2.11, O-CH_3), 3.6-3.7 (2H, J 0.38, CH_2-$\underline{CH_2}$-S), 3.85-3.96 (4H, J 1, N-$\underline{CH_2}$-CH_3).

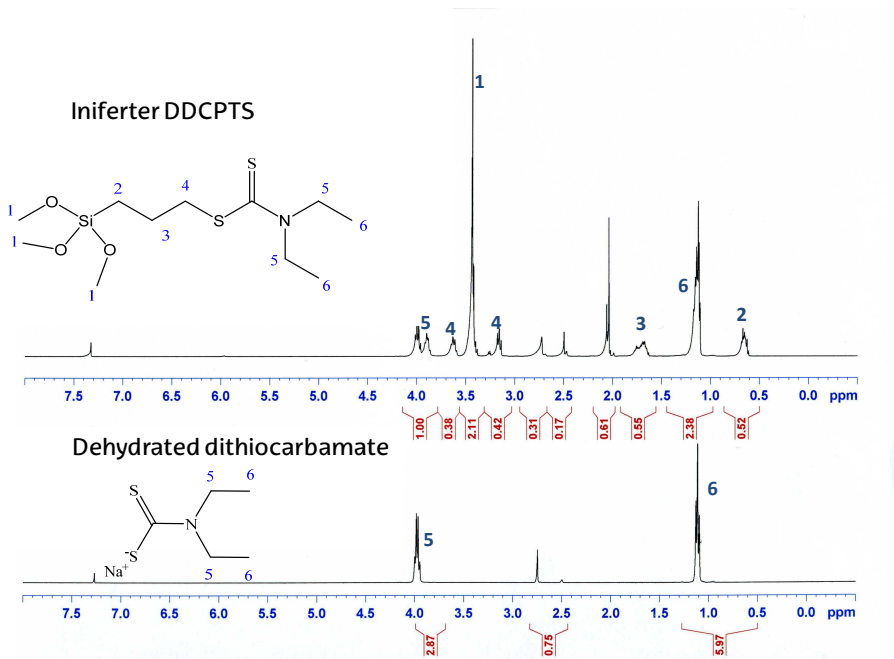

Figure 4.24. ^{1}HNMR spectra of the iniferter and the dehydrated sodium diethyl dithiocarbamate.

5.2.2. Iniferter immobilisation on silica surface

After the activation step, the silica was functionalised coupling the synthesised silane iniferter to the silica surface through its methoxy groups (figure 4.25). The minimum amount of DDCPTS to be employed for functionalisation was calculated based on the amount of silanols on the silica surface (8 μmol/m^2 of silica) and considering a 3:1 silanol: iniferter molar ratio. Nevertheless, an excess of iniferter was employed to avoid having uncoated silica particles.

Based on this, 4.3 g of DDCPTS, were dissolved in 250 mL of dry toluene and, subsequently, 4 g of dry silica particles were dispersed. The suspension was stirred, purged with nitrogen for 15 min and kept in the dark and under inert conditions for 24 h. Then silica beads were filtered out and rinsed successively with MeOH and ACN.

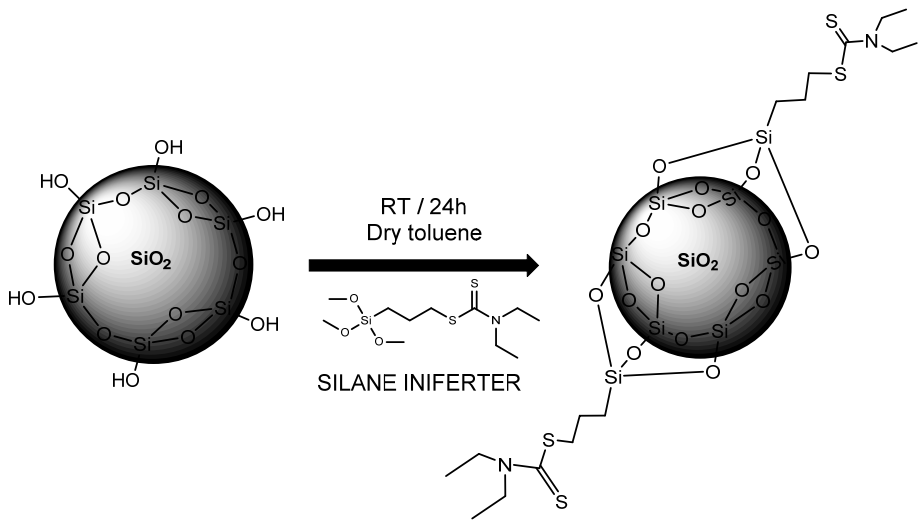

Figure 4.25. Functionalisation of the silica surface with the silane iniferter.

5.3. Silica surface coating with MIP thin layers

Polymer grafting on the functionalised silica was carried out by photo-initiated reversible deactivation radical polymerisation. As the chain growth was expected to be confined to the support surface, the grafting from approach was used. This technique allows having a better thickness control of the grafted polymer [133].

In the present work, an estimation of the polymer thickness to be grafted on the silica support was first carried out; this estimation directly depends on the pore size of the silica particles employed as solid substrate. For this estimation, based on the computational modelling detailed in chapter 3 and considering the preliminary results described in section 4, 1:4:24 was selected as template:functional-monomer:cross-linker molar ratio.

Silica particles used in chromatography applications have very high surface area in order to provide strong analyte retention. This surface area is mainly influenced by its pore size, that is, the higher the pore size, the smaller the surface area. In this context, considering that the pore size of the silica used in this work was 9 nm, a maximum thickness of 4 nm could be grafted on the surface without pore collapse (figure 4.26).

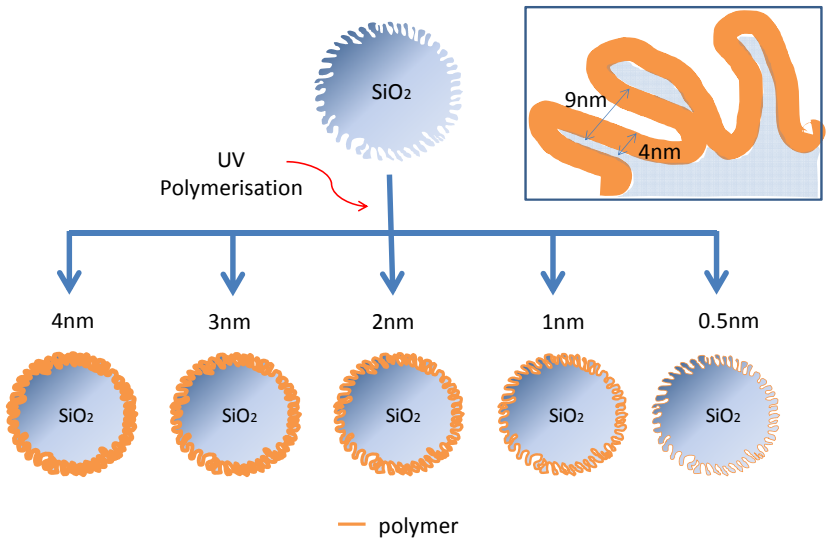

Figure 4.26. Schematic representation of the silica surface coated with different thicknesses of polymer films.

Initially, from the radius of the silica pores (4.5 nm, as provided by the manufacturer), the area (A_i) of each pore was calculated and then, considering the desired polymer thickness, the final uncoated pore area (A_f) is estimated subtracting the desired layer thickness to the pore radius. Then, the pore area difference (A_i-A_f) and its ratio with respect to the initial area (A_i-A_f)/A_i were calculated. This ratio indicates the pore area decrease as a consequence of the grafted polymer layer. Based on this ratio, from the pore volume value (V_i) provided by the manufacturer (9.7 mL/g) the final pore volume (V_f) was calculated using the equation (4.4):

$$V_f = \frac{A_i - A_f}{A_i} V_i \qquad 4.4$$

The difference between the initial and final pore volume is the volume that will be occupied by the polymer thin film. Based on this volume, the relative amount of

monomer moles are calculated (equation 4.5) considering the desired functional monomer:cross-linker ratio and the density of each of the used monomers. As described by the group of Sellergren [78], the amount of monomers in the polymerisation mixture can be adjusted assuming a near to full conversion of all monomers by RDRP polymerisation, what leads to a thin liquid film coating in the inner pores of the silica support.

$$n = \frac{V_f}{\sum\left(\frac{monomer\ ratio \cdot M_w}{\rho}\right)} \qquad 4.5$$

Where V_f is the pore volume difference that is to be occupied by the polymer thin film. M_W is the molecular weight of each monomer in the polymerisation mixture and ρ is the density (g/mL) of that monomer. By this equation, the n value provides the relative amount of monomers (mmol) required in the polymerisation mixture. In this case, as the ratio is 24:4:1 cross-linker: functional monomer: SCIT the mmol necessary of cross-linker will be 24n and for the functional monomer, 4n.

Based on the preliminary results obtained with MIP synthesised by bulk polymerisation, IA and EDMA were chosen as functional monomer and as cross-linker respectively. If a 4 nm coating is to be grafted, the initial and final pore areas would be 63.617 nm^2 and 0.785 nm^2, being the area difference ratio 0.987. Based on this data, a final non-polymerised pore volume of 0.958 g/mL would be obtained (see equation 4.4). Considering the pore volume provided by the manufacturer (0.970 g/mL), the pore volume difference is equal to 0.012 g/mL, a volume that must be occupied by the polymer thin film on the silica support. A polymer that, as previously stated, must be comprised of a 24:4:1 molar ratio of EDMA:IA:SCIT.

In this work, different polymer thicknesses were tested in order to select the one that led to best chiral resolution. Considering the pore size of the solid support, films ranging from 0.5 to 4 nm were grafted on its surface. Depending on the desired

polymer film thickness, different amounts of IA and SCIT (table 4.4) were dissolved in 15 mL of ACN in a 50 mL round bottom flask, and then, the mixture was deoxygenated with high-purity nitrogen for 3 min. Then, the cross-linker (EDMA) and 2 g of the functionalised silica, suspended in 5 mL of ACN, were added. Finally, the whole mixture was deoxygenated by the freeze–pump–thaw degassing method. This is one of the most reliable methods for deoxygenation of laboratory solvents on a small scale and It consists of several steps: a) a degassing step with pure nitrogen, in order to ensure that the flask environment is free of oxygen to prevent from condensing liquid oxygen upon freezing, b) a second step that consists in freezing the solvent with liquid nitrogen and 3) a final step that involves vacuum application for 10-30 minutes, or until the space above the frozen liquid is completely evacuated. These steps should be repeated at least twice more for a total of three free-pump-thaw cycles in order to ensure the complete removal of the dissolved gases. Once the mixture is deoxygenated, ultraviolet irradiation was applied to for 3 h under constant stirring in a multiMovilROD tube shaker (J. P. Selecta, Barcelona, Spain) at a rolling speed of 15 rpm. Finally, polymerised silica particles (Si-MIP) were collected, filtered and washed with 250 mL of ACN.

Table 4.4. Composition of the different polymerisation mixtures depending on the estimated coating thickness.

	Thickness (nm)	SCIT (mmol)	IA (mmol)	EDMA (mmol)	Silica (g)
SI-MIP/NIP 1	4	0.19	0.79	4.74	2
SI-MIP/NIP 2	3	0.18	0.71	4.27	2
SI-MIP/NIP 3	2	0.14	0.55	3.32	2
SI-MIP/NIP 4	1	0.08	0.32	1.90	2
SI-MIP/NIP 5	0.5	0.04	0.17	1.00	2

The NIP-coated silica particles (Si-NIP) were synthesised using the same procedure but in the absence of SCIT in the polymerisation mixture.

5.4 Characterisation of the MIP-modified silica

Characterisation of the structure and the morphology of the materials is crucial to get information concerning the homogeneity of the stationary phase, which influences sample loading capacity and mass transfer kinetics [134]. Methods such as Elemental Analysis (EA) are useful to obtain information concerning the polymer yield on the surface of a solid support. Spectroscopic techniques including Fourier Transform Infrared (FTIR), Raman, Ultraviolet-Visible or Nuclear Magnetic Resonance or emission spectroscopies, are regularly used to get information of the chemical and structural composition [34]. Other techniques such as Thermogravimetric Analysis (TGA), are also important as a tool for the study of conformational transitions, thermostability and therefore degradation processes in polymers [134]. Concerning the pore size, surface area or MIP morphology, techniques such as porosimetry, Scanning Electron Microscopy (SEM) and swelling and solvent uptake are commonly used. In this study, EA, FTIR, TGA and SEM have been employed to characterise the silica particles coated with MIP thin films.

5.4.1. Elemental Analysis

Elemental Analysis on carbon, hydrogen and nitrogen (sometimes also on oxygen and sulphur) is the most essential and classical method performed to characterise the elemental composition of an organic sample. In EA, the sample is completely and instantaneously oxidised by oxygen combustion at an approximate temperature of 1020° C. For instance, carbon and hydrogen are determined in organic compounds by conversion through combustion to carbon dioxide and water. Likewise, nitrogen containing compounds are converted into nitrogen gas [134]. A thermal conductivity detector provides the signal for each element, what allows obtaining the relative weight percentages of the elements.

In this study, Elemental Analyses were carried out to unmodified silica, iniferter-modified silica and MIP or NIP-grafted silicas to estimate its surface coverage based on the change in carbon and nitrogen contents.

In the first instance, this technique allowed for determining the final density of the iniferter-modified silica, which was expected to be around 2.66 μmol/m^2, calculated considering a maximum silanol density of 8 μmol/m^2 and a stoichiometric 3:1 silanol: iniferter ratio. For this purpose, the Berendsen-de Galan equation (eq. 4.6) [135] was employed. Where δ is the area density (in μmol of grafted group per m^2 of native silica), p is the carbon or nitrogen percentage (w/w %), S is the specific surface area (m^2/g) of the native silica, C is the atomic weight of carbon or nitrogen, n is the number of carbon or nitrogen atoms per grafted group and M the molecular weight of the attached group.

$$\delta = \frac{10^6 p}{S(100\ Cn - pM)} \qquad 4.6$$

Obtained results are shown in table 4.5. As illustrated, the elemental composition of the iniferter-modified silica and the native one is significantly different. The estimated area density (1.88 μmol/m^2) was close to the theoretical maximum value of 2.67 μmol/m^2. From the estimated area density, surface coverage was calculated based on equation 4.7. Calculated coverage (C) was found to be 70% of the silica surface.

$$C_{Si-iniferter} = \frac{100\delta}{8/3} \qquad 4.7$$

Table 4.5. Elemental Analysis results.

Support	Thickness	Elemental composition			Area density	Coverage
		%N	%C	%H	(μmol/m^2)	(%)
Silica	-	‹0.10	‹0.30	1.12	-	-
Si-Iniferter	-	0.98	6.62	1.89	1.88	70.83
Si-MIP 1	4	0.90	21.30	3.23	-	-
Si-NIP 1	4	0.86	22.83	3.36	-	-
Si- MIP 2	3	0.85	23.35	3.60	-	-
Si-NIP 2	3	0.82	24.7	3.51	-	-
Si-MIP 3	2	0.77	19.48	2.85	-	-
Si-NIP 3	2	0.75	18.91	3.75	-	-
Si-MIP 4	1	0.75	19.22	3.14	-	-
Si-NIP 4	1	0.66	17.8	2.93	-	-
Si-MIP 5	0.5	0.61	13.73	5.58	-	-
Si-NIP 5	0.5	0.63	14.65	4.78	-	-

Concerning NIP and MIP modified materials, the carbon content was significantly higher than the one observed in the iniferter-modified silica. In contrast, the nitrogen percentage remained almost equal. Given that the iniferter was the only molecule containing nitrogen among the ones employed, only the carbon percentage increase can be attributed to the polymer growth on silica surface. Actually, as it is shown in table 4.5. the higher the thickness the higher the percentage of carbon. Unexpectedly, an increment of hydrogen percentage was appreciated in the SI-MIP 5 and the SI-NIP 5, which are relative to columns with lowest thickness (0.5 nm). This could be attributed to an excess of unreacted silanols on the silica surface. Given that the coverage of the silica surface with the iniferter is not 100%, the silanol groups are more exposed than when the polymer is thicker.

5.4.2. Fourier Transform Infrared Spectroscopy

ATR/FTIR microscopy was employed for the elucidation of the specific functional groups of the silane iniferter and the monomers employed for the MIP synthesis, thereby confirming the proper functionalisation and the synthesis of the polymer on the silica surface. In this regard, the IR spectra of bare silica, iniferter-functionalised silica and MIP/NIP-modified silica were acquired by placing the material directly over the ATR crystal of the equipment. Prior to FTIR measurements, all samples were dried at room temperature.

As shown in figure 4.27, a broad and intense band at 1110-1000 cm^{-1} can be appreciated in all infrared spectra. This band was attributed to the Si-O stretching vibration of the silica. The inset (figure 4.27) depicts magnifications of each of the registered spectra. Weak bands close to 2950 cm^{-1} can be distinguished, which could be indicative of the iniferter coupling or polymer grafting. These bands were assigned to -C-H stretching vibrations of methyl and methylene groups and, as it can be deduced from the inset, they were slightly more intense in Si-MIP and Si-NIP spectra than in the spectrum of the iniferter-modified silica. In Si-MIP and Si-NIP spectra, apart from these bands, a moderately intense band is noticeable at 1723 cm^{-1} which was assigned to C=O stretching vibration. Both the cross-linker (EDMA) and the functional monomer (IA) are the only molecules among the employed ones that contain C=O groups, so the presence of this band in the IR spectrum can be indicative of the polymer formation on the silica surface.

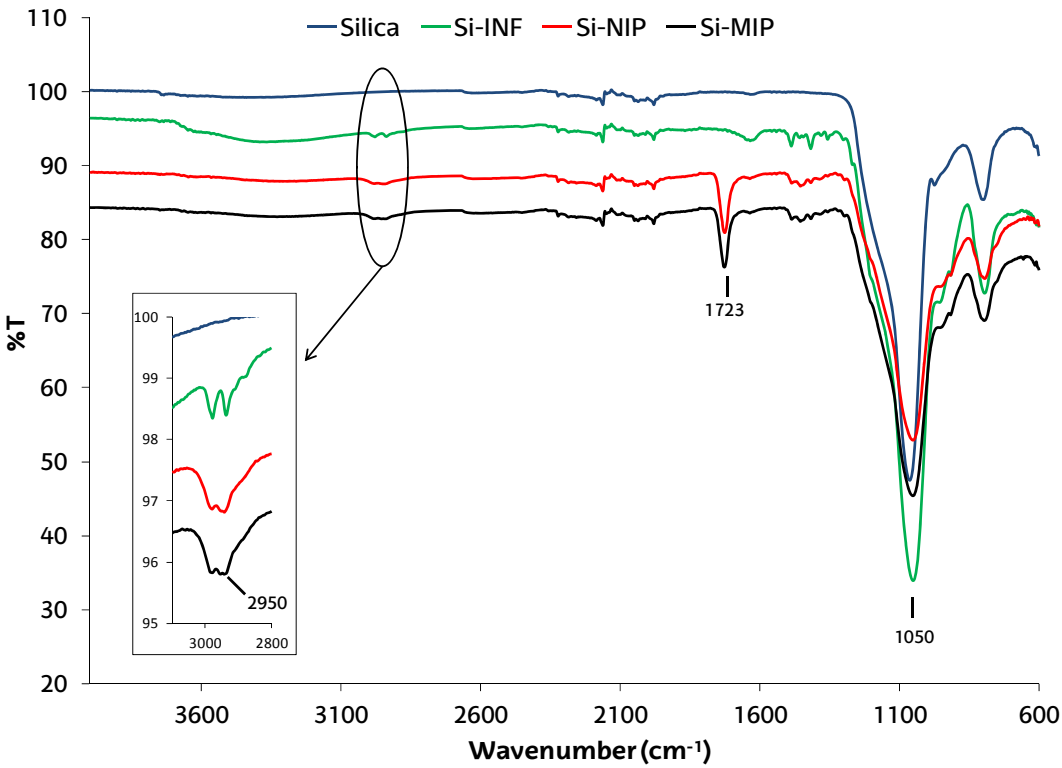

Figure 4.27. FTIR spectra of bare silica, iniferter modified silica (Si-INF), non-imprinted polymer-modified silica (Si-NIP) and molecularly imprinted polymer-modified silica (Si-MIP).

When Si-MIP coated with different polymer thicknesses were measured by this technique, no significant difference was observed (figure 4.28). However, in the Si-MIP 5 spectrum, which corresponds with the one with the smallest film of polymer over the silica, a broad band from 3070 to 3600 cm^{-1} can be distinguished. This was assigned to the O-H stretching vibration of unreacted silanol groups that may be uncoated due to the low polymer thickness, that is, 0.5 nm. As discussed in the previous section, this fact

seems to confirm that the amount of monomers in the synthesis step was not enough to the completely coat the silica particles.

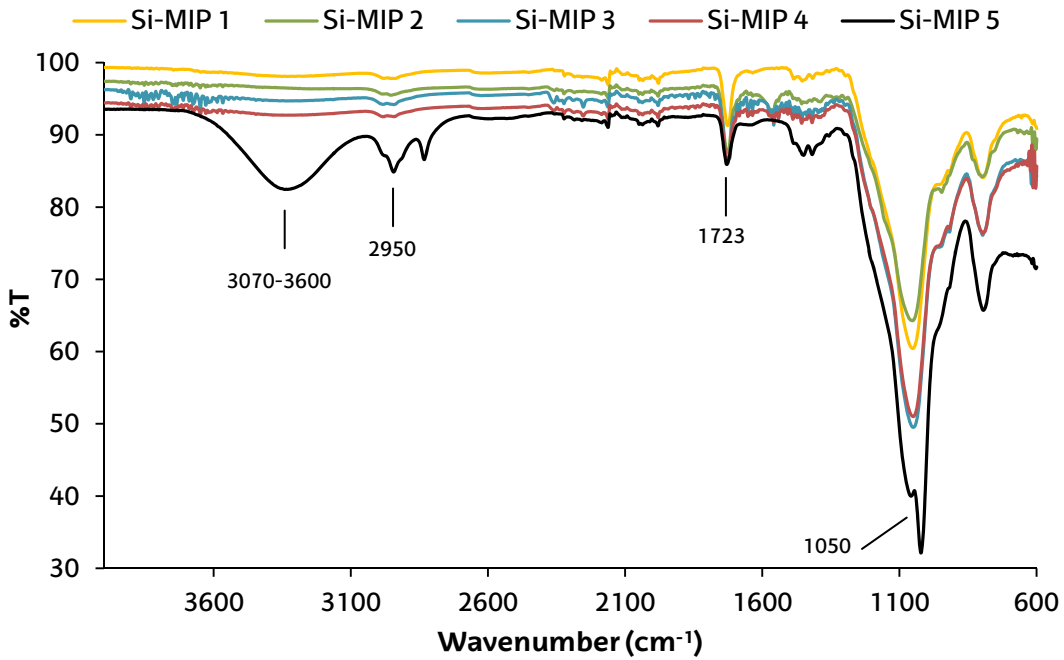

Figure 4.28. FTIR spectra of the different molecularly imprinted polymer-modified silica with different estimated coating thicknesses.

5.4.3. Thermogravimetric Analysis

Thermogravimetric Analysis (TGA) is a thermal method that involves the measurement of weight loss as a function of temperature or time. This technique can be used not only to quantify the mass change in a polymer associated with degradation processes [34], but also to obtain a qualitative determination of the polymer mass adhered to the silica surface.

Initially, TGA were carried out for all the MIP and NIP synthesised with different thicknesses. As it was expected, even if the differences between the weight losses are slightly different, it can be observed in figure 4.29 how the lower the calculated thickness, the smaller the weight loss related to the polymer coating.

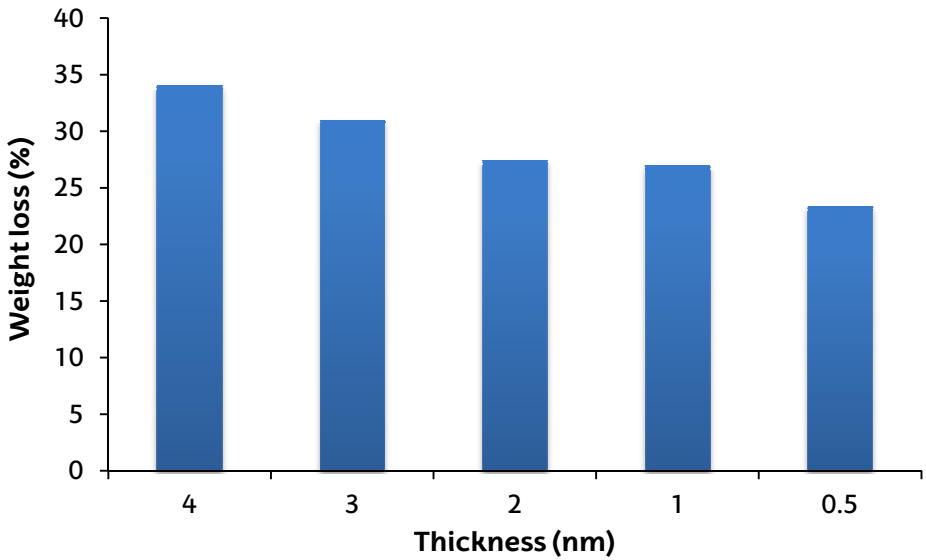

Figure 4.29. Weigh loss percentage estimated by TGA for silica particles coated with different polymer thicknesses.

Secondly, thermal stability of the iniferter-modified silica and its derivatives, Si-NIP1 and Si-MIP1, was compared, as they were the ones having highest polymer thickness. As depicted in figure 4.30, in all cases, an initial mass loss can be observed at 100ºC due to the solvent content of the material. As regards Si-INF, weight loss at this point is higher due to the fact that the material was not dried in order to prevent it from thermal premature initiation. The weight loss observed around 400ºC is due to the organic matter on the silica. In the iniferter modified silica, the weight loss was lower

than the one observed in the Si-MIP1 or Si-NIP1, due to the polymeric absence on the silica surface. As could be expected, the polymer mass in the NIP and the MIP is quite similar. However, weight loss in the NIP is slightly higher, what may indicate a slightly lower polymer amount in the MIP material due to defects in the polymer structure associated with the presence of the template in the synthesis step.

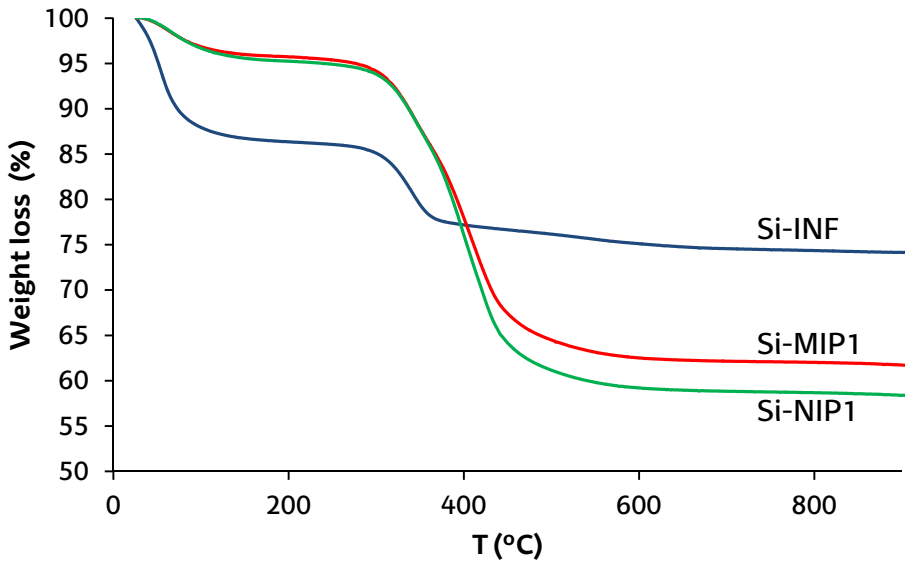

Figure 4.30. TGA measurements of the iniferter modified silica (SI-INF), molecularly imprinted polymer-modified silica (Si-MIP1) and non-imprinted polymer-modified silica (Si-NIP1).

5.4.4. Scanning Electron Microscopy

In order to become a "true" HPLC material, a MIP-based stationary phase should be composed of monodispersed and very regular beads with an average diameter from 2 to 10 µm [37]. That means that the performance of the MIP is not exclusively dictated by the interaction of the template with the functional monomer at a molecular level in the pre- and post-polymerisation, but also by their overall morphological

features [136]. Scanning Electron Microscopy (SEM) gives information on the morphology and surface texture of the materials. In this study in particular, it also provided information about the effectiveness of the synthesis inside the pores of the silica support.

Figure 4.31 depicts SEM micrographs of uncoated and coated silica materials. As illustrated, no significant difference is appreciable between bare silica (figure 4.31a) and the iniferter-modified one (figure 4.31b). Nevertheless, in MIP and NIP coated silicas (figure 4.31c and d) slight differences on their surface are appreciable in contrast to bare silica. Moreover, as it can be deduced from the figure, the MIP-coated silica shows higher roughness, probably due to the presence of the template during polymerisation what favours the formation of defects on the polymer layer. In addition optical SEM images showed that there was no particle agglomeration, what confirms that the synthesis of this material has successfully been carried out and therefore it can be considered as a "true" material for liquid chromatography.

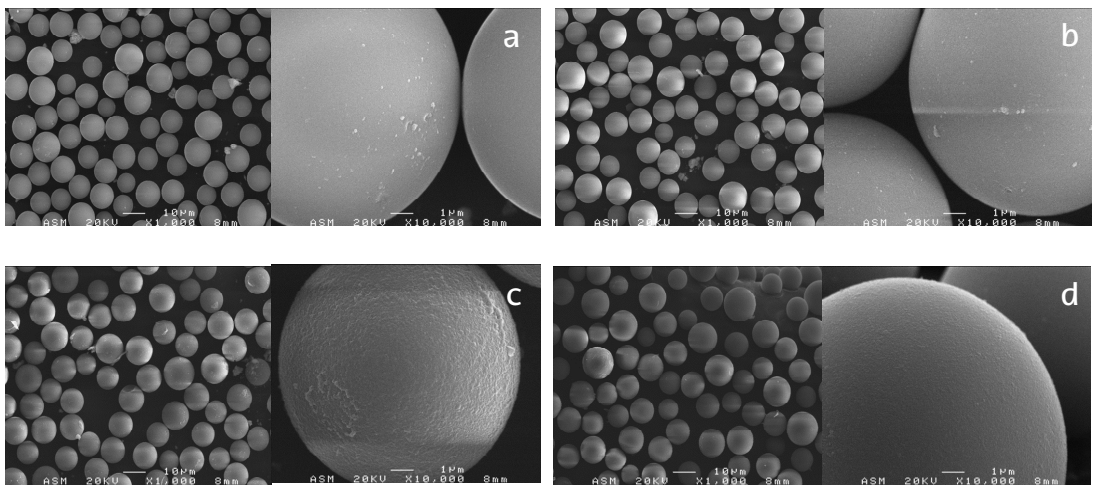

Figure 4.31. SEM micrographs at different magnifications of a) bare silica, b) iniferter-modified silica, (c) molecularly imprinted polymer-modified silica and (d) non-imprinted polymer modified silica.

6. Chromatographic evaluation of the chiral stationary phase

The developed MIP-coated silica was finally evaluated as stationary phase for the chiral resolution of citalopram racemate by liquid chromatography. To this end, different experimental variables that may influence on chiral separation were assessed such as pH, temperature and buffer percentage in the mobile phase.

6.1. Column packing

Stainless steel chromatographic columns (100 mm L x 4.6 mm i.d.) were packed with the MIP or NIP-coated silica material using a slurry packing procedure. For this purpose, 1.5 g of the developed material was suspended in 20 mL of ACN and it was then packed using the Pack in a Box column packing system at constant pressure (2000 psi), employing ACN as the pressurising agent. Afterwards, the column was connected to the chromatographic system and a mobile phase that consisted of 200 mM formic acid in MeOH was passed through it, at a flow rate of 1 mL/min, for 5 hours for template removal. Finally the column was washed with a ACN: water (10:90 v/v) mixture and then with 100% ACN.

6.2. Optimisation of the chiral separation

In order to maximise the separation of target enantiomers, different experimental variables that may contribute in chiral separation were assessed first. In this regard, the concentration of the buffer used as aqueous phase, its pH and its percentage over the organic phase was evaluated. This evaluation was carried out using the Si-MIP/NIP 1 material due to fact that it was the silica with highest polymer thickness coating (4 nm) and therefore higher retention of both SCIT and RCIT could be expected.

Separation efficiency was assessed based on the separation factor (α) and the resolution (R) whereas imprinting effect was evaluated through the Imprinting

Factor (IF). The resolution (R) is defined as the retention times differences between two chromatographic peaks, divided by the combined widths of the elution peaks (Eq.4.8). It is a measure of the degree of chromatographic separation of two adjacent peaks.

$$R = \frac{(t_B - t_A)}{0.5(W_B + W_A)} \qquad 4.8$$

Where B is the analyte with longest retention time, and t and W are the retention time and elution peak width respectively. Rs = 0 indicates complete co-elution or no separation. Rs = 1 indicates partial separation and is the minimum separation required for quantification. Rs = 1.5 indicates baseline separation. Ideally, the goal of most HPLC methods is to achieve baseline separation (Rs = 1.5–2.0) [137].

Figure 4.32 depicts the influence of a) buffer percentage in the mobile phase, b) its pH and c) its concentration, on peak resolution and separation factor. The Imprinting Factor has also been calculated for every tested condition. As can be deduced from figure 4.32a buffer percentages higher than 30% contributed to peak broadening what made resolution decrease. This effect was attributed to non-specific hydrophobic interactions which would be favoured as water content in the mobile phase increased. However, the IF does not follow a similar behaviour; even if small buffer percentages led to higher IF, an increasing tendency was observed as buffer percentage was higher became higher. Based on this finding, 30% was selected as the IF was highest at this point.

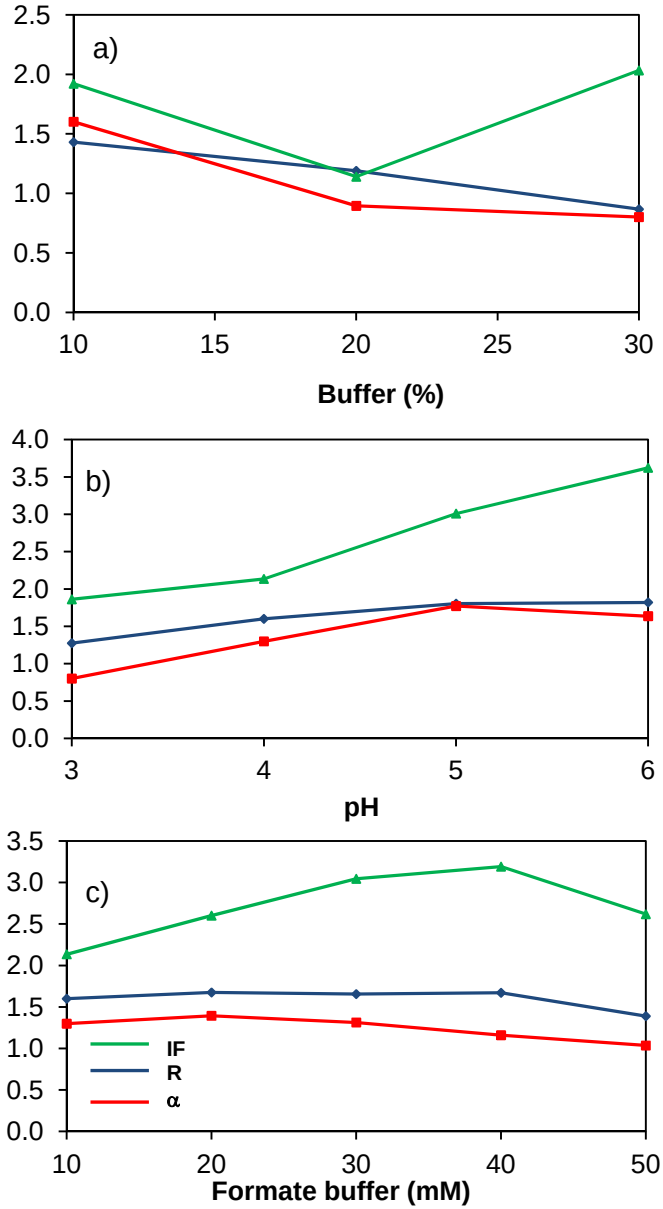

Figure 4.32. Effect of buffer a) percentage, b) pH and c) concentration on the separation factor (α), resolution (R) and imprinting factor (IF) of the CSP.

Considering that the functional monomer, IA, is not a neutral monomer (pKa_1 3.80 and pKa_2 5.45), pH optimisation was crucial in order to minimise non specific interactions with randomly distributed carboxylic groups of the functional monomer. As it is shown in figure 4.32b, the higher the pH value, the higher the retention of both enantiomers. In fact, even if the IF values were best at pH 6, it was discarded for further research due to the high retention times registered, what led to excessive peak broadening. On the other hand, pH values lower than 4 were not enough to get appropriate enantiomer separation. This effect could be attributed to the neutralisation of carboxylic groups of the functional monomer leading to weaker analyte binding in the imprinted sites and, in consequence, a worse peak resolution. In contrast, less acidic pHs led to too high retention times with the consequent peak broadening. pH 4 was found to be the one providing best enantiomer resolution in a shorter time, figure 4.33.

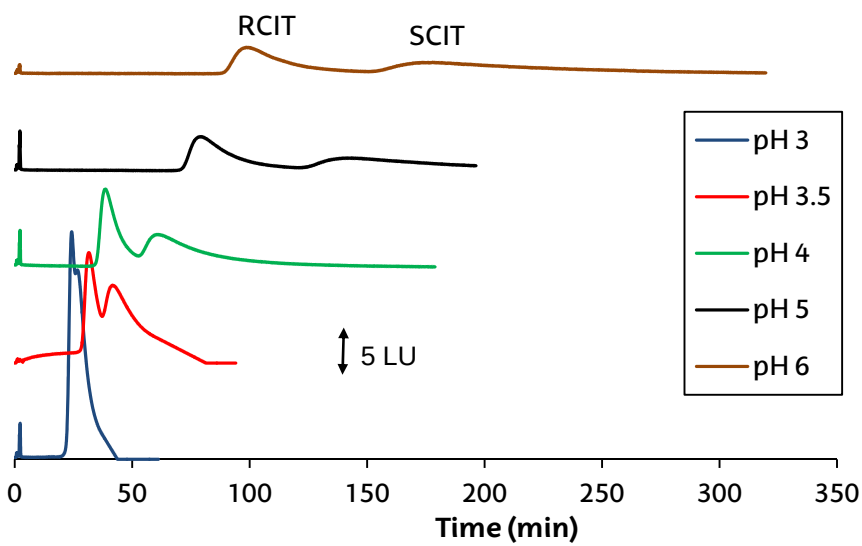

Figure 4.33. Chromatograms registered after the injection of 25 µg/mL of citalopram using a 70:30 v/v mixture of ACN and formate buffer (10mM) at different pH.

As regards buffer concentration (figure 4.32c), resolution and separation factors remained almost constant at all tested values. However, the best IF value was registered using 40 mM of formate buffer, hence, this was chosen for further experimental.

In conclusion, best enantiomeric resolution was observed working at pH 4, at a buffer percentage of 30% and a buffer concentration of 40 mM. The chromatograms registered with the MIP and the NIP columns at these conditions are shown in figure 4.34. As depicted, the NIP column was not capable of resolving the racemate, being the signal of both enantiomers overlapped in a single peak.

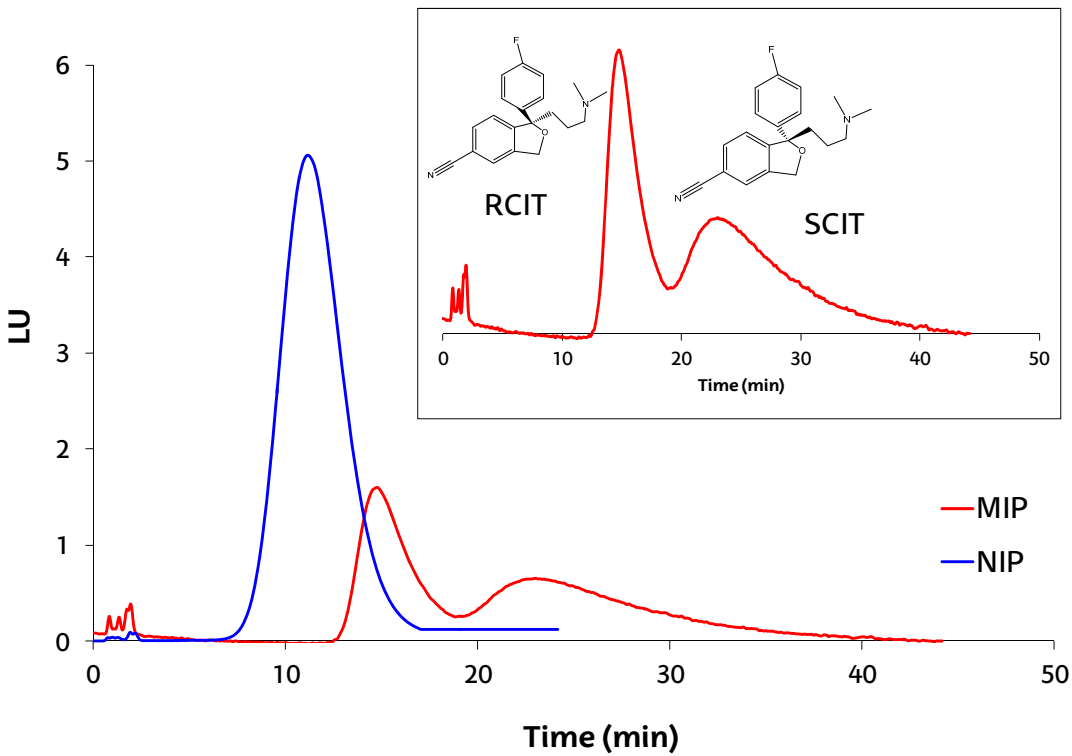

Figure 4.34. Chromatographic profile of citalopram using a MIP and a NIP column. ACN : 40mM formate buffer (70:30 v/v).

6.3. Thermodynamic study

The temperature under which the chromatographic process is carried out, may be another factor that contributes in proper chromatographic resolution of analytes. It has thermodynamic and kinetic effects on chromatographic separations [138]. The former is the one that influences the MIP selectivity, which arises from the differences of binding free energies of different substrates in an imprinted site [139]. Concerning enantiomers, MIP selectivity will be determined from their differences in Gibbs free energies, which depend on the temperature employed during the separation process (T) and the retention factor of the analyte (k), as detailed in equation 4.9:

$$\Delta G = -RTlnk \qquad 4.9$$

Where R is the ideal gas constant (8.314 J/mol·K). The difference between free energies of both enantiomers can be referred to as the separation factor (α), by equation 4.10:

$$\Delta G_2 - \Delta G_1 = \Delta(\Delta G) = -RTln\alpha = \Delta(\Delta H) - T\Delta(\Delta S) \qquad 4.10$$

And consequently,

$$ln\alpha = -\frac{\Delta(\Delta H)}{RT} + \frac{\Delta(\Delta S)}{R} \qquad 4.11$$

Where Δ(ΔG), Δ(ΔH), and Δ(ΔS) represent, respectively, the difference of Gibbs free energy increment of the enantiomer-MIP phase transfer and the differences in the enthalpy and entropy for a given pair of enantiomers [140]. Through Van't Hoff plot, where the experimental ln α values are represented versus the temperature inverse, 1/T (K^{-1}), the enthalpy, ΔH, and entropy, ΔS, of the global interaction of each enantiomer

can be estimated from the slope and the intercept value of the plot. For this purpose, the chromatographic separation of both enantiomers is necessarily to be performed at different temperatures calculating the α value at every single temperature [141].

In this work, temperature effect was evaluated injecting separate solutions of RCIT and SCIT independently in the chromatographic system. Column heater was set to the desired temperature and it was kept constant at least for 20 minutes before injection. From the retention values of each compound, the retention factor (k), and the separation factor (α), were calculated. Subsequently, Van't Hoff plot was constructed by plotting the experimental ln α values versus 1/T. As illustrated in figure 4.35, two linear sections can be clearly distinguished. This is an indicative of the differences of the thermodynamic processes and it happens as a result of conformational changes of the analyte or the stationary phase as a consequence of their interaction [142].

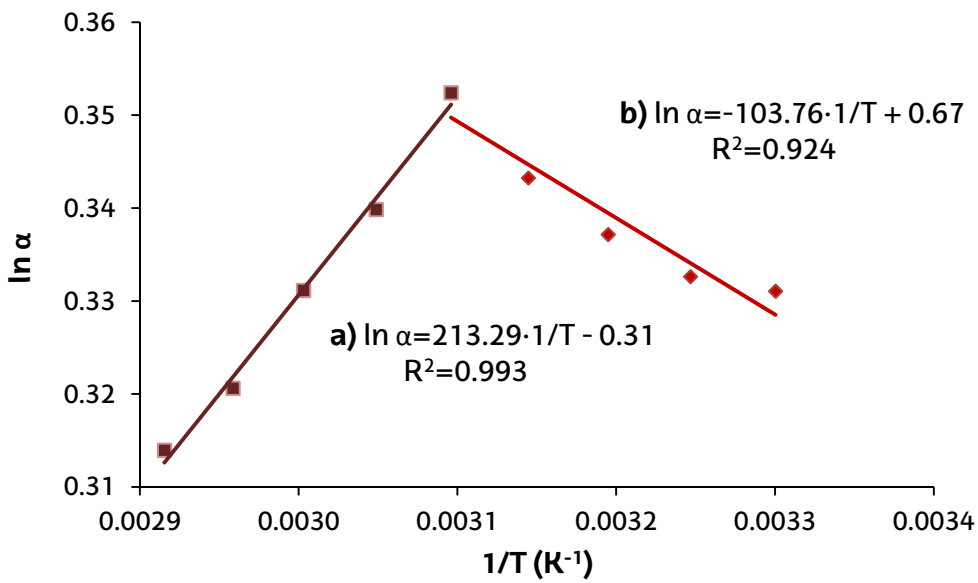

Figure 4.35. Van't Hoff plot.

For each section, experimental data was fitted by linear regression and Δ(ΔS) and Δ(ΔH) were calculated from the intercept and the slope of each equation. At temperatures ranging from 50 to 70ºC (section a), Δ(ΔH) was found to be -1.77 KJ/mol and Δ(ΔS) was equal to -2.57 J/mol. Negative Δ(ΔH) values indicate an exothermic transfer of the preferentially adsorbed enantiomer from the mobile phase to the stationary phase and therefore chiral recognition is favoured. The more negative the value, the stronger the interaction with the stationary phase [143]. However, too negative Δ(ΔS) can counteract chiral recognition spontaneity making Δ(ΔG) increase (equation 4.10). In this case, since $|\Delta(\Delta H)| > |T\Delta(\Delta S)|$, the process in section a) is enthalpy controlled and temperature increase worsens enantioselectivity.

On the other hand, in section b, the opposite effect occurs. Here Δ(ΔH) and Δ(ΔS) values are 0.86 KJ/mol and 5.57 J/mol respectively so $|\Delta(\Delta H)| < |T\Delta(\Delta S)|$ and the process is entropy controlled. In consequence, from 30 to 50ºC, as temperature increases, enantioselectivity is enhanced. However, even if the temperature of HPLC analysis increases enantioselectivity, the differences between 40ºC and 50ºC were insignificant, and in order to prevent the MIP stationary phase from getting damaged and to extend column life (the higher the temperature the faster the MIP degradation), a temperature of 40ºC was chosen for further analysis.

6.4. Layer thickness effect on polymer capacity

The thickness of the polymer coating is known to affect MIP performance. Making thin grafted films, it could be expected that mass transfer problems associated with most of MIP could be overcome in a greater or lesser extent [42].

In this work, different coating thicknesses were tested in order to know the one that led to the best MIP performance in comparison with the NIP. The total monomer amount was estimated to get films of 0.5, 1, 2, 3 and 4 nm in average thickness, as described in section 5.3. The binding capacity of each of the prepared materials was then determined by frontal chromatography. To this end, different thickness materials

were packed in chromatographic columns and a solution of 25 µg/mL SCIT in ACN was percolated through the columns to evaluate the retention capacity of the materials. As a result, a sigmoid chromatogram was obtained for each tested concentration. From the inflexion point of the sigmoid curve the retention volume was calculated.

Finally, the binding capacity was calculated from the retention volume, the mass of stationary phase packed in the column and the analyte concentration percolated through the column, using the following equation:

$$B_C(mg/g) = \frac{V_R(mL)\ x\ C\ (mg/mL)}{m\ (g)} \qquad 4.12$$

As it could be expected, the highest MIP capacity was appreciated when 4 nm coatings were employed (table 4.6). It should be emphasised that NIP retention capacity was higher than the one observed for the MIP for thicknesses below 3 nm. As previously reported by Sulitzky *et al.* [42], 10 nm pore size silica containing ultrathin grafted films (1 nm approximately) exhibited highest chromatographic efficiency.

Table 4.6. Binding capacities of the surface-modified silicas at different thicknesses

Thickness (nm)	Binding capacity (mg SCIT/g polymer)	
	MIP	NIP
4	2.29	1.06
3	1.58	1.37
2	1.02	1.49
1	1.16	2.06

However, particles with thinner films (‹1 nm) were unable to separate the enantiomers. In the present work, these columns were chromatographically tested at

optimised chromatographic conditions, (section 6.2). It was observed that thicknesses below 4 nm were unable to resolve the racemate. Moreover, NIP retention capacity was higher than the one observed for the MIP. This fact could be attributed to the lower number of binding sites as coatings were thinner.

6.5. Binding experiments and adsorption isotherms

For batch rebinding experiments, stocks solutions of SCIT were prepared in ACN in a concentration range from 2.5 to 90 µg/mL (7.71×10^{-3} – 0.28 mM). 2mL aliquots of these solutions were incubated with 20 mg of MIP or NIP-coated silica, for 24 h, under stirring in a rotating shaker (15 rpm) at room temperature. Thereafter, the silica was left to decant and the supernatant was removed carefully and filtered through 0.22 µm filters. The SCIT concentration that remained free in each solution was determined by HPLC-FD.

Analyte concentration bound to the receptor was plotted versus the free ligand concentration at every tested SCIT level. The adsorption isotherms resulting from this data are depicted in figure 4.36. It is clearly noticeable the different tendencies between the MIP and the NIP materials. The NIP-coated silica shows an almost linear behaviour whereas the MIP-coated one displays saturation kinetics. The appreciated differences may be indicative of the different binding mechanisms in the NIP and MIP materials. SCIT binding to NIP-coated silica may be governed by non-specific interactions with the randomly distributed carboxylic groups of the functional monomer, since hydrophobic binding is not likely to happen in the solvent selected for binding experiments. This binding does not show a saturation-like behaviour, since no imprinted site is expected to be present in the NIP material.

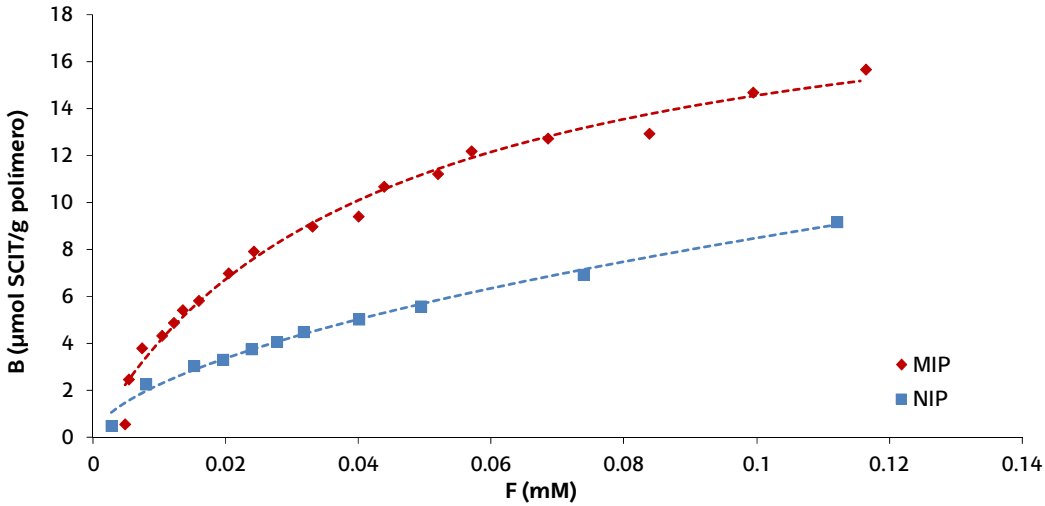

Figure 4.36. Binding isotherms, registered by batch rebinding experiments, using the MIP-coated and the NIP-coated silica as adsorbents.

The experimental isotherms were fitted to different binding models such as the Langmuir, Bi-Langmuir, Freundlich and Freundlich-Langmuir isotherm models. The binding parameters calculated with each model are summarised in table 4.7.

Table 4.7. Fitting parameters for the experimental binding isotherms.

Langmuir model		**MIP**	**NIP**
Number of binding sites	N_t (µmol/g)	19.99 ± 0.59	13.56 ± 1.23
Affinity constant	K_a (mM^{-1})	$2.59\ 10^{-2} \pm 0.18\ 10^{-2}$	$1.58\ 10^{-2} \pm 0.26\ 10^{-2}$
Coefficient of determination	R^2	0.991	0.976
Absolute sum of squares		2.346	1.323
Bi-Langmuir model		**MIP**	**NIP**
Number of binding sites	N_{t1} (µmol/g)	$68.95 \pm 1.19\ 10^{3}$	3.79 ± 1.85
Number of binding sites	N_{t2} (µmol/g)	13.46 ± 7.96	$394.80 \pm 10.60\ 10^{3}$
Affinity constant	K_{a1} (mM^{-1})	$0.58\ 10^{-3} \pm 11.95\ 10^{-3}$	$8.79\ 10^{-2} \pm 5.76\ 10^{-2}$
Affinity constant	K_{a2} (mM^{-1})	$4.13\ 10^{-2} \pm 2.16\ 10^{-2}$	$0.13\ 10^{-3} \pm 3.46\ 10^{-3}$
Coefficient of determination	R^2	0.994	0.995
Absolute sum of squares		1.500	0.279
Freundlich model		**MIP**	**NIP**
Average binding affinity	a (mM^{-1})	1.51 ± 0.12	0. 60 ± 0.05
Heterogeneity factor	m	0.50 ± 0.02	0.58 ± 0.02
Coefficient of determination	R^2	0.983	0.990
Absolute sum of squares		4.491	0.521
Freundlich-Langmuir		**MIP**	**NIP**
Number of binding sites	N_t (µmol/g)	24.97 ± 3.09	206.40 ± 1334
Average binding affinity	a (mM^{-1})	$3.16\ 10^{-2} \pm 0.26\ 10^{-2}$	$2.80\ 10^{-3} \pm 17.4\ 10^{-3}$
Heterogeneity factor	m	0.82 ± 0.07	0.59 ± 0.10
Coefficient of determination	R^2	0.985	0.990
Absolute sum of squares		1.632	0.516

In order to determine which model fitted best to experimental data, a statistical comparative test was carried out by the Graphpad® software (table 4.8).

Table 4.8. Comparative results employing the F test.

Comparative test between models			
Comparison	Preferred model	F value	*p*
Langmuir (h_0) vs Bi-Langmuir (h_1)	Langmuir	3.668	0.0546
Langmuir (h_0) vs Freundlich-Langmuir (h_1)	Freundlich-Langmuir	6.132	0.0267
Freundlich (h_0) vs Freundlich-Langmuir (h_1)	Freundlich-Langmuir	24.530	0.0002

The Freundlich-Langmuir isotherm model was found to be the best fitting one, which is described by equation 4.13.

$$B = \frac{N_t a F^m}{1 + a F^m} \qquad 4.13$$

For the Freundlich-Langmuir model (see table 4.7), the average binding affinity of the MIP ($3.16\ 10^{-2} \pm 0.26\ 10^{-2}$ mM^{-1}) was noticeably higher than the one observed for the NIP ($2.80\ 10^{-3} \pm 17.4\ 10^{-3}$ mM^{-1}). The heterogeneity factor of the imprinted material was 0.82, whereas the *m* value of the NIP was found to be 0.59, what clearly denotes a more homogeneous binding site distribution of the MIP. In what concerns the number of binding sites, the value observed for the NIP material was around 10 times higher than the one observed for the MIP, 206.4 ± 1334 μmol/g versus 24.97 ± 3.09 μmol/g. This could be attributed to a higher amount of non-specific low-affinity binding sites related with randomly distributed carboxylic functional groups in the polymer. In other words, as could be expected, a higher number of binding sites with a more heterogeneous distribution and with much lower binding affinity was observed for non-imprinted materials in comparison with imprinted ones.

7. Molecularly imprinted chiral nanoparticles grafted to the surface of silica beads for the chromatographic resolution of the citalopram racemate

Surface grafting of MIP layers onto performed silica beads has been proposed in previous sections as an attractive and successful technique to obtain imprinted materials for chromatographic chiral separation. These materials provide faster mass transfer, more accessibility to imprinted sites and more higher recognition capacity for the target enantiomer over conventional MIP stationary phases synthesised by traditional bulk polymerisation [144]. However, MIP prepared by surface polymerisation still suffer from binding site heterogeneity [145] which is responsible for poor chromatography efficiency, peak asymmetry and tailing [146, 147]. These drawbacks limit their application in chiral chromatography in comparison with stationary phases based on chiral selectors [12, 148].

With the aim of improving chromatographic resolution, several imprinting strategies that enhance binding site homogeneity, such as stoichiometric imprinting [25, 149] or post-imprinting modification [150, 151], have been reported so far. Similarly, MIP formats other than bulky MIP or thin-grafted layers have also been employed. In this regard, the development of polymer nanoparticles [152] has played an important role. Molecularly imprinted nanoparticles have been almost exclusively applied to sensors, catalysts, as antibody mimics and in controlled drug delivery [153]. In chromatographic separation, so far, the direct use of MIP nanoparticles as stationary phase in HPLC is limited by the high back pressure due to their small size [40]. However, their small dimensions and their large number of feature per volume, make possible obtaining large surface-to-volume ratios, shortening the diffusion distances and improving the access to binding sites [32]. These intrinsic characteristics make MIP nanoparticles very attractive to be used in chromatography.

It is well known that the formation of binding sites in the synthesis process is the most critical stage in MIP synthesis [1, 148, 154]. Having the template in solution may widen binding site heterogeneity of MIP due to template translation and rotation. In this regard, templates immobilised on solid supports offer significant advantage since the template is not in motion, giving rise to the formation of more homogeneous and accessible imprinted sites [148].

Considering the benefits of the immobilised templates, the synthesis of molecularly imprinted nanoparticles (MIN) by the solid-phase approach emerged, which was first developed by Poma *et al.* [148]. This technique consists in the immobilisation of the template on the surface of a solid support, usually glass beads. In a second step, the polymerisation mixture is poured onto these beads and they are irradiated with UV for a short time. As nanoparticles are formed around the template, the binding sites, which will be only present on the surface of the nanoparticle, will remain accessible after template removal. In addition, the template amount would never be in excess, what prevents the loss of site integrity due to coalescence of the binding site which can cause the prolonged retention of template and therefore the template leaching [154]. In the solid-phase approach, the chemical modification of the nanoparticle surface can be carried out without affecting binding sites, as modifications are produced before high-affinity nanoparticles are eluted, thereby being the binding sites still protected by the template.

This imprinting approach was first employed to develop MIN with high affinity for melamine [155]. The same authors also described a method to chemically modify the surface of MIN with poly (ethylene glycol) in order to improve their biocompatibility and stability [156], what allowed for the application of this method to templates incompatible with non-aqueous environments such as enzymes like trypsin [157]. Other applications of surface imprinting include ELISA immunoassays, employing nanoparticles as immunosorbents (ELISA) capable of measuring vancomycin in blood plasma [158], or even for the development of potentiometric sensors to measure

histamine in fish and wine samples [159]. More recently, these nanoparticles have also been successfully employed in the fabrication of sensors for microorganisms [160] and drugs [161, 162].

Based on their potential benefits as imprinted materials, it was hypothesised that these nanosized materials could provide better resolved chromatographic peaks than MIP grafted from the silica surface. In this regard, MIP nanoparticles were synthesised by two different strategies, the solid-phase approach and precipitation polymerisation. The former is based on a template immobilised on a solid support and the latter involves having the template free in solution during polymer synthesis. After nanoparticle synthesis, they were grafted on silica beads for chromatographic chiral separation. These two strategies were initially selected in order to determine whether high affinity nanoparticles provided better chiral resolution or not in comparison with precipitation polymerisation.

7.1. Development of S-citalopram imprinted nanoparticles by the solid-phase imprinting approach

Prior to nanoparticle synthesis, the template molecule was immobilised on the surface of a solid support (glass beads). Then, the glass beads were added to the polymerisation mixture that contained the functional and cross-linking monomers and the iniferter. The schematic representation of synthesis of surface imprinted nanoparticles, adapted from reference [148], is shown in figure 4.37.

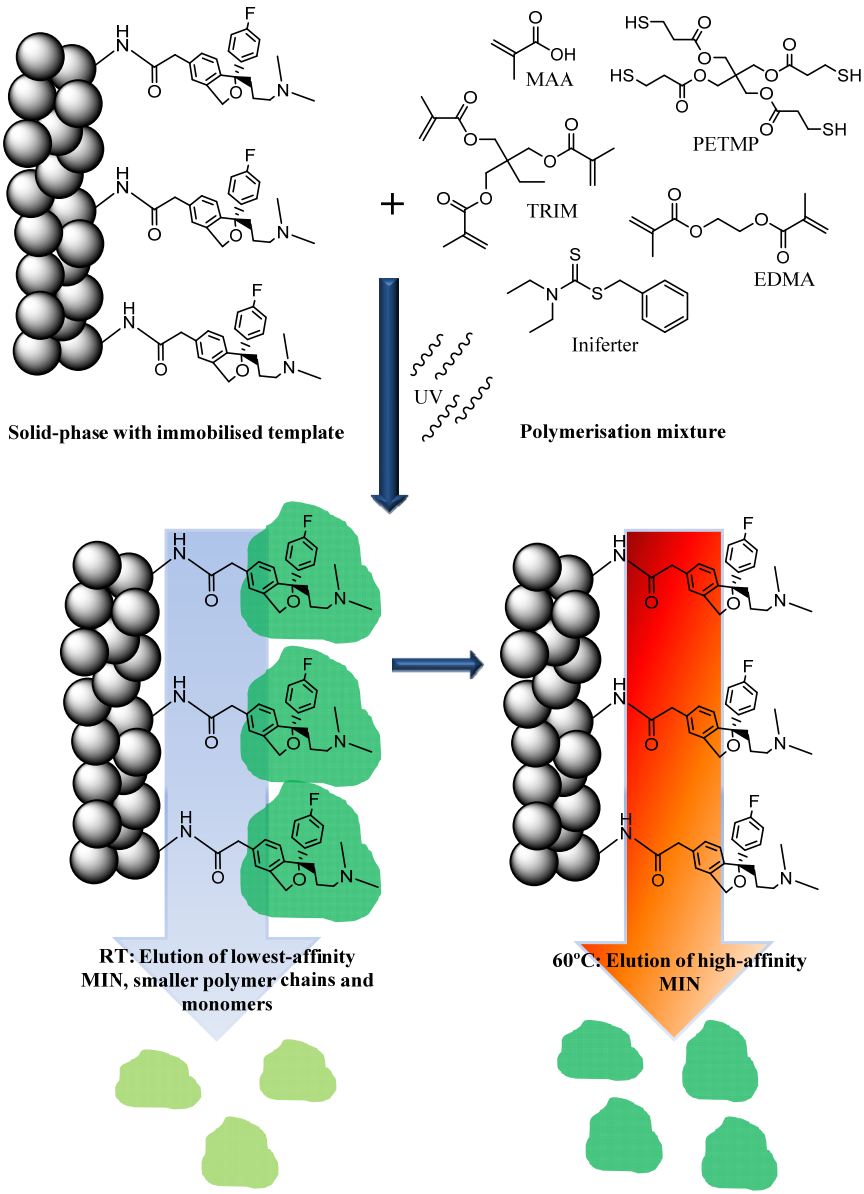

Figure 4.37. Schematic representation of solid phase synthesis of surface imprinted nanoparticles.

MAA: methacrylic acid, **PETMED:** pentaerythritol tetrakis (3-mercaptopropionate), **TRIM:** trimethylolpropane trimethacrylate, **EDMA:** ethylene glycol dimethacrylate and **Iniferter:** diethyldithiocarbamic acid benzyl ester

7.1.1. Immobilisation of S-citalopram to glass beads

500mg of glass beads were initially shaken together with ceramic beads for 5 h using a vibratory sieve shaker. This way, the surface of the glass is abraded and any kind of impurity is removed. Afterwards, the surface of the glass beads was activated in 250 mL of a boiling solution of NaOH 1 M for 15 min in order to increase the amount of silanols groups. The glass beads were washed next with water, then with HCl 2 M, deionised water and finally MeOH. Thereafter, they were dried in an oven at 80ºC.

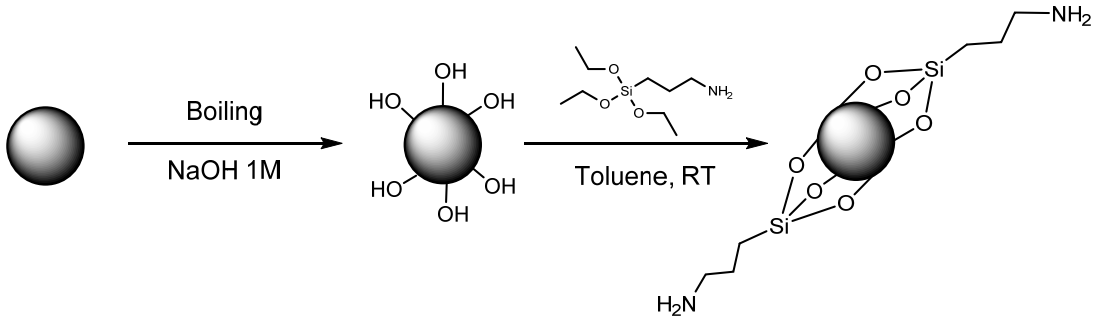

Figure 4.38. Schematic representation of the activation and functionalisation steps of the glass beads.

Once the surface of the glass beads was activated, they were functionalised in order to provide them with primary amino groups. To this end, dry glass beads were incubated overnight in a 2% v/v solution of 3-aminopropyltriethoxysilane (APTES) in toluene (figure 4.38). Next, glass beads were rinsed with acetone and MeOH. At this point, in order to confirm the presence of primary amino groups on the beads, a quick test was carried out. Briefly, a small amount of glass beads were put into a vial containing a few mg of dansyl chloride in ACN. As this compound reacts with primary amino groups leading to stable fluorescent sulfonamide adducts, after 15 min of reaction, the glass beads were taken out from the solution, then rinsed gently with ACN

and disposed under UV radiation observing fluorescence, what confirmed the presence of primary amino groups on glass beads.

Surface immobilisation of SCIT was performed on functionalised glass beads for 4 h at room temperature. Since SCIT itself does not contain any functional group capable of being linked to the silica beads, a carboxylic derivative of this compound was employed as pseudotemplate. In this regard, a derivative having the nitrile group substituted by a carboxylic group was employed for immobilisation (figure 4.39).

In the first instance, a solution of the carboxylated SCIT ((S)-1-(2-(dimethylamino) ethyl)-1-(4-fluorophenyl)-1,3-dihydroisobenzofuran-5-carboxylic acid), 1-ethyl-3-(3-dimethylaminopropyl) carbodiimide (EDC) and N-hydroxysuccinimide (NHS) was prepared in a 1:5:10 molar ratio in DMF:water (5:1 v/v) to derivatise the carboxylated SCIT. It was left to react for 15 min, and then, the functionalised glass beads were added. At this point, the pH of the solution (which was close to 5) was adjusted to pH 7.5 with NaOH 0.5 M. After 4 h of incubation, the beads were rinsed with 250 mL of MeOH first and with 250 mL of warm MeOH second, then dried under vacuum and stored at room temperature until use. A schematic representation of this procedure is shown in figure 4.39.

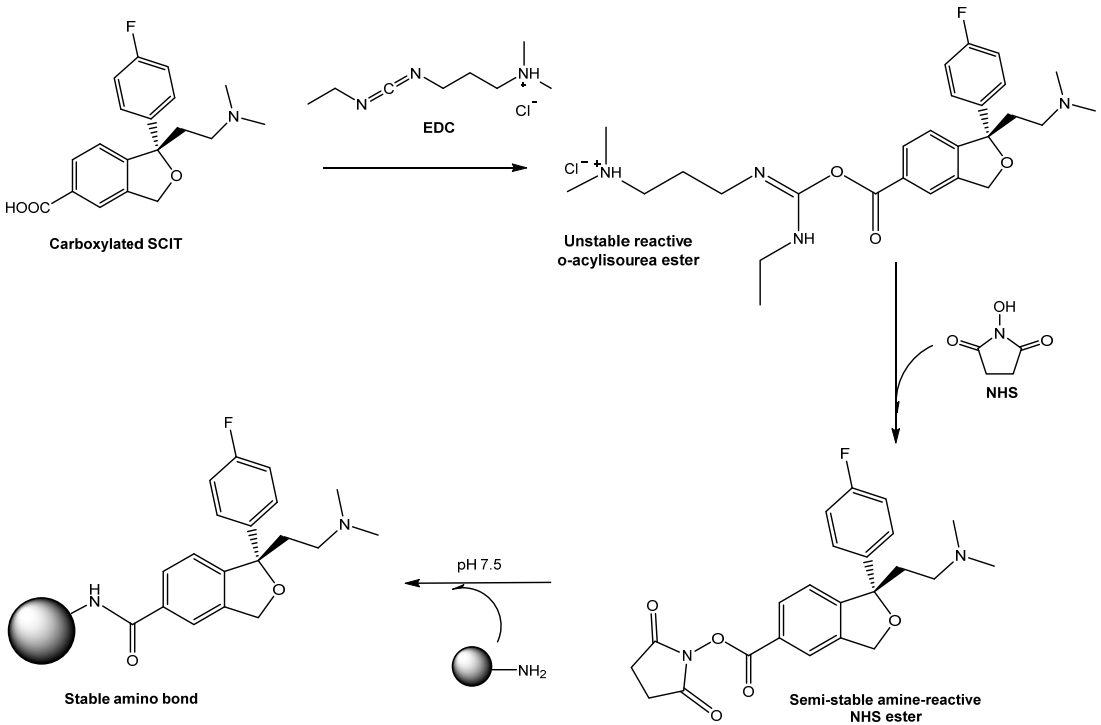

Figure 4.39. Schematic representation of SCIT immobilisation on the surface of glass beads through EDC-NHS coupling.

7.1.2. Synthesis of S-citalopram imprinted nanoparticles

In this work, two different types of nanoparticles were synthesised, ones using methacrylic acid (MAA) as functional monomer and other ones using itaconic acid (IA). IA was selected due to the excellent chiral discrimination capability shown by MIP developed with this monomer, as detailed in previous sections. Nevertheless, due to solubility limitations of this monomer in ACN, MAA was also tested. MAA is the most commonly employed functional monomer in molecularly imprinting [163] and it has already been used to synthesise MIP for the extraction [164] or controlled release [165] of the citalopram racemate. Both monomers have a carboxylic group which is an

excellent hydrogen bond donor and acceptor and therefore allows for the establishment of strong interactions with basic functional groups of the template (figure 4.40).

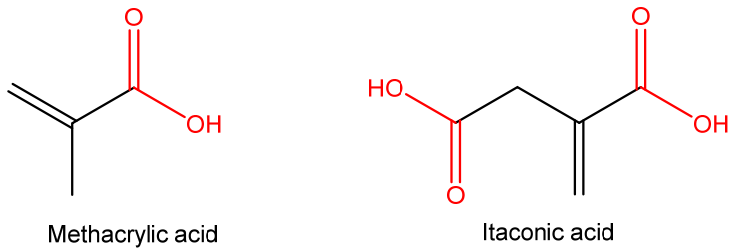

Figure 4.40. Chemical structure of the employed functional monomers.

Nanoparticles containing MAA as functional monomer were prepared as follows: 1.44 g of MAA were dissolved in 5.3 g of ACN, then 1.62 g of EDMA and 1.62 g of TRIM were added, and finally 0.37 g of the iniferter N, N-diethyldithiocarbamic acid benzyl ester and 0.09 g of the transfer agent pentaerythritol tetrakis(3-mercaptopropionate) (PETMP) were dissolved.

When IA was used as functional monomer for nanoparticle synthesis, the polymerisation mixture was prepared dissolving 1.43 g of IA, 1.08 g of EDMA, 1.08 g of TRIM, 0.25 g of *N,N*-diethyldithiocarbamic acid benzyl ester and 0.06 g of PETMP in 5 g of dimethylformamide (DMF).

Both mixtures were placed in a glass vial and bubbled with N_2 for 10 min to remove dissolved oxygen. The composition of these polymerisation mixtures was adapted from Guerreiro *et al*. [166] and Poma *et al*. [148] where it is reported that using a mixture of EDMA and TRIM provided nanoparticles with the right balance of flexibility/rigidity which determined the subsequent molecular recognition [166].

On the other hand, 30 g of SCIT-derivatised glass beads prepared as described in section 7.1.1 were placed in a 200 mL flat-bottomed glass beaker, which was covered with a flat glass slide, and vacuum degassed for 5 minutes. Then, inert atmosphere was

established inside the beaker using N_2 gas. This procedure was repeated at least three times in order to ensure complete oxygen removal. Finally, the polymerisation mixture was poured over the SCIT-derivatised glass beads and placed between two UV light sources for 75 seconds. As a result, MIP nanoparticles are formed on the surface of the glass beads; nevertheless, since the iniferter is present in the polymerisation mixture, non imprinted polymer particles may also be present in the solution after UV irradiation. In order to remove not only these particles but also unreacted monomers, the glass beads are to be washed. Moreover, this procedure allows for the separation of high affinity nanoparticles and other nanoparticles with lower affinities that may have been synthesised at the same time. To this end, after polymerisation, the beads were packed into a solid-phase extraction (SPE) cartridge fitted with 20 µm pore size polyethylene frits.

In the first instance, the washing of MAA nanoparticles was performed. After packing the beads in SPE cartridges, they were washed 8 times with 20 mL of ACN at room temperature to remove low affinity nanoparticles from the surface of the glass beads. Thereafter, it was proceed to a second washing procedure to elute high affinity nanoparticles bound to the template immobilised on the surface of glass beads. For this purpose, the SPE cartridge was conditioned at 60-65ºC and thereafter warm ACN (60-65 ºC) was percolated through it, 4 times. The total collected amount of molecularly imprinted nanoparticles (MIN) in ACN was concentrated down to 20-25 mL evaporating the ACN with pure N_2. IA containing MIN, were washed using the same protocol except for the initial 2 washing cycles. These washings were performed using DMF instead of ACN to avoid precipitation of unreacted IA.

As this procedure cannot be performed in the absence of the template, no non-imprinted polymer nanoparticles could be synthesised by this approach.

7.1.3. Characterisation of molecularly imprinted nanoparticles.

Two different techniques were used to characterise synthesised MIN. On one hand, average particle size was determined by Dynamic Light Scattering (DLS), whereas, on the other hand, binding affinity and the specificity for the target enantiomer was tested by Surface Plasmon Resonance (SPR).

7.1.3.1. Dynamic Light Scattering

The characterisation of particle size distribution in the nanoparticle suspension was performed by Dynamic Light Scattering. In DLS the light from a laser scattered by a colloidal suspension is measured. It is based on the measurement of the modulation of the scattered light intensity as a function of time. Analysing the fluctuations of such scattered light, the Brownian motion of particles can be determined and the particle size can be calculated.

To measure the average particle size of developed MIN, 1 mL of MIN dispersed in ACN was concentrated down by evaporation of the solvent under a nitrogen stream until almost complete evaporation. After that, 3 mL of milli-Q water was added and it was sonicated for 5 min. The dispersion was filtered next, through a 0.8 µm glass fibre syringe filter and analysed by DLS at 25ºC in a 3 mL disposable polystyrene cuvette. The results are summarised in table 4.9. It can be observed that the diameter of MIN synthesised with IA is smaller than the diameter of MIN synthesised with MAA. With regard to the polydispersity index (PDI), the lower the PDI the more monodisperse the sample, that is, the higher the particle size homogeneity. In both types of MIN the PDI is very close to 0, being particle size distribution very narrow.

Table 4.9. Average diameter and polydispersity index (PDI) of synthesised MIP nanoparticles (*n* =3).

	Diameter (nm ± SD)	PDI ±SD
MAA-MIN	170.5 ± 1.3	0.057 ± 0.040
IA-MIN	138.6 ± 2.0	0.059 ± 0.032

7.1.3.2. Surface Plasmon Resonance

Surface Plasmon resonance (SPR) is an optical method for measuring the refractive index of very thin layers of materials adsorbed on a certain metal. A fraction of the polarised light incident at a sharply defined angle can interact with the localised electrons in the surface of the metal film (surface plasmons) under conditions of total internal reflection, thus reducing the reflected light intensity. Whenever a plasmon is excited, it generates electron charge density waves producing a dip in reflected light at that specific resonance angle (figure 4.41).

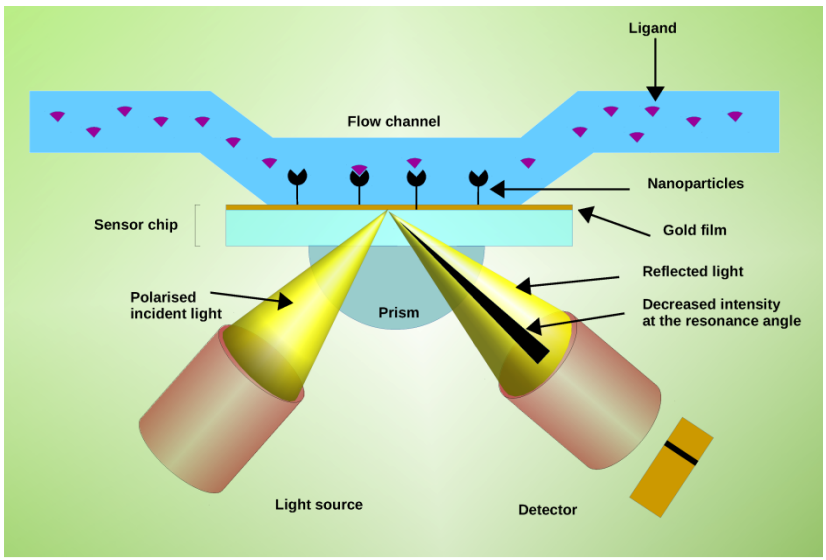

Figure 4.41. SPR instrument configuration.

The precise angle of incidence at which this occurs is determined by a number of factors, but in the Biacore system, which is the system employed in this work, the principal factor is the refractive index close to the surface of the metal film, to which the nanoparticles are immobilised and addressed by target ligand in the mobile phase running along a flow cell. If binding occurs to the immobilised nanoparticles, the local

refractive index changes, leading to a change in the resonance angle, which is monitored in real time by detecting changes in the intensity of the reflected light, what leads to a sensorgram similar to the one depicted in figure 4.42 [144]. The changes in the SPR signal can be analysed to yield apparent association and dissociation constants of a certain ligand with its corresponding receptor.

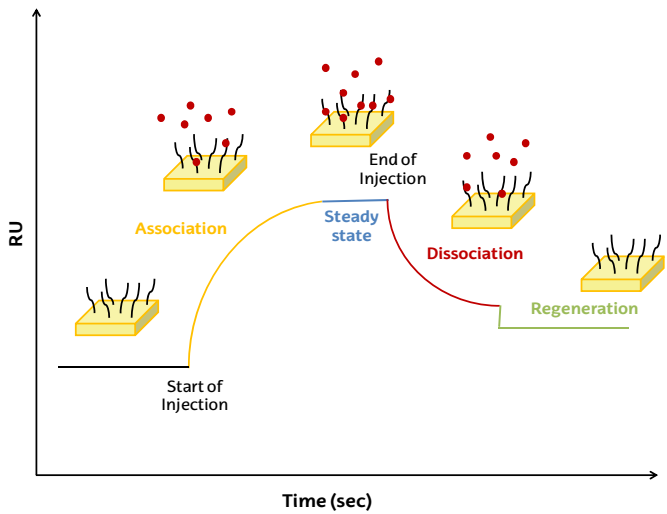

Figure 4.42. Association-dissociation sensorgram.

Surface activation of Biacore gold chips and nanoparticle immobilisation.

In the first instance, gold-coated chips were cleaned by immersion in piranha solution (H_2SO_4/H_2O_2, 3:1 v/v) for 5 min, and thoroughly rinsed next with deionised water. After that, the chips were dried under a N_2 stream and placed in 0.2 mg/mL of cysteamine in ethanol overnight in order to coat the gold surface with a cysteamine monolayer containing amino groups capable of subsequently linking target nanoparticles. Thereafter, the chips were rinsed with ethanol and deionised water and they were left to dry at room temperature until being used.

Immobilisation of the developed nanoparticles to the gold chip functionalised with amino groups, was performed directly in the Biacore system. To this end, initially, 5 mg of EDC were added to 1 mL of imprinted nanoparticles suspended in water. Then, 100 µL of this mixture was injected in the Biacore system in order to immobilise the nanoparticles. This procedure was carried out twice, the first one employing the nanoparticles synthesised with the IA monomer and secondly employing the ones synthesised with MAA. The MIN suspension was passed through the system at 10 µL/min to allow nanoparticles derivatised with EDC for reacting with amino groups on the surface of the gold chip.

Surface plasmon resonance (SPR) affinity analysis of MIN

Once the nanoparticles were immobilised, the flowing solvent was changed from water to phosphate buffer (pH 7.4) for SPR analysis. Solutions of SCIT at concentrations ranging from 0.001 to 0.78 nM and solutions of RCIT of concentrations comprised between 0.006 to 12.93 nM were prepared in phosphate buffer (pH7.4) for SPR measurements. 80 µL of each of these solutions were separately injected in the system using phosphate buffer (pH7.4) as flowing solvent at a flow rate of 35 µL/min. Dissociation constants (K_D) were calculated using the BiaEvaluation v4.1 software using a 1:1 binding model, assuming a Langmuir binding isotherm.

Figure 4.43 depicts SPR sensorgrams registered for SCIT and RCIT using imprinted nanoparticles, synthesised with MAA, as receptors. The calculated apparent K_D for RCIT was found to be 6.80×10^{-10} M, whereas, when SCIT was injected the obtained apparent K_D was about 500 times lower, that is, 1.20×10^{-12} M, what indicates a remarkably higher affinity for SCIT. In the sensorgrams of figure 4.43, this affinity difference can also be deduced from the difference in sensor response units (RU) between RCIT and SCIT, what corroborates the higher affinity of the nanoparticles for the S enantiomer.

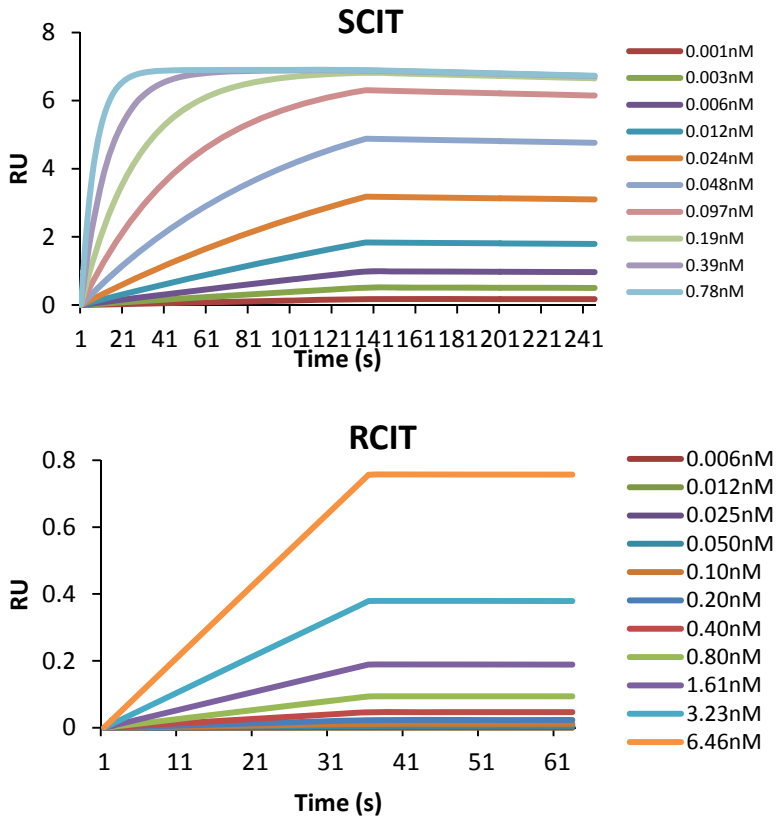

Figure 4.43. SPR sensorgrams for increasing concentrations of SCIT and RCIT registered with nanoparticles synthesised with MAA as functional monomer.

On the other hand, when the MIN synthesised with itaconic acid (IA) were tested, the dissociation constants were only two and a half times higher for RCIT (2.60×10^{-9} M) than for SCIT (1.05×10^{-9} M) as it is summarised in table 4.10. Figure 4.44 shows the SPR sensorgrams obtained with these nanoparticles. It can be observed a slightly higher response for SCIT than for RCIT, although it is not as significant as for MAA nanoparticles. This can be attributed to the use of DMF as porogen in the synthesis of IA based nanoparticles. As it is a polar solvent with moderate hydrogen bonding capacity,

it can lead to weaker monomer-template interactions in the prepolymerisation adduct, giving rise to binding sites with lower affinities.

Table 4.10. Summary of K_D values corresponding to SCIT and RCIT into a SPR sensor grafted with nanoparticles synthesised with two different functional monomers (IA and MAA).

Ligand	K_D(M)	
	MAA MIN	IA MIN
RCIT	6.80×10^{-10}	2.60×10^{-9}
SCIT	1.20×10^{-12}	1.05×10^{-9}

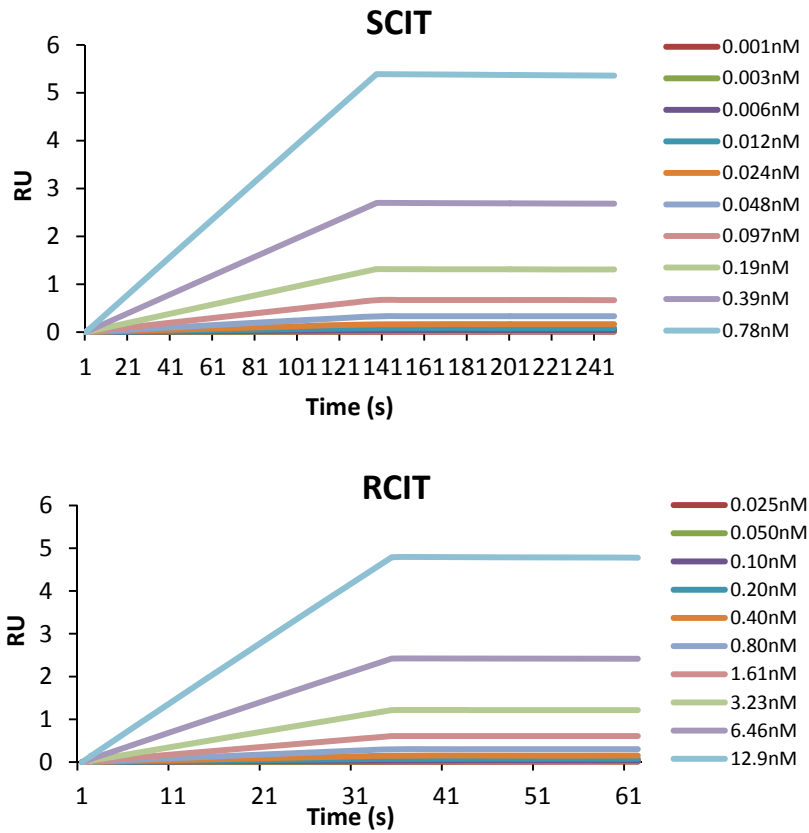

Figure 4.44. SPR sensorgrams for increasing concentrations of SCIT and RCIT registered with nanoparticles synthesised with IA as functional monomer.

7.2. Development of S-citalopram imprinted nanoparticles by precipitation polymerisation.

In section 7.1, MIP nanoparticles developed by the solid phase imprinting approach is detailed. Alternatively, MIN were also synthesised by precipitation polymerisation to be grafted on silica surface. This way, chiral resolution capability of two nanomaterials developed by different methodologies would be compared. MIN described here were synthesised by precipitation polymerisation according to the procedure detailed in chapter 3. However, in this case, the polymerisation time was considerably reduced in order to get smaller particle sizes, comparable to those obtained by solid phase imprinting. Moreover, this time, MIN synthesis was conducted using the same iniferter as that used in solid phase imprinting; not only to have control over particle size distribution, but also to get materials synthesised by the same polymerisation method, that is, reversible deactivation radical polymerisation.

The polymerisation mixture was prepared dissolving 450 mg of EDMA, 48 mg of IA and 31.1 mg of neutral SCIT in 27 mL of ACN, previously deoxygenated with N_2. 10 mg of diethyldithiocarbamic acid benzyl ester as iniferter was added next and the polymerisation mixture was deoxygenated again for another 2 min. Finally, the mixture was irradiated with UV light for 1 hour and 10 min, since this was the minimum time required to observe nanoparticles, suspended in the polymerisation mixture, in sol state.

Once the nanoparticles were synthesised, the mixture was washed with ACN and collected by centrifugation at 8000 rpm for 10 min at 20 ºC. This procedure was repeated three times.

The obtained particles were re-suspended in ACN and left to decant for at least 5 hours. The supernatant containing non-decanted nanoparticles was collected for immobilisation. This way, the smallest particles would be attached to the silica surface

eliminating both the largest particles and agglomerates that may be present in the mixture.

7.3. Development of chiral stationary phases based on molecularly imprinted nanoparticles

7.3.1. Silica surface activation and silanisation

The activation of the surface of the silica beads was carried out by rehydroxylation, as detailed in section 5.1. Once activated, 16 g of silica were suspended in 160 mL of dry toluene in a two-necked 500 mL round bottom flask connected to a N_2 stream and equipped with a condenser and a dropping funnel. Then, 15 mL of (3-aminopropyl)triethoxysilane was added dropwise and the mixture was refluxed for 5 h. Thereafter, the modified silica was filtered, washed with 100 mL of toluene and 250 mL of MeOH. It was finally left to dry at room temperature overnight.

7.3.2. End-capping of the amino functionalised silica

The physical stability and well-defined and controllable pore structure and morphology of the silica-based packing materials ensure a rapid mass transfer, good loadability and high reproducibility when they are used as stationary phases in liquid chromatography [167]. However, a significant fraction of silanol groups remain unreacted even when the porous silica particles have been exhaustively derivatised. These unreacted silanols are capable of interacting with polar and charged analytes in pH values commonly used with silica-based columns (2.5-7.5). Consequently, they have a negative influence on the separation of basic compounds such as citalopram, which lead to ionic interactions with ionised silanols as it is represented in equation 4.14[168, 169]. Where BH^+ is the basic compound protonated and bc^+ the mobile phase buffer cation.

$$BH^+ + SiO^-bc^+ \rightarrow SiO^-BH^+ + bc^+ \qquad 4.14$$

In order to avoid the access to the residuals silanols on the silica surface, an end-capping procedure is highly recommended [127]. Using low molecular weight organosilanes capable of generating trimethylsilyl groups ($(CH_3)_3Si$-) such as trimethylchlorosilane (TMCS) or hexamethyldisilazane (HMSD) [170, 171], the quality of the original chemically bonded phase is improved. In this work, end-capping was carried out with HMDS, for being the most suitable reagent for basic analytes [172, 173]. For that, 15 g of the silanised silica beads obtained in the previous step were suspended in 150 mL of dichloromethane (DCM) in a 500 mL two-necked round bottom flask equipped with a condenser, a dropping funnel and under N_2 stream. 3 mL of HMDS in 50 mL of dry DCM was added drop-wise next to the suspension. The mixture was refluxed for 3 h and the product was filtered and washed with 100 mL of MeOH in order to remove traces of unreacted HMDS. The silica beads were dried overnight at room temperature.

7.3.3. Linkage of the molecularly imprinted nanoparticles to the silica surface

The linkage of both MIN synthesised by precipitation polymerisation and solid phase imprinting was carried out by the NHS-EDC coupling, similarly to the procedure described in section 7.1.1.

20 mL of imprinted nanoparticles suspended in ACN were added to 20 mL of deionised water in which 700 mg of EDC and 800 mg of NHS were dissolved. The mixture was left to react for 15 min and then 2 g of the amino-derivatised silica (section 7.3.1) was added. The pH of the solution (that was close to 5) was changed to pH 7.5 in order to start the reaction. This reaction was left under gentle stirring (15 rpm) for 2 hours, and then it was left to react for another 3 hours without stirring.

Afterwards, the resulting silica was washed with water and ACN to remove unreacted reagents and it was left for 1 hour in a carbonate buffer solution adjusted to pH 9. This is a critical step, since unstable reactive o-acylisourea ester can be formed in

the binding cavities and a pH 9 is necessary in order to reverse this formation between the carboxylic groups and the EDC reagent.

7.4. Characterisation of the chiral stationary phases

Once the chiral stationary phases were synthesised, they were characterised by FTIR spectroscopy and Scanning Electron Microscopy as described in section 5.4.

Figure 4.45 depicts SEM micrographs of the developed stationary phases. It can be observed that only MIN synthesised by precipitation polymerisation (Si-P-MIN) are appreciable on the silica surface (figure 4.45 d). MIN synthesised by solid-phase imprinting (Si-SP-MIN) (figure 4.4 b and c) are much more difficult to distinguish on the silica surface, probably due to its lower diameter, or even due to its lower yield. The nanoparticles obtained by solid-phase imprinting are below 180 nm in diameter in all cases (see table 4.9, section 7.1.3), however, by precipitation polymerisation nanoparticles of 249 ± 4 nm in diameter (PDI 0.245 ± 0.065) were obtained. In conclusion, SEM images did not allow for confirming the correct linkage of the nanoparticles synthesised by solid-phase imprinting to the silica surface.

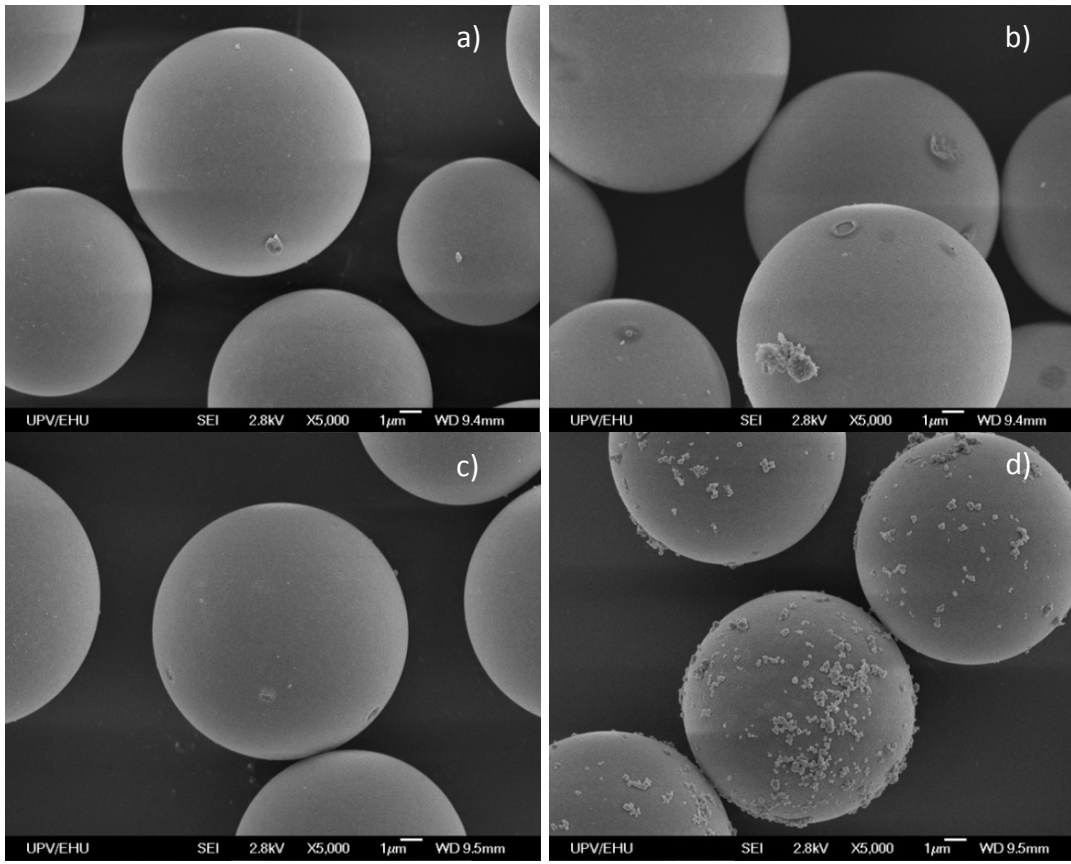

Figure 4.45. SEM micrographs at different magnifications of a) amino functionalised silica after end-capping, b) Si-SP-MIN using MAA as functional monomer, c) Si-SP-MIN using IA as functional monomer d) Si-P-MIN using IA as functional monomer.

The correct attachment of MIN to the silica surface was additionally corroborated by FTIR analysis of the developed stationary phases. figure 4.46 depicts all recorded spectra. Every one presents a characteristic band at 1052 cm^{-1} relative to Si-O stretching vibrations of the silica support. In the spectra corresponding to silica grafted with MIP nanoparticles (figure 4.46 b, c and d) another band appears between 1600 and 1650 cm^{-1}. This moderately intense band may be attributed to the C=O stretching vibration. This functional group, is only present in the chemical structure of the

monomers used in the polymerisation of the nanoparticles, consequently, this band may be indicative of the successful linking of MIN to the silica surface.

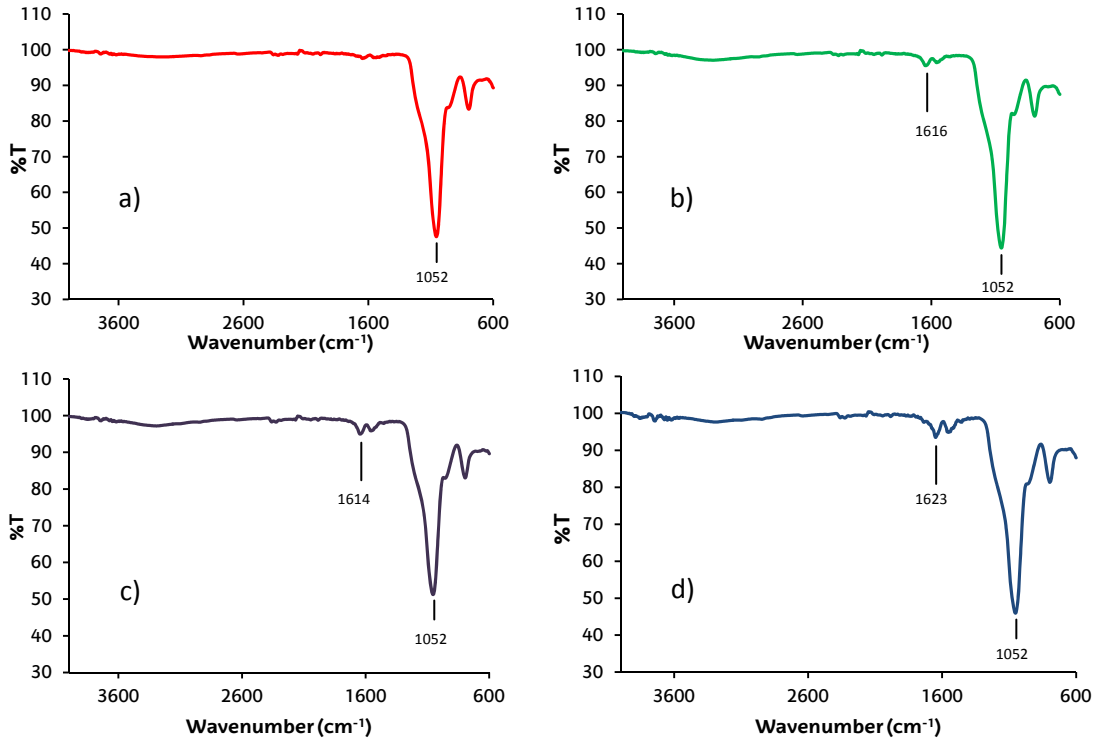

Figure 4.46. FTIR spectra of a) a control blank stationary phase based on silica beads functionalised with amino groups and end-capped b) A CSP based on Si-SP-MIN using MAA as functional monomer, c) A CSP based on Si-SP-MIN with IA as functional monomer and d) A CSP based on Si-P-MIN with IA as functional monomer.

7.5. Chromatographic evaluation

The chiral separation capability of the stationary phases developed using MIN synthesised by solid-phase imprinting (Si-SP-MIN) and by precipitation polymerisation (Si-P-MIN) was assessed by liquid chromatography. To this end, based on the retention times of each enantiomer in each stationary phase, the separation factor and peak resolution were calculated and compared. For these experiments, ACN was used as

organic modifier in the mobile phase. When it was not mixed with an aqueous phase, ACN itself favoured full retention of S and R citalopram in all tested stationary phases. In contrast, no retention was appreciated using a blank control column which consisted of a column packed with the end-capped amino-derivatised silica, without any MIP nanoparticle immobilised on its surface.

For proper analyte elution, being ACN a solvent with poor hydrogen bonding capacity, an aqueous percentage was required in the mobile phase in order to displace hydrogen bonds between the analyte and binding sites. Initially, a 40 mM formate buffer solution at pH 3 was employed as aqueous phase. Different percentages of this buffer solution in the mobile phase were tested to determine its influence on chiral resolution. In Si-SP-MIN columns made with IA and MAA, when buffer percentages over 5% were employed, neither SCIT nor RCIT were retained. However, using the Si-P-MIN phase, at least 10% of buffer was required to appreciate this effect, what denoted higher binding strength of the enantiomers to this stationary phase.

Based on these preliminary findings, the pH effect of the aqueous phase was assessed keeping constant the mobile phase composition at 98:2 v/v of ACN: formate buffer and varying the pH of the buffer from 3 to 9. Table 4.11 shows the calculated separation parameters obtained with the tested stationary phases. As illustrated, the highest retention times were observed at pH 6 using the phases Si-SP-MIN (MAA) and Si-SP-MIN (IA). However, when Si-P-MIN was used, the lower the pH the higher the retention time. As regards the retention factor (k), in all cases the value is above the unit, which is indicative of the proper separation of the analyte from the injection peak. The adequate separation of the enantiomers can be determined by the value of the separation factor (α) or even the resolution (R). However, as the capability of a stationary phase for proper peak separation (when $\alpha > 1$) does not necessarily involve perfect peak resolution, in this study, the resolution was taken into consideration. Considering the R values, column Si-P-MIN was the only one presenting chiral

separation capability. Si-SP-MIN stationary phases were never able to resolve the racemate.

Table 4.11. Separation parameters registered at different pHs. Mobile phase composition: 98:2 v/v ACN: formate 40 mM.

Stationary Phase	pH	Analyte	Tr	k	α	R
Si-SP-MIN (MAA)	3.00	RCIT	4.83	1.68	1.00	0.00
		SCIT	4.83	1.68		
	5.00	RCIT	6.08	3.12	0.99	0.00
		SCIT	6.05	3.10		
	6.00	RCIT	6.58	3.39	1.00	0.00
		SCIT	6.59	3.39		
	7.00	RCIT	5.94	3.01	1.01	0.10
		SCIT	6.00	3.06		
	8.00	RCIT	6.26	3.17	1.01	0.10
		SCIT	6.32	3.21		
Si-SP-MIN (IA)	3.00	RCIT	3.88	2.02	1.01	0.10
		SCIT	3.89	2.03		
	5.00	RCIT	4.31	1.97	1.03	0.20
		SCIT	4.40	2.03		
	6.00	RCIT	4.86	2.88	1.01	0.10
		SCIT	4.90	2.92		
	7.00	RCIT	4.57	2.26	1.01	0.10
		SCIT	4.60	2.29		
	8.00	RCIT	4.23	1.93	1.01	0.00
		SCIT	4.25	1.94		
Si-P-MIN	3.00	RCIT	19.19	14.19	1.45	1.44
		SCIT	27.32	20.62		
	5.00	RCIT	12.76	9.11	1.15	0.70
		SCIT	14.43	10.43		
	7.00	RCIT	12.95	9.61	1.18	0.90
		SCIT	15.07	11.34		
	9.00	RCIT	3.38	1.78	1.08	0.4
		SCIT	3.56	1.93		

Based on these findings, it was hypothesised that the reason for chiral separation absence in Si-SP-MIN phases may be correlated with the derivatisation of the nitrile group of the template to get a carboxylated pseudotemplate linkable to the surface glass beads for solid-phase imprinting. This approach may conduct to nanoparticles having imprinted sites with less functional groups for binding interactions, thereby leading to lower selectivity. Moreover, as described in the modelling section of chapter 3, the nitrile group of the target enantiomer is the group that strongest binds to carboxylic groups of the functional monomer, IA. As a consequence, having substituted the nitrile group for a carboxylyc one and having sacrificed the carboxylic group to link the pseudotemplate to the surface of glass beads, has not proved to be a good attempt to develop MIN by solid phase imprinting for small molecules. Especially when functional imprintable groups are sacrificed to be attached to the surface of the solid phase.

In contrast, when MIN are synthesised by precipitation polymerisation, there is no need to sacrifice any functional group for immobilisation on a solid support. Moreover, SCIT itself is directly imprinted instead of a pseudotemplate. As a result, remarkably different retention times where observed for SCIT and RCIT when Si-P-MIN was used as stationary phase, being the value of resolution close to 1.5 (table 4.11). Based on these findings, the stationary phase composed of nanoparticles synthesised by precipitation polymerisation (Si-P-MIN) was selected for further experimental.

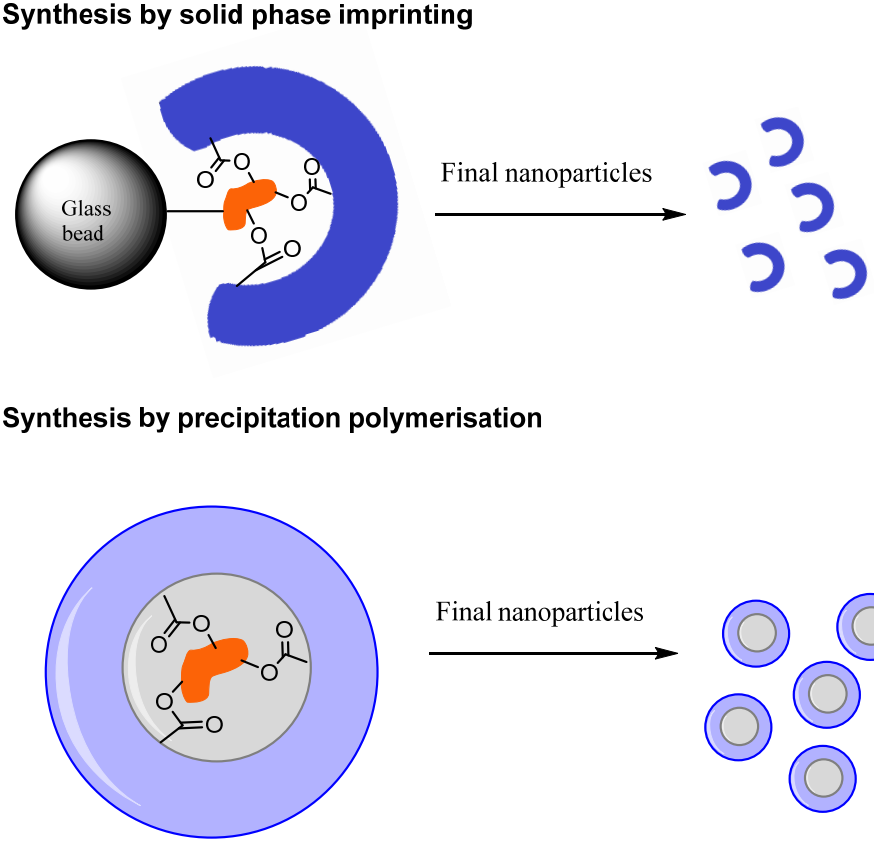

Figura 4.48. Schematic representation of imprinted nanoparticles developed by the solid-phase imprinting approach and by precipitation polymerisation.

7.6. Optimisation of chromatographic conditions for chiral separation

Different parameters that could influence on chiral separation of CIT were evaluated next in order to know the experimental conditions at which the developed Si-P-MIN chiral stationary phase showed best performance.

In the first instance, the effect of buffer percentage on chiral separation was evaluated. To this end, mobile phases consisting of different buffer percentages at pH 3 were tested, results are summarised in table 4.12. As depicted, the higher the water content, the higher the chiral resolution. As expected, the presence of water leads to contributes in weaker binding to imprinted sites, and consequently, lower retention times are registered.

Table 4.12. Separation parameter values in function of buffer percentage in the mobile phase.

Column	%Buffer	Analyte	Tr	k	α	R
Si-P-MIN	2	RCIT	19.19	14.19	1.45	1.44
		SCIT	27.32	20.62		
	3	RCIT	6.95	4.59	1.22	0.74
		SCIT	8.18	5.58		
	4	RCIT	4.82	2.92	1.20	0.75
		SCIT	5.55	3.52		
	5	RCIT	3.42	1.83	1.10	0.36
		SCIT	3.64	2.02		

Once evaluated the buffer percentage effect, it was determined if buffer concentration had any influence on chiral resolution. In this regard, buffer solutions comprised between 1 mM and 40 mM were mixed with ACN (95:5 v/v ACN:buffer). Results are shown in figure 4.49. It can be observed that the lower the buffer concentration the higher the resolution. However concentrations lower than 1 mM did not improve significantly chiral separation.

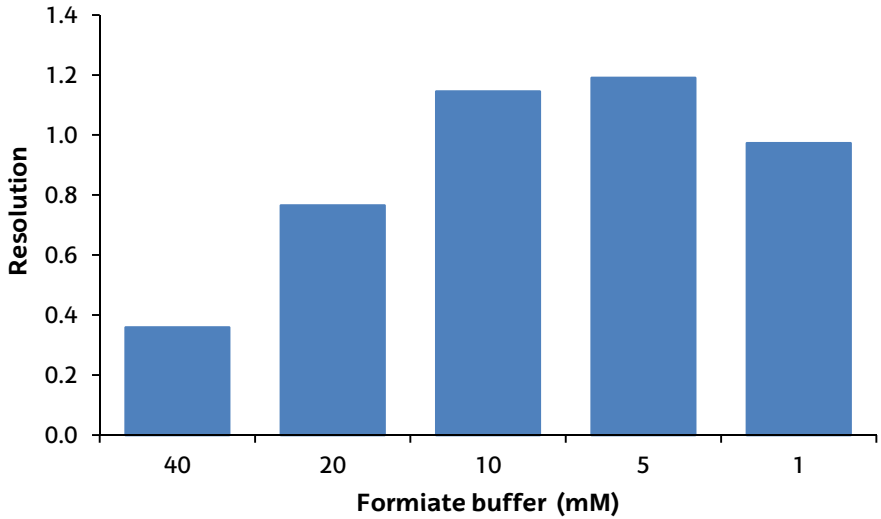

Figure 4.49. Effect of buffer concentration on enantiomer resolution. Mobile phase: 95:5 v/v ACN: formate buffer pH 3.

pH optimisation is crucial in order to minimise non specific interactions with randomly distributed carboxylic groups of the functional monomer, outside binding sites. Usually, average pKa values of carboxylic functional groups in binding sites are slightly lower, more acidic, than pKa of carboxylic groups outside these sites. Consequently, carboxylic groups, responsible for non-specific binding, would be neutralised at higher pHs than the ones inside the cavities. In this sense, a careful pH evaluation should always be performed in order to select the proper pH value at which non specific interactions are minimised. In this study, formate buffer solutions at pH comprised between 2.5 and 9 were tested in the mobile phase. Registered retention times are summarised in table 4.13. As it can be observed, the separation factor is, in all cases, above the unit. The resolution, however, is quite close to 1 at lowest pH (3.5 and 2.5) whereas the highest value was registered at pH 4.5.

Table 4.13. Separation parameters calculated at different buffer pH. Mobile phase composition: 95:5 (v/v) ACN: formate buffer 5 mM.

pH	Analyte	Tr	k	α	R
2.50	RCIT	7.76	5.36	1.41	1.09
	SCIT	10.47	7.57		
3.50	RCIT	7.62	5.20	1.38	0.94
	SCIT	10.02	7.16		
4.50	RCIT	7.43	5.08	1.61	1.35
	SCIT	11.20	8.16		
6.00	RCIT	8.37	5.86	1.57	1.25
	SCIT	12.43	9.18		
7.00	RCIT	8.94	6.33	1.54	1.20
	SCIT	13.10	9.74		
9.00	RCIT	8.86	6.22	1.54	1.25
	SCIT	13.00	9.60		

The mobile phase temperature effect on chiral separation was finally evaluated. In this regard, three different temperatures (25, 40 and 60 ºC) were tested. The enantiomer resolution values were 1.19, 1.73 and 1.33 at 25, 40 and 60 ºC respectively. It was observed that the higher the temperature the lower the retention times and the thinner the peaks, however, over 40 ºC the resolution was negatively affected and, consequently, 40 ºC was selected as optimum.

Once the mobile phase composition was optimised, chromatographic columns with different lengths (100, 150 and 250 mm) were packed with the developed Si-P-MIN material to determine whether longer columns provided better chiral resolution. Figure 4.50 shows the chromatograms recorded with each of these columns. As it can be deduced, the longer the column the better the resolution of the racemic mixture.

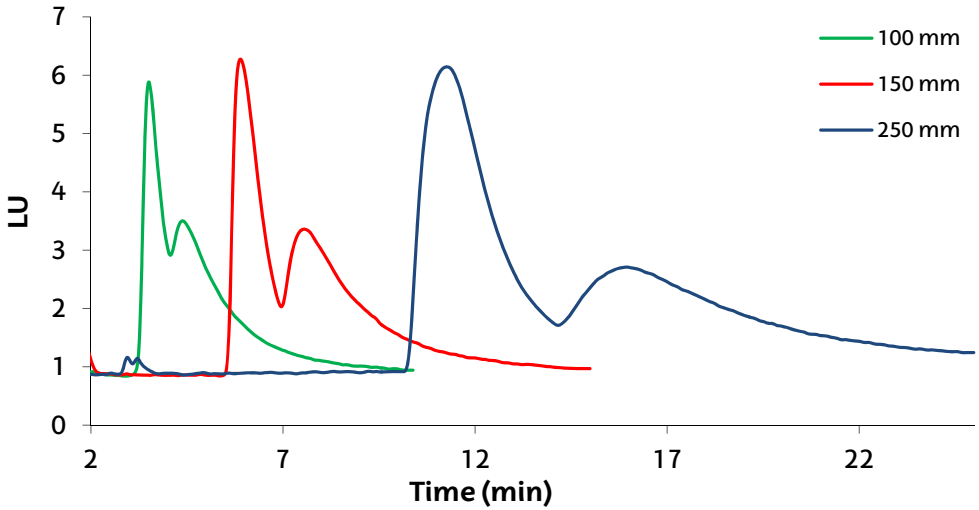

Figure 4.50. Chromatograms registered using columns with different lengths. 20 µL of 1 µg/mL of racemic citalopram was injected in all cases. Mobile phase: 95:5 v/v ACN: formate buffer 5 mM, pH 4.5. Temperature 40 ºC.

In order to improve the separation, instead of working in isocratic mode, different gradients were tested. Best results were obtained increasing gradually the buffer percentage in the mobile phase from 2% to 10%, from the beginning of the run to 20 min and then it was kept constant until the end of the analysis (25 min). The registered chromatogram is depicted in figure 4.51.

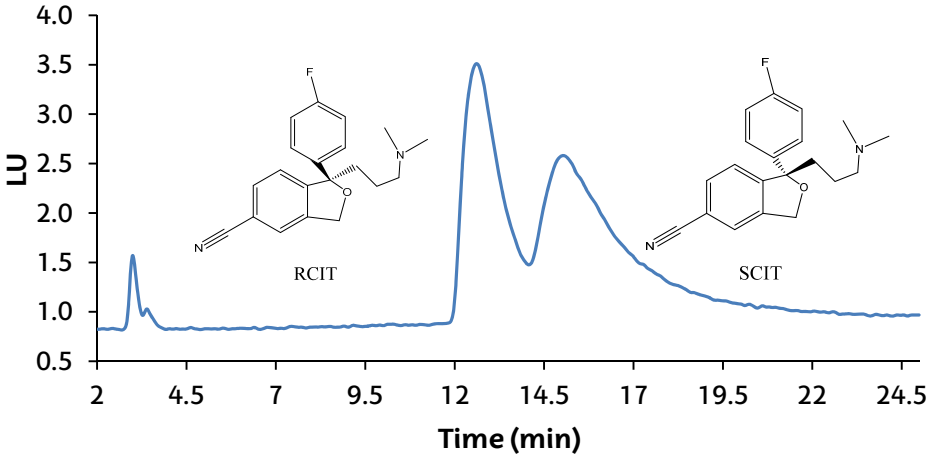

Figure 4.51. Chromatogram registered injecting 20 µL of 1 µg/mL citalopram in gradient mode.

The resolution improvement of racemic citalopram in this column in comparison with the stationary phase developed by the grafting from approach Si-MIP 1 (figure 4.52) can be clearly distinguished.

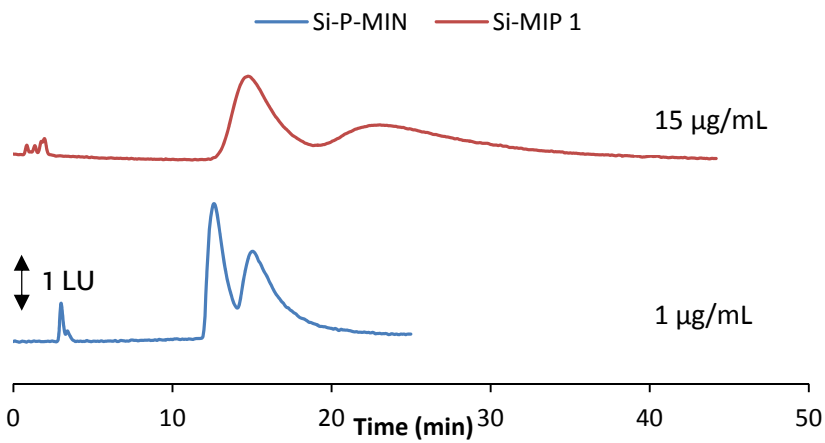

Figure 4.52. Chromatograms recorded injecting 1 µg/mL and 15 µg/mL of racemic CIT using CSP developed by surface imprinting (Si-MIP1) and by precipitation polymerisation (Si-P-MIN).

8. Analytical parameters

After the selection of the best CSP (Si-P-MIN), and the optimisation of chromatographic conditions for the chiral resolution of citalopram, the analytical evaluation was carried out. In this regard, a calibration curve was constracted in order to determine the linear range and the instrumental detection (LOD) and quantification (LOQ) limits.

8.1. Method calibration

For method calibration a series of standard solutions of S and R citalopram were injected in a concentration range comprised between 0.02 and 10 µg/mL (n=3). The obtained calibration curve was adjusted by the least squares method, giving rise to the following expressions for SCIT (4.15) and RCIT (4.16):

$$A_S = (336.35 \pm 4.12)C - (32.28 \pm 15.66) \quad 4.15$$

$$A_R = (229.00 \pm 2.74)C - (15.74 \pm 10.43) \quad 4.16$$

Where A_S and A_R are the peak area of SCIT and RCIT respectively, expressed in LU·s, and C is the concentration expressed in µg/mL. As it shown intable 4.14, for both enantiomers the coefficient of determination (R^2) confirms an adequate linear correlation of the analytical signal versus the enantiomer concentration.

Table 4.14. Parameters obtained in the calibration (n=3)

	Slope ± S.D (LU·s·mL/µg)	Intercept ± S.D (LU.s)	R^2
SCIT	336.4 ± 4.1	-32.3 ± 15.7	0.999
RCIT	229.0 ± 2.7	-15.7 ± 10.4	0.999

In order to corroborate the goodness of fit of the proposed regression, a statistical analysis of the distribution of the residuals was carried out. The residual (r_i) is the difference between the experimental value of the dependent variable (y_{exp}) and the predicted value (y_{calc}) which is calculated by the interpolation of the theoretical concentration value in the calibration curve. This value for each data point is calculated based on the following expression:

$$r_i = y_{calc} - y_{exp} \qquad 4.17$$

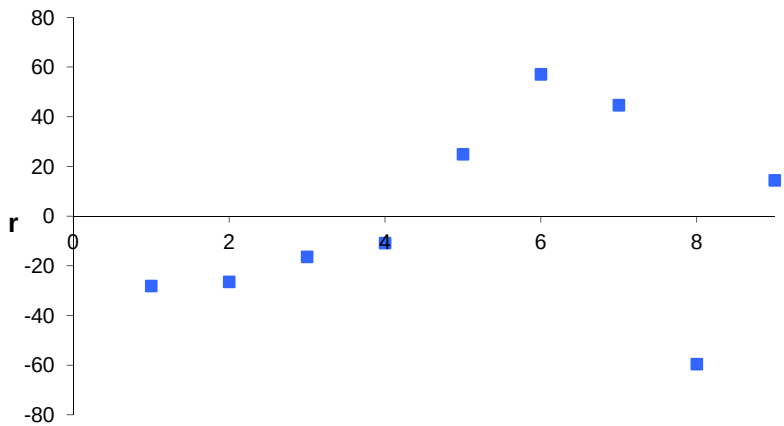

Figure 4.53. Distribution diagram of the residuals for the calibration of SCIT.

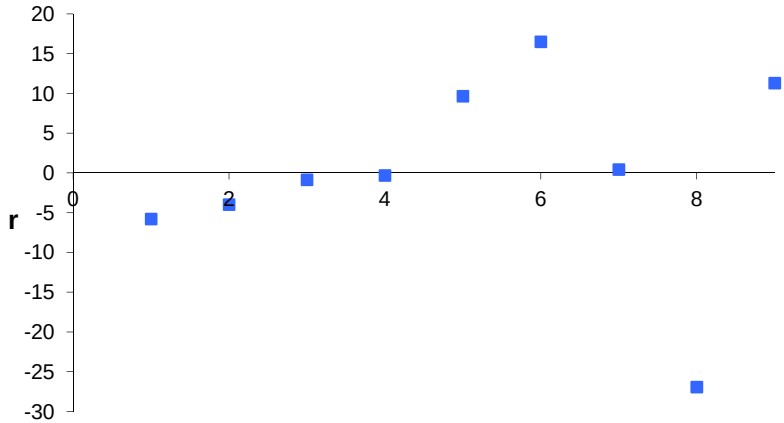

Figure 4.54. Distribution diagram of the residuals for the calibration of RCIT.

As depicted in figure 4.53 and 4.54, a random distribution of the residuals can be observed, what indicates that the proposed regression adequately fits experimental data. Additionally, in order to confirm this randomness, different parameters that indicate if calculated residuals follow a normal distribution, have been evaluated.

Arithmetic median of the residuals

$$\bar{r} = \frac{\sum(y_{calc} - y_{exp})}{N_P} \qquad 4.18$$

Where N_p is the number of the calibration points. A normal distribution of the residuals would result in a value of $\bar{r}$=0.

Standard deviation of the residuals

$$\sigma(r) = \sqrt{\left(\frac{\sum r_i^2}{N_P}\right) - \left(\frac{\sum r_i}{N_P}\right)} \qquad 4.19$$

This value must be lower or equal to the total standard deviation, σ_{TOT}, in order for the distribution of the residuals to be Gaussian.

Average residual

$$\overline{|r|} = \frac{\sum |y_{calc} - y_{exp}|}{N_P} = \frac{\sum |r_i|}{N_P} \qquad 4.20$$

To ensure that the distribution of the residuals is Gaussian, the resulting residual average value must be lower or equal to the standard deviation of the residuals.

Asymmetry coefficient

$$C_s = \frac{\sum (r_i - \bar{r})^3}{N_P\ \sigma(r)^3} \qquad 4.21$$

It indicates the degree of symmetry of the Gaussian curve. This parameter should be zero when the distribution of the residuals is symmetrical, and therefore Gaussian.

Kurtosis coefficient

$$C_{ku} = \frac{\sum (r_i - \bar{r})^4}{N_P\ \sigma(r)^4} \qquad 4.22$$

The coefficient of kurtosis is a measure for the degree of peakedness/flatness in the variable distribution. A normal distribution of the residuals has a value of 3.

Global standard deviation

$$\sigma_{TOT} = \sqrt{\frac{\sum_{i=1}^{N_P}\left(y_{calc} - y_{exp}\right)^2}{N_p - 2}} \qquad 4.23$$

Table 4.15. Experimental and theoretical values of the statistical analysis of the residuals.

	Experimental value		Theoretical value for a normal distribution
	SCIT	RCIT	
$\bar{r}$	2.37 x 10^{-14}	1.25 x 10^{-13}	$\bar{r} \approx 0$
σ_{TOT}	40.5	13.5	
$\sigma(r)$	35.8	11.9	$\sigma(r) \leq \sigma_{TOT}$
$\lvert\bar{r}\rvert$	31.4	8.5	$\lvert\bar{r}\rvert \leq \sigma(r)$
Cs	0.09	-0.84	$C_S \cong 0$
C_{KU}	2.0	3.4	$C_{KU} \cong 3$

As shown in table 4.15, most of the parameters approach theoretical values indicating a Gaussian distribution of the residuals. It can be stated that the proposed regression model adequately fits experimental data in a concentration range comprised between 0.02 and 10 µg/mL.

8.2. Detection and quantification limits

The detection (LOD) and quantification (LOQ) limits were calculated using the sensitivity values (S) obtained from the slope of the calibration curves and the standard deviation of the signals recorded from blank measurements(σ_B).

$$C_{LOD} = \frac{K\sigma_B}{S} = \frac{3\sigma_B}{S} \quad 4.24$$

$$C_{LOQ} = \frac{K\sigma_B}{S} = \frac{10\sigma_B}{S} \quad 4.25$$

The blank signals were obtained injecting ACN under the same conditions (n=5).

Table 4.16. Summary of the detection and quantification limits obtained for S and RCIT.

	SCIT (µg/mL)	RCIT (µg/mL)
LOD	0.006	0.007
LOQ	0.020	0.023

The detection limits obtained with this stationary phase by liquid chromatography coupled with a fluorescence detector, would allow for the quantification of the SCIT levels expected in urine in patients treated chronically with common SCIT doses (10 mg/day) [174].

9. Conclusions

In reference to the previously established objectives, it can be concluded that a new MIP based CSP capable of resolving the enantiomers of the antidepressant citalopram has successfully been synthesised. The methodology presented along this chapter could be extrapolated to other enantiomers of drugs for the controlled development of CSP that could separate racemates.

In the same way, different operational objectives have been fulfilled, allowing to conclude that:

- A new MIP capable of the separating citalopram enantiomers has successfully been synthesised by Reversible Deactivation Radical Polymerisation on the surface of silica support through different polymerisation strategies.

- The new MIP based CSP have been characterised by Elemental Analysis, Fourier Transform Infrared Spectroscopy, Thermogravimetric Analysis and Scanning Electron Microscopy what allowed concluding that the MIP chiral selector had been successfully grafted on silica particles.

- Among tested polymerisation strategies, the immobilisation of chiral nanoparticles developed by precipitation polymerisation, has been found to be the one providing best chromatographic resolution.

- The chromatographic conditions as well as the effect of the temperature in the CSP have been optimised in order to obtain the best enantioseparation of the drug citalopram.

- The proposed method may serve to quantify usual levels of SCIT in urine.

References

1. Kempe M: **Molecularly imprinted polymers in enantiomer separations**. In: *Molecularly Imprinted Polymers Man-made mimics of antibodies and their applications in analytical chemistry*. Edited by Sellergren B, 1 edn. Amsterdam: Elsevier; 2001: 395-415.
2. Wang Y, Ng SC: **HPLC enantioseparation on cyclodextrin-based chiral stationary phases**. In: *Chiral separations methods and protocols*. Edited by Scriba GKE, 2 edn. New York: Humana Press; 2013: 69-79.
3. Xiao Y, Ng S-C, Tan TTY, Wang Y: **Recent development of cyclodextrin chiral stationary phases and their applications in chromatography**. *Journal of Chromatography A* 2012, **1269**:52-68.
4. Zheng Y, Wang X, Ji Y: **Monoliths with proteins as chiral selectors for enantiomer separation**. *Talanta* 2012, **91**:7-17.
5. Paik M-J, Kang JS, Huang B-S, Carey JR, Lee W: **Development and application of chiral crown ethers as selectors for chiral separation in high-performance liquid chromatography and nuclear magnetic resonance spectroscopy**. *Journal of Chromatography A* 2013, **1274**:1-5.
6. Hyun MH: **Development of HPLC chiral stationary phases based on (+)-(18-crown-6)-2,3,11,12-tetracarboxylic acid and their applications**. *Chirality* 2015, **27**(9):576-588.
7. Ilisz I, Pataj Z, Aranyi A, Peter A: **Macrocyclic antibiotic selectors in direct HPLC enantioseparations**. *Separation and Purification Reviews* 2012, **41**(3):207-249.
8. Shen J, Ikai T, Okamoto Y: **Synthesis and application of immobilized polysaccharide-based chiral stationary phases for enantioseparation by high-performance liquid chromatography**. *Journal of Chromatography A* 2014, **1363**:51-61.
9. Yashima E: **Polysaccharide-based chiral stationary phases for high-performance liquid chromatographic enantioseparation**. *Journal of Chromatography A* 2001, **906**(1-2):105-125.
10. Perrin C, Vu VA, Matthijs N, Maftouh M, Massart DL, Vander Heyden Y: **Screening approach for chiral separation of pharmaceuticals. Part I. Normal-phase liquid chromatography**. *Journal of Chromatography A* 2002, **947**(1):69-83.
11. Perrin C, Matthijs N, Mangelings D, Granier-Loyaux C, Maftouh M, Massart DL, Vander Heyden Y: **Screening approach for chiral separation of pharmaceuticals Part II. Reversed-phase liquid chromatography**. *Journal of Chromatography A* 2002, **966**(1-2):119-134.

12. Sellergren B: **Recognition of enantiomers using molecularly imprinted polymers**. In: *Molecularly imprinting of polymers*. Edited by Piletsky S, Turner A, 1 edn. Georgetown: Landes Bioscience; 2006: 95-121.
13. Bai LH, Chen XX, Huang YP, Zhang QW, Liu ZS: **Chiral separation of racemic mandelic acids by use of an ionic liquid-mediated imprinted monolith with a metal ion as self-assembly pivot**. *Analytical and Bioanalytical Chemistry* 2013, **405**(27):8935-8943.
14. Sellergren B, Nilsson KGI: **Molecular imprinting by multiple noncovalent host-guest interactions: synthetic polymers with induced specificity**. *Methods in Molecular and Cellular Biology* 1989, **1**(2):59-62.
15. Wang X-N, Meng X-Y, Liang R-P, Qiu J-D: **One-step synthesis of mussel-inspired molecularly imprinted magnetic polymer as stationary phase for chip-based open tubular capillary electrochromatography enantioseparation**. *Journal of Chromatography A* 2014, **1362**:301-308.
16. Wulff G, Biffis A: **Molecular Imprinting with covalent or stoichiometric non-covalent interactions**. In: *Molecularly imprinted polymers Man-made mimics of antibodies and their applications in analytical chemistry*. Edited by Sellergren B, vol. 23, 1 edn. Amsterdam: Elsevier; 2001: 71-112.
17. Sellergren B: **The non-covalent approach to molecular imprinting**. In: *Molecularly imprinted polymers Man-made mimics of antibodies and their applications in analytical chemistry*. Edited by Sellergren B, vol. 23, 1 edn. Amsterdam: Elsevier; 2001: 113-184.
18. Kempe M, Fischer L, Mosbach K: **Chiral separation using molecularly imprinted heteroaromatic polymers**. *Journal of Molecular Recognition* 1993, **6**(1):25-29.
19. Kempe M: **Antibody-mimicking polymers as chiral stationary phases in HPLC**. *Analytical Chemistry* 1996, **68**(11):1948-1953.
20. Vidyasankar S, Ru M, Arnold FH: **Molecularly imprinted ligand-exchange adsorbents for the chiral separation of underivatized amino acids**. *Journal of Chromatography A* 1997, **775**(1–2):51-63.
21. Hebert B, Meador DS, Spivak DA: **Scalemic and racemic imprinting with a chiral crosslinker**. *Analytica Chimica Acta* 2015, **890**:157-164.
22. Kempe M, Mosbach K: **Separation of amino acids, peptides and proteins on molecularly imprinted stationary phases**. *Journal of Chromatography A* 1995, **691**(1-2):317-323.
23. Fischer L, Mueller R, Ekberg B, Mosbach K: **Direct enantioseparation of β-adrenergic blockers using a chiral stationary phase prepared by molecular imprinting**. *Journal of the Americal Chemical Society* 1991, **113**(24):9358-9360.
24. Kempe M, Mosbach K: **Direct resolution of naproxen on a non-covalently molecularly imprinted chiral stationary phase**. *Journal of Chromatography A* 1994, **664**(2):276-279.

25. Manesiotis P, Osmani C, McLoughlin P: **An enantio-selective chromatographic stationary phase for S-ibuprofen prepared by stoichiometric molecular imprinting**. *Journal of Materials Chemistry* 2012, **22**(22):11201-11207.
26. Ansell RJ, Kuah JKL, Wang D, Jackson CE, Bartle KD, Clifford AA: **Imprinted polymers for chiral resolution of (±)-ephedrine, 4: Packed column supercritical fluid chromatography using molecularly imprinted chiral stationary phases**. *Journal of Chromatography A* 2012, **1264**:117-123.
27. Ramstrom O, Yu C, Mosbach K: **Chiral recognition in adrenergic receptor binding mimics prepared by molecular imprinting**. *Journal of Molecular Recognition* 1996, **9**(5/6):691-696.
28. Hart BR, Rush DJ, Shea KJ: **Discrimination between enantiomers of structurally related molecules: separation of benzodiazepines by molecularly imprinted polymers**. *Journal of the American Chemical Society* 2000, **122**(3):460-465.
29. Hosoya K, Shirasu Y, Kimata K, Tanaka N: **Molecularly imprinted chiral stationary phases: requirement for the chiral template**. *Analytical Chemistry* 1998, **70**(5):943-945.
30. Torres JJ, Gsponer N, Ramirez CL, Vera DMA, Montejano HA, Chesta CA: **Experimental and theoretical studies on the enantioselectivity of molecularly imprinted polymers prepared with a chiral functional monomer**. *Journal of Chromatography A* 2012, **1266**:24-33.
31. Jiang J, Zhou Q, Kang C, Wu S, Tang Y, Zuo X: **Preparation and characterization of a pseudo-template imprinted polymer with a chirality-matching monomer for the separation of cinchona alkaloids by high-performance liquid chromatography**. *Journal of Applied Polymer Science* 2013, **129**(6):3425-3431.
32. Bompart M, Haupt K, Ayela C: **Micro and nanofabrication of molecularly imprinted polymers**. In: *Molecularly imprinting*. Edited by Haupt K, 1 edn. Heidelberg: Springer-Verlag; 2012: 83-111.
33. Otsu T, Matsumoto A: **Controlled synthesis of polymers using the iniferter technique: developments in living radical polymerization** In: *Microencapsulation/Microgels/Iniferters* Edited by Abe A, Albertson AC, Cantow HJ, Dugek K, Edwards S, Höcker H, Joanny JF, Kausch HH, Kobayashi T, Lee KS *et al*. Heidelberg: Springer-Verlag; 1998: 75-139.
34. Stuart BH: **Polymers**. In: *Infrared spectroscopy. Fundamentals and applications.* Edited by Stuart BH, 1 edn. Chichester: John Wiley & Sons; 2004: 113-135.
35. Moad G, Solomon DH: **Living radical polymerization**. In: *The chemistry of radical polymerization.* Edited by Moad G, Solomon DH, 2 edn. Oxford: Elservier; 2006: 451-585.

36. Sellergren B: **Imprinted chiral stationary phases in high-performance liquid chromatography**. *Journal of Chromatography A* 2001, **906**(1-2):227-252.
37. Baggiani C: **Chromatographic techniques**. In: *Molecularly imprinted materials science and technology*. Edited by Yan M, Ramström O, 1 edn. New York: Marcel Dekker; 2005: 517-552.
38. Kempe H, Kempe M: **Novel method for the synthesis of molecularly imprinted polymer bead libraries**. *Macromolecular Rapid Communications* 2004, **25**(1):315-320.
39. Haginaka J, Kagawa C: **Uniformly sized molecularly imprinted polymer for d-chlorpheniramine. Evaluation of retention and molecular recognition properties in an aqueous mobile phase**. *Journal of Chromatography A* 2002, **948**(1-2):77-84.
40. Wang J, Cormack PAG, Sherrington DC, Khoshdel E: **Monodisperse, molecularly imprinted polymer microspheres prepared by precipitation polymerization for affinity separation applications**. *Angewandte Chemie International Edition* 2003, **42**(43):5336-5338.
41. Perez-Moral N, Mayes AG: **Noncovalent imprinting in the shell of core-shell nanoparticles**. *Langmuir* 2004, **20**(9):3775-3779.
42. Sulitzky C, Rueckert B, Hall AJ, Lanza F, Unger K, Sellergren B: **Grafting of molecularly imprinted polymer films on silica supports containing surface-bound free radical initiators**. *Macromolecules* 2002, **35**(1):79-91.
43. Lu CH, Zhou WH, Han B, Yang HH, Chen X, Wang XR: **Surface-imprinted core-shell nanoparticles for sorbent assays**. *Analytical Chemistry* 2007, **79**(14):5457-5461.
44. Jenkins AD, Jones RG, Moad G: **Terminology for reversible-deactivation radical polymerization previously called "controlled" radical or "living" radical polymerization (IUPAC Recommendations 2010)**. *Pure and Applied Chemistry* 2010, **82**(2):483-491.
45. Salian VD, Byrne ME: **Living radical polymerization and molecular imprinting: improving polymer morphology in imprinted polymers**. *Macromolecular Materials and Engineering* 2013, **298**(4):379-390.
46. Jenkins AD, Kratochvil P, Stepto RFT, Suter UW: **Glossary of basic terms in polymer science**. *Pure and Applied Chemistry* 1996, **68**(12):2287-2311.
47. Matyjaszewski K: **Radical polymerization**. In: *Controlled and living polymerizations*. Edited by Müller AHE, Matyjaszewski K, 1 edn. Weinheim: Wiley-VCH verlag GmbH & Co; 2009: 103-166.
48. Solomon DH, Rizzardo E, Cacioli P: **Free radical polymerization and the produced polymers**. In.: Commonwealth Scientific and Industrial Research Organization, Australia . 1985: 63 pp.

49. Moad G, Rizzardo E: **Alkoxyamine-initiated living radical polymerization: factors affecting alkoxyamine homolysis rates**. *Macromolecules* 1995, **28**(26):8722-8728.
50. Marque S, Fischer H, Baier E, Studer A: **Factors influencing the C-O bond homolysis of ‹lkoxyamines: effects of H-bonding and polar substituents**. *The Journal of Organic Chemistry* 2001, **66**(4):1146-1156.
51. Marque S, Le Mercier C, Tordo P, Fischer H: **Factors influencing the C-O-bond homolysis of trialkylhydroxylamines**. *Macromolecules* 2000, **33**(12):4403-4410.
52. Nicolas J, Guillaneuf Y, Lefay C, Bertin D, Gigmes D, Charleux B: **Nitroxide-mediated polymerization**. *Progress in Polymer Science* 2013, **38**(1):63-235.
53. Guegain E, Guillaneuf Y, Nicolas J: **Nitroxide-mediated polymerization of methacrylic esters: insights and solutions to a long-standing problem**. *Macromolecular Rapid Communications* 2015, **36**(13):1227-1247.
54. Boonpangrak S, Whitcombe MJ, Prachayasittikul V, Mosbach K, Ye L: **Preparation of molecularly imprinted polymers using nitroxide-mediated living radical polymerization**. *Biosensors and Bioelectronics* 2006, **22**(3):349-354.
55. Banerjee S, Paira TK, Mandal TK: **Surface confined atom transfer radical polymerization: access to custom library of polymer-based hybrid materials for speciality applications**. *Polymer Chemistry* 2014, **5**(14):4153-4167.
56. Wang JS, Matyjaszewski K: **Controlled/"living" radical polymerization. halogen atom transfer radical polymerization promoted by a Cu(I)/Cu(II) redox process**. *Macromolecules* 1995, **28**(23):7901-7910.
57. Wang JS, Matyjaszewski K: **Controlled/"living" radical polymerization. atom transfer radical polymerization in the presence of transition-metal complexes**. *Journal of the American Chemical Society* 1995, **117**(20):5614-5615.
58. Wang JS, Matyjaszewski K: **"Living"/controlled radical polymerization. transition-metal-catalyzed atom transfer radical polymerization in the presence of a conventional radical initiator**. *Macromolecules* 1995, **28**(22):7572-7573.
59. Kato M, Kamigaito M, Sawamoto M, Higashimura T: **Polymerization of methyl methacrylate with the carbon tetrachloride/dichlorotris-(triphenylphosphine)ruthenium(II)/methylaluminum bis(2,6-di-tert-butylphenoxide) initiating system: possibility of living radical polymerization**. *Macromolecules* 1995, **28**(5):1721-1723.
60. Percec V, Barboiu B: **"Living" radical polymerization of styrene initiated by arenesulfonyl chlorides and CuI(bpy)nCl**. *Macromolecules* 1995, **28**(23):7970-7972.
61. Kharasch MS, Jensen EV, Urry WH: **Addition of carbon tetrachloride and chloroform to olefins**. *Science* 1945, **102**:128.

62. Matyjaszewski K, Xia J: **Atom transfer radical polymerization**. *Chemical Reviews* 2001, **101**(9):2921-2990.
63. Bompart M, Haupt K: **Molecularly imprinted polymers and controlled/living radical polymerization**. *Australian Journal of Chemistry* 2009, **62**(8):751-761.
64. Mao X, Sun H, He X, Chen L, Zhang Y: **Well-defined sulfamethazine-imprinted magnetic nanoparticles via surface-initiated atom transfer radical polymerization for highly selective enrichment of sulfonamides in food samples**. *Analytical Methods* 2015, **7**(11):4708-4716.
65. Niu Y, Ma M, Gong Y, Wang Y, Gong B: **Synthesis of chlorogenic acid imprinted chromatographic packing by surface-initiated atom transfer radical polymerization and its application**. *Chemical Research in Chinese Universities* 2014, **30**(5):855-862.
66. Yang F, Hu D, Dong X: **Molecularly imprinted mesoporous SBA-15 synthesized by surface-initiated atom transfer radical polymerization for bisphenol A recognition**. *Chromatographia* 2015, **78**(1-2):45-54.
67. Ji J, Sun X, Tian X, Li Z, Zhang Y: **Synthesis of acrylamide molecularly imprinted polymers immobilized on graphite oxide through surface-initiated atom transfer radical polymerization**. *Analytical Letters* 2013, **46**(6):969-981.
68. American Chemical Society: **Scifinder**. In. https://scifinder.cas.org; 2015.
69. Chiefari J, Chong YK, Ercole F, Krstina J, Jeffery J, Le TPT, Mayadunne RTA, Meijs GF, Moad CL, Moad G *et al*: **Living free-radical polymerization by reversible addition-fragmentation chain transfer: the RAFT process**. *Macromolecules* 1998, **31**(16):5559-5562.
70. Tu YF, Cheng ZP, Zhang ZB, Zhu J, Zhang W, Zhou NC, Ni PH, Zhu XL: **Mechanism study and molecular design in controlled/"living" radical polymerization**. *Science China Chemistry* 2010, **53**(8):1605-1619.
71. Charmot D, Corpart P, Adam H, Zard SZ, Biadatti T, Bouhadir G: **Controlled radical polymerization in dispersed media**. *Macromolecular Symposia* 2000, **150**(Polymers in Dispersed Media):23-32.
72. Moad G, Rizzardo E, Thang SH: **Living radical polymerization by the RAFT process**. *Australian Journal of Chemistry* 2005, **58**(6):379-410.
73. Xu S, Li J, Chen L: **Molecularly imprinted core-shell nanoparticles for determination of trace atrazine by reversible addition-fragmentation chain transfer surface imprinting**. *Journal of Materials Chemistry* 2011, **21**(12):4346-4351.
74. Li J, Dong R, Wang X, Xiong H, Xu S, Shen D, Song X, Chen L: **One-pot synthesis of magnetic molecularly imprinted microspheres by RAFT precipitation polymerization for the fast and selective removal of 17 β-estradiol**. *RSC Advances* 2015, **5**(14):10611-10618.

75. Xie X, Chen L, Pan X, Wang S: **Synthesis of magnetic molecularly imprinted polymers by reversible addition fragmentation chain transfer strategy and its application in the Sudan dyes residue analysis**. *Journal of Chromatography A* 2015, **1405**:32-39.
76. Halhalli MR, Sellergren B: **Cover and uncover: chiral switching exploiting templating and layer-by-layer grafting**. *Chemical Communications* 2013, **49**(64):7111-7113.
77. Halhalli MR, Schillinger E, Aureliano CSA, Sellergren B: **Thin walled imprinted polymer beads featuring both uniform and accessible binding sites**. *Chemistry of Materials* 2012, **24**(15):2909-2919.
78. Halhalli MR, Aureliano CSA, Schillinger E, Sulitzky C, Titirici MM, Sellergren B: **An improved grafting technique for producing imprinted thin film composite beads**. *Polymer Chemistry* 2012, **3**(4):1033-1042.
79. Kadhirvel P, Azenha M, Schillinger E, Halhalli MR, Silva AF, Sellergren B: **Recognitive nano-thin-film composite beads for the enantiomeric resolution of the metastatic breast cancer drug aminoglutethimide**. *Journal of Chromatography A* 2014, **1358**:93-101.
80. Peeters M, Kobben S, Jiménez-Monroy KL, Modesto L, Kraus M, Vandenryt T, Gaulke A, van Grinsven B, Ingebrandt S, Junkers T *et al*: **Thermal detection of histamine with a graphene oxide based molecularly imprinted polymer platform prepared by reversible addition–fragmentation chain transfer polymerization**. *Sensors and Actuators B: Chemical* 2014, **203**:527-535.
81. Zhao L, Zhao F, Zeng B: **Synthesis of water-compatible surface-imprinted polymer via click chemistry and RAFT precipitation polymerization for highly selective and sensitive electrochemical assay of fenitrothion**. *Biosensors and Bioelectronics* 2014, **62**:19-24.
82. Niu H, Yang Y, Zhang H: **Efficient one-pot synthesis of hydrophilic and fluorescent molecularly imprinted polymer nanoparticles for direct drug quantification in real biological samples**. *Biosensors and Bioelectronics* 2015, **74**:440-446.
83. Kamra T, Zhou T, Montelius L, Schnadt J, Ye L: **Implementation of molecularly imprinted polymer beads for surface enhanced raman detection**. *Analytical Chemistry* 2015, **87**(10):5056-5061.
84. Ferington TE, Tobolsky AV: **Organic disulfides as initiators of polymerization: tetramethylthiuram disulfide**. *Journal of the American Chemical Society* 1955, **77**:4510-4512.
85. Otsu T, Yoshida M: **Role of initiator-transfer agent-terminator (iniferter) in radical polymerizations: polymer design by organic disulfides as iniferters**. *Die Makromolekulare Chemie, Rapid Communications* 1982, **3**(2):127-132.
86. Otsu T: **Iniferter concept and living radical polymerization**. *Journal of Polymer Science Part A: Polymer Chemistry* 2000, **38**(12):2121-2136.

87. Tasdelen MA, Yagci Y: **Controlled/living radical polymerization in the presence of iniferters**. In: *Fundamentals fo Controlled/Living Radical Polymerization*. Edited by Tsarevsky NV, Sumerlin BS, 1 edn. Cambridge: Royal Society of Chemistry (RSC); 2013: 78-111.
88. Arnold FH, Plunkett S, Dhal PK, Vidyasankar S: **Surface modification with molecularly-imprinted polymers for selective recognition**. *Polymer Preprints* 1995, **36**(1):97-98.
89. Piletsky SA, Matuschewski H, Schedler U, Wilpert A, Piletska EV, Thiele TA, Ulbricht M: **Surface functionalization of porous polypropylene membranes with molecularly imprinted polymers by photograft copolymerization in water**. *Macromolecules* 2000, **33**(8):3092-3098.
90. Dyer DJ: **Photoinitiated synthesis of grafted polymers**. In: *Surface Initiated polymerization I*. Edited by Jordan R, vol. 197, 1 edn. Heidelberg: Springer-Verlag; 2006: 48-65.
91. Norrloew O, Glad M, Mosbach K: **Acrylic polymer preparations containing recognition sites obtained by imprinting with substrates**. *Journal of Chromatography A* 1984, **299**(1):29-41.
92. Ou J, Li X, Feng S, Dong J, Dong X, Kong L, Ye M, Zou H: **Preparation and evaluation of a molecularly imprinted polymer derivatized silica monolithic column for capillary electrochromatography and capillary liquid chromatography**. *Analytical Chemistry* 2007, **79**(2):639-646.
93. Masoumi M, Jahanshahi M: **Synthesis and recognition of nano pore molecularly imprinted polymers of thymol on the surface of modified silica nanoparticles**. *Advances in Polymer Technology* 2015:doi: 10.1002/adv.21548.
94. Lin Z, Xia Z, Zheng J, Zheng D, Zhang L, Yang H, Chen G: **Synthesis of uniformly sized molecularly imprinted polymer-coated silica nanoparticles for selective recognition and enrichment of lysozyme**. *Journal of Materials Chemistry* 2012, **22**(34):17914-17922.
95. du Fresne von Hohenesche C, Ehwald V, Unger KK: **Development of standard operation procedures for the manufacture of n-octadecyl bonded silicas as packing material in certified reference columns for reversed-phase liquid chromatography**. *Journal of Chromatography A* 2004, **1025**(2):177-187.
96. Giovannoli C, Passini C, Baravalle P, Anfossi L, Giraudi G, Baggiani C: **An innovative approach to molecularly imprinted capillaries for polar templates by grafting polymerization**. *Journal of Molecular Recognition* 2012, **25**(6):377-382.
97. Edmondson S, Osborne VL, Huck WTS: **Polymer brushes via surface-initiated polymerizations**. *Chemical Society Reviews* 2004, **33**(1):14-22.
98. Haginaka J: **Monodispersed, molecularly imprinted polymers as affinity-based chromatography media**. *Journal of Chromatography B* 2008, **866**(1-2):3-13.

99. Baht RRT, Wu MR, Jan T: **Surface-grafted polymer gradients: formation, characterization and applications**. In: *Surface-initiated polymerization II*. Edited by Jordan R, vol. 198, 1 edn. Heidelberg: Springer-Verlag; 2006: 54-124.
100. Minko S: **Grafting on solid surfaces: "grafting to" and "grafting from" methods**. In: *Polymer surfaces and interfaces*. Edited by Stamm M, 1 edn. Heidelberg: Springer-Verlag; 2008: 215-234.
101. de Boer B, Simon HK, Werts MPL, van der Vegte EW, Hadziioannou G: **"Living" free radical photopolymerization initiated from surface-grafted iniferter monolayers**. *Macromolecules* 2000, **33**(2):349-356.
102. Luo N, Hutchison JB, Anseth KS, Bowman CN: **Surface-initiated photopolymerization of poly(ethylene glycol) methyl ether methacrylate on a diethyldithiocarbamate-mediated polymer substrate**. *Macromolecules* 2002, **35**(7):2487-2493.
103. Bossi A, Whitcombe MJ, Uludag Y, Fowler S, Chianella I, Subrahmanyam S, Sanchez I, Piletsky SA: **Synthesis of controlled polymeric cross-linked coatings via iniferter polymerization in the presence of tetraethyl thiuram disulphide chain terminator**. *Biosensors and Bioelectronics* 2010, **25**(9):2149-2155.
104. Rahane SB, Metters AT, Kilbey SM, II: **Impact of added tetraethylthiuram disulfide deactivator on the kinetics of growth and reinitiation of poly(methyl methacrylate) brushes made by surface-initiated photoiniferter-mediated photopolymerization**. *Macromolecules* 2006, **39**(26):8987-8991.
105. Barahona F, Turiel E, Cormack PAG, Martin-Esteban A: **Chromatographic performance of molecularly imprinted polymers: core-shell microspheres by precipitation polymerization and grafted MIP films via iniferter-modified silica beads**. *Journal of Polymer Science Part A: Polymer Chemistry* 2010, **48**(5):1058-1066.
106. Gallego-Gallegos M, Garrido ML, Olivas RM, Baravalle P, Baggiani C, Camara C: **A new application of imprinted polymers: speciation of organotin compounds**. *Journal of Chromatography A* 2010, **1217**(20):3400-3407.
107. Singh M, Tarannum N, Kumar A: **Selective recognition of fenbufen by surface-imprinted silica with iniferter technique**. *Journal of Porous Materials* 2014, **21**(5):677-684.
108. Xu W, Su S, Jiang P, Wang H, Dong X, Zhang M: **Determination of sulfonamides in bovine milk with column-switching high performance liquid chromatography using surface imprinted silica with hydrophilic external layer as restricted access and selective extraction material**. *Journal of Chromatography A* 2010, **1217**(46):7198-7207.
109. Martins N, Carreiro EP, Simoes M, Cabrita MJ, Burke AJ, Garcia R: **An emerging approach for the targeting analysis of dimethoate in olive oil: The role of**

molecularly imprinted polymers based on photo-iniferter induced "living" radical polymerization. *Reactive and Functional Polymers* 2015, **86**:37-46.

110. Song RY, Hu XL, Guan P, Li J, Qian LW, Wang QL: **Synthesis of glutathione imprinted polymer particles via controlled living radical precipitation polymerization**. *Chinese Journal of Polymer Science* 2015, **33**(3):404-415.
111. Li J, Zu B, Zhang Y, Guo X, Zhang H: **One-pot synthesis of surface-functionalized molecularly imprinted polymer microspheres by iniferter-induced "living" radical precipitation polymerization**. *Journal of Polymer Science Part A: Polymer Chemistry* 2010, **48**(15):3217-3228.
112. Liu W, Qin L, Yang Y, Liu X, Xu B: **Synthesis and characterization of dibenzothiophene imprinted polymers on the surface of iniferter-modified carbon microspheres**. *Macromolecular Chemistry and Physics* 2014, **148**(3):605-613.
113. Marchyk N, Maximilien J, Beyazit S, Haupt K, Sum Bui BT: **One-pot synthesis of iniferter-bound polystyrene core nanoparticles for the controlled grafting of multilayer shells**. *Nanoscale* 2014, **6**(5):2872-2878.
114. Piletsky SA, Mijangos I, Guerreiro A, Piletska EV, Chianella I, Karim K, Turner APF: **Polymer cookery: influence of polymerization time and different initiation conditions on performance of molecularly imprinted polymers**. *Macromolecules* 2005, **38**(4):1410-1414.
115. Mijangos I, Navarro-Villoslada F, Guerreiro A, Piletska E, Chianella I, Karim K, Turner A, Piletsky S: **Influence of initiator and different polymerisation conditions on performance of molecularly imprinted polymers**. *Biosensors and Bioelectronics* 2006, **22**(3):381-387.
116. Chen L, Xu S, Li J: **Recent advances in molecular imprinting technology: current status, challenges and highlighted applications**. *Chemical Society Reviews* 2011, **40**(5):2922-2942.
117. Vasapollo G, Del Sole R, Mergola L, Lazzoi MR, Scardino A, Scorrano S, Mele G: **Molecularly imprinted polymers: present and future prospective**. *International Journal of Molecular Sciences* 2011, **12**(9):5908-5945.
118. **IUPAC. Compendium of Chemical Terminology-The Gold Book** http://goldbook.iupac.org/ **Access data:** 2015.11.30
119. Francotte E: **Isolation and production of optically pure drugs by enantioselective chromatography**. In: *Chirality in drug research*. Edited by Francotte E, Linder W, vol. 33, 1 edn. Weinheim: Wiley-VCH Verlag GmbH & Co. KGaA; 2006: 155-189.
120. Francotte E, Wolf RM, Lohmann D, Mueller R: **Chromatographic resolution of racemates on chiral stationary phases : I. Influence of the supramolecular structure of cellullose triacetate**. *Journal of Chromatography A* 1985, **347**:25-37.
121. Mosbach K: **Molecular imprinting**. *Trends Biochem Sci* 1994, **19**(1):9-14.

122. Kempe M, Mosbach K: **Molecular imprinting used for chiral separations**. *Journal of Chromatography A* 1995, **694**(1):3-13.
123. Tamayo FG, Titirici MM, Martin-Esteban A, Sellergren B: **Synthesis and evaluation of new propazine-imprinted polymer formats for use as stationary phases in liquid chromatography**. *Analytica Chimica Acta* 2005, **542**(1):38-46.
124. Haginaka J, Takehira H, Hosoya K, Tanaka N: **Uniform-sized molecularly imprinted polymer for (S)-naproxen selectively modified with hydrophilic external layer**. *Journal of Chromatography A* 1999, **849**(2):331-339.
125. Haginaka J, Tabo H, Kagawa C: **Uniformly sized molecularly imprinted polymers for d-chlorpheniramine: Influence of a porogen on their morphology and enantioselectivity**. *J Pharm Biomed Anal* 2008, **46**(5):877-881.
126. Vansant EF, Van Der Voort P, Vrancken KC: **Chemical modification of silica: applications and procedures**. In: *Characterization and chemical modification of the silica surface*. Edited by Vansant EF, Van Der Voort P, Vrancken KC, vol. 93, 1 edn. Amsterdam: Elsevier; 1995: 149-187.
127. Nawrocki J: **The silanol group and its role in liquid chromatography**. *Journal of Chromatography A* 1997, **779**(1 + 2):29-72.
128. Koehler J, Chase DB, Farlee RD, Vega AJ, Kirkland JJ: **Comprehensive characterization of some silica-based stationary phases for high-performance liquid chromatography**. *Journal of Chromatography A* 1986, **352**:275-305.
129. Koehler J, Kirkland JJ: **Improved silica-based column packings for high-performance liquid chromatography**. *Journal of Chromatography A* 1987, **385**:125-150.
130. Unger KK, Lork KD, Pfleiderer B, Albert K, Bayer E: **Impact of acidic/hydrothermal treatment on pore structural and chromatographic properties of porous silicas. I. The conventional approach**. *Journal of Chromatography A* 1991, **556**(1-2):395-406.
131. Colthup NB, Daly LH, Wiberley SE: **Compounds containing boron, silicon, phosphorus, sulfur or halogen**. In: *Introduction to Infrared and Raman Spectroscopy*. Edited by Colthup NB, Daly LH, Wiberley SE, 3 edn. London: Elsevier; 1990: 355-387.
132. Colthup NB, Daly LH, Wiberley SE: **Amines, C=N, and N=O compounds**. In: *Introduction to Infrared and Raman Spectroscopy*. Edited by Colthup NB, Daly LH, Wiberley SE, 3 edn. London: Elsevier; 1990: 339-354.
133. Prucker O, Ruehe J: **Mechanism of radical chain polymerizations initiated by azo compounds covalently bound to the surface of spherical particles**. *Macromolecules* 1998, **31**(3):602-613.
134. Sellegren B, Hall AJ: **Fundamental aspects on the synthesis and characterisation of imprinted network polymers**. In: *Molecularly imprinted*

polymers. Man-made mimics of antibodies and their applications in analytical chemistry Edited by Sellergren B, vol. 23. Amsterdam, The Netherlands: Elsevier; 2001: 21-57.

135. Sandoval JE: **Equation for calculating surface coverage from end-capping of chromatographic bonded phases**. *Journal of Chromatography A* 1999, **852**(2):375-381.
136. Simões M, Martins N, Cabrita M, Burke A, Garcia R: **Tailor-made molecularly imprinted polymers for dimethoate and deltamethrin recognition: synthesis, characterization and chromatographic evaluation**. *Journal of Polymer Research* 2014, **21**(3):1-13.
137. Dong MW: **Basic terms and concepts**. In: *Modern HPLC for practicing scientists*. Edited by Dong MW, 1 edn. Hoboken: John Wiley & Sons; 2006: 15-46.
138. Peter A, Torok G, Armstrong DW, Toth G, Tourwe D: **Effect of temperature on retention of enantiomers of β-methyl amino acids on a teicoplanin chiral stationary phase**. *Journal of Chromatography A* 1998, **828**(1 + 2):177-190.
139. Spivak DA: **Optimization, evaluation, and characterization of molecularly imprinted polymers**. *Advanced Drug Delivery Reviews* 2005, **57**(12):1779-1794.
140. Berthod A, He BL, Beesley TE: **Temperature and enantioseparation by macrocyclic glycopeptide chiral stationary phases**. *Journal of Chromatography A* 2004, **1060**(1-2):205-214.
141. Berthod A: **Chiral recognition mechanism in enantiomers separations: a general view**. In: *Chiral recognition in separation methods*. Edited by Berthod A, 1 edn. Paris: Springer-Verlag; 2010: 1-32.
142. Lao W: **Thermodynamic and extrathermodynamic studies of enantioseparation of imidazolinone herbicides on Chiralcel OJ column**. *ISRN Chromatography* 2013, **2013**(Article ID: 460787):1-9.
143. Oberleitner WR, Maier NM, Lindner W: **Enantioseparation of various amino acid derivatives on a quinine based chiral anion-exchange selector at variable temperature conditions. Influence of structural parameters of the analytes on the apparent retention and enantioseparation characteristics**. *Journal of Chromatography A* 2002, **960**(1-2):97-108.
144. Dong H, Zheng M, Ou Y, Zhang C, Liu L, Li J, Yang X: **A chiral stationary phase coated by surface molecularly imprinted polymer for separating 1,1'-binaphthalene-2,2'-diamine enantiomer by high performance liquid chromatography**. *Journal of Chromatography A* 2015, **1376**:172-176.
145. Umpleby RJ, II, Bode M, Shimizu KD: **Measurement of the continuous distribution of binding sites in molecularly imprinted polymers**. *Analyst* 2000, **125**(7):1261-1265.
146. Sellergren B, Shea KJ: **Origin of peak asymmetry and the effect of temperature on solute retention in enantiomer separations on imprinted chiral stationary phases**. *Journal of Chromatography A* 1995, **690**(1):29-39.

147. Scriba GKE: **Chiral recognition mechanisms in analytical separation sciences**. *Chromatographia* 2012, **75**(15-16):815-838.
148. Poma A, Guerreiro A, Whitcombe MJ, Piletska EV, Turner APF, Piletsky SA: **Solid-phasesynthesis of molecularly imprinted polymer nanoparticles with a reusable template-"plastic antibodies"**. *Advanced Functional Materials* 2013, **23**(22):2821-2827.
149. Ambrosini S, Serra M, Shinde S, Sellergren B, De Lorenzi E: **Synthesis and chromatographic evaluation of molecularly imprinted polymers prepared by the substructure approach for the class-selective recognition of glucuronides**. *Journal of Chromatography A* 2011, **1218**(39):6961-6969.
150. Kirsch N, Alexander C, Lubke M, Whitcombe MJ, Vulfson EN: **Enhancement of selectivity of imprinted polymers via post-imprinting modification of recognition sites**. *Polymer* 2000, **41**(15):5583-5590.
151. Takeuchi T, Murase N, Maki H, Mukawa T, Shinmori H: **Dopamine selective molecularly imprinted polymers via post-imprinting modification**. *Organic & Biomolecular Chemistry* 2006, **4**(3):565-568.
152. Ding X, Heiden PA: **Recent developments in molecularly imprinted nanoparticles by surface imprinting techniques**. *Macromolecular Materials and Engineering* 2014, **299**(3):268-282.
153. Cheong WJ, Yang SH, Ali F: **Molecular imprinted polymers for separation science: a review of reviews**. *Journal of Separation Science* 2013, **36**(3):609-628.
154. Sellergren B, Hall AJ: **Fundamental aspects on the synthesis and characterisation of imprinted network polymers**. In: *Molecularly imprinted polymers: Man-made mimics of antibodies and their applications in analytical chemistry* Edited by Sellergren B, vol. 23, 1 edn. Amsterdam: Elsevier; 2001: 21-57.
155. Moczko E, Poma A, Guerreiro A, Perez de Vargas Sansalvador I, Caygill S, Canfarotta F, Whitcombe MJ, Piletsky S: **Surface-modified multifunctional MIP nanoparticles**. *Nanoscale* 2013, **5**(9):3733-3741.
156. Moczko E, Guerreiro A, Piletska E, Piletsky S: **PEG-stabilized core-shell surface-imprinted nanoparticles**. *Langmuir* 2013, **29**(31):9891-9896.
157. Poma A, Guerreiro A, Caygill S, Moczko E, Piletsky S: **Automatic reactor for solid-phase synthesis of molecularly imprinted polymeric nanoparticles (MIP NPs) in water**. *RSC Advances* 2014, **4**(8):4203-4206.
158. Chianella I, Guerreiro A, Moczko E, Caygill JS, Piletska EV, De Vargas Sansalvador IMP, Whitcombe MJ, Piletsky SA: **Direct replacement of antibodies with molecularly imprinted polymer nanoparticles in ELISA-development of a novel assay for vancomycin**. *Analytical Chemistry* 2013, **85**(17):8462-8468.
159. Basozabal I, Guerreiro A, Gomez-Caballero A, Goicolea MA, Barrio RJ: **Direct potentiometric quantification of histamine using solid-phase imprinted**

nanoparticles as recognition elements. *Biosensors and Bioelectronics* 2014, **58**:138-144.
160. Altintas Z, Gittens M, Guerreiro A, Thompson KA, Walker J, Piletsky S, Tothill IE: **Detection of waterborne viruses using high affinity molecularly Imprinted polymers**. *Analytical Chemistry* 2015, **87**(13):6801-6807.
161. Altintas Z, Guerreiro A, Piletsky SA, Tothill IE: **NanoMIP based optical sensor for pharmaceuticals monitoring**. *Sensors and Actuators B* 2015, **213**:305-313.
162. Karim K, Giannoudi L, Piletska E, Chianella I, Henry OYF, Laitenberger P, Piletsky SA, Cowen T: **Development of MIP sensor for monitoring propofol in clinical procedures**. *Journal of the Chinese Advanced Materials Society* 2015, **3**(3):149-160.
163. Yilmaz E, Schmidt RH, Mosbach K: **The noncovalent approach**. In: *Molecularly imprinted materials science and technology*. Edited by Yan M, Ramström O, 1 edn. New York: Marcel Dekker; 2005: 25-59.
164. Abdouss M, Azodi-Deilami S, Asadi E, Shariatinia Z: **Synthesis of molecularly imprinted polymer as a sorbent for solid phase extraction of citalopram from human serum and urine**. *Journal of Materials Science: Materials in Medicine* 2012, **23**(6):1543-1552.
165. Abdouss M, Asadi E, Azodi-Deilami S, Beik-mohammadi N, Aslanzadeh SA: **Development and characterization of molecularly imprinted polymers for controlled release of citalopram**. *Journal of Materials Science: Materials in Medicine* 2011, **22**(10):2273-2281.
166. Guerreiro AR, Chianella I, Piletska E, Whitcombe MJ, Piletsky SA: **Selection of imprinted nanoparticles by affinity chromatography**. *Biosensors and Bioelectronics* 2009, **24**(8):2740-2743.
167. Bocian S, Buszewski B: **Residual silanols at reversed-phase silica in HPLC - a contribution for a better understanding**. *Journal of Separation Science* 2012, **35**(10-11):1191-1200.
168. McCalley DV: **The challenges of the analysis of basic compounds by high performance liquid chromatography: some possible approaches for improved separations**. *Jorunal of Chromatography A* 2010, **1217**(6):858-880.
169. McCalley DV: **Selection of suitable stationary phases and optimum conditions for their application in the separation of basic compounds by reversed-phase HPLC**. *Journal of Separation Science* 2003, **26**(3/4):187-200.
170. Pirkle WH, Readnour RS: **The influence of end-capping on the enantioselectivity of a chiral phase**. *Chromatographia* 1991, **31**(3-4):129-132.
171. Oliveros L, Minguillón C, Desmazières B, Desbène PL: **Chiral-bonded silica gel stationary phases obtained from chiral silanes for high-performance liquid chromatography**. *Journal of Chromatography A* 1992, **606**(1):9-17.

172. Lochmuller CH, Marshall DB, Wilder DR: **An examination of chemically modified silica surfaces using fluorescence spectroscopy**. *Analytica Chimica Acta* 1981, **130**(1):31-43.
173. Vervoort RJM, Debets AJJ, Claessens HA, Cramers CA, De Jong GJ: **Optimization and characterization of silica-based reversed-phase liquid chromatographic systems for the analysis of basic pharmaceuticals**. *Journal of Chromatography A* 2000, **897**(1+2):1-22.
174. Unceta N, Gomez-Caballero A, Garcia D, Diaz G, Guerreiro A, Piletsky S, Goicolea MA, Barrio RJ: **Enantioselective extraction of (+)-(S)-citalopram and its main metabolites using a tailor-made stir bar chiral imprinted polymer for their LC-ESI-MS/MS quantitation in urine samples**. *Talanta* 2013, **116**:448-453.

Chapter 5

General conclusions

This Page Intentionally Left Blank

1. General conclusions

Based on the objectives established previously and in compliance with the results presented along this thesis, it can be concluded that chiral synthetic receptors, based on molecular imprinting technology, have been successfully developed in different formats. These artificial receptors have been applied both as chiral selectors in chromatographic separation and as recognition elements for potentiometric sensing of the S-enantiomer of the chiral antidepressant drug, the serotonin reuptake inhibitor citalopram.

In the first part of the presented work, a potentiometric sensor has been developed, capable of quantifying usual therapeutic levels of SCIT in urine. To this end, Molecularly Imprinted Nanoparticles (MIN) have been developed to be employed as recognition elements implemented in a PVC based membrane. The membrane composition has been optimised obtaining a sensor with Nernstian response. The artificial receptors implemented in the membrane have provided the sensor with excellent selectivity, being capable of recognising the target S enantiomer over the R. Additionally, sensor preference for the target analyte has also been tested in the presence of other cations which are at very high levels urine matrix, since these may be the ones that would preferably hinder proper analyte detection. It has been found that sensor response has not been affected by any of these ions, what has allowed

concluding that the MIN-based potentiometric electrode could be undoubtedly employed as a sensitive and selective sensor for the direct, fast and low-cost quantification of the S enantiomer of citalopram. The methodology presented here may also be extrapolated to other chiral drugs to obtain potentiometric devices that may serve for the fast monitorisation of chiral drugs in clinical samples.

Alternatively to potentiometric sensing, the research carried out along this thesis has also focused on developing new molecularly imprinted chiral stationary phases (CSP) capable of resolving the enantiomers of citalopram. To this end Reversible Deactivation Radical Polymerisation has been employed to modify the surface of silica microparticles with MIP developed in different formats. Initially, CSP were developed by surface imprinting through the grafting from approach, obtaining silica particles coated with MIP thin films. Alternatively, imprinted nanoparticles synthesised by solid-phase imprinting and precipitation polymerisation were also immobilised on silica surface.

Surface imprinting through the grafting from approach provided successful chiral separation, but poor chromatographic resolution for an adequate compound quantification. However, immobilising imprinted nanoparticles on the surface of silica beads, was found to be a really interesting approach to develop MIP-based stationary phases for analytical chromatography. Nevertheless, only nanoparticles developed by precipitation polymerisation presented chiral separation capability. These differences observed in enantioseparation could be due to different reasons. On the one hand, in the solid-phase imprinting approach, the template is linked to the surface of glass beads through the nitrile group of the target compound. This makes this nitrile group unable for imprinting, since it would be never free to establish the prepolymerisation adduct with the functional monomer. Moreover, this functional group was the one which, *a priori*, was capable of strongest binding the functional monomer itaconic acid. On the other hand, in order to synthesise high affinity nanoparticles by the solid-phase approach, a functional group of the template is always sacrificed, which in enantiomeric resolution, can be a key aspect considering that a chiral selector must have at least three point of interaction with the template to be able to discriminate

between the two enantiomers. This sacrifice does not happen in precipitation polymerisation, what could have been the principal factor that may have contributed in the final outcome.

The potential benefits provided by imprinted polymers, in combination with the advantages presented by nanomaterials, have been jointly exploited all along this work in developing artificial receptors with selective recognition capability. It was initially hypothesised if imprinting nanoparticles with a single target enantiomer could lead to nanosized artificial receptors presenting chiral recognition capability. In compliance with the presented results, it can be stated that the presented methodology serves as a very promising approach to get synthetic chiral receptors that may be implemented on different supports to develop enantioselective devices for analytical purposes.

Annex

Articles published in scientific journals

This Page Intentionally Left Blank

Special Issue Article

Journal of Molecular Recognition

Received: 2 June 2014, Revised: 23 September 2014, Accepted: 27 October 2014, Published online in Wiley Online Library

(wileyonlinelibrary.com) DOI: 10.1002/jmr.2443

Iniferter-mediated grafting of molecularly imprinted polymers on porous silica beads for the enantiomeric resolution of drugs

Raquel Gutiérrez-Climente[a], Alberto Gómez-Caballero[a], Mahadeo Halhalli[b], Börje Sellergren[c], M. Aránzazu Goicolea[a] and Ramón J. Barrio[a]*

A surface-imprinted chiral stationary phase for the enantiomeric resolution of the antidepressant drug, citalopram, is presented in this work. N, N'-diethylaminodithiocarbamoylpropyl(trimethoxy)silane has been used as silane iniferter for the surface functionalization of the solid silica support. A molecularly imprinted polymer thin film, in the nm scale, was then grafted on the silanized silica using itaconic acid as the functional monomer and ethylene glycol dimethacrylate as the cross-linker in the presence of the template S-citalopram. The total monomer amount was calculated to obtain the desired thickness. Non-imprinted stationary phases were prepared similarly in the absence of S-citalopram. Characterization of the materials was carried out by scanning electron microscopy, thermogravimetric analysis, elemental analysis and Fourier transform infrared spectroscopy. Stationary phases have been applied to the chromatographic separation of the target. Conditions for best chromatographic resolution of the enantiomers were optimized, and it was found that a mobile phase consisting of a mixture of formate buffer (40 mM, pH 3) and acetonitrile (30:70 v/v) at 40 °C provided best results. Binding behaviour of the developed material was finally assessed by batch rebinding experiments. The obtained binding isotherm was fitted to different binding models being the Freundlich–Langmuir model, the one that best fitted the experimental data. The developed material has shown high selectivity for the target enantiomer, and the stationary phase could be undoubtedly exploited for chiral separation of the drug.

Additional supporting information may be found in the online version of this article at the publisher's web site.

Keywords: iniferter; MIP; citalopram; chiral stationary phase

INTRODUCTION

Molecular imprinting is a technique where a tailor-made polymer is synthesized under the guidance of a template molecule. The presence of this molecule during the polymer formation, in combination with functional and cross-linking monomers, leads to the generation of molecular imprints with specific recognition capability. The subsequent removal of the template is crucial to leave the imprinted sites free, which are chemically and sterically complementary in shape, size and functional groups to the template itself or structural analogues (Piletsky and Turner, 2006).

Molecularly imprinted polymers (MIPs) have been employed over the last years (Whitcombe *et al.*, 2014) as a useful tool for different analytical applications including chromatography (Sulitzky *et al.*, 2002; Chen *et al.*, 2012), capillary electrochromatography (Turiel and Martin-Esteban, 2005), sensor technology (Piletsky *et al.*, 2012) or even in sample treatment procedures such as solid-phase extraction (Sellergren and Esteban, 2010), solid phase microextraction (Prasad *et al.*, 2008) or stir bar sorptive extraction (Gomez-Caballero *et al.*, 2011). In what concerns chromatography, MIP-based stationary phases, traditionally, have been almost exclusively synthesized by bulk polymerization, obtaining irregular particles because of grinding and sieving processes after radical polymerization. This approach has been widely employed for imprinting, not only because of its economic viability, but also because of the fact that resulting polymers are very stable and are able to withstand high pressures without cracking or collapsing. However, this procedure is far long from ideal because the process is time consuming and often leads to highly irregular, variable dimensions and poor yield of useful MIP particles (Baggiani, 2005).

In order to have a better control of MIP particle morphology and to provide materials having improved chromatographic characteristics, different strategies such as suspension polymerization (Kempe and Kempe, 2004), multi-swelling polymerization (Haginaka and Kagawa, 2002), precipitation polymerization (Wang *et al.*, 2003) and imprinting core-shell particles (Perez-Moral and Mayes, 2004) have been employed. However, the conditions required to generate high-affinity binding sites are in most cases incompatible with the conditions needed to obtain the desired particle characteristics

* Correspondence to: Ramón J. Barrio, Department of Analytical Chemistry, Faculty of Pharmacy, University of the Basque Country, 01006 Vitoria-Gasteiz (Álava), Spain.
E-mail: r.barrio@ehu.es

a R. Gutiérrez-Climente, A. Gómez-Caballero, M. A. Goicolea, R. J. Barrio
Department of Analytical Chemistry, Faculty of Pharmacy, University of the Basque Country, Vitoria-Gasteiz (Álava), Spain

b M. Halhalli
INFU, Faculty of Chemistry, Technical University of Dortmund, Dortmund, Germany

c B. Sellergren
Department of Biomedical Sciences, Faculty of Health and Society, Malmö University, Malmö, Sweden

(size, porosity, pore volume and surface area) (Sulitzky *et al.*, 2002). To overcome these problems, surface-imprinting technique (Lu *et al.*, 2007) emerged. Surface imprinting can be carried out by different types of reversible-deactivation radical polymerizations such as iniferter polymerization (Tamayo *et al.*, 2005; Su *et al.*, 2008; Barahona *et al.*, 2010), atom transfer radical polymerization and reversible addition fragmentation chain transfer polymerization.

End-functionalized monomers or polymeric chains can be inserted on the surface of solid supports by 'grafting to' or 'grafting from' approaches. These grafting methods allow the growth of MIPs on preformed support materials of known morphology (Arnold *et al.*, 1995; Piletsky *et al.*, 2000). Traditionally, the preparation of bonded stationary phases based on silica has been carried out almost exclusively by the 'grafting to' approach. Despite its potential benefits improving kinetic characteristics and the simplicity of the procedure, the synthesis of imprinted thin layers is not a simple goal because of the difficulties in controlling film thickness (Giovannoli *et al.*, 2012) because of the presence of an initiator in solution and the molecular weight of the polymers. Moreover, grafting densities are limited because of kinetic and steric factors (Edmondson *et al.*, 2004). On the other hand, in the 'grafting from' approach, the polymerization can start from the surface itself if reactive groups are previously attached (Quaglia *et al.*, 2003). The greater control of the polymerization process, in terms of length and density of surface polymer chains above all, has favoured the recent increase of the use of this technique (Giovannoli *et al.*, 2012).

In this work, the 'grafting from' approach has been employed to develop a surface-imprinted chiral stationary phase for the chromatographic separation of the enantiomers of the antidepressant drug, citalopram (Unceta *et al.*, 2011). The surface-imprinted stationary phase was synthesized via initiator, transfer agent, terminator (iniferter) technique (Tamayo *et al.*, 2005; Barahona *et al.*, 2010), what led to the formation of a chiral stationary phase (CSP) based on a MIP. This application of MIP as CSP provides benefits, such as selectivity and elution predictability, which are not often found in commercial CSPs (Ansell *et al.*, 2012) where organic compounds with chiral functionalities are immobilized.

MATERIALS AND METHODS

Materials

(S)-citalopram (SCIT) and (R)-citalopram (RCIT) oxalate were purchased from Trademax (Shanghai, China). The monomers itaconic acid (IA) ≥99% and ethylene glycol dimethacrylate (EDMA) 98% were supplied from Sigma-Aldrich (Madrid, Spain). Porous silica particles (SiliCycle®) were from Teknokroma (Barcelona, Spain) whose average diameter, pore size and surface area were 10 μm, 10 nm and 432 $m^2 g^{-1}$ respectively. The iniferter N, N'-diethylaminodithiocarbamoylpropyl(trimethoxy)silane (DDCPTS) was synthesized as reported elsewhere (Bossi *et al.*, 2010). Reagents required for its synthesis, that is sodium diethyl dithiocarbamate trihydrate and chloropropyl trimethoxysilane ≥97%, were obtained

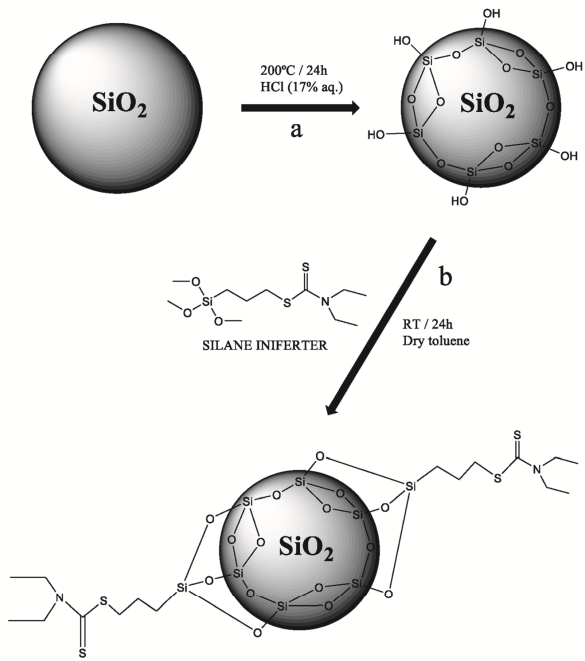

Figure 1. (a) Silica surface activation and (b) functionalization.

from Sigma-Aldrich (Madrid, Spain). Acetone, acetonitrile (ACN) and methanol (MeOH), were acquired from Scharlab (Barcelona, Spain) and dry toluene from Panreac (Barcelona, Spain), all of them were analytical or high-performance liquid chromatography (HPLC) grade and used as received. Mass spectrometry grade ammonium formate >99% and formic acid ≥98% were acquired from Sigma-Aldrich (Madrid, Spain). Every buffer solution was prepared with doubly deionized water Milli-Ro and Milli-Q water purifications system (Millipore, Bedford, MA, USA).

For the MIP synthesis, SCIT was required to be used in its neutral form. This procedure was carried out as reported elsewhere (Gomez-Caballero *et al.*, 2011).

Instrumentation

A Philips UV model HP/3151/A (Amsterdam, the Netherlands) fitted with 4 × 75 W lamps was used for photo-polymerizations. Elemental analysis (EA) was performed with a Eurovector 3000 (Milan, Italy) elemental analyzer. Fourier transform infrared spectroscopy analysis of polymers was performed using a FT-IR spectrometer, model 6300 type A, from Jasco (Madrid, Spain). Thermogravimetric analysis (TGA) was carried out in a Mettler Toledo SDTA 851 analyzer (Mettler Toledo International Inc., Greifensee, Switzerland) at a heating rate of 10 °C min^{-1} up to 900 °C under nitrogen atmosphere. Morphological studies were carried out by scanning electron microscopy (SEM) in a JSM-6400 scanning microscope (JEOL Ltd., Tokyo, Japan), with an accelerating voltage set to 20 kV. Samples were mounted on conductor tape and were chromium coated (20 nm thickness). EA, SEM and TGA analysis were performed by the Advanced Research Facilities (SGIker) of the University of Basque Country.

Chromatographic experiments were carried out using stainless-steel columns (4.6 × 100 mm) (Phenomenex-Micron Analitica, Madrid, Spain) packed with surface-modified silica. The packing was performed using the Pack in a Box column packing system from Restek (Bellefonte, USA) comprised of a dual piston pump and a 20-ml reservoir. Chromatographic evaluation of MIP and non-imprinted polymer (NIP) columns was performed in an Agilent 1100-series binary pump system (Agilent Technologies Inc., Palo Alto, CA, USA) at a flow rate of 1 ml min^{-1} and a temperature of 40 °C. The mobile phase consisted of a mixture of formate buffer (40 mM, pH 4) and ACN (30:70 v/v). Fluorescence detection was carried out at 240nn (excitation) and 308 nm (emission).

Preparation of the chiral molecularly imprinted stationary phase

Initially, the surface of commercial silica particles was activated by rehydroxylation (Figure 1). There are various methods for rehydroxylation whose impact on the quality of bonded phases has been thoroughly evaluated by Köhler and Kirkland (Koehler *et al.*, 1986; Koehler and Kirkland, 1987) and Unger *et al.* (1991) who studied acidic/hydrothermal treatment of a series of commercially available silicas. In this work, an acid treatment was applied to commercial silica using HCl. 4 g of silica were suspended in 150 ml of a 17% HCl solution, and the mixture was kept under reflux during 24 h. Once the mixture had cooled down, silica particles were filtered and rinsed several times with water and then twice with 250 ml of MeOH to avoid clotting during drying (du Fresne von Hohenesche *et al.*, 2004). Finally, silica particles were dried at 120 °C at least for 12 h. After this step, an amount of 8 μmol of silanols per m^2 of silica was assumed as a physicochemical constant (Vansant *et al.*, 1995).

After the activation step, the silica surface was functionalized using DDCPTS as silane iniferter (Figure 1). For this, 4.3 g of iniferter were dissolved in 250 ml of dry toluene where, subsequently, 4 g of dry silica particles were dispersed. The suspension was stirred, purged with nitrogen for 15 min and kept in the dark for 24 h. Then silica beads were filtered out and rinsed successively with MeOH and ACN. The minimum amount of DDCPTS to be employed for functionalization was calculated based on the amount of silanols on the silica surface (8 μmol m^{-2}) and considering a 3:1 silanol: iniferter molar ratio. An excess of iniferter was employed to avoid having uncoated silica particles. The final iniferter density on silica particles was determined by EA.

Polymer grafting on the functionalized silica was finally carried out by photo-initiated radical polymerization. Based on a previously reported computational modelling (Gomez-Caballero *et al.*, 2011), IA was chosen as functional monomer because of its strong binding energy with SCIT. Initially, depending on the desired polymer film thickness (Table 1), different amounts of IA and SCIT were dissolved in 15-ml ACN in a 50-ml flask, and it was degassed with high-purity nitrogen for 3 min. Then, the cross-linker (EDMA) and the functionalized silica (2 g) suspended in 5 ml of ACN were added. The mixture was degassed by the freeze–pump–thaw degassing method using liquid nitrogen and a vacuum pump. Finally, ultraviolet irradiation was applied to the mixture for 3 h, and polymerized silica particles were collected, filtered and washed with ACN. The NIP-coated silica particles were synthesized using the same procedure but in the absence of SCIT.

Column packing

Stainless steel analytical (100 mm L × 4.6 mm i.d) columns were packed using a slurry packing procedure: 1.5 g of the chiral molecularly imprinted material was suspended in 20 ml of ACN. The slurry was packed in the column at constant pressure (2000 PSI), using ACN as the pressurizing agent.

Once the material packed, MIP and NIP columns were placed in a chromatograph and a mobile phase that consisted of 200-mM formic acid in MeOH was passed through at 1 ml min^{-1} for 5 h. Finally, the columns were washed with a water:ACN 90:10 mixture and then with 100% ACN.

Binding capacity and adsorption isotherms

Batch rebinding analyses were performed using the following procedure: 20 mg of the surface-modified silica (imprinted or non-imprinted) were weighted into a 5-ml glass vials followed by the addition of 2 ml of different standard solutions of SCIT

Table 1. Composition of the different polymerization mixtures depending on the estimated coating thickness

Thickness (nm)	SCIT (mmol)	IA (mmol)	EDMA (mmol)	Silica (g)
0.5	0.04	0.17	1.00	2
1	0.08	0.32	1.90	2
2	0.14	0.55	3.32	2
3	0.18	0.71	4.27	2
4	0.19	0.79	4.74	2

SCIT, (S)-citalopram; IA, itaconic acid; EDMA, ethylene glycol dimethacrylate.

Table 2. Elemental analysis results

Support	Elemental composition			Area density	Coverage
	%N	%C	%H	(μmol m^{-2})	(%)
Silica	<0.1	<0.3	1.12	—	—
Si-iniferter	0.98	6.62	1.89	1.88	70.83
Si-MIP	0.86	22.83	3.36	—	—
Si-NIP	0.9	21.3	3.23	—	—

MIP, molecularly imprinted polymer; NIP, non-imprinted polymer.

and RCIT independently (concentration range 3–90 mg L^{-1}). Next, the vials were stirred at room temperature with a MovilROD tube shaker (J. P. Selecta, Barcelona, Spain) at a rolling speed of 15 rpm. After 24 h, the silica was left to decant, and the supernatant was removed carefully, filtered and analyzed by HPLC in order to measure the amount of free (unbound) analyte in solution. To this end, a ZORBAX Eclipse XDB-C18 (4.6 × 150 mm, 5 μm) column from Agilent Technologies (Palo Alto, CA, USA) was used, and a mixture of tetramethylammonium chloride (0.4%, pH 4) and ACN (70:30 v/v) was employed as mobile phase at a flow rate of 1 ml min^{-1} at room temperature.

RESULTS AND DISCUSSION

Characterization of surface-modified silica

Characterization of the surface modified silica was performed by Fourier transform infrared spectroscopy, TGA and EA. Morphological analysis of the material was carried out by SEM.

Elemental analysis data for unmodified silica, iniferter-modified silica and MIP-grafted or NIP-grafted silica are shown in Table 2. From these results the surface coverage of the functionalized silica was calculated using the Berendsen-de Galan equation, Equation (1) (Sandoval, 1999).

$$\delta = \frac{10^6 p}{S(100Cn - pM)} \quad (1)$$

Where δ is the area density (in μmol of grafted group per m^2 of native silica), *p* is the carbon percentage (w/w %), *S* is the specific surface area (m^2 g^{-1}) of the native silica, *C* is the atomic weight of carbon, *n* is the number of carbon atoms per grafted group and *M* is the molecular weight of the anchored group.

As illustrated in Table 2, the elemental composition of the iniferter-modified silica and the native one are significantly different. The estimated area density (1.88 μmol m^{-2}) was close to the theoretical maximum value of 2.67 μmol m^{-2}, calculated considering a maximum silanol density of 8 μmol m^{-2} and a stoichiometric 3:1 silanol: iniferter ratio. From the estimated area density, surface coverage was calculated based on Equation (2). Calculated coverage (*C*) was found to be 70% of the silica surface.

$$C_{Si-Iniferter} = \frac{100\,\delta}{8/3} \quad (2)$$

Concerning NIP and MIP modified materials, the carbon content was significantly higher than the one observed in the iniferter-modified silica. In contrast, the nitrogen percentage remained constant. The only molecule containing nitrogen among the ones employed (apart from the template) is the iniferter. In this sense, carbon percentage increase can be attributed to the polymer growth on silica surface.

Infrared spectra of the bare silica support, the iniferter-modified silica and the MIP-grafted or NIP-grafted silica were registered and compared next (Figure 2). The infrared spectrum of the bare silica shows a broad and intense band at 1110 − 1000 cm^{-1} that was attributed to the Si-O stretching vibration. This band can be distinguished in each of the recorded spectra. Insets 1 and 2 (Figure 2) depict magnifications of each of the registered spectra. In inset 1, bands around 2950 cm^{-1} are clearly distinguished that were assigned to -C-H stretching vibrations of methyl and methylene groups. In spectrum (b), the presence of these bands in comparison with spectrum (a) is clear, what is indicative of the iniferter coupling. In (c) and (d) spectra, a moderately intense band is noticeable at 1723 cm^{-1} (inset 2, Figure 2), which was assigned to C = O stretching vibration. Both the cross-linker (EDMA) and

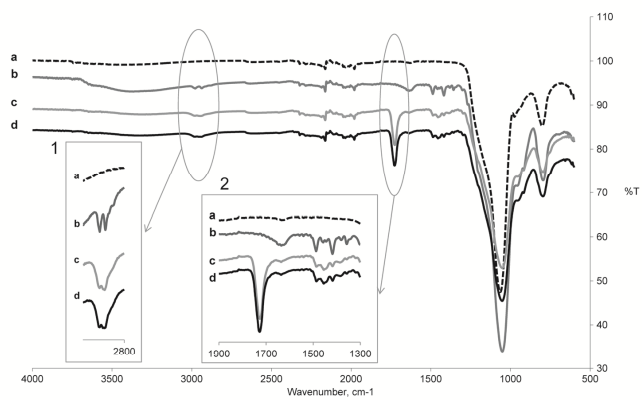

Figure 2. Fourier trasnsform infrared spectroscopy spectra of (a) silica, (b) iniferter modified silica, (c) non-imprinted polymer-modified silica and (d) molecularly imprinted polymer-modified silica.

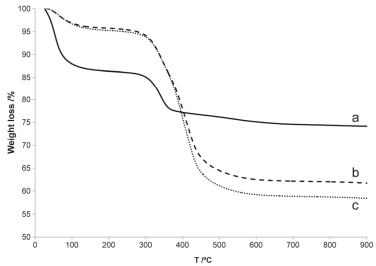

Figure 3. Thermogravimetric analysis measurements of the (a) iniferter-modified silica (SI-INF), (b) molecularly imprinted polymer-modified silica and (c) non-imprinted polymer-modified silica.

the functional monomer (IA) are the only molecules among the employed ones that contain C=O groups, so the presence of this band in the infrared spectrum can be indicative of the polymer formation.

Thermal stability of native silica, iniferter-modified silica and its derivatives, Si-NIP and Si-MIP, were investigated by TGA. As depicted in Figure 3, in all cases, an initial mass loss can be observed at 100 °C because of the solvent content of the material. As regards the iniferter modified-silica (Si-INF), weight loss at this point is higher because of the fact that the material was not dried in order to prevent it from thermal premature initiation. The weight loss observed around 400 °C is due to the organic matter on the silica. In the iniferter modified silica, the weight loss was lower than the one observed in the Si-MIP or Si-NIP, because of the polymeric absence on the silica surface. As could be expected, the polymer mass in the NIP and the MIP is almost equal; so, the polymer coating in both cases could be assumed to be similar.

A MIP-based stationary phase should have different properties that make it a 'true' HPLC material. First of all, the column should be composed of monodispersed and very regular beads, with an average diameter from 2 to 10 μm (Baggiani, 2005). Because of that, the performance of the MIPs is not exclusively dictated by the interaction of the template with the functional monomer pre-polymerization and post-polymerization at a molecular level but also by their overall morphological features (Simoes *et al.*, 2014). Optical SEM images showed that the silica surface, both in the MIP (Figure 4c) and the NIP (Figure 4b) modified silicas, had been coated with the polymer without any appreciable difference concerning particle morphology. No particle agglomeration was observed, and based on the morphological similarities between the MIP-silica, NIP-silica and the bare silica, it was concluded that polymerization had occurred in the silica pores.

Polymer thickness optimization

Being the chain growth mainly confined to the support surface, the 'grafting from' approach allows to have a better control of the thickness of the grafted polymer (Prucker and Ruehe, 1998). It could be expected that mass transfer problems associated with most of MIPs would be largely overcome by thin grafted films (Sulitzky *et al.*, 2002).

In this work, different coating thicknesses were tested in order to know the one that led to the best MIP performance in comparison with the NIP. The total monomer addition was adjusted to get films of 0.5, 1, 2, 3 and 4 nm in average thickness, as described elsewhere (Halhalli *et al.*, 2012). The binding capacity of each of the prepared materials was determined next by classical frontal chromatography. Table 3 summarizes the binding capacities of MIP and NIP modified silicas. The highest MIP capacity was appreciated when 4-nm coatings were employed. Higher coating thicknesses were not employed to avoid collapsing silica pores and the subsequent surface area decrease. Sulitzky *et al.* (2002) had previously reported that a 10-nm-pore-sized silica containing ultrathin grafted films (1 nm approximately) exhibited the highest chromatographic efficiency. However, particles with thinner films (<1 nm) were unable to separate the enantiomers. In the present work, it was observed that thicknesses below 4 nm were unable to resolve the racemate. Moreover, NIP retention capacity was higher than the one observed for the MIP. This fact could be attributed to the lower number of binding sites when coatings were thinner.

Mobile phase optimization

The effect of the mobile phase composition was investigated next in order to know the solvent mixture that led to best enantiomeric resolution. The pH effect, buffer concentration and organic modifier percentage on the chromatographic separation of citalopram enantiomers was investigated. Separation efficiency was assessed based on the separation factor (α) and the resolution (R), whereas imprinting effect was evaluated through the imprinting factor. Figure S1 depicts the effect of each of the tested variables on these three parameters. Best enantiomeric resolution was observed working at pH:4, at a buffer percentage of 30% and a buffer concentration of 40 mM (Supporting information).

Figure 5 depicts overlaid chromatograms registered with the MIP and the NIP columns at the optimized mobile phase composition. It is noticeable that the NIP is not capable of resolving the racemate it constrast to what can be observed with the MIP.

The effect of column temperature

Molecularly imprinted polymer selectivity is based on the difference of binding free energies of different substrates in an imprinted site (Spivak, 2005), and these differences are affected by temperature. Temperature has, at least, two different effects on the resolution of chromatographic separations: the thermodynamic and the kinetic effect (Peter *et al.*, 1998). The former is the one that influences the separation factor (α). Temperature dependence of thermodynamic parameters is described in Equations (3) and (4) (Berthod *et al.*, 2004).

$$\Delta(\Delta G) = -R\,T\,\ln\alpha = \Delta(\Delta H) - T\Delta(\Delta S) \quad (3)$$

$$\ln\alpha = -\frac{\Delta(\Delta H)}{RT} + \frac{\Delta(\Delta S)}{R} \quad (4)$$

Where Δ(ΔG), Δ(ΔH) and Δ(ΔS) represent respectively, the difference of the Gibbs free energy change of the enantiomer-selector phase transfer and the differences in the enthalpy and entropy for a given pair of enantiomers (Berthod *et al.*, 2004). *R* is the gas constant (8.314 J mol^{-1} K^{-1}), *T* is the absolute temperature and α the separation factor.

Temperature effect was evaluated through the injection of RCIT and SCIT independently in the chromatograph. Column

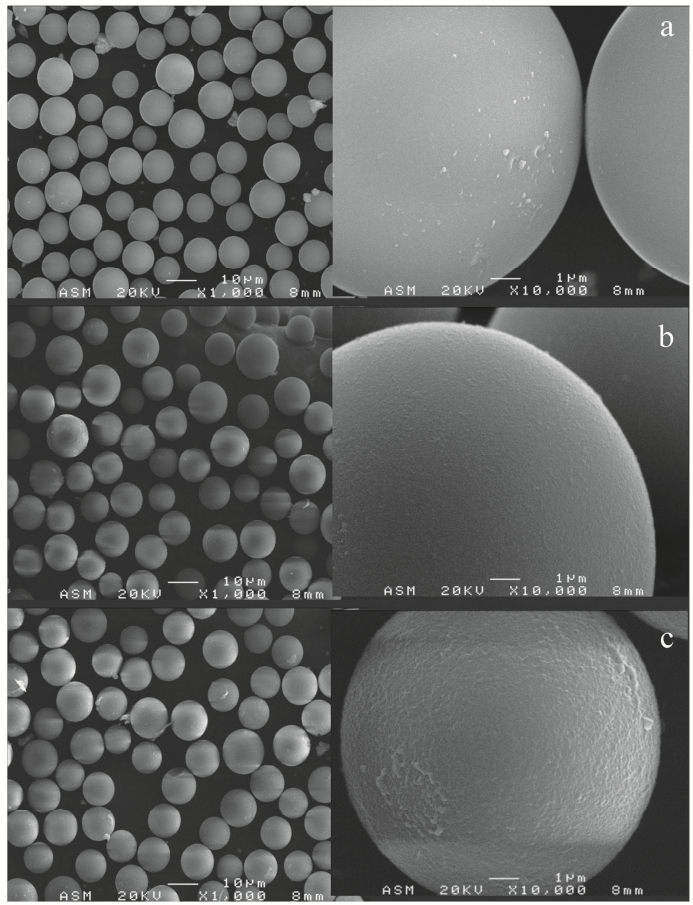

Figure 4. Scanning electron microscopy micrographs at different magnifications of (a) bare silica, (b) non-imprinted polymer-modified silica and (c) molecularly imprinted polymer-modified silica.

Table 3. Binding capacities of the surface-modified silicas at different thicknesses

Thickness (nm)	Capacity (mg SCIT g^{-1} material)	
	MIP	NIP
4	2.29	1.06
3	1.65	1.37
2	1.13	1.69
1	1.16	2.06

SCIT, (S)-citalopram; MIP, molecularly imprinted polymer; NIP, non-imprinted polymer.

heater was fixed to the desired temperature and kept constant at least for 20 min before injection. From the retention values of each compound, the retention factor (k) and the separation factor (α) were calculated. Van't Hoff plot was constructed next plotting the experimental ln α values versus 1/T (K^{-1}). As illustrated in Figure 6, two linear sections can be distinguished. The nonlinearity of the plot is an indicative of the differences of the thermodynamic processes, and it happens as a result of conformational changes of the analyte, the stationary phase or as a consequence of their interaction (Lao, 2013).

Experimental data of each section were fitted by linear regression and from the intercept, and the slope of each equation $\Delta(\Delta S)$ and $\Delta(\Delta H)$ were obtained. In Section A, which corresponds to temperatures ranging from 50–70 °C, $\Delta(\Delta H)$ was found to be -1.77 KJ mol^{-1} and

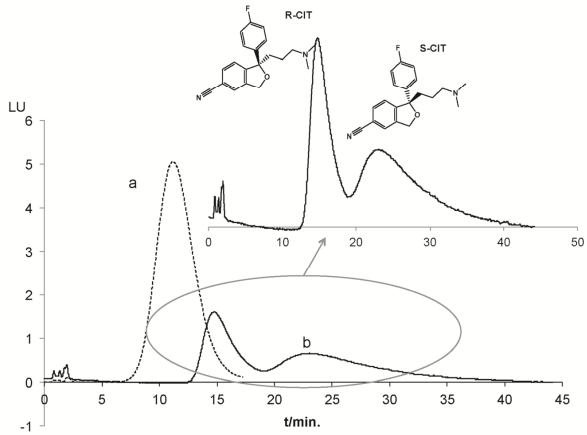

Figure 5. Chromatographic profile of citalopram at (a) a non-imprinted stationary phase and (b) an imprinted stationary phase. Mobile phase was 40 mM formate buffer:ACN (30:70 v/v) at a flow rate of 1 ml min^{-1} and a temperature of 40 °C.

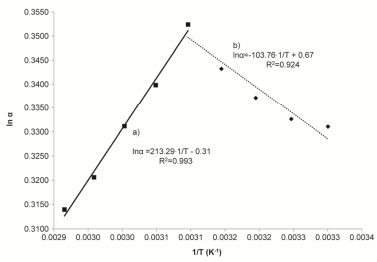

Figure 6. Van't Hoff plot where ln α versus 1/T is represented for each of the tested temperatures.

Δ(ΔS) was equal to -2.57 J mol^{-1}. Negative ΔΔH values indicate an exothermic transfer of the preferentially adsorbed enantiomer from the mobile phase to the stationary phase and therefore chiral recognition is favoured. The more negative the value, the stronger the interactions with the stationary phase (Oberleitner *et al.*, 2002). However, too negative Δ(ΔS) can counteract the chiral recognition spontaneity making ΔG increase (Equation (3)). In this case, because $|\Delta\Delta H| > |T\Delta\Delta S|$, the process in Section (a) is enthalpy controlled and temperature increase worsens enantioselectivity.

In Section (b), the opposite effect occurs. Here, ΔΔH and ΔΔS values are 0.86 KJ mol^{-1} and 5.58 J mol^{-1} respectively, so $|\Delta\Delta H| < |T\Delta\Delta S|$, and the process is entropy controlled. In consequence, from 30 to 50 °C, as temperature increases, enantioselectivity is enhanced.

Binding capacity and adsorption isotherms

Experimental adsorption isotherms were obtained by batch rebinding experiments that are one of the best methods to characterize binding behaviour of MIPs (Spivak, 2005). Results are described in supporting information (Figure S3 and Table S1).

Adsorption isotherms were fitted using different mathematical models including Langmuir, Bi–Langmuir, Freundlich and Freundlich–Langmuir isotherm models (Supporting information). Freundlich–Langmuir model was found to be the best fitting one, which is described by Equation (5). Where N_t is the binding site number, *a* is the average affinity binding and *m* is the heterogeneity factor. Fitting parameters are summarized in Table S1 for both the MIP and the NIP.

$$B = \frac{N_T a F^m}{1 + a F^m} \quad (5)$$

The average binding affinity of the MIP ($3.16\ 10^{-2} \pm 0.26\ 10^{-2}$ mM^{-1}) was noticeably higher than the one observed for the NIP ($2.80\ 10^{-3} \pm 1.74\ 10^{-3}$ mM^{-1}). The heterogeneity factor of the imprinted stationary phase was 0.82, whereas the *m* value of the NIP column was found to be 0.59, what clearly denotes a more homogeneous binding site distribution of the MIP material. In what concerns the number of binding sites, the value observed for the NIP material was around 10 times higher than the one observed for the MIP, 206.4 ± 133.5 µmol g^{-1} versus 24.97 ± 3.09 µmol g^{-1}. This could be attributed to a higher amount of non-specific low-affinity binding sites related with randomly distributed carboxylic functional groups in the polymer. In other words, as could be expected, a higher number of binding sites with a more heterogeneous distribution and with much lower binding affinity was observed for non-imprinted materials in comparison with imprinted ones.

CONCLUSIONS

Iniferter-mediated polymerization of an imprinted polymer has been demonstrated here to be a useful tool to coat silica based solid support. The MIP chiral selector has been successfully grafted on porous silica particles leading to a homogeneous material that recognizes preferably the S enantiomer of the

drug. Grafted polymer thickness has been optimized, and best MIP performance was observed using 4-nm-thick films. Lower thicknesses did not provide a good resolution of the tested racemate. The MIP-coated silica particles have demonstrated their performance as CSP for the enantiomeric resolution of the drug citalopram. The methodology presented here could be easily extrapolated to other enantiomers of drugs for the controlled development of thin film CSP that could separate drug racemates.

Acknowledgements

The authors wish to acknowledge the Spanish Ministry of Economy and Competitiveness (project CTQ2013-47921-P) and the University of the Basque Country (project PPM12/08) for the financial support. The Basque Government (Department of education, language policy and culture) is also gratefully acknowledged for a predoctoral BFI-2011-122 grant for R. Gutiérrez-Climente. Technical and human support provided by SGIker (UPV/EHU, MICINN, GV/EJ, ESF) is also acknowledged.

REFERENCES

Ansell RJ, Kuah JKL, Wang D, Jackson CE, Bartle KD, Clifford AA. 2012. Imprinted polymers for chiral resolution of (±)-ephedrine, 4: packed column supercritical fluid chromatography using molecularly imprinted chiral stationary phases. *J. Chromatogr. A* **1264**: 117–123.

Arnold FH, Plunkett S, Dhal PK, Vidyasankar S. 1995. Surface modification with molecularly-imprinted polymers for selective recognition. *Polym. Prepr. (Am. Chem. Soc., Div. Polym. Chem.).* **36**: 97–98.

Baggiani C. 2005. Chromatographic techniques. In Molecularly imprinted materials. Science and Technology. Ramström O, Yan M (eds). Marcel Dekker: New York; 517–734.

Barahona F, Turiel E, Cormack PAG, Martin-Esteban A. 2010. Chromatographic performance of molecularly imprinted polymers: core-shell microspheres by precipitation polymerization and grafted MIP films via iniferter-modified silica beads. *J. Polym. Sci., Part A: Polym. Chem.* **48**: 1058–1066.

Berthod A, He BL, Beesley TE. 2004. Temperature and enantioseparation by macrocyclic glycopeptide chiral stationary phases. *J. Chromatogr. A* **1060**: 205–214.

Bossi A, Whitcombe MJ, Uludag Y, Fowler S, Chianella I, Subrahmanyam S, Sanchez I, and Piletsky SA. 2010. Synthesis of controlled polymeric cross-linked coatings via iniferter polymerization in the presence of tetraethyl thiuram disulphide chain terminator. *Biosens. Bioelectron.* **25**: 2149–2155.

Chen X, Yang W, Zhou Y, Jiao F. 2012. *In situ* synthesis of monolithic molecularly imprinted stationary phases for liquid chromatographic enantioseparation of dibenzoyl tartaric acid enantiomers. *J. Porous Matter.* **19**: 587–595.

Edmondson S, Osborne VL, Huck WTS. 2004. Polymer brushes via surface-initiated polymerizations. *Chem. Soc. Rev.* **33**: 14–22.

du Fresne von Hohenesche C, Ehwald V, Unger KK. 2004. Development of standard operation procedures for the manufacture of n-octadecyl bonded silicas as packing material in certified reference columns for reversed-phase liquid chromatography. *J. Chromatogr. A* **1025**: 177–187.

Giovannoli C, Passini C, Baravalle P, Anfossi L, Giraudi G, Baggiani C. 2012. An innovative approach to molecularly imprinted capillaries for polar templates by grafting polymerization. *J. Mol. Recognit.* **25**: 377–382.

Gomez-Caballero A, Guerreiro A, Karim K, Piletsky S, Goicolea MA, Barrio RJ. 2011. Chiral imprinted polymers as enantiospecific coatings of stir bar sorptive extraction devices. *Biosens. Bioelectron.* **28**: 25–32.

Haginaka J, Kagawa C. 2002. Uniformly sized molecularly imprinted polymer for d-chlorpheniramine. Evaluation of retention and molecular recognition properties in an aqueous mobile phase. *J. Chromatogr. A.* **948**: 77–84.

Halhalli MR, Aureliano CSA, Schillinger E, Sulitzky C, Titirici MM, Sellergren B. 2012. An improved grafting technique for producing imprinted thin film composite beads. *Polym. Chem.* **3**: 1033–1042.

Kempe H, Kempe M. 2004. Novel method for the synthesis of molecularly imprinted polymer bead libraries. *Macromol. Rapid Commun.* **25**: 315–320.

Koehler J, Kirkland JJ. 1987. Improved silica-based column packings for high-performance liquid chromatography. *J. Chromatogr.* **385**: 125–150.

Koehler J, Chase DB, Farlee RD, Vega AJ, Kirkland JJ. 1986. Comprehensive characterization of some silica-based stationary phases for high-performance liquid chromatography. *J. Chromatogr.* **352**: 275–305.

Lao W. 2013. Thermodynamic and extrathermodynamic studies of enantioseparation of imidazolinone herbicides on chiralcel OJ column. *ISRN Chromatogr.* **2013**: 460787–460789.

Lu C-H, Zhou W-H, Han B, Yang H-H, Chen X, Wang X-R. 2007. Surface-imprinted core-shell nanoparticles for sorbent assays. *Anal. Chem.* **79**: 5457–5461.

Oberleitner WR, Maier NM, Lindner W. 2002. Enantioseparation of various amino acid derivatives on a quinine based chiral anion-exchange selector at variable temperature conditions. Influence of structural parameters of the analytes on the apparent retention and enantioseparation characteristics. *J. Chromatogr. A.* **960**: 97–108.

Perez-Moral N, Mayes AG. 2004. Noncovalent imprinting in the shell of core-shell nanoparticles. *Langmuir* **20**: 3775–3779.

Peter A, Torok G, Armstrong DW, Toth G, Tourwe D. 1998. Effect of temperature on retention of enantiomers of β-methyl amino acids on a teicoplanin chiral stationary phase. *J. Chromatogr. A* **828**: 177–190.

Piletsky S, Turner A. 2006. Molecular imprinting of polymers. Landes Bioscience: Texas.

Piletsky SA, Matuschewski H, Schedler U, Wilpert A, Piletska EV, Thiele TA, Ulbricht M. 2000. Surface functionalization of porous polypropylene membranes with molecularly imprinted polymers by photograft copolymerization in water. *Macromol.* **33**: 3092–3098.

Piletsky S, Piletsky S, Chianella I. 2012. MIP-based sensors. In Molecularly imprinted sensors Li S et al. (eds). Elsevier: Amsterdam; 339–354.

Prasad BB, Tiwari K, Singh M, Sharma PS, Patel AK, Srivastava S. 2008. Molecularly imprinted polymer-based solid-phase microextraction fiber coupled with molecularly imprinted polymer-based sensor for ultratrace analysis of ascorbic acid. *J. Chromatogr. A* **1198-1199**: 59–66.

Prucker O, Ruehe J. 1998. Mechanism of radical chain polymerizations initiated by azo compounds covalently bound to the surface of spherical particles. *Macromol.* **31**: 602–613.

Quaglia M, De Lorenzi E, Sulitzky C, Caccialanza G, Sellergren B. 2003. Molecularly imprinted polymer films grafted from porous or nonporous silica: novel affinity stationary phases in capillary electrochromatography. *Electrophoresis* **24**: 952–957.

Sandoval JE. 1999. Equation for calculating surface coverage from end-capping of chromatographic bonded phases. *J. Chromatogr. A* **852**: 375–381.

Sellergren B, Esteban AM. 2010. The use of molecularly imprinted polymers for sampling and sample preparation. In Handbook of sample preparation, Pawliszyn J, Lord HL (eds). John Wiley and Sons: Hoboken; 445–473.

Simoes M, Martins N, Cabrita MJ, Burke AJ, Garcia R. 2014. Tailor-made molecularly imprinted polymers for dimethoate and deltamethrin recognition: synthesis, characterization and chromatographic evaluation. *J. Polym. Res.* **21**: 1–13.

Spivak DA. 2005. Optimization, evaluation, and characterization of molecularly imprinted polymers. *Adv. Drug Delivery Rev.* **57**: 1779–1794.

Su S, Zhang M, Li B, Zhang H, Dong X. 2008. HPLC determination of sulfamethazine in milk using surface-imprinted silica synthesized with iniferter technique. *Talanta* **76**: 1141–1146.

Sulitzky C, Rueckert B, Hall AJ, Lanza F, Unger K, Sellergren B. 2002. Grafting of molecularly imprinted polymer films on silica supports containing surface-bound free radical initiators. *Macromol.* **35**: 79–91.

Tamayo FG, Titirici MM, Martin-Esteban A, Sellergren B. 2005. Synthesis and evaluation of new propazine-imprinted polymer formats for use as stationary phases in liquid chromatography. *Anal. Chim. Acta* **542**: 38–46.

Turiel E, Martin-Esteban A. 2005. Molecular imprinting technology in capillary electrochromatography. *J. Sep. Sci.* **28**: 719–728.

Unceta N, Goicolea MA, Barrio RJ. 2011. Analytical procedures for the determination of the selective serotonin reuptake inhibitor antidepressant citalopram and its metabolites. *Biomed. Chromatogr.* **25**: 238–257.
Unger KK, Lork KD, Pfleiderer B, Albert K, Bayer E. 1991. Impact of acidic/hydrothermal treatment on pore structural and chromatographic properties of porous silicas I. The conventional approach. *J. Chromatogr.* **556**: 395–406.
Vansant EF, Van Der Voort P, Vrancken KC, and Editors. 1995. Characterization and chemical modification of the silica surface. Elsevier Science B. V: Amsterdam.
Wang J, Cormack PAG, Sherrington DC, Khoshdel E. 2003. Monodisperse, molecularly imprinted polymer microspheres prepared by precipitation polymerization for affinity separation applications. *Angew. Chem. Int. Ed.* **42**: 5336–5338.
Whitcombe MJ, Kirsch N, Nicholls IA. 2014. Molecular imprinting science and technology: a survey of the literature for the years 2004–2011. *J. Mol. Recognit.* **27**: 297–401.

SUPPORTING INFORMATION

Additional supporting information may be found in the online version at the publisher's web site.

Supporting Information

Iniferter-mediated grafting of molecularly imprinted polymers on porous silica beads for the enantiomeric resolution of drugs

Raquel Gutiérrez-Climente, Alberto Gómez-Caballero, Mahadeo Halhalli, Börje Sellergren, Mª Aránzazu Goicolea and Ramón J. Barrio.

Mobile phase optimisation

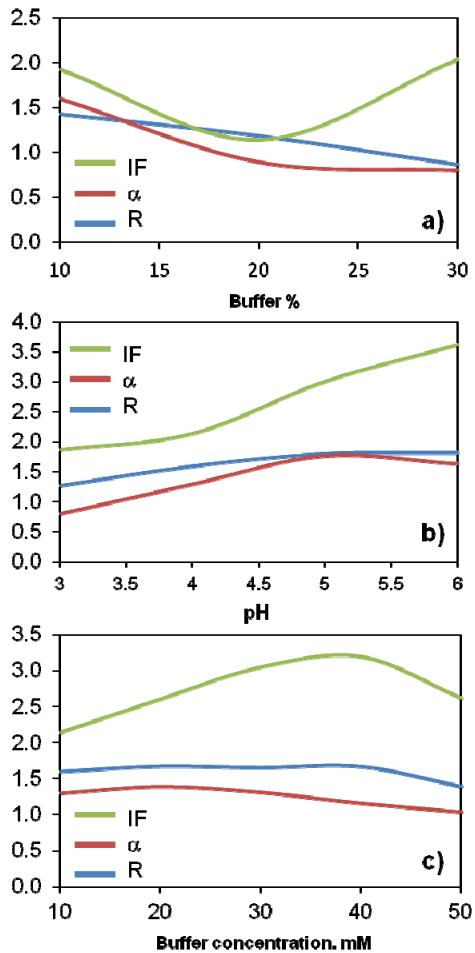

Figure S1: Effect of a) buffer percentage, b) pH and c) buffer concentration on the separation factor (α), the resolution (R) and the imprinting factor (IF).

As shown in figure S1a the resolution declines when the buffer content in the mobile phase is higher. When buffer percentages higher than 40% were employed, the enantioselectivity of the MIP worsened due to band broadening attributed to non-specific hydrophobic interactions with the cross-linker. 30% of buffer was finally selected as adequate due to the IF was highest at this point.

pH optimisation was crucial in order to minimise non specific interactions on randomly distributed carboxylic groups of the functional monomers in non-imprinted sites. As can be deduced from figure S1b, the higher the pH value, the higher the retention. pH values lower than 4 were not enough to get a good separation of enantiomers (figure S2). This effect could be attributed to the neutralisation of carboxylic groups of the functional monomer (pka_1 3.8 and pKa_2 5.45) leading to a weaker analyte binding in the imprinted sites and in consequence a worse enantiomer resolution. In contrast, less acidic pHs led to too high retention times and the consequent band broadening was observed. pH 4 was found to be the one providing good enantiomer resolution. Even if the IF, α and R values were better at pH 5 or 6, these ones were discarded for further research due to the high RT appreciated.

Buffer concentration was also assessed in order to test the effect of the ionic strength of the solution on chromatographic separation. As depicted in figure S1c, best IF was observed at 40mM.

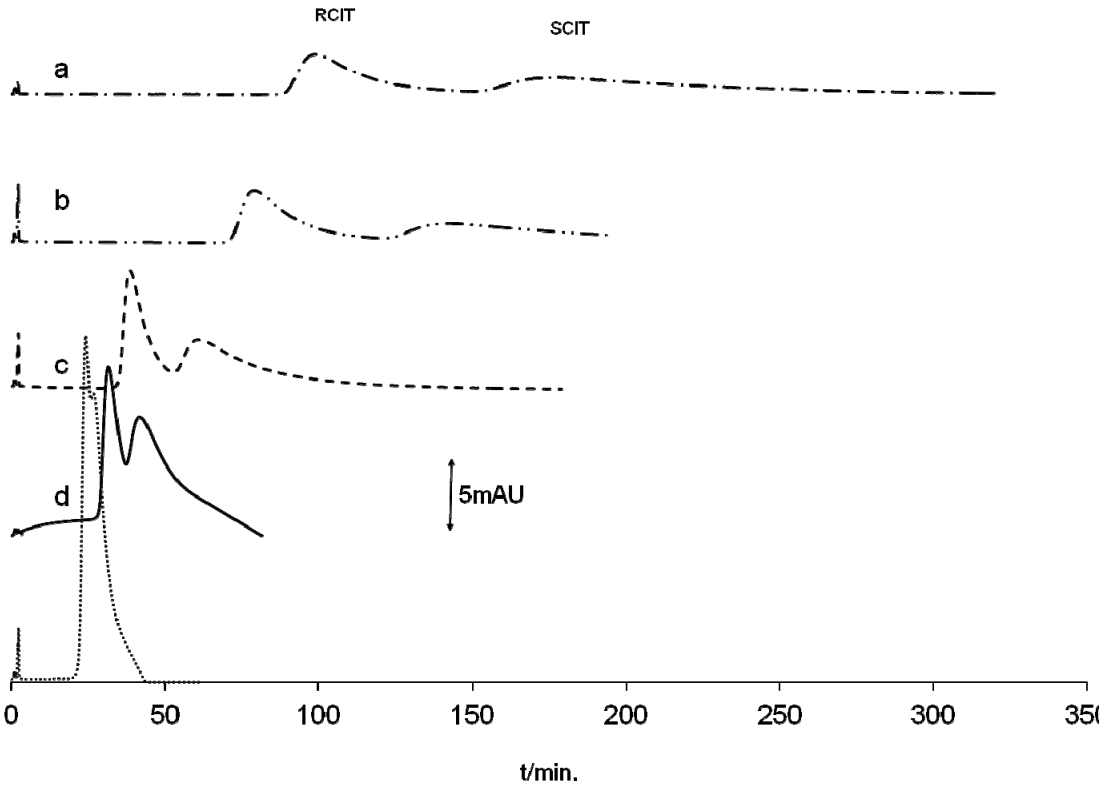

Figure S2: Chromatograms registered after the injection of 25 mg L^{-1} of citalopram using a 30:70 v/v mixture of formate buffer (10mM) and ACN at a) pH 6 b) pH 5 c) pH 4 d) pH 3.5 and e) pH 3.

Binding isotherms

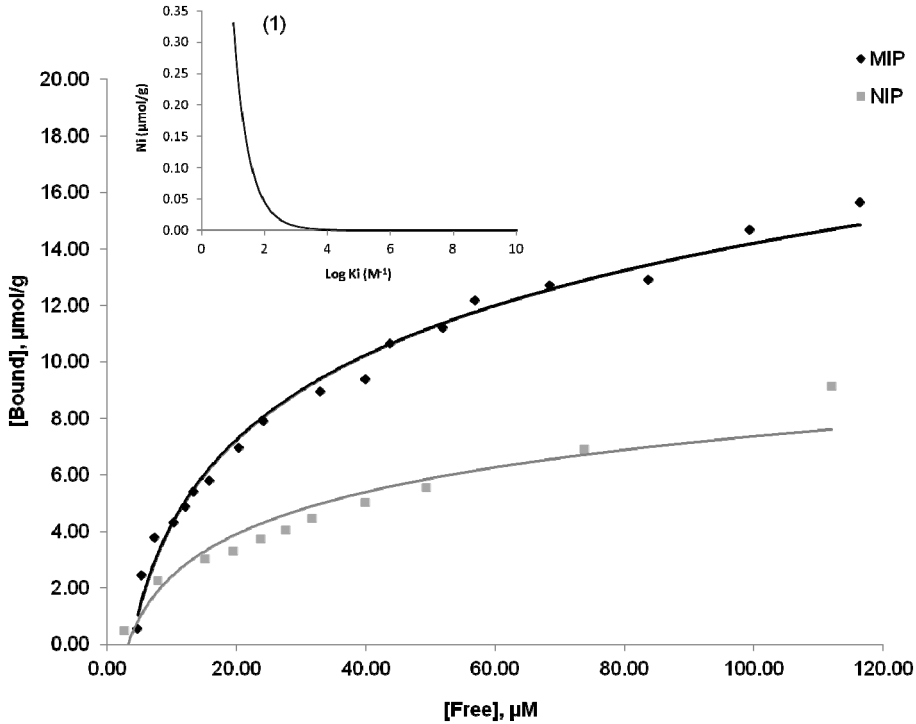

Figure S3. Binding isotherms registered using the MIP coated silica and the corresponding non-imprinted one. Isotherms are fitted to the Freundlich-Langmuir model and from the fitting parameters, the corresponding affinity distribution diagram is shown in the inset.

Figure S3 describes the experimental isotherm where free analyte concentration is plotted versus the bound concentration. The difference of the MIP and NIP behaviours is clearly noticeable. The experimental curve was fitted to different binding models such as the Langmuir, Bi-Langmuir, Freundlich and Freundlich-Langmuir isotherm models. A statistical comparative test was carried out by the Graphpad® software in order to know the model that best fitted experimental data. The program calculates Fischer's F value and the corresponding P value for the comparative study. When Langmuir was tested as null hypothesis (h0) and Bi-Langmuir as the alternative one (h1), the preferred model was the Langmuir model with an F value of 3.729 and P value of 0.0525. When Langmuir and Freundlich-Langmuir were compared, Freundlich-Langmuir was preferred (F: 6.174 and P: 0.0262). Between Freundlich and Freundlich-Langmuir models, Freundlich-Langmuir fitted better (F: 24.63 and P: 0.0002).

Table S1. Fitting parameters for the experimental MIP and NIP isotherms using the Langmuir, Bi-Langmuir, Freundlich and Freundlich-Langmuir isotherm models.

Langmuir	**MIP**	**NIP**
N_t (µmol g^{-1})	19.99 ± 0.59	13.56 ± 1.23
K_a (mM^{-1})	$2.59\ 10^{-2} \pm 0.18\ 10^{-2}$	$1.58\ 10^{-2} \pm 0.26\ 10^{-2}$
Bi-Langmuir	**MIP**	**NIP**
Nt_1 (µmol g^{-1})	$2773 \pm 1.23\ 10^{10}$	846.4 ± 52626
Nt_2 (µmol g^{-1})	$740.1 \pm 2.04\ 10^{10}$	1.09 ± 0.84
K_{a1} (mM^{-1})	$5.96\ 10^{-5} \pm 72.52$	$8.25\ 10^{-5} \pm 5.18\ 10^{-3}$
K_{a2} (mM^{-1})	$1.39\ 10^{-5} \pm 1053$	$1.38\ 10^{15} \pm 1.72\ 10^{25}$
Freundlich	**MIP**	**NIP**
a (mM^{-1})	2.51 ± 0.12	0. 60 ± 0.05
m	0.50 ± 0.02	0.58 ± 0.02
Freundlich-Langmuir	**MIP**	**NIP**
N_t (µmol g^{-1})	24.97 ± 3.09	206.4 ± 133.5
a (mM^{-1})	$3.16\ 10^{-2} \pm 0.26\ 10^{-2}$	$2.80\ 10^{-3} \pm 1.74\ 10^{-3}$
m	0.82 ± 0.07	0.59 ± 0.05

N_t: Number of binding sites. K_a: Affinity constant. a: Average binding affinity. m: Heterogeneity factor.

± Standard error

Synthesis of Molecularly Imprinted Polymers for the Speciation of Chiral Compounds

Universidad del País Vasco
Euskal Herriko Unibertsitatea